DOCTOR OF PHILOSOPHY

Microencapsulation : studies on the preparation and characterisation of liquid filled capsules

Amey, Jennifer Rachel

Award date:
2005

Awarding institution:
University of Wales, Bangor

MICROENCAPSULATION: STUDIES ON THE PREPARATION AND CHARACTERISATION OF LIQUID FILLED CAPSULES

A thesis submitted for the degree of

Doctor of Philosophy

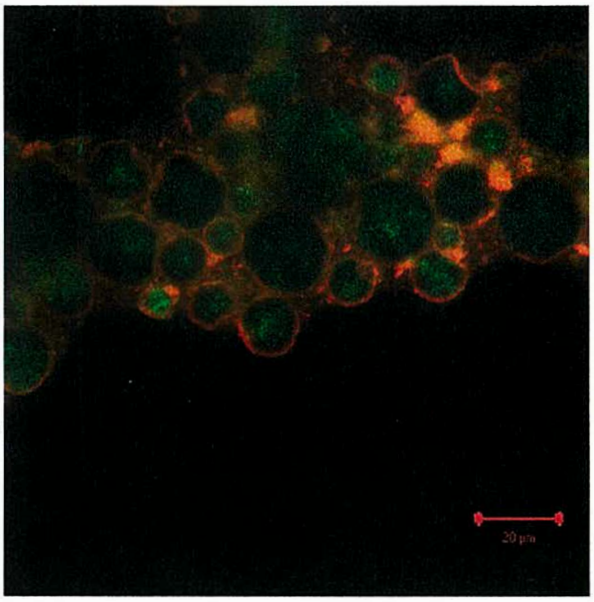

Prifysgol Cymru • University of Wales Bangor

by

Jennifer Rachel Amey

Contents

Abstract

The *in situ* interfacial polymerisation microencapsulation technique has been studied in detail by preparing liquid filled melamine-formaldehyde microcapsules. To examine the effect of microencapsulation variables upon microcapsule structure and morphology, three variables; internal phase, surfactant and mixing speeds, were studied. The resultant microcapsules were characterised using optical microscopy, SEM, and particle sizing. Thereafter, solutions of dyes and fluorophores were encapsulated to enhance microcapsule characterisation using optical, fluorescence and confocal laser scanning microscopy. Leaching experiments were conducted on three separate batches of microcapsules; phenanthroline, ferrocene and chlorobenzene containing microcapsules. Microcapsule leaching was monitored using UV/Visible spectroscopy and gas chromatography. In a separate experiment, a ruthenium homogeneous catalyst was encapsulated and the resultant microcapsules were characterised using SEM, EDAX and UV/Visible spectroscopy.

Acknowledgements

Firstly, my sincerest gratitude and thanks go to my PhD supervisors, Dr. Ian Butler and Dr. Peter Holliman. Thank you for providing me with a PhD CASE award which enabled me to continue my studies at Bangor University for an additional four years. Thank you for the continual guidance, encouragement and efforts put in during the past four years to help me reach my goal. I shall always remember, and never underestimate, just how much time, energy and patience both of you invested to me during my PhD.

Thereafter, I'd like to thank the following; EPSRC and Thermographic Measurements Ltd (TMC) for funding the research; all the departmental technicians, Denis Williams, Glyn Connolly, Kevin Spencer, Mike Lewis, John Charles, Gwynfor Davies and Steve Jones, who have helped me enormously during my PhD; Andrew Davies for his microscopy expertise; Caroline Naylor, Tracey Parry and Barbara Kinsella for all their help over the years.

Special thanks go to, Dafydd Thomas for all his invaluable help during the past four years, Chris Gwenin for proof reading various chapters of my PhD, Dan Lamb for helping me to get all my scans straight! These thanks extend to all students and staff (past and present) who I have at one time or another either worked alongside or played sport with, thank you all for keeping me sane during my PhD! You will all be remembered with fond memories.

And finally, the deepest thanks are reserved for all members of my family (on both sides of the Atlantic!). Thank you all for your continued unconditional love and support.

"Sow your seed in the morning,

and at evening let not your hands be idle,

for you do not know which will succeed,

whether this or that,

or whether both will do equally well."

Ecclesiastes 11: 6

CHAPTER 1

INTRODUCTION

1. Introduction

1.1. Area of Study

The aim of the work carried out in this PhD thesis was to produce liquid filled microcapsules containing homogeneous catalysts. Microencapsulation is a widely used technique, employed to offer protection and controlled delivery of the chosen encapsulatant. The reason for microencapsulating homogeneous catalysts arises from various problems associated with the catalysts themselves. For example, homogeneous catalysts are often air sensitive and some contain toxic metals. Therefore, a protective barrier coating homogeneous catalysts would solve these two specific problems. Homogeneous catalysts are also difficult to separate from the product at the end of reaction and it was envisaged that microencapsulation would offer a solution to this problem. Given that these catalysts are also high cost, controlled delivery of homogeneous catalysts from microcapsules would be of particular use for chemical industry, since despite homogeneous catalysts being both highly active and selective, they are not used as widely in chemical industry as they could be.

Much literature exists on methods developed to try to overcome separation and recovery problems associated with homogeneous catalysts. In particular, there is a significant volume of literature citing "polymer-supported" homogeneous catalysts as one method to tackle these problems. However, there is a dearth of literature on microencapsulated homogeneous catalysts, in particular liquid filled microcapsules containing homogeneous catalysts. To the authors knowledge no such literature exists on liquid filled microcapsules containing homogeneous catalysts but literature has been found describing the production of solid microcapsules containing homogeneous catalysts and their use in organic reactions. Solid microcapsules contain the intact homogeneous catalyst (or catalyst metal only) embedded within a solid core polymer matrix. Such solid core microcapsules catalyze organic reactions in similar ways to polymer supported catalysts by allowing liquid reagents to pass into and over the microcapsules. They also have the advantage over traditional homogeneous catalysts of being filtered and re-used in the same

way as polymer supported catalysts. The work in this thesis differs from literature work because it is concerned with the preparation and characterisation of liquid filled microcapsules containing homogeneous catalysts rather than solid microcapsules. Liquid filled microcapsules offer an advantage over solid core microcapsules use in homogeneous catalysis because the homogenous catalyst is already dissolved in the liquid core of the capsule, and therefore is ready for catalytic activity upon release. The literature that has been reviewed in this chapter focuses upon solid microcapsules containing catalysts with a discussion of relevant liquid filled microcapsules. The thesis introduces such relevant background literature in chapter 1. The preparation and characterisation of liquid filled melamine-formaldehyde microcapsules containing various dyes and fluorophores is presented in chapter 2 which is the first results and discussion chapter of this thesis. Thereafter, results from microcapsule leaching experiments are presented and discussed in chapter 3. Chapter 4 focuses upon the microencapsulation of a ruthenium homogeneous catalyst and the characterisation of the resultant catalyst containing microcapsules. Conclusions drawn from results discussed in this thesis are given at the end of each relevant chapter. The final chapter of this thesis (chapter 5) gives the experimental procedures used.

1.2. Microencapsulation

Microencapsulation is a well established process whereby micron-sized particulate matter (solids) or liquid droplets are coated with a polymer. The products obtained from microencapsulation processes are termed microcapsules or microspheres. A number of reviews on the subject have been published within the scientific and patent literature which summarize procedures and microcapsule applications, the most recent reviewing the role of microencapsulation in the pharmaceutical industry. [1] In addition to this, there are a number of texts on the subject; the most recently published comprehensive text covers all aspects of microencapsulation. [2] There is also an international journal on the subject. [3] It should be noted at this stage that microencapsulation terminology can often be ambiguous. Microcapsules exhibit essentially two different types of structure (Figure 1.1). The internal phase (alternatively known as core material) is the chemical species that forms the inside of

the capsule. The internal phase can be either solid or liquid. This thesis focuses primarily upon liquid filled microcapsules. The surface area of the internal phase is completely covered by the polymer wall (also known as capsule wall or capsule shell), and hence, the internal phase is termed "encapsulated".

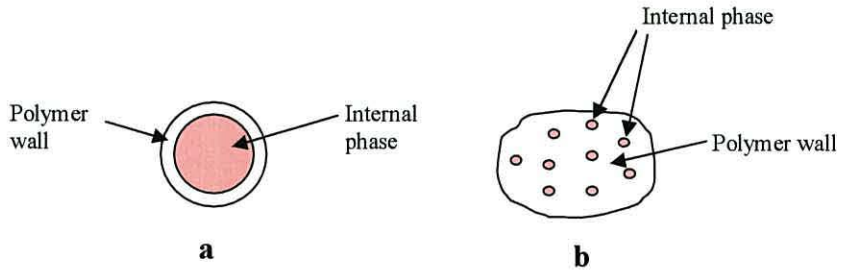

Figure 1.1. Schematic diagrams of two microcapsules: (a) continuous core/shell microcapsule, and (b) multinuclear microcapsule. [2]

Continuous core/shell microcapsules (Figure 1.1, a) can be considered as individual spherical vesicles containing a thin polymeric coating around the internal phase. Alternatively, multinuclear microcapsules (Figure 1.1, b) contain a number of liquid droplets or solid particles of internal phase embedded within the polymer matrix of each capsule. The resulting shape of multinuclear microcapsules can either be spherical or irregular whereas continuous core/shell microcapsules are normally spherical. Clearly, the shapes and sizes of both types of microcapsules are determined by the type of microencapsulation process used in manufacture. It is often unclear whether the product from a microencapsulation procedure is to be labelled a microcapsule or a microsphere, since both types of microcapsule in Figure 1.1 have also been alternatively labelled as "microspheres" by many workers in the field. Also, several other terms may be used when labelling the individual components of a microcapsule or microsphere; for example, terms such as core material, active fill, capsule wall, shell material and others are regularly used in the description of microcapsules/microspheres. In this thesis the following terms will be used exclusively to avoid ambiguity. Internal phase will be used to describe the inside of a microcapsule, and polymer wall to describe the material that coats the internal phase. At the time of writing, there is no universally accepted size range that particles must have in order to be classified as microcapsules. However, it is common to classify capsules smaller

than 1 μm as nanocapsules and capsules larger than 1000 μm as macrocapsules, and hence between these two limits are microcapsules. [2] This thesis will use this size classification.

Capsule Functions and Applications

Microcapsule functions can be several-fold. Microencapsulation can offer protection of the internal phase from the surrounding environment, therefore improving the storage life and stability of the internal phase. In addition, undesirable properties of the internal phase (for example, if the internal phase is toxic or hazardous) can be masked by encapsulation. Related to this is odour or taste masking, or masking chemical properties of the internal phase such as extreme pH. Microencapsulation can be employed to separate incompatible components by encapsulating the reactive species separately within a blend, and liquid components can be converted to free-flowing powders upon encapsulation. Microcapsules can be engineered to release the internal phase in a controlled manner and this can mean either timed release through rupture of the polymer wall or sustained release, where often the internal phase diffuses through the polymer wall. Microcapsules can also be engineered to target the site of release of active material, most common for pharmaceutically active materials, giving targeted site delivery and controlled release. [1,2]

Some of the most interesting examples demonstrating such functions of capsules are found in nature. [4] For example, plant seeds and bacteria spores have remained viable for periods over 100 years because of their outer protection. In another example, the black pigmentation within the cellular wall of certain types of fungi spores provides protection in hostile environments by filtering out sunlight. Release of internal phase in natural samples can be demonstrated by observing the action of charged lipid bilayers within a cell membrane. Such bilayers act selectively as permeability valves; for example, the permeability of water through these cytoplasmic membranes may be 10^{10} times larger than the permeability of ions. The final example, a chicken egg, although a macroscopic example, does demonstrate the concept of "protection and release" of microencapsulation particularly well. The chicken egg has been engineered by nature with a protective wall which is thick enough to provide maximum protection during incubation, yet still thin enough to allow breakage at the moment of hatching. Research in the field of microencapsulation first began in the late 1930s where Green and co-workers were

developing a product that would give multiple paper copies without the use of carbon paper. Combining the idea of dispersions (which had already been used in photographic applications), and investigating de Jong's coacervation studies on gelatin microspheres at the time, led Green to develop and patent the first commercially available gelatin based microcapsules containing a liquid colourless dye-precursor for the application of carbonless copy paper. [4,5] The microcapsules were screen printed onto paper that contained a top layer of clay coating. Pressure induced microcapsule rupture causes the internal phase (colourless liquid dye-precursor) to release from the microcapsules, which upon contact with the acidic clay coating, forms a coloured complex that is displayed on the paper (Figure 1.2).

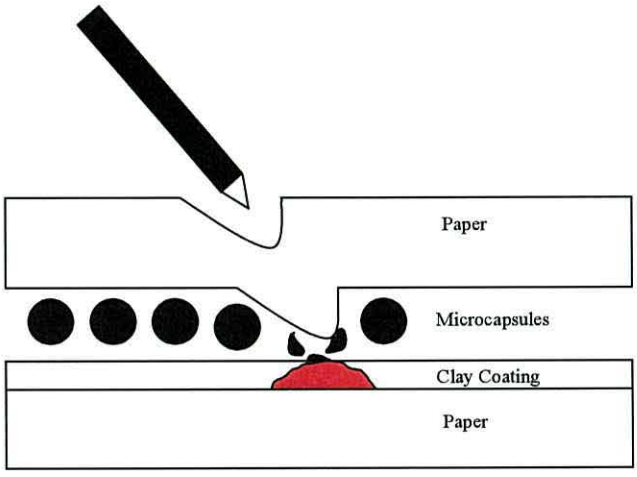

Figure 1.2. Pressure activated release of encapsulated dye-precursor to give a colour reaction on paper coated with acidic clay. [4]

Since then, microencapsulation has been utilised throughout the chemical and food industries in numerous applications. Materials ranging from adhesives, agrochemicals, live cells, active enzymes, flavours, fragrances, pharmaceuticals, and inks have all been encapsulated. [2,6] Such microcapsules are now commonplace in everyday items such as cosmetics, washing powders, and pharmaceutical pills. Various novelty items such as colour changing T-shirts and mood rings using microencapsulated liquid crystals became popular in the early 1990s, as did "scratch and sniff" products which used microencapsulated fragrances to manufacture such products.

Microcapsule Preparation

Several methods exist to make microcapsules. The methods currently known for microencapsulation are categorized into chemical and physical (mechanical) techniques [2,4], often referred to as Type A and Type B processes since some chemical techniques rely exclusively on physical phenomena and some so-called physical techniques actually involve a chemical reaction. Each of the processes has been developed to produce microcapsules with specific properties in mind. Microcapsule properties (structure, size, wall thickness, internal phase (wt % of capsule), wall permeability, etc.) depend upon both the microencapsulation method and the physical properties of materials chosen for encapsulation. For example, variables within a microencapsulation synthetic method include stirring speeds, temperature, pH, stoichiometry, rate and sequence of addition of different reagents to one another. Material properties include surfactant type and concentration, viscosity and volatility of liquid phases, immiscibility of liquid phases and polymer type. Alteration of any of these variables, however small, can lead to significant changes in microcapsule properties and therefore, it is difficult to make generalisations. Table 1.1 lists these "Type A" and "B" encapsulation processes.

Table 1.1. List of types A and B encapsulation Processes. [2]

Type A (chemical) processes	**Type B (mechanical) processes**
Complex coacervation	Spray drying
Polymer-polymer incompatibility	Spray chilling
Interfacial polymerization in liquid media	Fluidized bed
In situ polymerization	Electrostatic deposition
In-liquid drying	Centrifugal extrusion
Thermal and ionic gelation in liquid media	Spinning disk/rotational suspension separation
Desolvation in liquid media	Polymerization at liquid-gas or solid-gas interface

Most materials used to form the capsule wall are organic polymers, though fats and waxes may be used in special cases. A range of internal phases (both liquids and solids) have been encapsulated using such wall materials. [2] Most microencapsulation methods use dispersions and the interface between the immiscible phases is often the nucleation point

for polymerization to form the capsule wall. Depending upon the method and materials chosen, most commercial microcapsules have diameters ranging between 3 and 800 μm and can vary in the concentration of internal phase from 10-90 % by weight. Complex coacervation was the first encapsulation process to be used commercially (see Figure 1.2, carbonless copy paper example discussed earlier).

Another example of this particular process used to encapsulate a liquid is outlined in Figure 1.3. Complex coacervation is based upon the ability of cationic and anionic water-soluble polymers interacting in water to form a liquid, polymer-rich phase known as a complex coacervate. Most commonly, gelatin is the cationic polymer used and gum arabic (comprised of the following composition; L-arabinose (30.3 %), L-rhamnose (11.4 %), D-galactose (36.8%), D-glucuronic acid (13.8 %) and water (7.7 %)) is the anionic water soluble polymer used in this process. The resulting coacervate (loosely linked coils of these hydrophilic colloids), at this stage is in equilibrium with an excess of aqueous supernatant. Therefore, this aqueous solution can be thought of as a pseudo two-phase system containing a dispersed phase (coacervate) within a continuous external phase (aqueous supernatant).

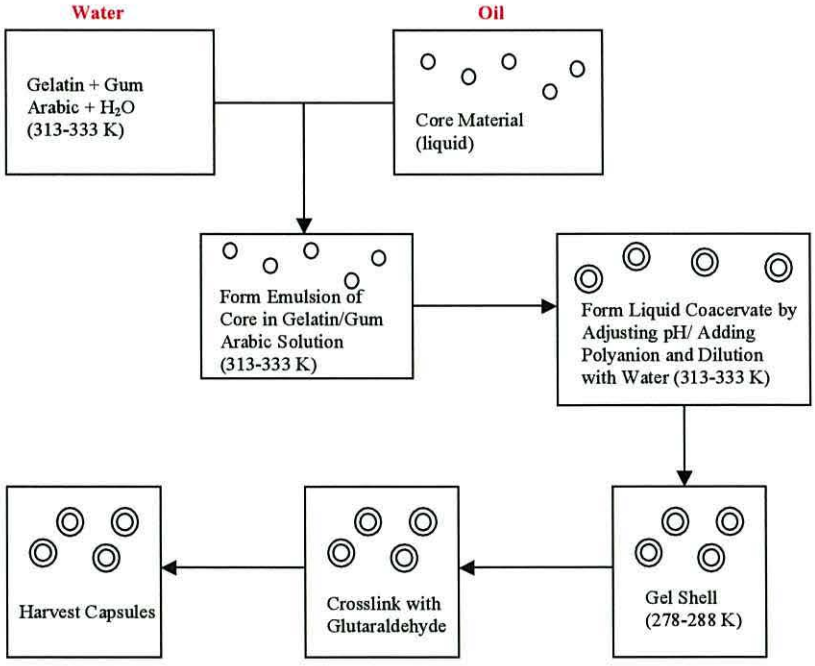

Figure 1.3. Schematic flow diagram of the gum arabic/gelatin encapsulation process based upon complex coacervation. [2]

An oil (water immiscible) liquid phase is then poured into this mixture whilst stirring, thus forming an oil-in-water emulsion, since the oil phase is dispersed into the aqueous phase which contains the coacervate. Providing the complex coacervate has the correct properties to wet this liquid phase, each droplet is spontaneously coated with a thin film of coacervate to produce microcapsules. Often, the soft gelatin-gum arabic polymer wall is hardened using a crosslinking agent such as glutaraldehyde before the microcapsules are harvested (Figure 1.4). Glutaraldehyde crosslinks gelatin-gum arabic polymers by a Schiff base reaction between the aldehyde functional groups in glutaraldehyde and amino groups in the gelatin-gum arabic polymer. Also, crosslinking occurs by an aldol condensation between two adjacent aldehydes. [7] Complex coacervation has been used to produce microcapsules for a variety of other applications such as perfumes for advertising inserts and liquid crystals for display devices. The microcapsules produced from this type of encapsulation technology are simple continuous core/shell microcapsules (Figure 1.1, a), often with a capsule diameter range 20-800 μm that, depending upon polymer/internal phase ratio, contain 80-90 % wt. internal phase.

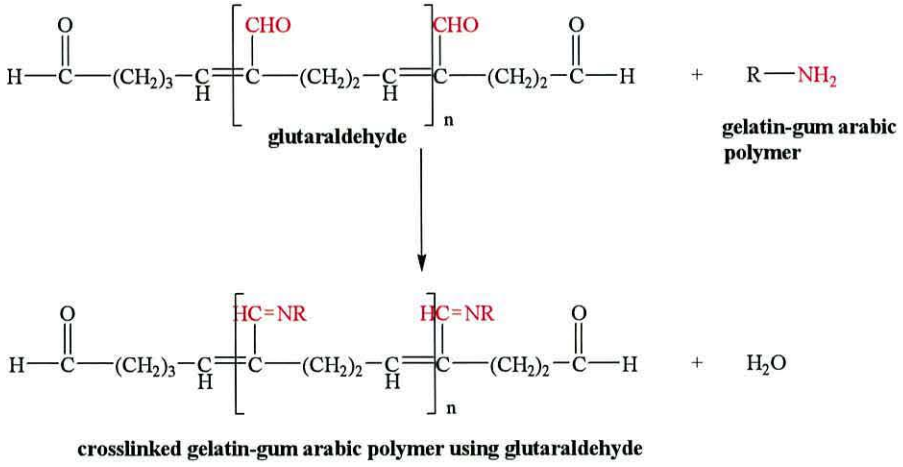

Figure 1.4. Chemical crosslinking of gelatin-gum arabic polymer using glutaraldehyde. [7]

Interfacial polymerisation is a microencapsulation process whereby the polymer wall is formed at the interface of an oil-in-water emulsion (or water-in-oil emulsion). An emulsion is formed by the dispersion of one immiscible liquid in another, and it is

stabilized by a third component, the surfactant. [2] The surfactant concentration in the external phase plays an integral part of stabilizing the emulsion. Interfacial polymerisation differs from the previous example in that soluble monomers are dissolved in each phase. Often, the reagents chosen for this type of process are water soluble amines and organic soluble isocyanates or acids which react together to form a polyurea wall. The microcapsules produced from this type of encapsulation technology are simple continuous core/shell microcapsules (Figure 1.1, a). Interfacial polymerisation is routinely used to produce 20-30 μm diameter microcapsules loaded with pesticides and herbicides. [2] These agrochemicals are relatively water insoluble, low-melting solids or high-boiling liquids that are free of functional groups which could react with the monomers needed to form the polymer wall. Therefore, many commercial encapsulated agrochemical formulations are prepared by interfacial polymerisation. The exterior surface of microcapsules formed by this process is smooth and uniform. However, capsule fracture studies have shown that the interior surface often appears cratered and irregular, leading to observations that the polymer wall is not uniformly deposited around the internal phase except for a comparatively thin outer region of the capsule wall. Therefore, in such cases the polymer wall is a thin skin membrane resting on a thick porous support. [2]

In situ polymerisation is a similar microencapsulation process to both complex coacervation and interfacial polymerisation, in that polymerisation occurs in the presence of an emulsion. The difference here is that polymerization occurs exclusively in the continuous phase (*i.e.* outer phase) and on the continuous-phase side of the interface formed by the dispersed internal phase and continuous phase. As the process continues, polymerization with crosslinking occurs, eventually creating a solid polymer wall. Various water-immiscible liquids have been encapsulated using amine based resins such as urea-formaldehyde and melamine-formaldehyde as polymer wall. [8] Studies into the *in situ* melamine-formaldehyde polymerisation process showed that the addition of anionic polymers to the aqueous continuous phase can have a significant effect on polymerisation. [9] *In situ* polymerization encapsulation technology is used to produce microcapsules with a diameter range; 3-6 μm for commercial applications such as carbonless paper inks and perfumes. Larger microcapsules (containing mineral oil) are also produced using this

method for use in cosmetics. This thesis focuses upon the *in situ* polymerisation of water soluble melamine-formaldehyde oligomers to produce liquid filled microcapsules.

Other microencapsulation techniques mentioned in Table 1.1 are; (i) spray drying was the first type of process to introduce the concept of microencapsulation (in the 1930s) by preparing small particles carrying an internal phase trapped within a polymer wall. The technique uses water soluble polymers for encapsulation with no crosslinking involved, therefore the microcapsules produced can be used for food applications as the polymer wall will simply dissolve in water leaving no residue. Spray drying is a low cost microencapsulation method, usually used nowadays for the encapsulation of fragrances and flavours, (ii) centrifugal extrusion is the process where two mutually immiscible liquids are pumped through a spinning two-fluid nozzle, producing a continuous two-fluid column of liquid that breaks up into a stream of spherical droplets immediately after it emerges from the nozzle. Each droplet contains a continuous core region surrounded by a liquid shell (Figure 1.5).

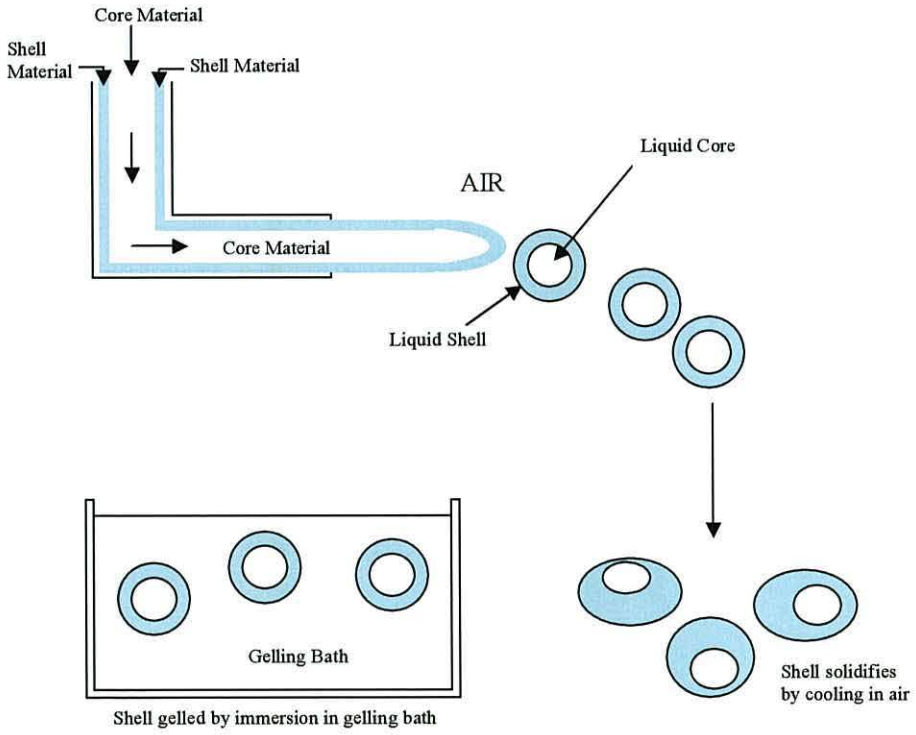

Figure 1.5. Schematic diagram of the microencapsulation technique, centrifugal extrusion. [2]

The droplets are converted into capsules by several different methodologies which depend on the nature of the shell material. For example, if the shell material is a relatively low-viscosity hot melt that crystallises on cooling (*eg.* a wax), then droplets are converted into capsules as they fall away from the nozzle. This method is limited to producing relatively large microcapsules, often in the size range 250 μm to several mm, (iii) polymer-polymer incompatibility, which uses the polymer phase-separation phenomenon that occurs when two chemically incompatible polymers are dissolved in a common solvent. The two polymers repel each other, forming two distinct liquid phases. One phase is designed to form the polymer wall, whereas the other phase is present in the system only to form the second phase (it is not used in forming microcapsules). This process is used for the commercial production of encapsulated aspirin and encapsulated potassium chloride, (iv) fluidised bed microencapsulation process is limited to the encapsulation of solid particles or porous particles into which a liquid has been absorbed. To summarize, a range of different microencapsulation processes exist and many different types of materials have been encapsulated within different types of polymers using such methods discussed.

1.3. Microcapsule Leaching and Characterisation

In vitro characterisation of microcapsules typically consists of determining how fast the internal phase is lost by a known weight of capsules under a given set of conditions. [10] Normally, data of this type is presented by plotting the amount of material released against time to give a release curve. It should be made clear that such curves actually represent the average release behaviour of a population of capsules rather than the release behaviour of individual microcapsules themselves. Often, the interpretation of release data is complicated. For example, microcapsules which might be expected to individually release their internal phase at a constant rate may show first order population release. It should be realized that individual capsules in a given population differ from one another in release kinetics. This is due to differences between individual capsules in size, internal phase, geometry, and/or other factors that influence the release kinetics of a capsule. The exact form of the release behaviour of a population of capsules depends on the functional form characterising the release behaviour of the individual capsules, and on a rate parameter

distribution function which characterises the population. Rates of release from such capsules depend largely on the structure of the polymer formed, which in turn is influenced by the conditions employed in the preparation.

It is widely known that several different parameters affect polymer permeability. [11] For example, an increase in polymer density, crystallinity, orientation, degree of crosslinking, and plasticizer level will all reduce polymer permeability. The shape of the microcapsule also plays a significant part in affecting polymer capsule wall permeability. For example, larger sized microcapsules, an increase in capsule wall thickness, a higher proportion of spherical microcapsules, post treatment of microcapsules (such as hardening, spray coating, crosslinking), and multiple wall formation will all reduce microcapsule permeability. [11] There have been many studies on structure-permeability correlations carried out in polymeric membranes. These are often conducted by systematically changing the monomers used and observing the differences in resultant physical structure.

The effect of polymer crystallinity upon permeability has been investigated in polyurea liquid filled microcapsules containing cyclohexane as internal phase. [12] The polyurea polymer wall was made by reacting together the monomers, hexamethylene-1,6-diisocyanate (HMDI) and hexamethylene-1,6-diamine (HMDA). Batches of microcapsules with varying degrees of polymer crystallinity were made using different reaction conditions and the dependence of release rates on degree of polymer crystallinity was examined. The parameters varied in the preparation were; monomer mole ratio (the ratio of moles of diisocyanate to amine), the number of moles of the limiting monomer and the ratio of dispersed phase (cyclohexane) to the continuous phase in the final mixture. The microcapsules were characterised initially for size using a particle sizer and the capsules produced were found to have a size range 0.5-10 μm. The polymer wall thickness could not be directly measured but the polymeric reaction was known to go to completion (as measured by pH measurements) therefore an average polymer wall thickness was calculated from the stoichiometry and the average size of the capsules.

The permeability of the polyurea membrane was determined by monitoring the rate of release of cyclohexane into an *n*-heptane environment. The microcapsules were filtered from the slurry and washed 3-4 times with distilled water. The capsules were then lightly bottled to remove surface moisture and placed into a release cell containing 100 ml *n*-

heptane. The ratio of the dispersed phase to the continuous phase was maintained at 0.5 % (wt/wt). Samples of the continuous phase were taken at intervals using a syringe and analysed for cyclohexane by gas chromatography. Two samples of polyurea microcapsules, one batch containing the most amorphous polymer and one containing the most crystalline polymer (as determined by XRD analysis) were examined. The release rates were shown to be significantly different for the two samples, although in both cases the data followed the trend expected for a diffusional release process. The data was interpreted in terms of a permeation model which was developed from an existing model. [13] Using the model, the permeabilities for both polyurea samples were calculated to be 3.75 x 10^{-8} moles per second (mol s^{-1}) for the most amorphous polymer and 1.20 x 10^{-8} (mol s^{-1}) for the most crystalline polymer, showing that the more crystalline the polymer, the less permeable it is.

Studies using polyurea microcapsules containing fragrant Migrin oil doped with the dye molecule, 1,4-diaminoanthraquinone (DAA) showed that an increased thickness polymer capsule wall reduces the polymer permeability, hence reducing the rate at which the internal phase is released. [14] Two separate batches of polyurea microcapsules were made from using 2,4-toluene diisocyanate (TDI) as the organic soluble monomer and either ethylene diamine (EDA) or 1,6-hexane diamine (HDA) as the water soluble amine monomer. Release profiles of DAA from the microcapsules were obtained by adding the microcapsules to 100 ml of *N,N'*-dimethyl acetamide and methanol with stirring at 293 K over a total time period of 400 minutes. When EDA was used the microencapsulation proceeded faster in comparison with HDA based monomers. This was attributed to the rapid reactivity of EDA. Also EDA – based microcapsules had the slowest release rate compared to the HDA – based microcapsules which is explained simply because the EDA – microcapsules having a thicker polymer wall.

The transfer of azo-dyes from an internal phase of dioctylphthlate to methanol through poly(urea-urethane) microcapsule membrane has similarly been measured. [15] Poly(urea-urethane) microcapsules containing an internal phase of dioctyl(diethyl hexyl)phthalate with the oil soluble dye; *N*-[2,5-bis(heptyloxy)phenyl]-2-[(2,5-dibutoxy-4-p-tolylthiophenyl)hydrazono]-3-oxobutylamide were prepared according to a standard interfacial polymerization microencapsulation technique. The resulting microcapsules

were spread homogeneously onto a polyethylene terephthalate (PET) sheet and dried. The protective colloid PVA was found to be an effective binder between the PET sheet and microcapsule thin layer. The thickness of the microcapsule layer was measured to be approximately 20 μm. The film was then cut into squares 1cm x 1cm. Ten sheets of the square films were put into a glass vessel containing 20 ml of methanol. The solution was gently stirred and thermally controlled at various temperatures in the range from 303 to 328 K. The optical density (OD) of the outer dispersing medium was measured at $\lambda = 430$ nm as a function of time. The results showed that the dye concentration in methanol increases with temperature, T and smoothly saturates at a long time, t. The observed data was found to fit a permeation model based upon the chemical potential of the releasing solute, further details of which can be found in the paper.

Confocal laser scanning microscopy (CLSM) is a technique that uses lasers to image fluorescent specimens by single point illumination at the focal plane. It has been used to image and characterise microcapsules. [16] The confocal principle in epi-fluorescence scanning optical microscopy is shown in Figure 1.6.

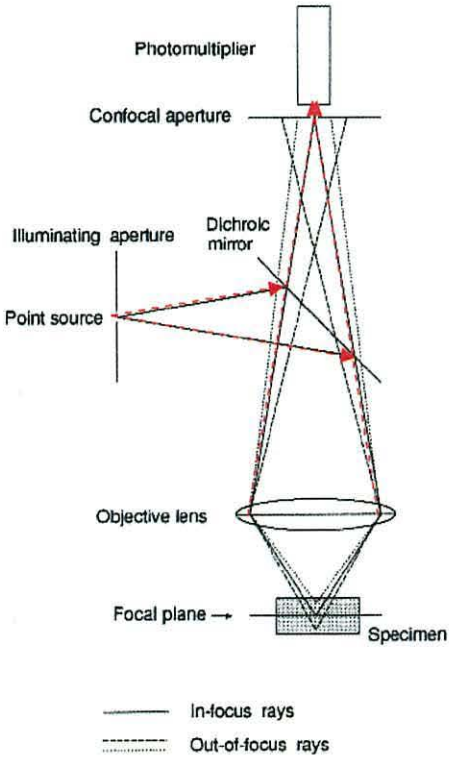

Figure 1.6. The confocal principle in epi-fluorescence scanning optical microscopy. [17]

The diagram in Figure 1.6 shows excitatory laser light from the illuminating aperture passes through an excitation filter (not shown) and is reflected by the dichroic mirror. Thereafter, the excitatory laser light is focussed by the microscope objective lens to a diffraction limited spot at the focal plane within the 3D specimen. Fluorescent emissions excited both within the illuminated in-focus voxel and within the illuminated cones above and below it, are collected by the objective and pass through the dichroic mirror and the emission filter (not shown). Only those emissions from the in-focus voxel are able to pass unimpeded through the confocal aperature to be detected by the photomultiplier. Fluorescence emissions from the regions below and above the focal planes (out-of-focus rays) contribute essentially nothing to the final confocal image. This is in direct contrast to conventional epi-illumination light/fluorescence microscopy which images specimens using full-field illumination. [17] Providing the material is sufficiently translucent, CLSM is capable of non-invasive serial optical sectioning of the specimens, leading to the possibility of generating three-dimensional images of thick transparent objects such as biological cells and tissues.

By labelling microcapsules using different fluorophores, the unambiguous identification of several compounds within the microcapsule is possible. In one example, the internal oil phase (eicosapentaenoic acid ethyl ester) of gelatine-gum arabic microcapsules was labelled with the fluorophore, Nile Red and imaged using CLSM (Figure 1.7). [16]

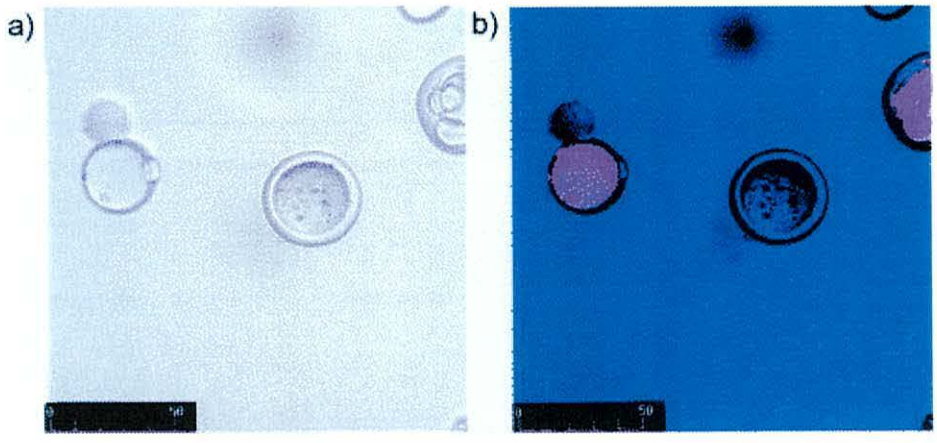

Figure 1.7. Visualization of microcapsules containing a Nile Red stained oil phase by a light microscopy image (a) and by CLSM using the red fluorescence channel and transmitted light detection (b). [16]

In addition to labelling the internal phase, gelatin was labelled with the fluorophore, fluorescein isothiocyanate and gum arabic was labelled with the fluorophore, rhodamine B isothiocyanate. Upon CLSM imaging the fluorescently labelled microcapsules, a visualisation of the polymer distribution throughout the capsule wall was possible which allowed detection of an inhomogeneous distribution of the capsule wall polymers. [16]

1.4. Melamine-Formaldehyde

Melamine-formaldehyde (a thermosetting polymer) is an amine containing resin formed by reacting melamine and formaldehyde together under a range of different experimental conditions. Melamine-formaldehyde polymers account for approximately 20 % of industrially produced amine resins with the remainder largely comprised of urea-formaldehyde polymers. Other aldehydes and other amines may be used to make amino resins but are less frequently used. [18] The principal attraction of amino resins are water solubility before curing, which enables easy application to substrate materials and their transparency which allows combinations with dyes and pigments, solvent resistance in the cured state, hardness and abrasion resistance, and heat resistance. The limitations of these resins include release of formaldehyde upon polymer curing and in some cases after cure. Other limitations of amine resins may be resin specific; for example, urea-formaldehyde resins are easily weathered when used for outdoor applications, in comparison to the more robust melamine-formaldehyde.

The procedure for producing melamine-formaldehyde resin was first patented in 1936 and thereafter these resins then became commercially important, rapidly replacing earlier urea resins mainly due to their greater stability towards chemical attack once the resin had been cured to the insoluble cross-linked state. [19] Since then, amine resins have been used commercially for a wide variety of products, however their use as adhesives represents the largest single market particularly for plywood, chipboard and sawdust board. Alternative applications involve modifying the properties of other materials; for example, small amounts of amine resin are added to textile fabrics to increase durability of clothing. [18] In a second example, the material; Dacron (Du Pont) polyester, which forms the sails of racing boats is modified using amino resins to increase the wind resistance of the sail. [20]

Other applications are as follows: in the automotive industry, tyres are strengthened by amine resins which improves the adhesion of rubber to the tyre cord and further uses of amine resins in the form of molding compounds are used for parts of electrical devices, bottle and jar caps, and molded plastic dinnerware. [18]

Resin Formation

The initial step in the formation of amine resins is the addition of the amino containing compound to formaldehyde. Formalin, an aqueous solution of formaldehyde (37 % by volume) is often used as the formaldehyde source. Upon solvation, formaldehyde readily coverts from its monomeric form to a mixture of several oligomers. Consequently, aqueous solutions contain less than 0.1 % of formaldehyde in monomeric form. The five most common oligomers groups in formalin are as follows: methylene glycol ($CH_2(OH)_2$), polyoxymethylene glycol ($H(CH_2O)_nOH$ ($2<n<100$)), formaldehyde hemiformal (H-O-CH_2-O-CH_3), polyoxymethylene hemiformal (H-O-$(CH_2$-O$)_m$-OCH_3) ($2<m<80$)) and trioxane ($(CH_2O)_3$). The dominant species in formalin is methylene glycol (Figure 1.8) formed in equilibrium by the addition of the nucleophilic oxygen atom in water to the carbonyl carbon in formaldehyde. [21]

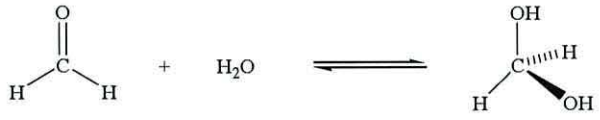

Figure 1.8. Formation of methylene glycol in formalin. [21]

Addition of the amino group to formaldehyde occurs under either neutral or alkaline conditions. This step is known as methylolation or hydroxymethylation, since it is the hydroxymethyl species being introduced into the structure.

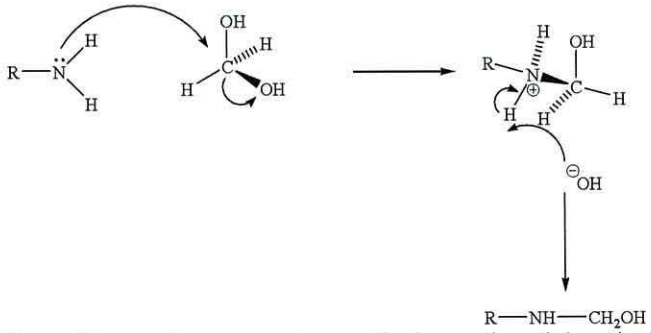

Figure 1.9. Addition of an amino group to methylene glycol (methylolation). [21]

The amino precursor compounds commonly used for making amino resins, such as urea and melamine contain two and three amine groups respectively, *i.e.* they are multi-functional and thus react with formaldehyde to form mixed methylol oligomers. In Figure 1.10 two oligomers (from a possible six) of methylolmelamine oligomers formed from the process of methylolation of melamine where there is one triazine core molecule, are shown.

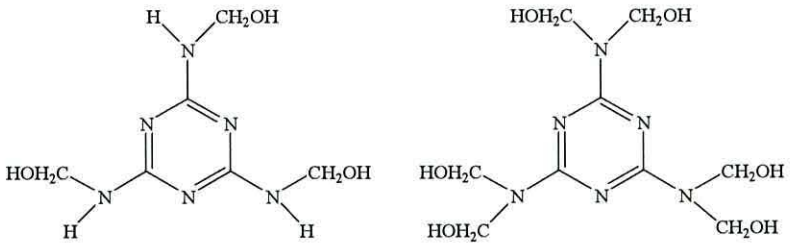

Figure 1.10. Examples of 50 % and 100 % converted methylolmelamine oligomers.

The second step of resin formation involves condensation reactions that occur under acidic conditions; that is, the linking together of the various oligomer units to form dimers, trimers, etc, then a polymer chain and eventually a vast crosslinked polymer network. For example, two methylol groups may condense to form a dimethylene ether linkage with the liberation of a molecule of water. [22]

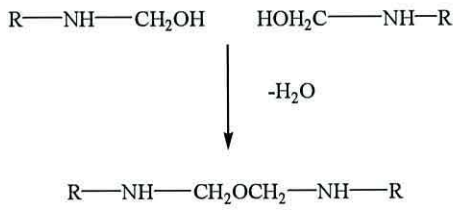

Figure 1.11. Self condensation of methylolamine structures forming an ether linkage. [22]

It has been reported that formation of such ether linkages can also liberate formaldehyde in the process. [23] An example follows. The polycondensation steps in melamine-formaldehyde type resin formation were investigated using the two model compounds; 2-amino-4,6-diphenoxy-s-triazine (A) and 2-amino-4,6-diphenyl- s- triazine (B) (Figure 1.12).

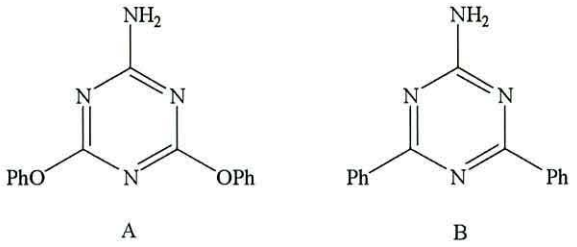

Figure 1.12. Model compounds; 2-amino-4,6-diphenoxy-s-triazine (A), 2-amino-4,6 diphenyl- s- triazine (B). [23]

In this study, for simplicity, both compounds were chosen with only one parent amine group compared to the trifunctional melamine molecule. The compounds were methylolated in separate reactions by dissolving each compound and a two molar equivalent of formalin in DMF which contained triethylamine (1.5 % by volume). The reaction mixtures were heated to 333 K for 4-5 h, yielding a product mixture of mono-methylolated and di-methylolated substituted triazines as well as starting material.

It was shown that self condensation of the mono-methylolated substituted triazines gave equal amounts of an ether bridged dimer and parent amine compound. Formaldehyde analysis (using a sodium bisulphite spot test) at this point gave inconsistent results. Also, subsequent formaldehyde analysis on the self condensation products of the di-methylolated substituted triazines indicated similar inconsistency. This was explained when it was realised that upon prolonged heating of the self condensation products, all products were converted to methylene bridged dimers with further loss of formaldehyde. It was concluded that a secondary reaction between the evolved formaldehyde and parent amine was taking place, regenerating the methylolated compounds as well as generation of the methylene bridge dimer.

In Figure 1.13, the proposed regeneration step leading to a repeating methylolation cycle is shown and in Figure 1.14 the mechanism for methylene bridge formation is shown. The mechanism for methylene bridge formation is thought to occur firstly with protonation of the methylol group in the acidic environment and loss of a water molecule (1) leaving the intermediate carbonium ion (2). This equilibrium mixture then reacts with an amino group to form a methylene link (3). The formation of this type of linkage is thought to be

favoured by a low pH, a relatively low formaldehyde to melamine ratio and a relatively high temperature during the final cure stage. [22]

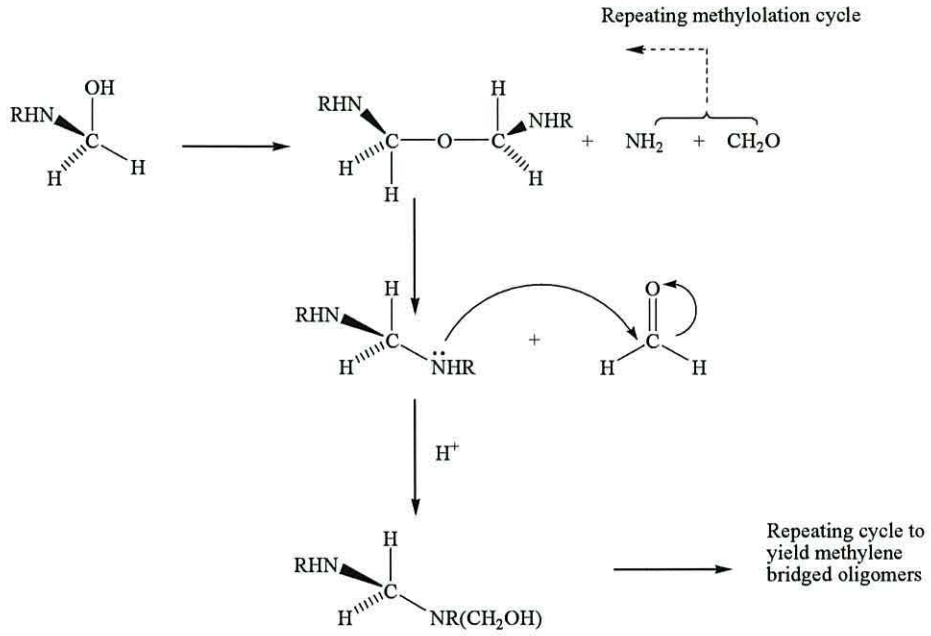

Figure 1.13. Repeating methylolation cycle. [23]

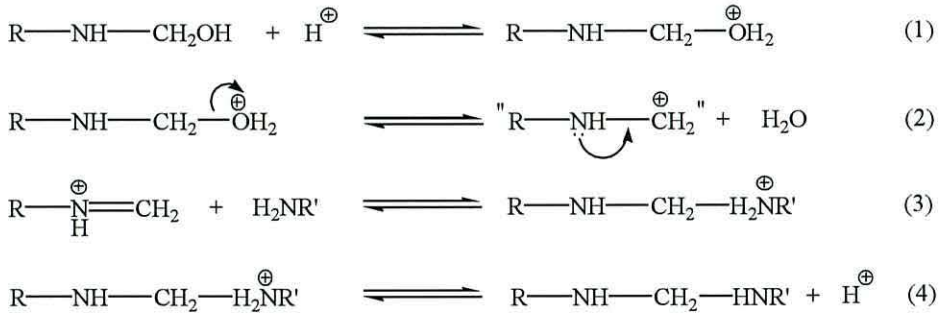

Figure 1.14. Mechanism of the condensation reaction (step 2) in amino resin formation.[22]

Therefore, the final mechanistic step is usually referred to as methylene bridge formation (or alternatively referred to as polymerization, resinification, or simply cure). Heating is normally required to cure the resin to the solid cross-linked state. Successful formation of an amino resin largely depends on the precise control of both methylolation and

condensation stages of the reaction; *i.e.* mole ratio of reactants, pH of reaction mixture, reaction time, temperature.

Clearly, melamine-formaldehyde resins are complex mixtures of melamine oligomers with different degrees of hydroxymethylolation and alkylation. [22] In commercial methylated formulations, these are defined by the general formula, MF_xMe_y; where M represents the melamine ring, F represents the formaldehyde unit on the three primary amino groups and Me represents the end-capping methyl groups.

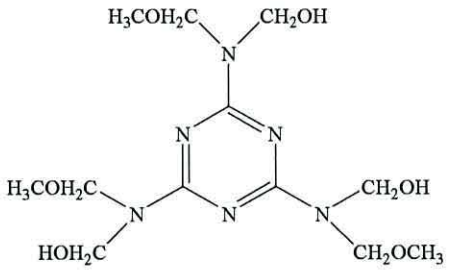

Figure 1.15. Example of a melamine resin; $MelamineFormaldehyde_{3.2}Methyl_{1.6}$ [24]

The mole ratios are determined by NMR analysis and titrimetric analysis of formaldehyde. Such information provides only a general profile of melamine resins without the necessary detail about individual components. The bulk properties of amino resins are influenced by a combination of chemical structure, morphology, orientation and chain dynamics. [22] Given the complex nature of these formulations, attempts at gaining an understanding of the relation between the structure on a molecular level and macroscopic behaviour of these resins prove difficult. Attempts have been made to quantify ratios of the individual components within these complex resins as a starting point for improving the bulk properties. For example, analytical techniques such as preparative HPLC has been used to separate and collect major components which have then been characterised using ^{13}C NMR. [25] In a separate investigation, major peak assignments of FAB/MS data have been compared with the HPLC profile of melamine formaldehyde resins but with a limited degree of success. [26] However, the combination of liquid chromatography and mass spectrometry (LC/MS) has been successfully used to separate and identify the individual components in various melamine formaldehyde resins. [27] Urea-formaldehyde and melamine-formaldehyde have been used extensively throughout the chemical industry as

coatings. The inherent properties of melamine-formaldehyde resin in its uncured state (water solubility) and in its cured state (good water resistance, thermostability and chemical resistance) indicate the resin to be a suitable candidate for use in phase separated *in situ* microencapsulation techniques as the polymer wall, a subject of this thesis.

1.5. Catalysis

A catalyst can be defined as "a substance that increases the rate of attainment of chemical equilibrium without itself undergoing chemical change". [28] A good catalyst must possess both high activity and long-term stability. Catalytic activity can be measured in terms of turnover frequency or turnover number. The turnover frequency (TOF) is simply the number of times *n* that the overall catalytic reaction in question takes place per catalytic site per unit time for a fixed set of reaction conditions (temperature, pressure or concentration, reaction ratio, extent of reaction).

Either:

$$TOF = \frac{number\ of\ molecules\ of\ a\ given\ product}{(number\ of\ active\ sites) \cdot (time)}$$

or,

$$TOF = (\frac{1}{S}) \cdot (\frac{dn}{dt})$$

(where S is the number of active sites).

When the number of active sites is known, as is often the case with homogeneously catalysed reactions, the turnover frequency can be specified quantitatively. High catalytic activity is characteristic of a good catalyst but selectivity, which reflects its ability to direct conversion of the reactant(s) along one specific pathway is also crucial in modern industrial processes. [28] Figure 1.16 shows an example of the subtleties involved in the phenomenon of catalysis; *i.e.* how diverse products can be obtained from the same starting material by selecting the appropriate catalyst.

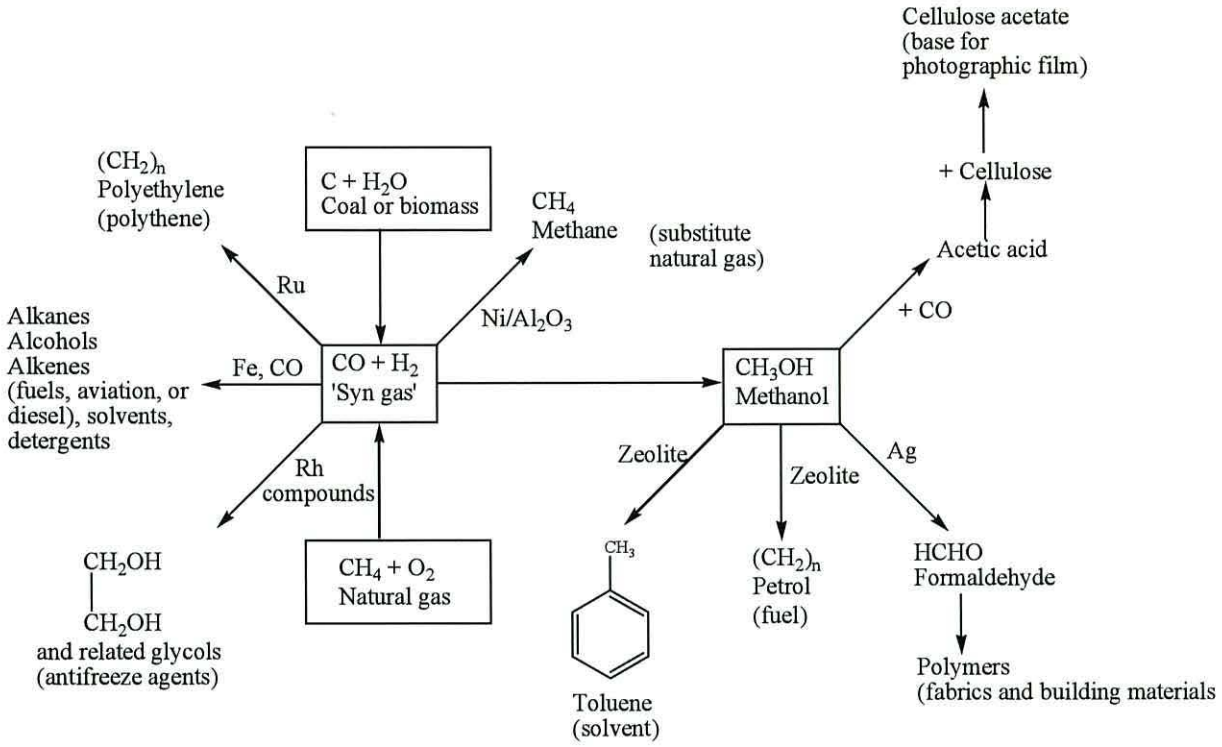

Figure 1.16. The importance of the catalyst in reactions of a common precursor: a wide diversity of products can be generated from 'syn-gas', using the appropriate catalyst, as shown. [28]

More than 90 % of the chemical manufacturing processes in use throughout the world use catalysts in one form or the other, generating a wide range of products that benefit society as a whole. Products considered essential such as food, medicine, materials and fuel are all generated using catalytic processes. [28] Industrial catalytic processes are essential for economic growth. In 1992, an article in Chemistry in Britain appeared stating that the value of catalysts installed world-wide per year was estimated to be about £2300 m and the value of products produced by using catalytic routes was three orders of magnitude higher. [29] One example of an important industrial catalytic process is the production of ammonia. Current world production of ammonia, required principally as an agricultural fertilizer, is *ca.* 140 million tons per annum. This figure is increasing at *ca.* 3% per annum due to the increasing need to feed mankind. [28] Hence, the science and technology of catalysis are of central practical importance. Current industrial catalytic processes use mainly heterogeneous catalysts, *i.e.* different phase catalysis rather than homogeneous catalysts

(same phase catalysis). This is widely due to the relative ease of catalyst separation from final product. [30] However, homogeneous catalysts are used industrially for manufacturing "high cost" fine chemicals such as pharmaceuticals and perfumes and they are now making inroads into the bulk manufacturing sector.

Homogeneous Catalysis

Homogeneous catalysis takes place when the catalyst is in the same phase as substrate, *i.e.* liquid phase. Homogeneous catalysts are normally organometallic complexes comprised of a metal centre surrounded by a number of ligands. Spectator ligands (*i.e.* ligands which are coordinated to the metal but are not directly involved in the reaction) can be fine tuned accordingly in order to tailor catalytic properties. Similar alteration of the catalytic properties can occur by exploitation of different metal (and ligand) oxidation states. This enables a wider range of catalyst activity and selectivity to be achieved. Chiral centres can be easily introduced into ligands producing the plethora of chiral ligands available for asymmetric synthesis. [31]

In most homogeneous catalytic processes, the active catalytic species is not the organometallic complex initially used, but a derivative of (or several derivatives of) this species. Therefore, since the initial organometallic complex doesn't normally occur within the catalytic cycle, it is often labelled a 'precatalyst'. Thus, to become the active catalytic species, the precatalyst often loses a ligand or changes oxidation state before it becomes the active catalyst. For example, the catalyst precursor $RhCl(PPh_3)_3$ (Wilkinson's catalyst) is used in the hydrogenation of alkenes. [32] Although this rhodium complex (precatalyst) is already coordinatively unsaturated (Rh (I), d^8, 16 electrons), it does not partake in the hydrogenation of alkenes in this form. Instead, it first looses a phosphine ligand to form the 14 electron complex $RhCl(PPh_3)_2$ (perhaps with solvent loosely attached) which is one of the kinetically active species occurring within the catalytic cycle. The mechanism of hydrogenation of alkenes by this catalyst has been studied in detail and it is found that oxidative addition of H_2 onto the precursor is the rate limiting step, followed by fast reductive elimination of the alkane and regeneration of the active catalyst. In addition to the catalytic cycle, several other equilibria are operating, complicating the system (Figure 1.17).

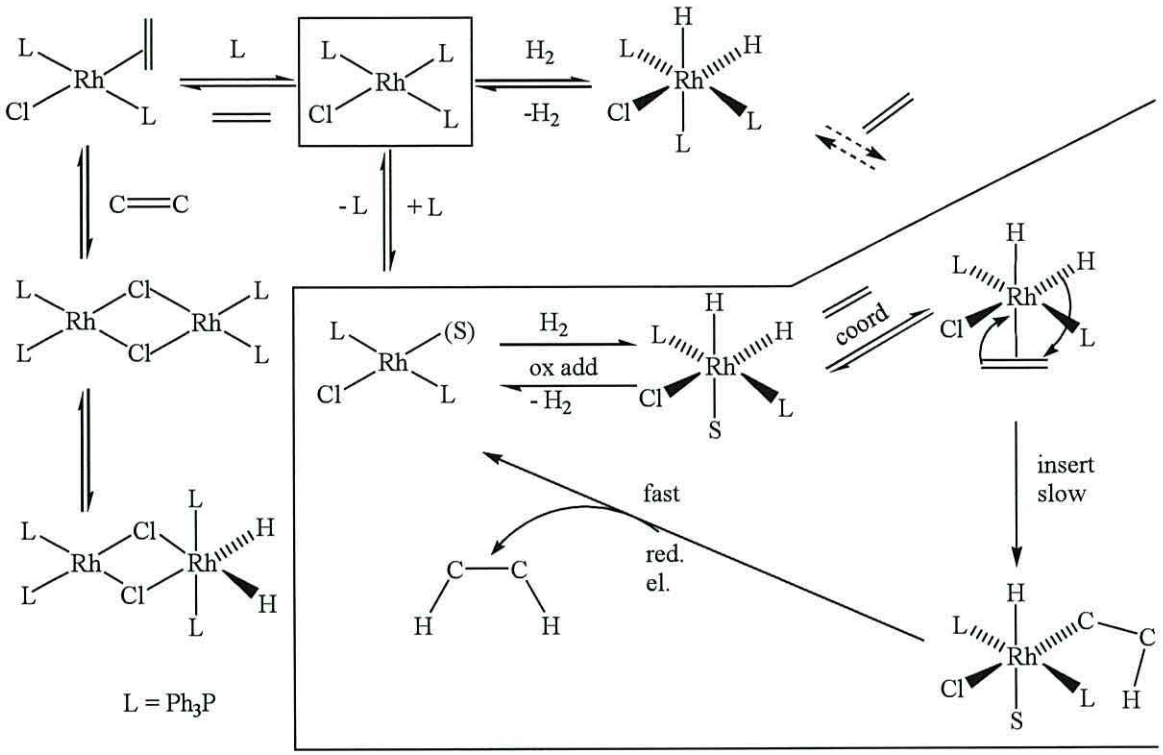

Figure 1.17. Standard mechanism for the reduction of alkenes by Wilkinson's catalyst.[32]

Homogeneous catalysts are generally more selective than their heterogeneous counterparts and lower catalyst loading is often used in homogeneous catalytic reactions since these catalysts possess higher specific activity for substrate conversion. However, homogeneous catalysts are not used as widely industrially as heterogeneous catalysts because of inherent problems. Common disadvantages of homogeneous catalysis along with low catalytic lifetimes and easy deactivation of catalyst are: (i) air-sensitivity, (ii) toxicity, and (iii) separation and recovery problems. The aforementioned Wilkinson's catalyst is an example of an air sensitive homogeneous catalyst; in solution this catalyst was found to catalyse the oxidation of triphenylphosphine, which in turn leads to the destruction of the complex, therefore air cannot be tolerated when using this catalyst. [32] Osmium tetroxide (OsO_4) is an example of a toxic homogeneous catalyst. See section 1.6 for a more detailed discussion about the toxicity of this catalyst.

Catalyst separation and recovery from products is a key challenge in homogeneous catalysis for commercial processes. [33] For many of these catalysts, the separation process is

often complicated by the air and thermal sensitivity associated with them. Traditional separation techniques, for example; product distillation, liquid-liquid solvent extraction, crystallization of the product, and flash chromatography have all been employed to separate homogeneous catalysts from the product but such techniques centre on the importance of product recovery rather than catalyst recovery and re-use. Using such techniques, further processing of the catalyst is required and such methods may deactivate particular sensitive catalysts. Several other methods have been investigated as possible contenders for solving the separation and recovery problems associated with homogeneous catalysts. For example, fluorous biphasic catalysis is one avenue that has been explored in great detail. One recent example of fluorous biphasic catalysis is the use of perfluoroalkyl-substituted bisoxazolines as chiral ligands in the aldol addition of silylketene thioacetals to methylpyruvate promoted by Cu(OTf). [34] Good enantiomeric excess (ee) was achieved using this reaction (85 %) and the recovery and recycling of the ligands were achieved by phase separation of the reaction solvents or by filtration through a short plug of fluorous silica gel.

The use of supercritical fluids in catalysis has also been investigated for the separation and recovery of homogeneous catalysts. [35] The continuous flow hydroformylation of 1-octene was catalysed by the complex, Rh/[RMIM][$Ph_2PC_6H_4SO_3$] (where R=1-propyl, 1-pentyl or 1-octyl) when only dissolved in the steady state reaction mixture and using supercritical carbon dioxide ($scCO_2$) as a transport vector for both substrates and products. The turnover numbers were relatively poor: 160-240 catalyst turnovers h^{-1}. Low rhodium leaching was reported over a 12 h period at a total pressure of 125-140 bar. Alternatively, homogeneous catalysts supported onto inert surfaces such as crystalline solids, silica and various inert polymers have been developed to enable recovery of catalyst. Extensive research has been devoted to homogeneous transition-metal reagents attached to such supports. The resulting species have been described in a variety of ways; immobilised, supported, hybrid and anchored. [36] Catalyst immobilization using polymeric supports should not be confused with microencapsulating catalysts using polymers. Microencapsulating a catalyst involves complete envelopment of the catalyst, therefore offering protection along with immobilization. Whereas immobilizing a catalyst using an

inert polymeric support, in most cases involves the displacement of a ligand attached to the metal centre by a pre-immobilized ligand.

For example, the catalyst precursor organometallic reagent; tris(triphenylphosphine)dichlororuthenium (II) $[RuCl_2(PPh_3)_3]$ was immobilized by agitating a dichloromethane solution of catalyst with resin (polystyrene cross-linked with 2% divinylbenzene; 3 mmol P/g resin) - bound triphenylphosphine overnight on a mechanical shaker. [37] Filtration, washing and drying of polymer gives a black powder characterised as resin-bound $[RuCl_2(PPh_3)_2(PPh_3)]$ (Figure 1.18).

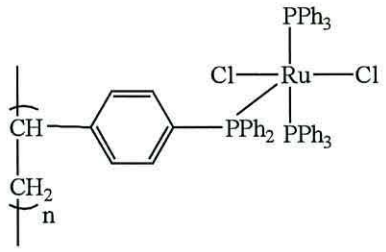

Figure 1.18. Resin-bound (polystyrene cross-linked with 2% divinylbenzene; 3 mmol P/g resin) $[RuCl_2(PPh_3)_2(PPh_3)]$. [37,38]

The development of polymer-bound metal catalysts is expected also to reduce metal toxicity and air sensitivity as well as to increase ease of separation of catalyst from product. For the polymer-bound catalyst to be successful, it must display comparable activity and selectivity with its homogeneous counterpart. Hypothetically, immobilized catalysts should combine the advantages of soluble catalysts, *i.e.* homogeneous reaction sites, utilization of all metal atoms, fast reaction rates and high selectivity with advantages of heterogeneous catalysts, facile separation of products from catalyst as well as recovery and reuse of the expensive catalyst. It is thought that, in some respects, immobilized catalysts should be superior to their soluble analogues by allowing highly unsaturated catalyst centres to be stabilized from aggregation or possibly used with a solvent in which the homogeneous catalyst is insoluble.

To date, most immobilized catalysts display either comparable or reduced activity. For example, the polymer-bound ruthenium catalyst $[RuCl_2(PPh_3)_2(PPh_3)]$ previously discussed was tested with a wide range of substrates in the oxidation reaction of

unsaturated hydrocarbons and transfer hydrogenation of ketones showed activity levels comparable with soluble analogues. [37] Characterization of supported catalysts is usually achieved using elemental analysis and comparison of spectroscopic data with that of the soluble analogue. Immobilized homogeneous catalysts have been shown to be separated from solution thus offering an advantage over traditional homogeneous catalysts. Therefore, immobilized catalysts have been used in a wide range of reactions including hydrogenation, [39] hydrosilylation, [40] and polymerization. [41]

In another example, the arene ruthenium dimer [Ru(*p*-cymene)Cl_2] was supported onto a resin bound (polystyrene cross-linked with 2% divinylbenzene; 3 mmol P/g resin) phosphine (triphenylphosphine derivative) and has been shown to be active in the reaction of phenylacetylene with formic acid. The catalyst was recycled five times without loss of activity and spectroscopic studies indicate that no leaching takes place during catalytic reaction. [42] Thus, it is clear that for a polymer-supported metal catalyst to be viable for industrial application it should possess the following attributes: high activity, high selectivity and, the metal must not leach off the support during the reaction. In summary, many attempts have been made to overcome the problems of separation and recovery in homogeneous catalysts with varying success. Therefore, a significant niche still exists in both academia and industry for the design of a generic "protection, release and recovery system" to benefit the problems associated with homogeneous catalysis. The subject of this thesis is the microencapsulation of homogeneous catalysts, *i.e.* organometallic complexes, organics etc, thereafter, collectively known in this thesis as target molecules. Therefore, existing literature containing such material has been surveyed in section 1.6.

1.6. Microencapsulation of Targets

Preparation of solid core microcapsules

Scandium trifluoromethanesulfonate ($Sc(OTf)_3$) is a water-compatible Lewis acid which has been used to catalyze the industrially important Friedel Crafts alkylation and acylation reactions. Its chemistry has recently been reviewed by Kobayashi. [43] Lewis acid catalysed reactions are of interest due to unique reactivities and selectivities that can be achieved under mild reaction conditions. However, despite the obvious success, these catalysts still

possess problems inherent to homogeneous catalysts; poor separation and recovery. "Polymer supported catalysts" are now well-recognised as alternatives to homogeneous catalysts (as previously discussed in section 1.5) offering ease of workup and separation of products and catalysts. [44] An extensive literature on this subject exists, which is beyond the scope of this thesis but generally, such catalysts are immobilized on polymers by coordinate or covalent bonds. Polymer supported catalysts made using coordinate bonds often possess low stability, and those made using covalent bonds often have a lower activity than their monomeric counterpart.

Therefore, a new type of catalyst immobilization has been sought. $Sc(OTf)_3$ has been "microencapsulated" using polystyrene as the polymer wall. [45] Such microcapsules contain a mixed solid core of $Sc(OTf)_3$ catalyst and polystyrene and differ to the type of microcapsules studied in this thesis, which contain a liquid internal phase that is contained within a solid polymeric capsule shell. Microencapsulated $Sc(OTf)_3$ differs from traditional polymer supported catalysts in that the microencapsulated catalyst is physically enveloped by polystyrene thin films and stabilised by the interactions between π electrons in the benzene rings of the polystyrene and vacant orbitals of the $Sc(OTf)_3$ (Figure 1.19).

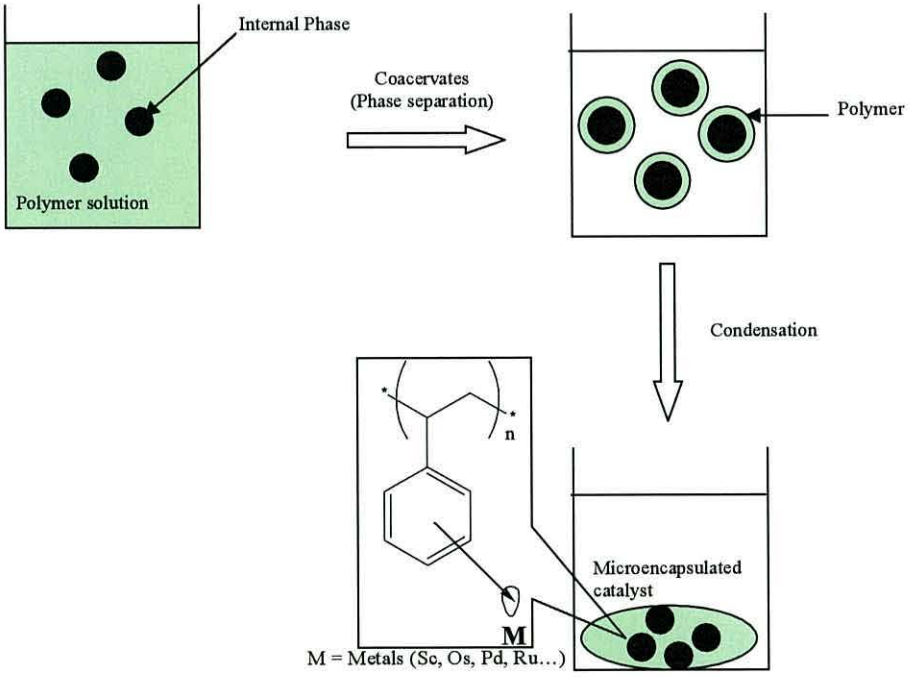

Figure 1.19. Microencapsulation of $Sc(OTf)_3$ [46]

Experiments conducted to prove π-interactions are present between the metal and the phenyl group have been carried out using polybutadiene and polyethylene as separate polymers for encapsulation of $Sc(OTf)_3$. Taking "100 % encapsulation" as the baseline, *i.e.* the amount of $Sc(OTf)_3$ catalyst which is encapsulated using polystyrene, it was shown that only 43 % was encapsulated using polybutadiene, whereas no $Sc(OTf)_3$ was trapped in the microcapsules prepared using polyethylene core. The interactions were further verified using ^{45}Sc NMR measurements on monomeric $Sc(OTf)_3$ catalyst, microencapsulated catalyst and $Sc(OTf)_3$ catalyst mixed with a model compound, 1,3,5-triphenylpentane, which was used as a polystyrene analogue in the investigation of effect of benzene rings upon the catalyst (Table 1.2).

Table 1.2. NMR experiments [a]

Sample	**^{45} Sc NMR peak shift data/δ**
$Sc(OTf)_3$	- 182.2
$Sc(OTf)_3$ + 1,3,5-triphenylpentane	- 168.4
Microencapsulated $Sc(OTf)_3$	- 163.9

[a] $ScCl_3$ was used as an external standard (δ=0) in CD_3CN

The data presented in Table 1.2 shows that in the presence of benzene rings, ^{45} Sc NMR signals are shifted downfield compared to monomeric $Sc(OTf)_3$, thus demonstrating that immobilization is from the interaction between $Sc(OTf)_3$ and the benzene rings in polystyrene. The microencapsulation procedure begins with dissolving polystyrene (MW 280,000) in cyclohexane at 323-333 K, followed by addition of powdered $Sc(OTf)_3$ as the internal phase. The resulting dispersion is stirred at this temperature for approximately 1 h, then slowly cooled to 273 K whereupon "coacervates" deposit onto the solid $Sc(OTf)_3$ particles, forming microcapsules (Figure 1.19). The soft polystyrene wall is hardened using hexane and the whole mixture is then stirred at room temperature for approximately 1 h. The microcapsules are subsequently washed with acetonitrile and dried at 323 K. Approximately 60 % of the $Sc(OTf)_3$ catalyst was encapsulated.

The resulting "microcapsules" were tested in catalytic reactions (imino aldol, aza Diels-Alder, cyanantion, and allylation, reactions) using aldimines as substrates. Figure

1.20 shows the imino aldol reaction chosen for testing the catalytic activity of the microcapsules using the aldimine, *N*-benzylideneaniline.

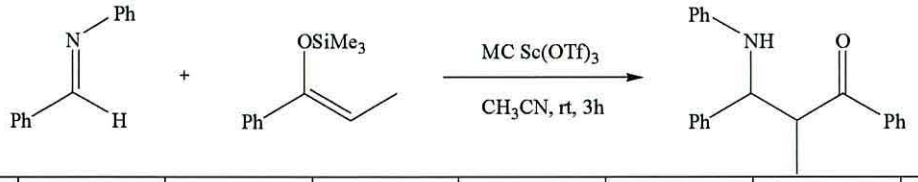

Run [a]	1	2	3	4	5	6	7
Yield (%)	90	90	88	89	89	88	90

[a] Recovered catalyst was used successfully (Use 2,3,4...)

Figure 1.20. Imino aldol reaction scheme showing re-use of MC $Sc(OTf)_3$ catalyst. [45]

All reactions were carried out on a 0.5 mmol reactant scale using approximately 0.12 g (0.2 mmols) of $Sc(OTf)_3$ catalyst. Kinetic studies revealed that the activating ability of PS-MC $Sc(OTf)_3$ for aldimines was superior to that of free $Sc(OTf)_3$, which as a Lewis acid is well known to be trapped and often deactivated by basic aldimines. However, it is stated that the origin of the high activity of PS-MC $Sc(OTf)_3$ is not clear at this stage. In later tests, the microcapsules were recycled three times successfully in three component reactions such as Mannich-type, Strecker and quinoline-forming reactions. PS-MC $Sc(OTf)_3$ were also tested in Friedel-Crafts alkylation and acylation reactions. Friedel-Crafts alkylation reactions normally proceed in the presence of a Lewis acid but acylation reactions generally require more than a stoichiometric amount of Lewis acid due to consumption of the Lewis acid by coordination of the products, aromatic ketones. When used in Friedel-Crafts acylation reactions, the microencapsulated $Sc(OTf)_3$ displayed high activity with the added advantage of recovery and re-use of the microcapsule without loss of activity. The reactions were carried out on a 0.5 mmol reactant scale using approximately 0.12 g (0.2 mmol) of $Sc(OTf)_3$ catalyst. An example is shown in Figure 1.21.

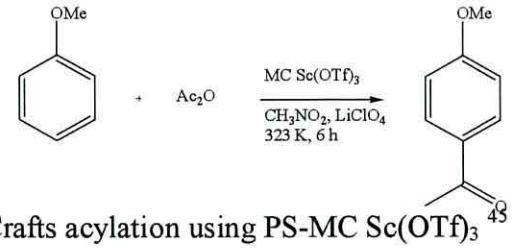

Figure 1.21. Friedel-Crafts acylation using PS-MC $Sc(OTf)_3$ [45]

The successful formation of $Sc(OTf)_3$ microcapsules led to the microencapsulation of a series of platinum group metal complexes containing (Os, Pd, Ru) using similar techniques. This work has been reviewed. [46] As an example, osmium tetroxide (OsO_4) which is a well known oxidation catalyst used to catalyze dihydroxylation reactions of olefins, such as that shown in Figure 1.22 has been encapsulated using polystyrene as polymer wall. [47]

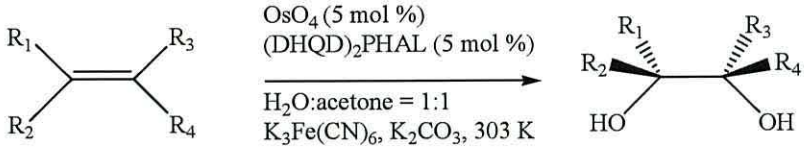

Figure 1.22. Dihydroxylation of an olefin using osmium tetroxide as a catalyst. [47]

Industrial applications using osmium tetroxide have been hampered because it is highly toxic, expensive, volatile and cannot be recovered. Using the technique of microencapsulation similar to that reported for the encapsulation of $Sc(OTf)_3$, it was reported that approximately 90 % of the catalyst was encapsulated within the polystyrene microcapsules (PS-MC OsO_4) by measuring recovered OsO_4. [47] Subsequently, it was used to catalyze a series of achiral olefin dihydroxylation reactions. It was observed that both cyclic and acyclic exo as well as internal olefins were oxidised with PS-MC OsO_4 (5 mol %), *N*-methyl-morpholine (NMO) as cooxidant in H_2O-acetone-CH_3CN (1:1:1) as solvent. The microcapsules were recovered quantitatively by simple filtration methods and re-used five times without loss of activity, thus indicating that no OsO_4 was released from the polymer during or after the reaction. This was initially determined by qualitative analysis of OsO_4 using iodometry on the reaction product which was later confirmed by using microwave induced plasma-mass spectrometry (MIP-MS).

Thus the polystyrene microcapsules containing osmium tetroxide were the first microcapsules to be used in achiral dihydroxylation reactions where complete recovery and re-use of osmium is achieved. Interestingly when kinetic studies were carried out on the achiral dihydroxylation of cyclohexene the results showed that the reaction proceeded slightly faster using the monomeric catalyst as would be expected than using the microencapsulated version but the difference was not truly significant. After 3 h, an 81 % yield of the diol was obtained using OsO_4 while a 75 % yield was obtained using

microencapsulated OsO_4 under the same reaction conditions. The polymer host used for encapsulation was later changed from polystyrene to the more polar polymer, acryronitrile-butadiene-styrene (ABS). [48] ABS microencapsulated OsO_4 (ABS-MC OsO_4) was made using a similar procedure to PS-MC OsO_4; ABS polymer was dissolved into tetrahydrofuran at 343-353 K and OsO_4 was added to this solution. The mixture was stirred at this temperature for 1 h, then cooled to 273 K whereupon "coacervates" deposit onto the solid OsO_4. Methanol was added to harden the microcapsules and after 8 h the microcapsules were washed with methanol and dried for 24 h at room temperature. Using this procedure, approximately 90 % of OsO_4 was reported to be encapsulated by measuring unencapsulated catalyst. A series of achiral dihydroxylation reactions were first examined using the modified microcapsules to check catalyst activity. Dihydroxylation of styrene was treated with NMO in H_2O-acteone-acetonitrile using the modified osmium microcapsules. After filtration, the corresponding diol was obtained in 93 % yield and ABS-MC OsO_4 was recovered quantitatively. The recovered catalyst was used in the second, third, and fourth runs, and no loss of activity was observed (93, 90, 87, and 89 % yields, respectively, and ABS-MC OsO_4 was recovered quantitatively in all cases). Similarly, various olefins tested including cyclic and acyclic, terminal, mono-, di-, tri-, and tetra-substituted olefins gave the corresponding diols in high yields, and the microcapsules were also recovered quantitatively and successfully re-used in these reactions.

Because the microcapsules proved highly active in achiral dihydroxylations, the catalyst containing microcapsules (ABS-MC OsO_4) were tested in an asymmetric dihydroxylation reaction. Using the Sharpless procedure, *trans*-methylstyrene was chosen as substrate, and 1,4,-bis(9-O-dihydroquinidinyl)phthalazine ($(DHQD)_2PHAL$) was chosen as the chiral ligand. The olefin was slowly added over 24 h to the mixture of ABS-MC OsO_4, $(DHQD)_2PHAL$ (5 mol % each) and NMO, the desired diol was obtained in 88 % yield with 84 % enantiomeric excess (ee). (See Figure 1.23 and Table 1.3).

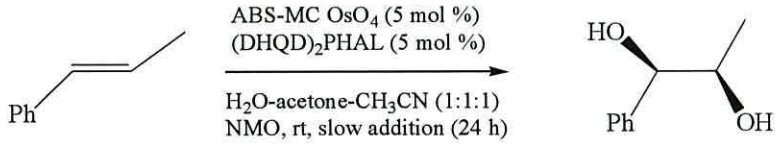

Figure 1.23. Asymmetric dihydroxylation reaction using ABS-MC OSO_4.

Table 1.3. Re-use of ABS-MC OsO_4 in the asymmetric dihydroxylation of *trans*-methylstyrene. [48]

Run	Yield (%)	Ee (%)	Recovery [a,b]
1	88	84	100 %
2	75	95	100 %
3	97	94	100 %
4	81	96	100 %
5	88	95	100 %

[a] Recovery of ABS-MC OsO4. [b] Recovery of $(DHQD)_2PHAL$ > 95 %

The microencapsulated osmium catalyst was recovered quantitatively by simple filtration and the chiral ligand was also recovered by simple acid/base extraction. Table 1.3 shows that both recovered catalyst and chiral source were re-used several times and no loss of activity was found after the fifth use. Asymmetric dihydroxylation using ABS-MC OsO_4 was extended to other olefin substrates using similar reaction conditions and in most cases the yield and selectivities obtained were reported as being comparable to those obtained using monomeric OsO_4. ABS-MC OsO_4 was also tested for activity in the two phase asymmetric dihydroxylation of styrene where the solvent mixture was changed from H_2O-acetone-acetonitrile to H_2O- *t*-BuOH and the cooxidation reagent was changed from NMO to $K_3Fe(CN)_6$. Under these conditions the yield and ee were both 84 % but the recovery of the microcapsules was found to be reduced. ^1H NMR spectra of the ABS – MC OsO_4 using swollen resin magic angle spectroscopy (SR-MAS) indicated that the olefin (derived from the butadiene monomer) reacts with OsO_4 upon microencapsulation making the polymer more hydrophilic and this partially dissolves in the reaction solvent mixture of H_2O- *t*-BuOH, which accounts for the reduced recovery of microcapsules. Thus the polymer for encapsulation was further modified with the objective to accommodate two phase asymmetric dihyroxylation reaction conditions. The polymer, phenoxyethoxymethyl-polystryene (PEM) (Figure 1.24) was chosen for the encapsulation of OsO_4. [49]

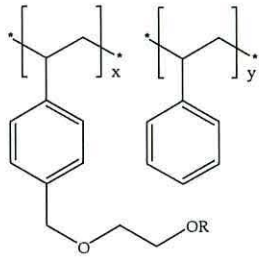

Figure 1.24. Structure of phenoxyethoxymethylpolystryene (PEM). [49]

The resulting microcapsules were tested in the two phase asymmetric oxidation of styrene using $(DHQD)_2PHAL$ as the chiral ligand source. It was found that using $K_3Fe(CN)_6$ as the cooxidant and a solvent mix of H_2O-acetone moderate yields were obtained with good enantiomer excesses and high catalyst recovery. It was confirmed from fluorescence X-ray analysis that no leaching of osmium occurred after the reaction and importantly, it was found that this reaction process does not require the slow addition of olefins. [49]

Subsequently, osmium tetroxide was microencapsulated using an *in situ* interfacial polymerization approach and polyurea microcapsules containing OsO_4 were obtained (Figure 1.25). [50] The polymer wall is initially formed by partial hydrolysis of the isocyanate into amine, which then reacts with the unhydrolysed isocyanate to form polyurea.

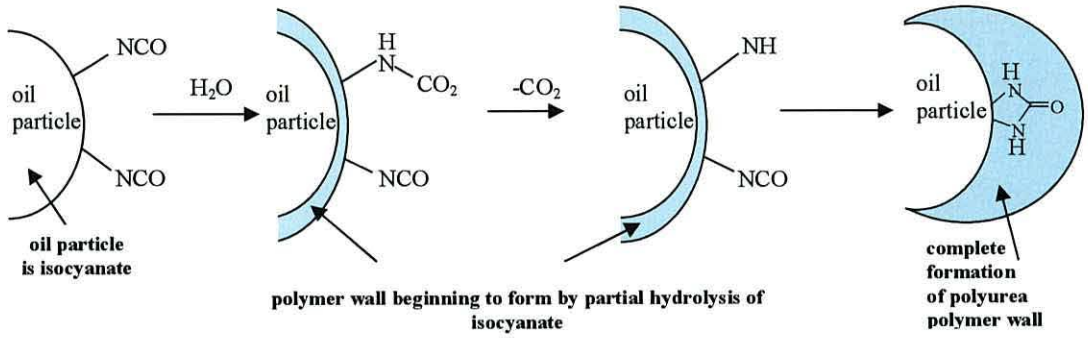

Figure 1.25. Schematic representation of the polyurea wall-forming reaction occurring at the oil-water interface. [50]

Polyurea microcapsules containing OsO_4 were prepared. The microcapsules were filtered and washed with deionised water and a range of organic solvents and dried. The resultant polyurea microcapsules are completely insoluble in aqueous and organic solvents and have proven to be extremely robust without any degradation under normal reaction conditions. It is thought that the urea functionality of the polymer ligates and hence retains the metal species within the polymer matrix. SEM analysis (in backscattered mode) of the microcapsules showed the metal to be distributed within the polyurea matrix.

The catalyst containing microcapsules were used in a series of tests and proved to be effective in the dihydroxylation of a range of olefins at room temperature using 5 mol %

of the polyurea catalyst in a 10:1 acetone-H_2O solvent system with NMO as cooxidant. Recovery and re-use of the microcapsules was possible. In five cycles no significant loss in activity was observed. Qualitative leach tests were carried out by stirring the microcapsules in solution for 24 h. No catalytic reaction occurred using the solution therefore it was reported that no significant leaching of an active species took place. No sign of cross contamination of the capsules by reagents and products was evident as shown by the analysis of the products. The microcapsules were also used as catalysts in the oxidative cleavage of olefins; treatment of a range of olefins with PEM-MC OsO_4 and $NaIO_4$ in 2:1 THF-H_2O yielded carbonyl compounds in good yields. Again, the microcapsules were easily recovered by a simple filtration and re-used several times. To summarize, these microcapsules have been reported as being effective catalysts that are easy to handle, that their manufacture is cost effective and could be easily scaled up for industrial applications.

In parallel work, the palladium complex, "[$Pd(PPh_3)$]" was first microencapsulated using polystyrene by Kobayashi and coworkers. [51] Solid state phosphorus NMR (^{31}P (SR-MAS) NMR) spectra of the catalyst capsules in $CDCl_3$ showed only one resonance signal at 29.1 ppm. ^{31}P NMR of PPh_3 ($CDCl_3$) = -4.7 ppm, O=PPh_3 ($CDCl_3$) = 55.3, therefore the resonance at 29.1 ppm was attributed to PPh_3 coordinating to the palladium. A catalytic asymmetric allylation reaction was successfully carried out using MC $Pd(PPh_3)$ and a chiral ligand (Figure 1.26).

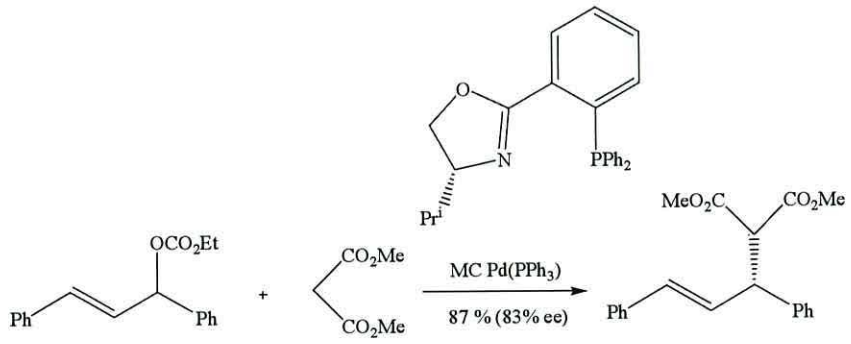

Figure 1.26. Asymmetric allylic substitution, *reagents and conditions*: MC $Pd(PPh_3)$ (20 mol %), chiral ligand (20 mol %), BSA (3.0 equiv.), KOAc (0.10 equiv.), CH_3CN, reflux, 12 h. [51]

The microcapsules were also tested for catalytic activity in the allylation reaction of allyl methyl carbonate with dimethyl phenylmalonate. It was found that when allyl methyl carbonate was combined with dimethyl phenylmalonate in the presence of 20 mol % of the encapsulated catalyst, the reaction did not proceed but upon adding various amounts of external ligand (PPh_3) to the test reactions, product was formed in varying yields. The highest yields were obtained when 20 mol % of the ligand was used. The microencapsulated palladium catalyst was recovered quantitatively and re-used five times with the catalytic activity retained.

Further studies of encapsulation have been carried out: palladium(II)acetate and tetraoctylammonium bromide stabilised nanoparticulate palladium were prepared by Ley and co-workers. Both were separately microencapsulated using polyurea as the polymer wall. [52,53] SEM and TEM analysis of the palladium(II)acetate microcapsules showed that the palladium metal was not bound on the surface but contained and evenly distributed within the polymer matrix and core. TEM analysis of the nanoparticulate palladium(0)microcapsules showed a higher presence of palladium along the channels formed within the polyurea matrix in comparison with the whole microcapsule, suggesting that the palladium nanoparticles were being stabilised and contained by the urea-linked polymer. Stabilization of the palladium nanoparticles using tetraoctylammonium bromide was eliminated as a cause of stabilization because traces of the stabiliser should have been removed by the washing procedures. The resulting palladium(II)acetate microcapsules were tested for catalytic activity in Suzuki type reactions involving the cross coupling of aryl boronic acids with aryl bromides. Reactions were carried out on a 1 mmol scale using 5 mol % of the catalyst (with respect to palladium content) in a solvent mix of toluene-ethanol-water system at 353 K. The various biaryl reaction products were produced in good yields using these reaction conditions. The microcapsules were able to be re-used four times without significant loss in activity.

Inductively coupled plasma (ICP) analysis of the crude product indicated approximately 0.2 % of Pd had leached from the $Pd(OAc)_2$ capsules, *i.e.* very low leaching. When the nanoparticulate palladium(0) microcapsules were tested in the same Suzuki reactions as the palladium(II)acetate microcapsules, they proved to be equally effective. In

a post modification experiment of the palladium(II)acetate polyurea microcapsules, capsules were treated with formic acid, resulting in deposition of Pd (0) in the polyurea support material. [54] The efficiency and stability of the palladium containing microcapsules was examined in a transfer hydrogenation reaction using acetophenone as a substrate. (Previously, homogeneous catalysis has focused upon the use of ruthenium based complexes for catalysing transfer hydrogenation reactions. However, cleaner methods requiring high selectivity, low cost, easy separation and production of minimum waste have been sought). The palladium containing microcapsules, were reported as giving excellent isolated yields through five successive runs. Importantly, no traces of by products from further hydrogenolysis or products from the over-reduction of the aromatic ring were detected in the analysis of the products as is found in alternative transfer hydrogenations using Pd/C. It was found that the encapsulated catalyst was more reactive than Pd/C in an identical study with higher conversion within the same reaction time (Figures 1.27 and 1.28).

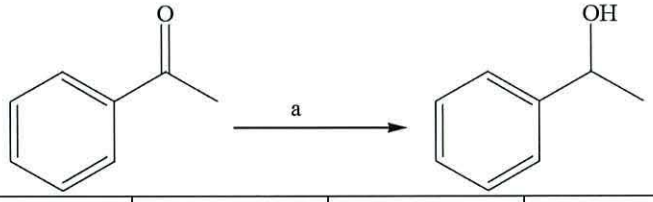

Run	1	2	3	4	5
Yield (%)	99	98	98	97	96
Time/h	21	22	24	26	28

[a] Reagents and conditions: 10 mol % palladium microcapsules, 200 μL EtOAc, 0.8 mmol HCOOH, 0.8 mmol Et_3N, 0.016 mmol acetophenone, 297 K. [54]

Figure 1.27. Recycling experiments [a]

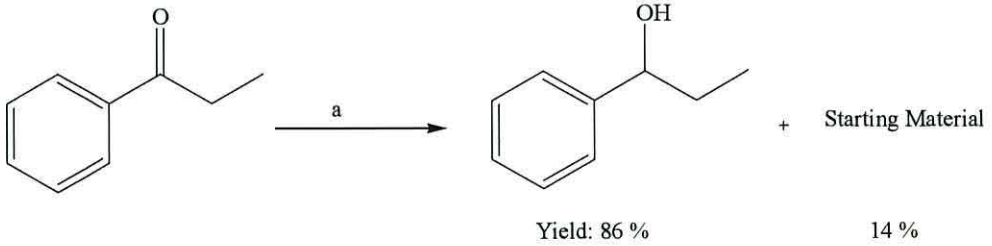

Figure 1.28. (a) Reagents and conditions: 10 mol % Pd/C (10 %), 200 μL EtOAc, 0.8 mmol HCOOH, 0.8 mmol Et_3N, 0.016 mmol propiophenone, 297 K, 22 h. [54]

Palladium on carbon (Pd/C) has also been encapsulated using polyoxyethylene-polypropoxylene (POEPOP). [55] The technique used for encapsulation was 'anionic suspension polymerization' and involved mixing PEG $_{1500}$ macromonomer, Pd/C (10 % by weight), ^{t} BuOK (acting as base) and surfactant into silicone oil at 393 K and left stirring. The resulting beads were washed with a range of organic solvents and water and dried. A series of solution phase hydrogenation reactions were carried out using the encapsulated catalyst which showed the activity to be marginally lower than standard 10 % Pd/C. It was thought that the Pd atoms coordinate to the PEG chain allowing for the microcapsules to be re-used for several times without loss of activity.

The ruthenium 4,5-dihydroimidazo-2-ylidene complex has also been microencapsulated using polystyrene as the polymer wall. [56] The procedure for the encapsulation of the ruthenium carbene catalyst is similar to previously mentioned organometallic complex encapsulations involving polystyrene. SEM analysis of the capsules showed the presence of polystyrene-enveloped microparticles across the polymer surface, and EDAX analysis of the microcapsules indicated the presence of ruthenium, chlorine and phosphorus within the particles. Ruthenium analysis of the microcapsules using ICP-AES showed that 87 % of the catalyst had been "encapsulated". Diene substrates were chosen for test ring closing metathesis reactions using the encapsulated catalyst, for example, *N,N*-diallyltolsylamide. The product isolated yield after column chromatography to remove leached ruthenium from microcapsule was found to be 92 %. The microcapsules were re-used in further test runs, ((2) 71, (3) 52, and (4) 40 %, respectively). The metathesis product was isolated from the small amount of leached ruthenium by column chromatography to give a 92 % isolated yield. The same complex was dispersed in molten paraffin wax to give a homogenous purple liquid. The mixture was then cooled, cut into pieces and stored without protection from air. The "encapsulated" catalyst in wax was used in a series of ring closing metathesis reactions to test catalytic activity. In all reactions, a high percentage yield was obtained and thus it was concluded that the catalyst can be stored in wax for many months without concern for loss of activity. [57]

In separate experiments, the arene-ruthenium complexes; $[Ru(\eta^6\text{-}C_6H_5CO_2Et)(PR_3)Cl_2]$, (where R = Ph, Cy) were encapsulated using polystyrene. [58] The

structure of the polymer supported arene-ruthenium complexes was confirmed by NMR spectroscopic analysis. The ^{31}P swollen resin magic-angle spinning NMR (SR-MAS) spectra showed only one resonance at arising from the phosphine coordinated to the ruthenium (R= Ph, 25.7 ppm; R=Cy, 28.5 ppm) hence, it was concluded that the catalyst was embedded as [(arene)$RuCl_2(PR_3)$]. The resulting microcapsules were used in ring – closing metathesis reactions as follows: firstly, a ruthenium-allyenylidene complex was prepared from the [(arene) $RuCl_2(PR_3)$] which was used in the ring closing metathesis reaction of *N,N*-diallyl-*p*-toluenesulfonamide. The choice of solvent was found to be crucial for reactions using the encapsulated catalyst with the solvent mixture *i*PrOH:hexane (1:1) giving the desired product in good yield, however the activity of the catalyst was significantly decreased when re-used. Reactivation conditions for the recovered catalyst was examined and after varying the reaction conditions, the best results were obtained when a mixture of the recovered catalyst, one equivalent of phosphine, and 1,1,-diphenyl-2-propynol were stirred for 1 h under reflux and, after addition of $NaPF_6$ further stirred for 12 h at room temperature. Resonances observed in the ^{31}P SR-NMR spectrum of the recovered catalyst were consistent with those of the original "encapsulated catalyst". In tandem with the microencapsulation of platinum group metals using polystyrene, the vanadium complex [$VO(acac)_2$] was microencapsulated and tested for activity in epoxidation reactions [59] of allylic alcohols (Figure 1.29)

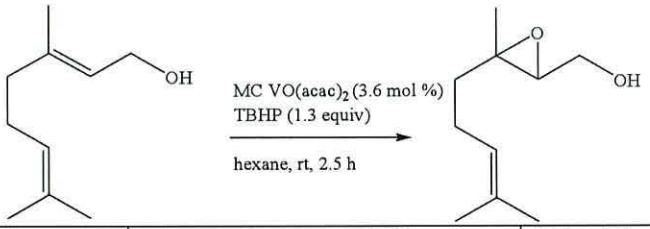

Run	Yield of epoxide (%)	Metal leaching
1	94	0.097 %
2	84	550 mg/L
3	83	275 mg/L
4	81	118 mg/L
5 [a]	5	-

[a] Use of $VO(acac)_2$ (0.1 mol %) in the place of MC -$VO(acac)_2$

Figure 1.29. Re-use of MC -$VO(acac)_2$ in the epoxidation of geraniol and determination of metal leaching [59]

A range of alternative solvents were tested and the highest yield of product was found using hexane. This was reported as being somewhat surprising since hexane is normally a poor solvent for the epoxidation of aliphatic hydrocarbons using monomeric $[VO(acac)_2]$. The epoxidation reaction using microencapsulated $[VO(acac)_2]$ was carried out at room temperature in comparison with the previously used elevated temperatures. Therefore, it was concluded that the catalytic activity of $[VO(acac)_2]$ is completely changed after microencapsulation. The microencapsulated $[VO(acac)_2]$ was recovered by simple filtration and was successfully re-used in the epoxidation of geraniol. The results showed the activity of these capsules were decreased after the fourth run. The leaching of the metal (determined by ICP analysis) after each run was found to decrease following that of the first run (Figure 1.29).

A recent organometallic complex to be encapsulated is bismuth(III)triflate $[Bi(OTf)_3]$ using polystyrene as polymer wall. [60] The microcapsules were tested in a range of organic reactions (Table 1.4).

Table 1.4. MC-$Bi(OTf)_3$ catalyzed allylation of aldehydes. [60]

Entry	Aldehyde	Time (min)	Yield (%) [b]
1	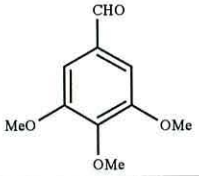	20	95
2	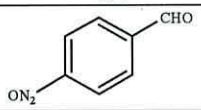	5 (110) 20	95 [c] (88) 90
3	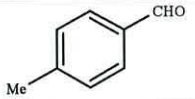	5 (90) 30	95 [c] (93) 90
4	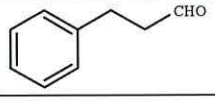	40	80

In Table 1.4; the values in parentheses refer to the $La(OTf)_3$ catalysed reaction, [a] reaction conditions: 1mmol of aldehyde, 1.5 mmol of allyltributylstannane, 100 mg of MC-$Bi(OTf)_3$, 1mmol of benzoic acid, 5 ml acetonitrile, [b] yields based on isolated yields, [c] with $Bi(OTf)_3$. Organic reactions such as allylation of aldehydes, Michael type addition of aliphatic amines to α, β- ethylenic compounds, acetylation of alcohols, Baeyer-Villiger

oxidations, and aldol condensations were all carried out using microencapsulated [$Bi(OTf)_3$]. In all cases, the microcapsules displayed comparable activity to their homogeneous counterparts and it was concluded from atomic absorption analysis that there is no leaching ($\leq$ 1ppm) of Bi from the microcapsules after reaction. An example of isolated % yields for MC-$Bi(OTf)_3$ catalyzed allylation of aldehydes is seen in Table 1.4. The microcapsules were also characterised using a variety of analytical techniques: SEM analysis showed adhesion of the microcapsules together as previously reported by other research groups. [46] Fourier-Transform Infrared (FT-IR) spectroscopy and X-ray Photoelectron Spectroscopy (XPS) analysis verified their nature, and thermogravimetric analysis - differential thermal analysis (TGA-DTA) indicated a small shift to both the endotherm signals compared to the unencapsulated compound and this shift was attributed to weak interactions between [$Bi(OTf)_3$] and the polystyrene support.

Microencapsulated Metals in Medicine

The organometallic complex; cis-diaminedichloroplatinum (II) (alternatively known as cisplatin) has been encapsulated using polylactic acid (PLA) as polymer wall. [61] PLA is a common polymer used for producing microcapsules that are used for foodstuffs or in medicinal applications. Microcapsules were prepared as follows: because the complex is poorly soluble in water, it was firstly suspended in albumin before encapsulation. To the cisplatin suspension, PLA dissolved in dichloromethane was added. The mixture was homogenised and a water–in-oil emulsion was formed which on solvent drying left solidified spherical microcapsules. The microcapsules were then centrifuged at 3,000 rpm for 10 min. To make the microcapsules a uniform size, they were suspended in 50 ml of 5 % mannitol solution for approximately 5 minutes. After this procedure was repeated several times, the microcapsules were resuspended in 50 ml of 1 % mannitol solution and immediately frozen. The water was sublimed using a lyophilizer, and the freeze dried product was obtained. The antitumour effects of these microcapsules were tested against Ehrlich ascites tumours *in vitro* and *in vivo* (in mice). The mice were given an injection of microcapsules 24 h after inoculation with the tumour cells. The microcapsules proved to be effective against Ehrlich ascites tumours and showed reduced acute toxicity compared with the standard treatment of cisplatin solution. It should be noted that all

microencapsulation literature surveyed so far under section 1.6 has involved the preparation of solid core microcapsules containing the various organometallic species discussed. To the best of the author's knowledge, no literature exists on liquid filled microcapsules containing an active catalytic homogeneous species. Therefore, the literature surveyed from hereon under section 1.6 is limited to the preparation and analysis of liquid filled microcapsules that are deemed relevant to the project of this thesis.

Preparation of liquid core microcapsules

Liquid filled urea-formaldehyde microcapsules containing lemon oil have been prepared by *in situ* interfacial polymerization. [62] The polymerization process was investigated by measuring the microencapsulation variables; surface functionality, thermal properties, and morphology. Key process parameters that affect formation and morphology of microcapsules for this particular type of microencapsulation technique have been identified as stirring time and speed, emulsifier sort and content, and internal phase viscosity. Microcapsules were prepared as follows (outlined in Figure 1.30).

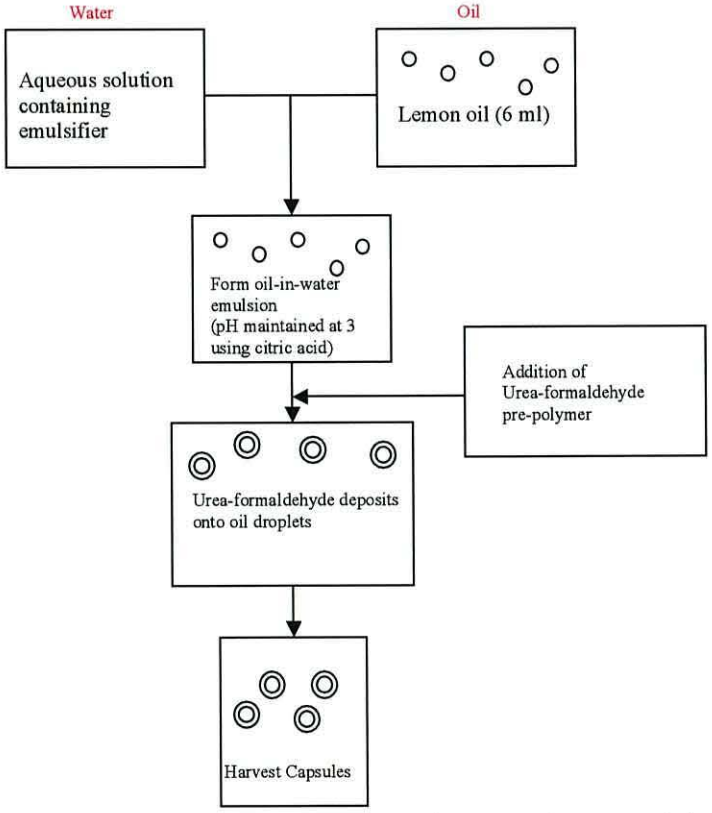

Figure 1.30. Preparation of urea-formaldehyde microcapsules containing lemon oil. [62]

An aqueous solution (100 ml) of urea (4 M) and formaldehyde (10 M) was adjusted to a pH of about 8-8.5 using triethanolamine and stirred at 343 K for 1 h to form the urea-formaldehyde pre-polymer to be used as polymer wall. An oil-in-water emulsion was formed by stirring lemon oil (6 ml) into an aqueous solution containing an emulsifier. The pH of the emulsion was maintained at about 3 using 10 % citric acid solution. The microcapsules were formed by addition of the pre-polymer to the stirring oil-in-water emulsion. Thermal analysis (differential scanning calorimetry (DSC) curves) of lemon oil, pre-polymer, and prepared urea-formaldehyde microcapsules containing lemon oil showed endothermic transitions at 453 K for the melting point in lemon oil, 523 K for the melting point in pre-polymer, and 453 and 523 K in the microcapsule, respectively. Therefore, the DSC results show that the microcapsule is composed of two materials. Thermogravimetric analysis (TGA) thermograms of the urea-formaldehyde pre-polymer and microcapsules containing lemon oil showed that the weight loss for both materials started at the melting point. The microcapsules show an initial weight loss of about 5 % from 323 to about 523 K (which is unaccounted for in the paper), but the pre-polymer did not show weight loss up until 453 K, then a subsequent weight loss of up to 80 and 95 % occurred for the pre-polymer and microcapsule respectively. The 15 % residual weight difference by temperature change of the pre-polymer and microcapsule containing lemon oil led the researchers to conclude that the microcapsules contain approximately 15 % lemon oil.

The structure of the microcapsules was carried out using FT-IR analysis on lemon oil, pre-polymer, and microcapsules containing lemon oil. It was found that the specific absorption bands of lemon oil were not observed in the microcapsule due to the sealing of lemon oil in the microcapsule. Particle size distributions of the microcapsules made using different stirring rates and different stirring times showed that the total particle sizes get smaller with increasing both stirring rates and stirring times. The particle distribution becomes narrower and the particles become smaller due to separation for longer periods of time by the stirrer in the emulsion phase, with increasing time. Four different emulsifiers; gelatin, span 80, polyvinylalcohol (PVA) and sodium dodecylsulphate (SDS) were used to study the effect of emulsifier type upon microcapsule production size and morphology. It was found that the use of gelatin (a cubic stabilizer) or PVA (a protective colloid) in microcapsule production gave a broad particle size distribution. Whereas, span 80 and

SDS both gave narrower size distributions (40-60 μm) due to dispersed particles in emulsions. The effect of emulsion concentration upon microcapsule size distribution was also investigated using four different concentrations of SDS emulsifier (1, 2.5, 5, 10 %). The study showed that as the emulsifier concentration is increased (up to 5 %), the size distribution maxima is shifted to a smaller particle size due to hydrolysis of the emulsifier and interaction of the micelles with increasing emulsifier concentration. A 10 % concentration of emulsifier showed a larger particle size distribution due to increased viscosity of the solution causing adhesion of the particles together. Investigations of the effect of viscosity of internal phase upon microcapsule size distribution showed increased size production with increased viscosity. This was attributed to the increased interfacial tension at high viscosity.

Similar investigations were carried out on melamine-formaldehyde microcapsules containing migrin oil. [63] The liquid filled microcapsules were prepared by *in situ* polymerization of a melamine-formaldehyde pre-polymer, using a similar process as described above for the preparation of urea-formaldehyde microcapsules containing lemon oil. The resulting microcapsules were characterized by analysing structure, a mean particle size and size distribution, morphologies, thermal properties and release behaviour. Structural analysis of migrin oil and microcapsules containing migrin oil was separately carried out using FT-IR measurements. Strong vibrational bands were observed at 3300 cm^{-1} (N-H stretching), 3100-3000 cm^{-1} (C-H stretching), 1380 cm^{-1} (C-N absorption band) and 1100 cm^{-1} (C-O stretching) for the microcapsules. From these results, it was concluded that migrin oil was encapsulated within the melamine-formaldehyde polymer wall.

The microcapsules formed using a stirring rate of 3000 rpm showed all particles to be below 10 μm with a narrow size distribution. Thermal analysis (TGA) of the microcapsules showed first a small weight loss due to the slow release of the internal phase trapped inside the capsule wall, then a sharp decrease in weight as the bulk of the internal phase, approximately 50 % was lost at 693 K. The DSC thermogram showed no thermal change up until 693 K, where upon a sudden absorption peak occurred. SEM analysis of the capsules showed surface smoothness. This surface smoothness was reported as being suitable for sustained release. The release behaviour of the microcapsules was investigated by encapsulating the dye molecule, 1,4-diaminoanthraquinone (DAA) which has the same

molecular weight as Migrin oil. Thus the internal phase consisted of DAA dissolved in Migrin oil. To obtain quantitative data of the microcapsule loading, the resultant microcapsules were suspended into methanol, stirred and then assayed using UV/Visible spectrometry. The obtained amount of dye from assaying was calculated and reported as the loading content of the microcapsules:

Loading content (%) = (Initial [DAA] – Encapsulated [DAA]) x 100

From UV/Visible spectroscopy measurements, the loading content was calculated to be 53 wt % which was in agreement with the TGA result of approximately 50 %. Release tests were conducted by storing the microcapsules under a drier for 60 days at two different temperatures, 298 K and 338 K. The weight of empty microcapsule was calculated by crushing, drying and weighing the microcapsules completely released for 24 h in methanol. The results were presented in the graph, resident weight (%) against release time (days) showing that release at 338 K progressed quickly, loosing up to 42 % of microcapsule weight. The results showed there to be an 8 % loss of microcapsule weight at 298 K. After extensive analysis of the melamine-formaldehyde microcapsules containing Migrin oil, they were then used to prepare fragrant fabrics. Microcapsules were applied onto cotton fabric, although it is not stated how they were applied. The fabric was then subjected to 15 laundry tests. Again, no detail is given in the paper concerning the laundry tests. SEM analysis was carried out on the fabric before and after laundry tests showing most of the microcapsules remaining on the fabric, appearing to be intact even after 15 times of the laundry test. Therefore, the paper concludes that durable microcapsules with long shelf-life are prepared using *in situ* polymerization of melamine-formaldehyde oligomers.

Liquid filled microcapsules containing dicyclopentadiene (DCPD) have been prepared by *in situ* polymerization of urea-formaldehyde. [64] The microencapsulation process is as follows. An aqueous solution (150 ml) containing urea (7.0 g), resorcinol (0.5 g), ammonium chloride (0.5 g) and ethylene maleic anhydride copolymer (EMA, 5 % wt, 100 ml) was made and the pH of the reaction mixture was adjusted to 3.5 using 10 % NaOH solution. The reaction mixture was agitated at a speed of 454 rpm and to the stirring

solution was added DCPD (60 ml) creating an average droplet size of 200 μm. Formaldehyde (0.23 ml) was added the agitated oil-in-water emulsion. The temperature of the reaction was raised to 323 K and maintained for 2 h. Water (200 ml) was added to the reaction and after 4 h the reaction mixture was cooled to room temperature. The microcapsule slurry was diluted with an additional 200 ml of water and washed with water (3 x 500 ml). The microcapsules were isolated by vacuum filtration and air dried.

Microcapsule size analysis was measured with an optical microscope using image analysis software. The average particle size of the microcapsules that were made using the agitation rate of 450 rpm was found to be 220 μm. Using this agitation rate, the typical yield of microcapsules was 79-92 %. Studies showed that increasing the rate of agitation up to 1800 rpm led to a reduced yield of 67%. A series of experiments varying agitation rate showed that agitation rate controls the average microcapsule diameter. Adjusting the agitation rate between 200 – 2,000 rpm, microcapsules with an average diameter in the range 10 – 1,000 μm were obtained (Figure 1.31).

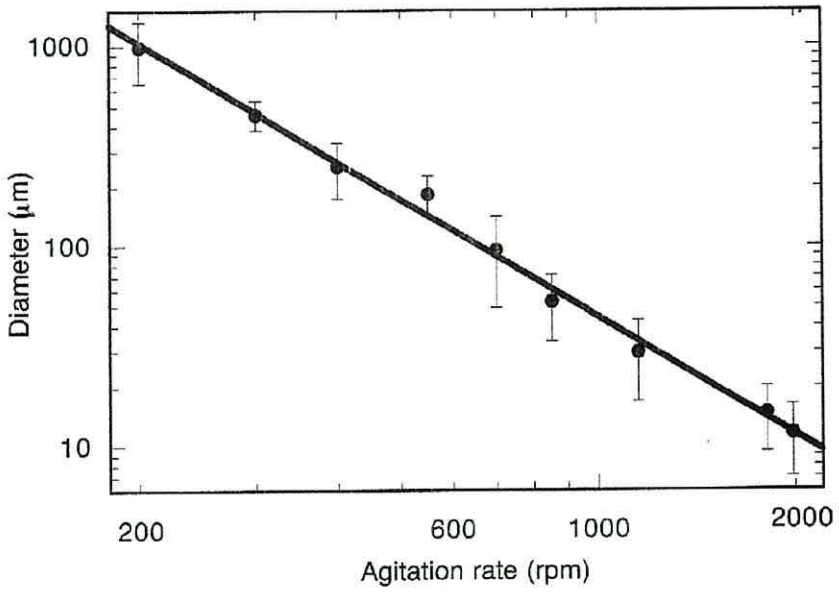

Figure 1.31. Mean microcapsule diameter *vs.* agitation rate. [64]

These results are explained by the following. Increasing the agitation rate generates a finer emulsion and therefore the average microcapsule diameter is decreased. The relationship between average diameter and agitation rate is shown to be linear in log-log scale over the

agitation rates investigated as shown in Figure 1.31. The agitation rates used to prepare microcapsules in this thesis vary between 2,000 – 10,000 rpm. Using the graph in Figure 1.31, microcapsules made using these mixing speeds can be predicted to be *ca.* 10 – 5 μm in diameter. The resulting microcapsules were characterised using a range of analytical techniques. Surface morphology and polymer wall thickness were investigated using both optical and electron microscopy. Environmental scanning electron microscopy (ESEM) showed the microcapsules to be spherical and free flowing after drying. The polymer wall was shown to possess a smooth inner membrane and a rough porous morphology on the outer surface. Similar investigations have shown these porous and non porous zones to be a common feature of urea-formaldehyde microcapsules. [62]

Investigations of the process parameters of microencapsulation showed variables such as excess reagents, addition of smaller volumes of DCPD, an unbalanced or unaligned mixer, and lower initial pH all dramatically increase the thickness of the outer, permeable layer. Contrary, the smooth nonporous inner region of the polymer wall was shown to be independent of processing parameters; the polymer wall thickness consistently was found to be between 160-220 nm over a full range of microcapsule diameters investigated. The rough porous structure on the outer surface of the polymer wall was found to be an agglomeration of urea-formaldehyde nanoparticles as determined by the following experiment. The bath temperature, solution temperature and pH were monitored during a standard microencapsulation process while simultaneously removing aquilots from the emulsion bath at periodic intervals and quenching in 20 ml of cold water. The aquilots were imaged optically with incident light, with a black background corresponding to an optically clear solution and white background indicating a milky solution.

During the time period of 0-50 minutes, the DCPD emulsion appears black (*i.e.* clear). It was observed at low agitation rates, individual DCPD droplets rapidly coalesced, forming a distinct second phase that floated above the aqueous phase if agitation was stopped. The pH was reduced from 3.50 to 2.35 and the solution temperature continuously increased during this time period. During the second time phase (50-70 minutes), a cloudy emulsion was observed in association with a slight increase in pH. Observations showed that although the droplets remained as microcapsules, if agitation was stopped, they clumped and were too fragile to isolate. The third time period (70-160 minutes) showed

the transition to a milky white emulsion in which the temperature stabilized and the pH peaked at 2.45, and then steadily decreased. The microcapsules were able to be separated at this stage if agitation was stopped. It was reported that the microcapsule shell reaches its maximum thickness with surface morphology transitions from smooth to rough during this time period. The milky white appearance of aliquot samples was explained by the hypothesis of formation of urea-formaldehyde nanoparticles in suspension. The particles were filtered from the solution and imaged using electron microscopy, the resulting electron micrographs of this sample were reported as being indistinguishable from those taken of the rough porous outer surface of the microcapsules and therefore, concluded to be urea-formaldehyde nanoparticles.

During this experiment, it was found that the onset of rough surface morphology occurs approximately 75 minutes into the microencapsulation reaction. In order to preserve the smooth surface of the polymer wall, attempts were made to end the reaction at this time. Therefore, agitation was stopped and the reaction was allowed to cool naturally. The result was that the emulsion formed a single gelatinous structure and individual microcapsules could not be obtained. Upon quenching with water at this stage, individual smooth microcapsules were reportedly produced but possessing poor quality and difficult to filter. After separation the microcapsules were found to turn yellow over a time period of 3-10 days as the DCPD diffuses through the shell. The paper suggests that the smooth non-porous microcapsule wall is believed to be the result of the deposition of low molecular weight pre-polymer at the DCPD-water interface while the pre-polymer remains soluble.

The formation of urea-formaldehyde nanoparticles is attributed to precipitation of higher molecular weight pre-polymer in the aqueous solution, the aggregation and deposition on the capsule surface results in the rough, porous outer layer of the urea-formaldehyde shell. This theory is supported by the following. It is widely reported that during *in situ* polymerization, the urea and formaldehyde react in the water phase to form a low molecular weight pre-polymer. The molecular weight of the pre-polymer increases over time, and during the microencapsulation of an oil (or alternative water immiscible liquid), it deposits at the oil-water interface. Eventually, over time the pre-polymer becomes highly crosslinked as the polymerisation process continues and forms the microcapsule polymer wall. [65] Studies have shown that gelation of bulk urea-formaldehyde

resin is attributed to the coalescence of a lyophobic colloidal sol, which is shown to precipitate out of solution as the molecular weight increases. [66,67]

The microcapsule fill content (encapsulation efficiency) was measured using elemental analysis. The measurements were based upon knowing the chemical compositions of urea-formaldehyde ($C_5H_8N_2O$, 53.56 wt% C and 24.98 wt% N) and DCPD ($C_{10}H_{12}$, 90.85 wt % C and O wt % N) and the assumption that water was the only impurity present in the combusted sample, the weight fractions of urea-formaldehyde (UF) and DCPD were calculated as:

$$W_{UF} = 4.003\ W_N$$
$$W_{DCPD} = 1.101\ W_C - 2.144\ W_N$$

(Where W_c and W_N are the weight fractions of C and N obtained by elemental analysis).

CHN analysis showed that immediately after manufacturing and drying, microcapsules contain 83-92 wt % DCPD and 6-12 wt % UF. After 30 days exposed to ambient laboratory conditions, the microcapsules were tested again and the results showed that the average fill content decreased by 2.3 wt %.

The DCPD filled microcapsules were then used as one of the key components to create a novel polymer composite that is reported as being inherently "self healing". [68] Polymer composites are routinely damaged in the form of cracks. Often induced by thermal or mechanical fatigue, cracking can lead to mechanical degradation of fibre-reinforced polymer composites. Where such polymer composites are used in microelectronics, cracking can lead to electrical failure. Cracking is also a long standing problem in polymer adhesives. Therefore, the development of a structural polymeric material with the ability to autonomically heal cracks ("self healing") is of great importance. The concept of "self healing" utilises the ring opening metathesis polymerization (ROMP) chemistry of dicyclopentadiene, a monomer well known to ROMP upon contact with the ruthenium based metathesis catalyst, Grubbs' catalyst (Figure 1.32).

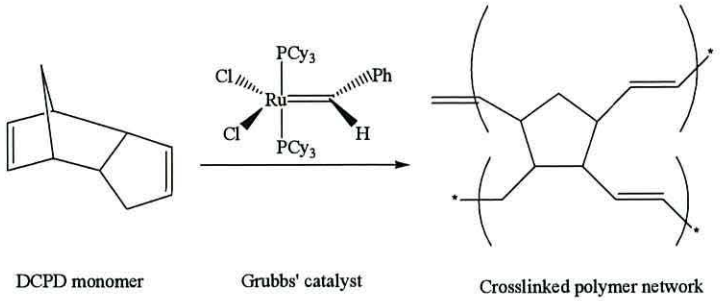

Figure 1.32. Chemistry of self-healing; ruthenium based Grubbs' catalyst initiates ring opening metathesis polymerization (ROMP) of dicyclopentadiene (DCPD).[68]

Placement of DCPD filled microcapsules into an epoxy resin matrix that contains ruthenium metathesis catalyst, showed that as cracking appeared within the polymer composite, the microcapsule polymer wall was also ruptured, thereby releasing the internal phase (DCPD). Polymerization of DCPD within the epoxy resin occurred upon contact with the metathesis catalyst to fill the cracks; *i.e* "self-healing" (Figure 1.33).

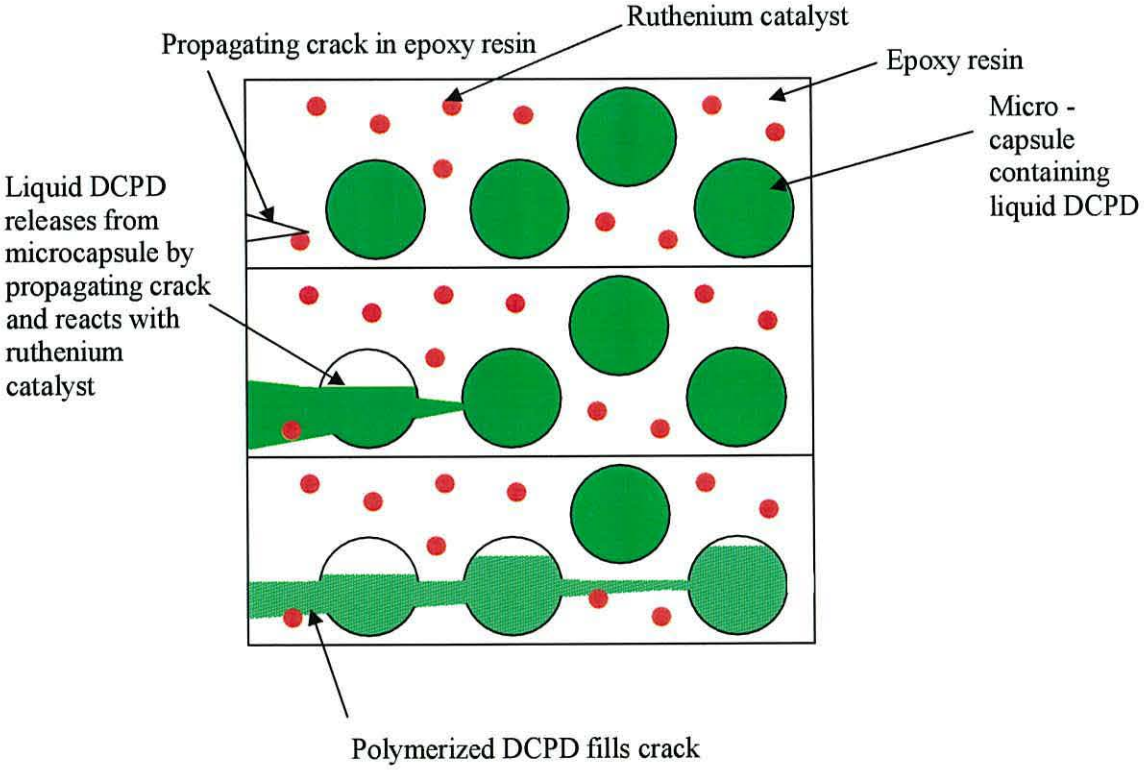

Figure 1.33. The autonomic healing concept ("self healing").[68]

Fracture experiments yielded as much as 75 % recovery in toughness of the polymer composite using self healing. The key feature of self-healing materials is the highly engineered microencapsulated healing agent; the microcapsules must possess sufficient strength to remain intact during processing of the host polymer, yet rupture when the polymer is damaged. Therefore, high bond strength to the host polymer combined with a moderate strength microcapsule wall is required. In order for the microcapsules to have a long shelf-life, they must be impervious to leakage and diffusion of the encapsulated liquid for a considerable time. It has been reported that these characteristics are achieved with a system based on the *in situ* polymerization of urea formaldehyde encapsulating dicyclopentadiene.

Several organic solvents have been encapsulated in a microencapsulation experiment using an alternative polymer wall to the amino resins discussed so far. For example, polyelectrolyte multilayer polymer walls formed by stepwise adsorption of polyelectrolytes into colloidal cores with subsequent dissolution of the core have been used to form microcapsules. [69] The materials used in this example for the polyelectrolyte shells were poly(styrene sulfonate, sodium salt) (PSS) and poly(allylamine hydrochloride) (PAH). The polyelectrolyte materials were first deposited onto a colloidal core of melamine latex particles. Subsequently, the melamine particles were dissolved by reducing the pH of the external environment. The hollow shells were then suspended in various organic media; methanol, ethanol, pentanol, hexanol, octanol, octane, and decane were all subsequently encapsulated by a gradual solvent exchange. The microcapsules were characterized using SEM, TEM, AFM, and confocal microscopy showing that the containment of solvents did not seem to significantly affect either the structure or appearance of the surface of the shells.

1.7. References

1 Sohi, H., Sultana, Y., Khar, R.K., *Drug Development and Industrial Pharmacy*, 2004, **30**, 429

2 Benita, S. (Ed.), *Microencapsulation: Methods and Industrial Applications*, Dekker, New York, 1996

3 Journal of Microencapsulation, Taylor & Francis

4 Vandegaer, J.E. (Ed.), *Microencapsulation: Processes and Applications*, Plenum Press, New York, 1974

5 Green, B.K., Schneidcher, L., 1958, U.S.Patent, 2,800,457 and 2,800,458

6 Vilstrup, P.(Ed.), *Microencapsulation of Food Ingredients*, Leatherhead, Surrey, 2001

7 Jayakrishnan, A., Jameela, S.R., *Biomaterials*, 1996, **17**, 471

8 Cakhshaee, M., Pethrick, R.A., Rashid, H., Sherrington, D.C., *Polymer Communication*, 1985, **26**, 185

9 Dietrich, K., Herma, H., Nastke, R., Bonatz, E., Tiege, W., *Acta Polymerica*, 1989, **40**, 243

10 Thies, C., Dappert, T., *Journal of Membrane Science*, 1978, **4**, 99

11 Billmeyer, F.W., *Textbook of Polymer Science*, Wiley, New York, 1984

12 Suresh, A.K., Yadav, S.K., Khilar, K.C., *Journal of Membrane Science*, 1997, **125**, 213

13 Kondo, T., Osada, Y., Nakagawa, T., (Ed)., *Membrane Science and Technology*, Marcel Dekker, New York, 1992

14 Park, S., Hong, K., *Materials Research Bulletin*, 1999, **34**, 963

15 Sato, T., Yamamoto, T., Shibako, S., Ichikawa, K., Dobashi, T., *Journal of Membrane Science*, 2003, **213**, 25

16 Lehr, C.M., Lamprecht, A., Schafer, U.F., *European Journal of Pharmaceutics and Biopharmaceutics*, 2000, **49**, 1

17 Sheppard, C.J.R., Shotton, D.M., *Confocal Laser Scanning Microscopy*, BIOS, Oxford, 1997

18 Mark, H.F.,(Ed.), *Encyclopedia of Polymer Science Technology (Vol 2)*, Wiley, New York,1965

19 Hentrich, W., Kohler, R., 1936, British Patent, GB 455,008

20 Bainbridge, R., *Sail*, 1977, **8**, 142

21 Meyer, B., *Urea-Formaldehyde Resins*, Addison-Wesley, USA, 1979

22 Scheepers, M.L., Gelan, J.M., Carleer, R.A., Adriaensens, P.J., Vanderzande, D.J., Kip, B.J., Brandts, P.M., *Vibrational Spectroscopy*, 1993, **6**, 55

23 Anderson, I.H., Cawley, M., Steedman, W., *British Polymer Journal*, 1969, **1**, 24

24 Cymel ® 385 resin brochure (Cytec, USA)

25 Ebdon, J., Hunt, B., O'Rourke, W., *British Polymer Journal*, 1987, **19**, 197

26 Longordo, E., Papazian, L., Chang, T., *Journal of Liquid Chromatography*, 1991, **14**, 2043

27 Chang, T., *Progress in Organic Coatings*, 1996, **29**, 45

28 Thomas JM, Thomas WJ, *Principles and Practice of Heterogeneous Catalysis*, VCH, Weinheim, 1997

29 Wells, P., *Chemistry in Britain*, 1992, **28**, 989

30 Shriver, D.F., Atkins, P.W., Langford, C.H., *Inorganic Chemistry (2nd Ed)*, Oxford University Press, Oxford, 1996

31 Noyri, R., *Asymmetric Catalysis in Organic Synthesis*, Wiley, New York, 1994

32 Hegedus, L.S., *Transition Metals in the Synthesis of Complex Organic Molecules* (2nd Ed) University Science Books, USA, 1999

33 Hanson, B., Zoeller, J.R., *Catalysis Today*, 1998, **42**, 371

34 Simonelli B, Orlandi S, Benaglia M, Pozzi G, *European Journal of Organic Chemistry*, 2004, **12**, 2669

35 Webb, P.B., Cole-Hamilton, D.J., *Chemical Communications*, 2004, **5**, 612

36 Colman, Hegedus, Norton, Finke., *Principles and Applications of Organotransition Metal Chemistry*, University Science Books, California, 1987

37 Sherrington, D.C., Kybett, A.P., (Eds), *Supported Catalysts and their Applications*, Royal Society of Chemistry, Cambridge, 2001

38 Farrall, M.J., Frechet, J.M.J., *Journal of Organic Chemistry*, 1976, **41**, 3877

39 M^{c}Morn, P., Hutchings, G.J., *Chemical Society Reviews*, 2004, **33**, 108

40 Drake, R., Sherrington, D.C., Thomson, S.J., *Reactive and Functional Polymers*, 2004, **60**, 65

41 Opstal, T., Melis, K., Verpoort, F., *Catalyst Letters*, 2001, **74**, 155

42 Leadbeater, N., Scott, K.A., Scott, L.J., *Journal of Organic Chemistry*, 2000, **65**, 3231

43 Kobayashi, S., Sugiura, M., Kitagawa, H., Lam, W.W.-L., *Chemistry Reviews*, 2002, **102**, 2227

44 Sherrington, D.C., *Journal of Polymer Science Part A-Polymer Chemistry*, 2001, **38**, 2364

45 Kobayashi, S., Nagayama, S., *Journal of the American Chemical Society*, 1998, **120**, 2985

46 Kobayashi, S., Akiyama, R., *Chemical Communications*, 2003, 449

47 Kobayashi, S., Nagayama, S., Endo, M., *Journal of Organic Chemistry*, 1998, **63**, 6094

48 Kobayashi, S., Nagayama, S., Endo, M., *Journal of the American Chemical Society*, 1999, **121**, 11229

49 Kobayashi, S., Ishida, T., Akiyama, R., *Organic Letters*, 2001, **3**, 2649

50 Ley, S., Ramarao, C., Lee, A-L., Ostergaard, N., Smith, S., Shirley, I., *Organic Letters*, 2003, **5**, 185

51 Kobayashi, S., Akiyama, R., *Angewandte Chemie-International Edition in English*, 2001, **40**, 3469

52 Ley, S., Ramarao, C., Smith, S., Shirely, I., DeAlmeida, N., *Chemical Communications*, 2002, 1132

53 Ley, S., Ramarao, C., Gordon, R., Holmes, A., Morrison, A., McConvey, I., Smith, S., Shirely, I., Smith, M., *Chemical Communications*, 2002, 1134

54 Ley, S., Yu, J-Q., Wu, H-C., Ramarao, C., Spencer, J., *Chemical Communications*, 2003, 678

55 Jansson, A.M., Grotli, M., Halkes, K.M., Meldal, M., *Organic Letters*, 2002, **4**, 27

56 Gibson, S.E., Swamy, V.M., *Advanced Synthetic Catalysis*, 2002, **344**, 619

57 Taber, D.F., Frankowski, K.J., *Journal of Organic Chemistry*, 2003, **68**, 6047

58 Kobayashi, S., Akiyama, R., *Angewandte Chemie-International Edition in English*, 2002, **41**, 2602

59 Lattanzi, A., Leadbeater, N.E., *Organic Letters*, 2002, **4**, 1519

60 Choudary, B.M., Sridhar, C., Sateesh, M., Sreedhar, B., *Journal of Molecular Catalysis A: Chemical*, 2004, **212**, 237

61 Araki, H., Tani, T., Kodama, M., *Artificial Organs*, 1999, **23**, 161

62 Park., S.J., Shin, Y.S., Lee, J.R., *Journal of Colloid and Interface Science*, 2001, **241**, 502

63 Hong, K., Park, S., *Materials Chemistry and Physics*, 1999, **58**, 128

64 Brown, E.N., Kessler, M.R., Sottos, N.R., White, S.R., *Journal of Microencapsulation*, 2003, **20**, 719

65 Thies, C., *Encyclopedia of Polymer Science and Engineering*, Wiley, New York, 1987

66 Pratt, T.J., William, E.J., Rammon, R.M., Plagemann, W.L., *Journal of Adhesion*, 1985, **17**, 275

67 Dunker, A.K., William, E.J., Rammon, R., Farmer, B., Johns, S.J., *Journal of Adhesion*, 1986, **19**, 153

68 White, S.R., *Nature*, 2001, **409**, 794

69 Moya, S., Sukhorukov, G.B., Auch, M., Donath, E., Mohwald, H., *Journal of Colloid and Interface Science*, 1999, **216**, 297

CHAPTER 2

RESULTS AND DISCUSSION

MICROCAPSULES AND MICROSCOPY

2. Microcapsules and Microscopy

2.1. Area of Study

In the academic literature there are many examples of dye containing microcapsules and microspheres that have been made using various methods and materials, such as poly(vinyl alcohol) microcapsules containing Disperse Red 1 (DR1), a photoresponsive group. [1] By comparison, there are few examples of dye containing melamine-formaldehyde microcapsules. However, one example is the encapsulation of the dye, 1,4 – diaminoanthraquinone (DAA). [2] The purpose of encapsulating DAA was to test the permeability of melamine-formaldehyde microcapsules towards fragrant Migrin oil which has the same molecular weight as DAA. Microcapsule permeability was measured by monitoring DAA release using UV/Visible spectroscopy. The overall aim was to produce long lasting fragrant fabric by coating melamine-formaldehyde microcapsules containing Migrin oil onto fabric. Also, surface structure and morphology of Migrin oil and DAA containing microcapsules was examined using scanning electron microscopy (SEM). Microscopy is a standard technique used for characterising microcapsules. For example, other than SEM, optical microscopy, [3] confocal scanning laser microscopy (CLSM), [4] and fluorescence microscopy [5] have all been employed to characterise microcapsules.

The work in this chapter focuses upon the preparation of dye filled melamine-formaldehyde microcapsules for the purposes of, characterising the structure and morphology of the microcapsule surface, examining the inside of the microcapsule, and probing the polymer wall. Specifically, the dyes used for this work were Rhodamine B, 9,10-bisphenylethynylanthracene, 9-anthraldehyde, and Pergascript blue dye. All aforementioned microscopy was employed to achieve such capsule characterisation. To the author's knowledge, these four dyes have not previously been encapsulated using the melamine-formaldehyde *in situ* interfacial microencapsulation technique. Therefore, although microscopy is a well known technique to characterise microcapsules, the specific preparation and characterisation of the microcapsules reported in this chapter is novel, thus forming the basis of this chapter.

2.2. Microencapsulation Investigations

The industrial CASE Award sponsors for this PhD, Thermographic Measurements Ltd (TMC) have a detailed knowledge on an established microencapsulation procedure that has been commercialized to manufacture melamine-formaldehyde microcapsules containing thermochromic materials. Thus, their microencapsulation tried and tested procedure was considered an appropriate starting point for the study of the microencapsulation of homogeneous catalysts. This commercial process from TMC is labelled as method 1 from hereon in this thesis. The constituents used for method 1 microencapsulations can be categorized into three types; external phase, internal phase and pre-polymer phase. All three constituents were initially investigated by various analytical techniques described below to determine the physicochemical properties associated with each material involved in the microencapsulation procedure. The external phase, internal phase, and pre-polymer phase are described from hereon in this thesis as solution 1, solution 2 and solution 3, respectively.

Solution 1

Solution 1 was an aqueous solution of surfactant and defined as the external phase. In method 1, the main requirements of the external phase were; an acidic pH (to initiate melamine-formaldehyde polymerization), immiscibility with the internal phase (*i.e.* to create an oil-in-water emulsion) and a surfactant concentration in excess of the critical micelle concentration to support and maintain a stable oil-in-water emulsion. [6] The surfactant used in all method 1 microencapsulation experiments was the co-polymer, ethylene-maleic anhydride (EMA) which was obtained from commercial suppliers (Zeeland Chemicals Inc, USA) as a white powder. The chemical structure of EMA was investigated using ^{1}H NMR spectroscopy by dissolving the fine white powder in D_2O at room temperature. The co-polymer proved to be only sparingly soluble in this so the solution was filtered through a cotton wool plug to remove particulate matter before NMR analysis. Two broad resonances were observed at 1.55 and 2.65 ppm, which integrated to 2 and 1, respectively. A proposed structure resulting from ^{1}H NMR analysis of the co-polymer EMA is shown (Figure 2.1) with the two different proton environments highlighted in the structure as H_a and H_b. The resonance occurring at 1.55 ppm was attributed to the proton environment on the ethylene backbone moiety

(labelled, H_a) and the signal occurring at 2.65 ppm was attributed to the deshielded proton environment on the maleic-anhydride backbone moiety (labelled, H_b).

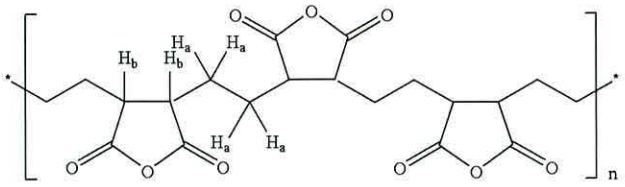

Figure 2.1. Proposed chemical structure of the co-polymer, EMA.

Dissolving the EMA co-polymer in water at 348 K will lead to the anhydride functions present in the molecule to be hydrolyzed by water. [7] This results in the formation of the diacid, which in turn is in equilibrium with its dissociated form (Figure 2.2). [7] The dissociated protons from the diacid were then available to protonate the melamine-formaldehyde oligomers, thus initiating polymerisation. The initial pH of solution 1 was measured to be 4.2.

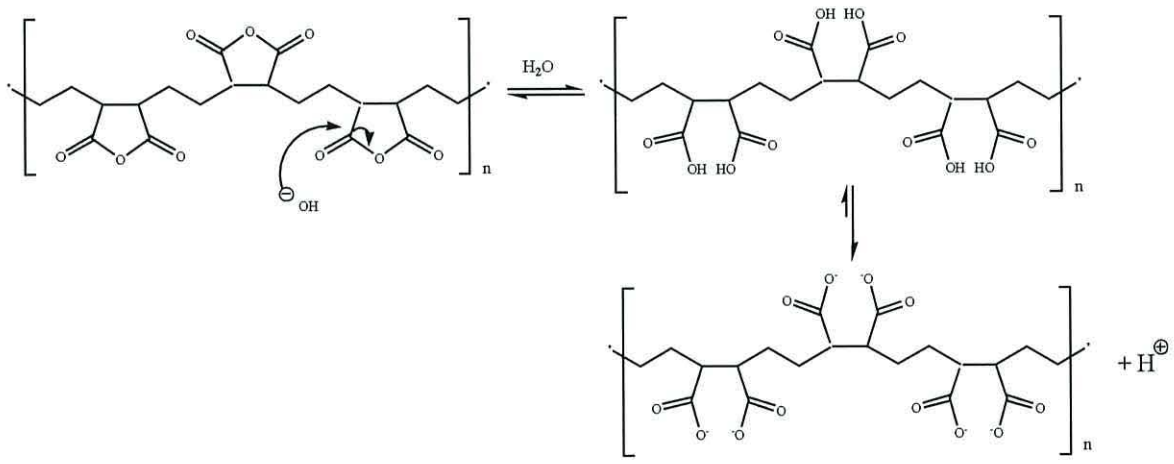

Figure 2.2. Structural representation of the processes that occur upon dissolving EMA into an aqueous environment.

The surfactant concentration used in all method 1 microencapsulation experiments was an aqueous solution of EMA (3 % solids by weight). This concentration exceeds the critical micelle concentration. The formation of an emulsion is a "fast" process, which is achieved by applying mechanical energy and takes place in a time period of milliseconds. [8] It has been reported that in the process of emulsion formation, firstly the interface between the two phases is deformed. A liquid film is then formed between the

two liquids, which later deforms to such an extent that droplets form. Such droplets are often relatively large and by continued shearing they are subsequently broken-up or disrupted into smaller droplets. To stabilize an emulsion, the system must be kept in a metastable state by opposing the mutual interfacial flow of liquids of one droplet to the other once the droplets approach each other as a result of Brownian motion in the system. [8] Surfactants are able to stabilize emulsions due to their chemical structure possessing both hydrophilic and hydrophobic moieties. For example, a surfactant with a sodium sulphate salt polar head and C_{12} alkane hydrophobic tail arranges itself around an oil droplet in an oil-in-water emulsion as shown in Figure 2.3. [8] EMA adsorbs onto the oil droplet surface in a similar manner, thus reducing the interfacial tension between the oil droplet and water, leaving the emulsion stabilized.

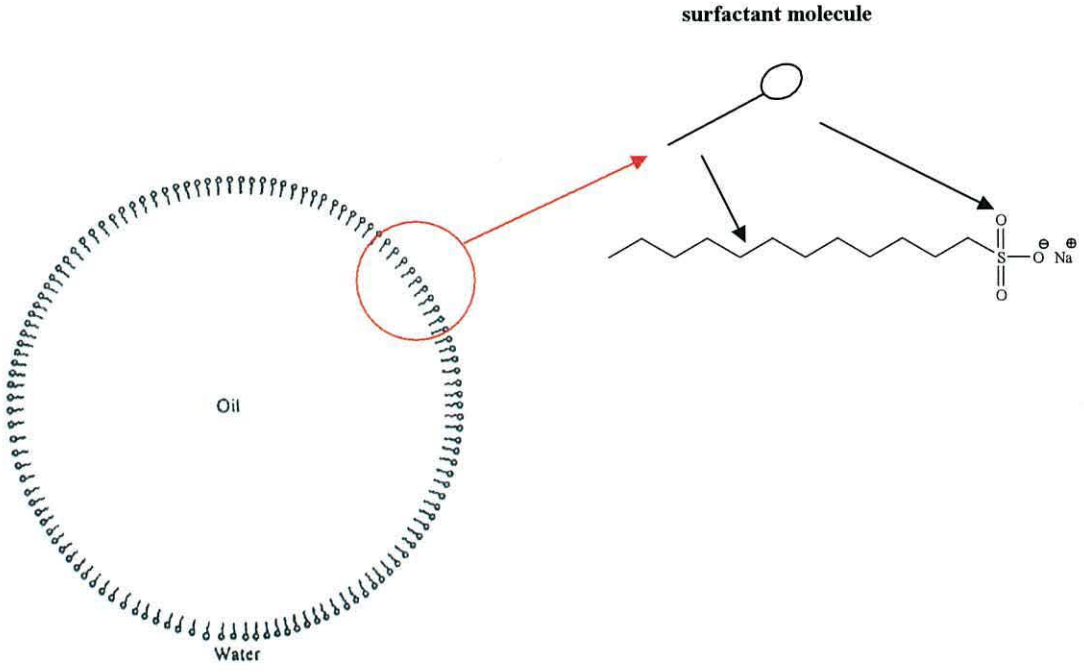

Figure 2.3. Schematic representation of an oil-in-water emulsion droplet stabilized by surfactant, sodium dodecyl sulphate (SDS) at the oil-water interface. [8]

Solution 2

The internal phase (IP) for all microencapsulation experiments carried out in this thesis consist of an organic solvent, either neat or containing a solute (specific details of IP are stated where appropriate in this thesis). While the microencapsulation procedure was being tested for catalyst encapsulation, it was considered appropriate for two reasons to carry out "blank" microencapsulations, *i.e.* using an internal phase of neat solvent

without the catalyst. Firstly, using an IP of neat solvent created a less complex system than using an IP of catalyst dissolved in solvent. Secondly, an IP of neat solvent was advantageous over a catalyst IP for economic reasons. Toluene was initially chosen as a test solvent for the internal phase because it met the criteria required for method 1 microencapsulation procedures, *i.e.* boiling point $\geq$ 343 K, immiscibility with water, and surfactant insolubility in IP. Toluene has a boiling point at 383 K and its solubility in water is 7.64 mmol/L at 328 K. [9] EMA was tested for solubility in toluene and found to be insoluble at both 298 K and 348 K (348 K is the temperature at which method 1 microencapsulations were carried out). The insolubility of EMA in toluene rules out the possibility of EMA being present in the internal phase of the microcapsule. However, it does not rule out the possibility of EMA being trapped within the melamine-formaldehyde polymer wall after encapsulation.

Solution 3

Solution 3 was always the pre-polymer. The pre-polymer was an aqueous solution of melamine-formaldehyde oligomers (trade name, Cymel 385) obtained from commercial suppliers; Cytec, USA. Cymel 385 is an aqueous solution of a mixture of various methylolmelamines (79 % by weight). Methylolmelamines are compounds containing the melamine ring with various methylol ($-CH_2OH$) substitutions on the three pendant nitrogen atoms. [10] In theory, each nitrogen atom can be substituted twice; therefore, each melamine ring will have six functional sites. Cymel 385 is represented as $MelamineFormaldehyde_{3.2}Methyl_{1.6}$ by the supplier company, Cytec (Figure 2.4). [11]

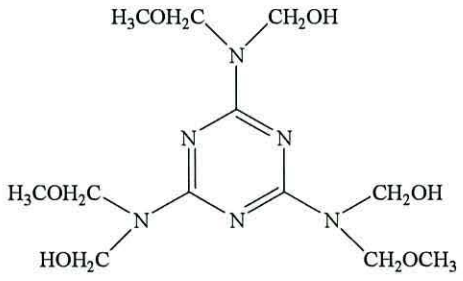

Figure 2.4. Representation of part of the structure of commercially available Cymel 385.

The above representation of Cymel 385 was confirmed using infrared (IR) analysis. IR analysis of a diluted sample of an aqueous Cymel 385 showed an OH stretch at 3363

cm^{-1}, alkane CH stretching at 2945 cm^{-1}, and CN double bond stretching at 1564 cm^{-1}. Since pre-polymers exhibit essentially the same core structure but different functional side groups to that of the final polymer, the data obtained IR analysis of Cymel 385 pre-polymer helps to give insight into the chemical structure of the cured Cymel 385 polymer. The method 1 microencapsulation procedure is outlined in the form of a flow diagram (Figure 2.5). High speed shearing (of the order of *ca.* 10,000 rpm) of the external phase with the internal phase was essential to create an oil-in-water emulsion (as mentioned earlier). Subsequent addition of the pre-polymer to the oil-in-water emulsion generated a high molecular weight polymer that envelopes the oil droplets, *i.e.* the polymer wall is formed at the surfactant interface of the external/internal phase. Curing of the polymer wall was activated by an acidic environment and heat over a 3 h period.

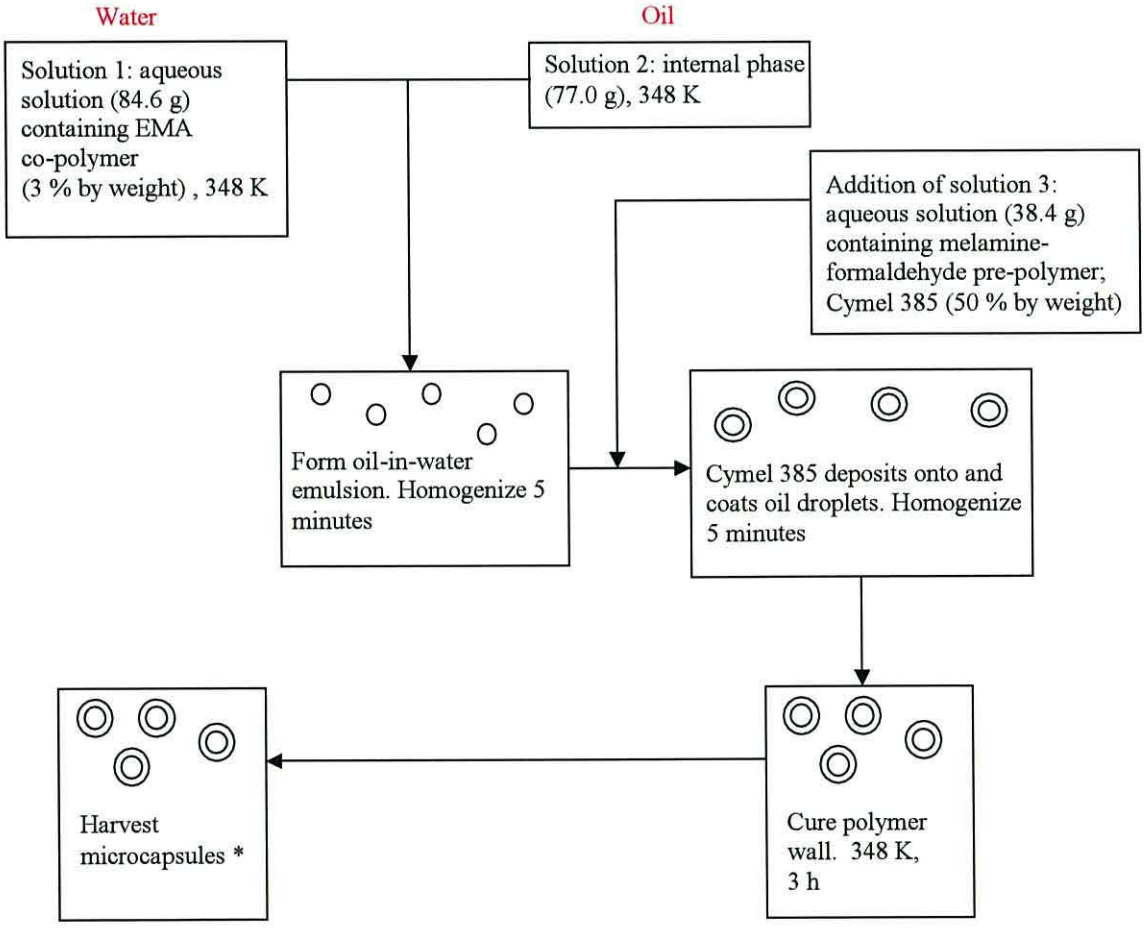

Figure 2.5. A flow diagram showing the microencapsulation process of method 1.

2.2.1. Microencapsulation Variables

Microencapsulation variables investigated were; mixing speeds, internal phase, surfactant, reaction time and temperature. The following microencapsulation experiments were carried out using toluene as internal phase for the reasons outlined earlier.

The Effect of Homogeniser Speed on Microcapsule Size

It is known (as discussed in section 1.6 in this thesis) that one of the main factors affecting microcapsule size is the mixing speed of microencapsulation components. [12] Therefore, the effect of homogenizing speed upon microcapsule particle size distribution under method 1 encapsulation conditions was examined in the following experiment. Five separate batches of microcapsules, using toluene as IP, were made using five different homogeniser speeds; 2,000 rpm, 4,000 rpm, 6,000 rpm, 8,000 rpm, and 10,000 rpm. The particle size distribution of each microencapsulation batch was measured by injecting diluted slurry (2 ml) into a Coulter LS particle sizer (Figure 2.6).

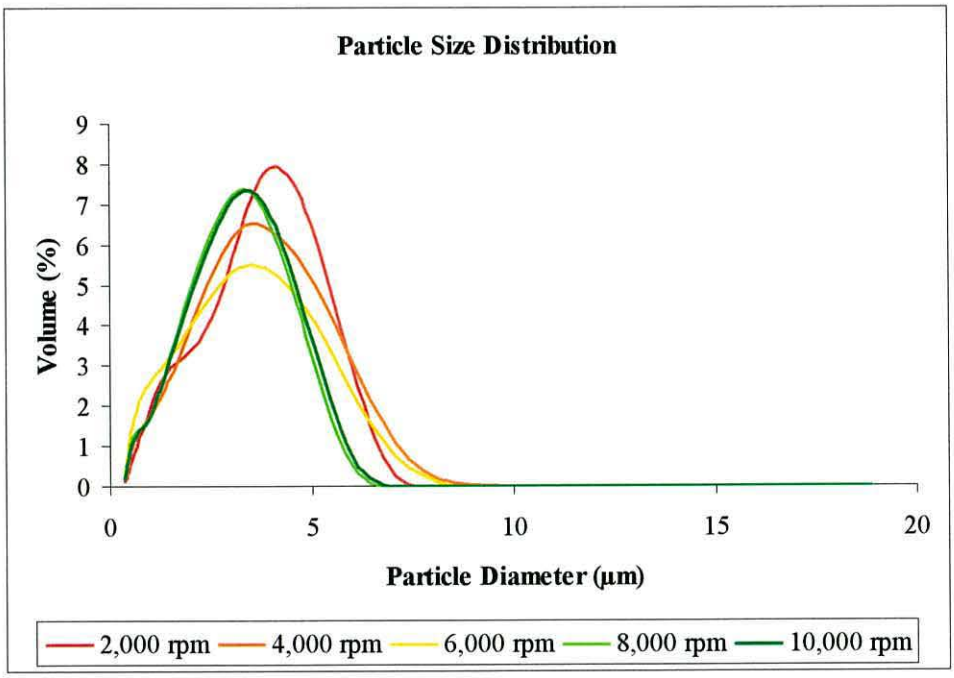

Figure 2.6. Particle size data showing the effect of homogeniser speed upon particle size distribution.

At 2,000 rpm, approximately 80 % volume of the resulting microcapsule slurry contains microcapsules that are *ca.* 4 µm ± 0.5 µm in diameter. As the homogenising speed was incremented by 2,000 rpm in each following experiment until a maximum mixing speed

of 10,000 rpm was reached, it was seen that the toluene containing microcapsules became smaller upon increasing mixing speed. This data fits with theory because the mechanical homogeniser highly shears the toluene (oil phase). [13] It is noted that the above results apply to a specific set of experimental conditions and equipment, and that changing such variables within method 1 encapsulations will result in a different set of particle size distribution curves. The toluene containing microcapsules made using a stirring speed of 2,000 rpm were characterised using both optical microscopy (Figure 2.7) and scanning electron microscopy (Figure 2.8).

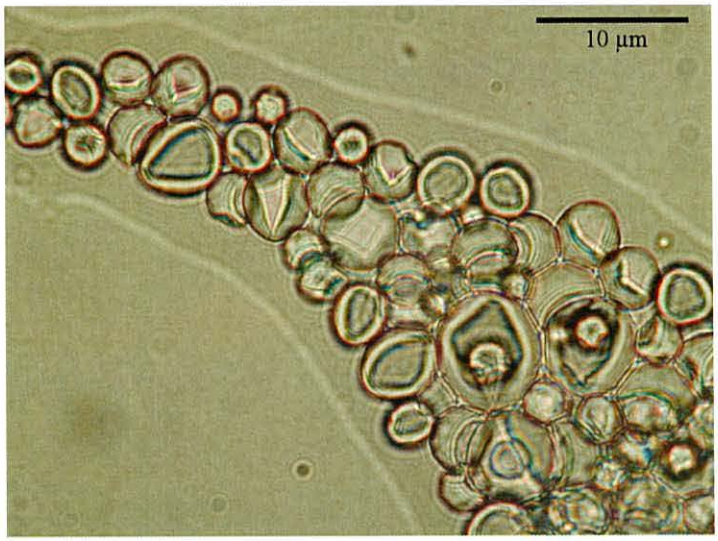

Figure 2.7. An optical micrograph of microcapsules containing an internal phase of toluene made using method 1. Magnification (x 1000).

The micrograph shows most of the microcapsules to be spherical in shape, however, closer examination of the microcapsule surface reveals that the majority of microcapsules do not appear to have a uniformly smooth surface but instead appear "deflated". The microcapsule size range shown in the optical micrograph correlates exactly with the particle size distribution graph (Figure 2.6). The particle size range of the microcapsule sample shown in the optical micrograph is between 2- 7.5 µm, however the majority of microcapsules shown are *ca.* 4-5 µm in diameter. A few of the microcapsules appear "blurred" in the optical micrograph. Such lack of focus is due to the difficulties arising from trying to focus three dimensional spherical microcapsules using an optical microscope which has a limited depth of focus. Therefore, the microcapsule surface and morphology was examined further using scanning electron microscopy (SEM) (Figure 2.8). SEM allows a more detailed examination of the microcapsule surface by offering both greater resolution and greater depth of focus in

comparison with optical microscopy. Also, three dimensional specimens are much better resolved in SEM than optical microscopy since the probing electron beam is precision guided towards the target specimen by a series of focusing and condensing mirrors housed inside the scanning electron microscope.

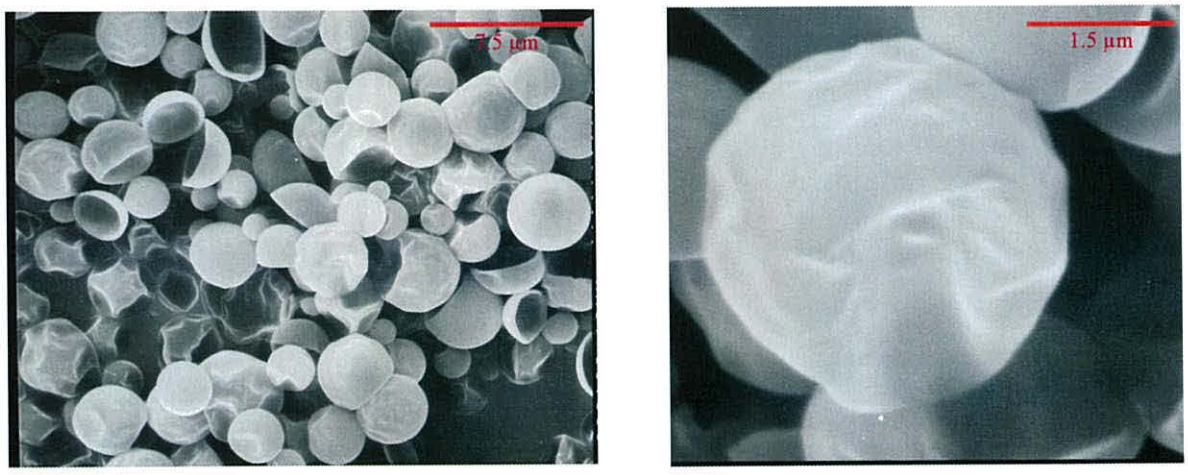

(a) (b)

Figure 2.8. SEM micrographs of toluene containing microcapsules.

The SEM image in Figure 2.8 (a) shows microcapsules ranging in size from *ca.* 1 – 5 µm which correlates with the particle size distribution curves seen earlier. Most of the microcapsules in (a) are seen to be intact, however some larger capsules appear "deflated". In Figure 2.8 (b), a close up of one microcapsule from the same sample in (a) is shown. The microcapsule size is *ca.* 3 µm in diameter. The surface morphology of the capsule in (b) is shown to be uneven. Such unevenness could be explained by two reasons. Firstly, the SEM image can be viewed as essentially a "snapshot" of the microencapsulation process. Therefore, it is feasible that upon mixing the microencapsulation components at such a high speed (*ca.* 2,000 rpm), the melamine-formaldehyde polymer will coat the toluene droplet unevenly, layer upon layer, thus resulting in the image seen in (b). Alternatively, the unevenness of the microcapsule surface could be explained by the onset of deflation.

The cause of microcapsule "deflation" was examined further. It could be one of the following; (i) as a consequence of filtering the microcapsules, (ii) the loss of internal phase (by leaching), or (iii) in the SEM under high vacuum. However, the final

statement can be ruled out since microcapsule deflation was also observed in the optical micrograph (*i.e.* no high vacuum). To eliminate filtering as the cause of deflation, SEM samples were prepared using a single drop of undiluted unfiltered slurry of microcapsules prepared using a mixing speed of *ca.* 2,000 rpm as before. The stubs were placed into a dessicator (under air) with silica gel and left to dry overnight for the water to evaporate. One example is shown (Figure 2.9).

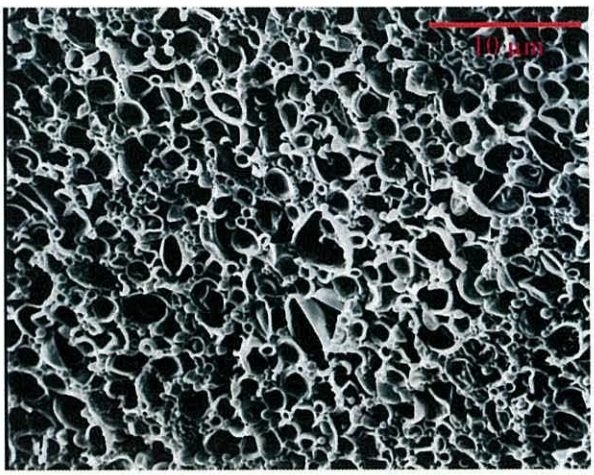

Figure 2.9. SEM micrograph of undiluted and unfiltered microcapsules taken from slurry and dried in air. All microcapsules appear "deflated".

The microcapsule size range in Figure 2.9 is shown to be between 1-3 µm in diameter. All microcapsules appear "deflated", thus eliminating the action of filtering as a possible cause of deflation. Therefore, the cause of deflation was concluded to be from internal phase leaching.

Variation of Morphology with Viscosity of Internal Phase

In a separate experiment to prevent microcapsule deflation, a solid internal phase (at room temperature) of cetyl alcohol was used. In order to visualise the internal phase using fluorescence microscopy, the fluorophore, 9,10-bisphenylethynylanthracene was dissolved into the cetyl alcohol (1 % by weight) by heating at 348 K. Microencapsulation of 9,10-bisphenylethynylanthracence has not been carried out before and therefore, preparation and characterisation of these microcapsules is novel. The resulting microcapsules were characterised by optical microscopy using epi fluorescence microscopy (Figure 2.10). Interestingly, the microcapsules shown in Figure 2.10 are spherical with a smooth outer coating. There are no signs of

microcapsule surface roughness and also none of the initial signs of "deflation". In (a), the particle size diameters observed range from 2-11 μm. However, a high distribution of the microcapsule sample in (a) is seen to have diameters ranging between 5-8 μm. In Figure 2.10 (b), two large microcapsules are shown in focus. The largest microcapsule is shown to have a diameter of *ca.* 14 μm, whereas the smaller capsule has a diameter of *ca.* 10 μm. Both microcapsules show the polymer wall clearly as a thin smooth coating around the internal phase.

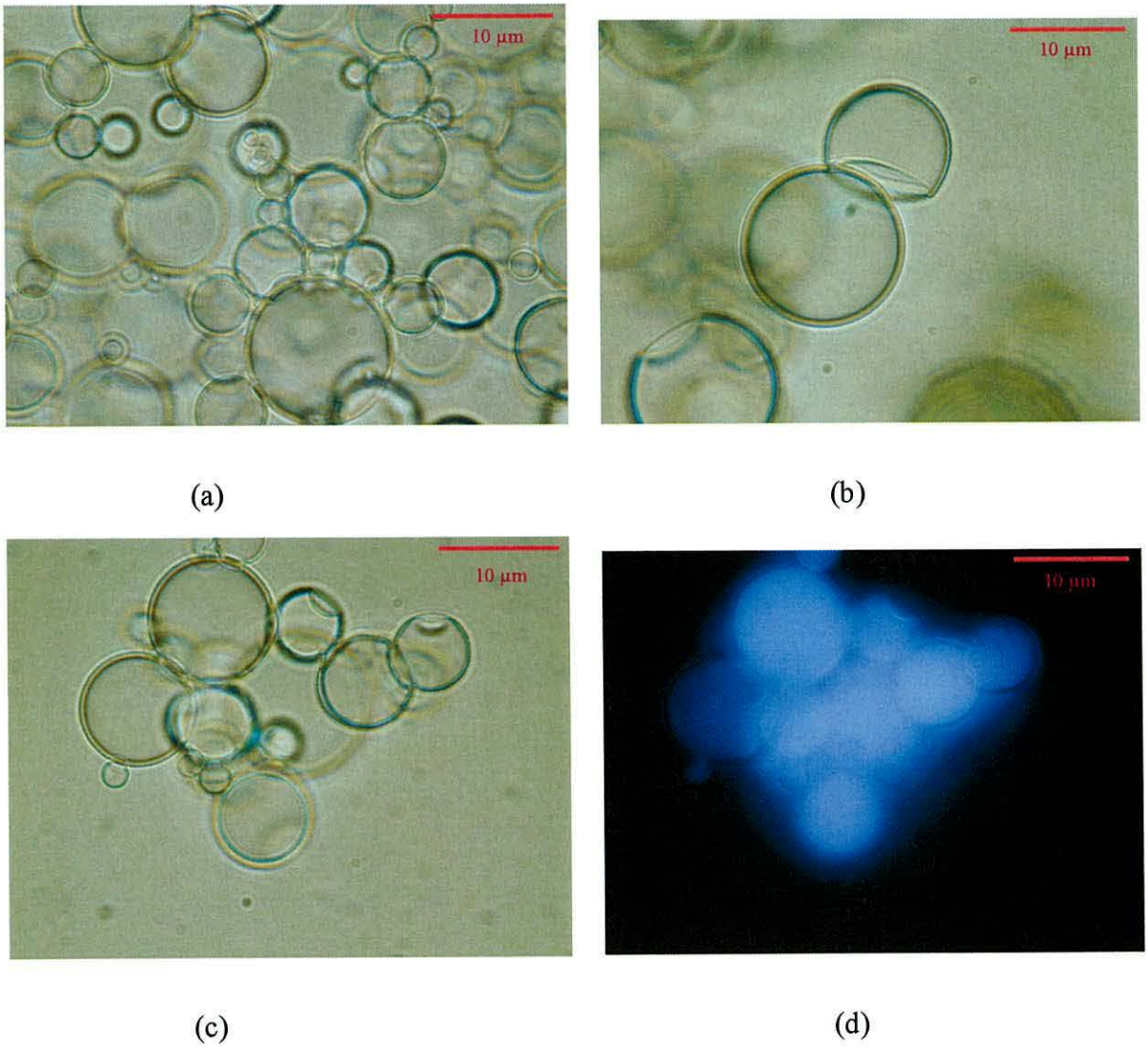

Figure 2.10. Optical micrographs (a)-(c) showing a collection of melamine-formaldehyde microcapsules containing an internal phase of fluorophore, 9,10-bisphenylethynylanthracene in cetyl alcohol. Fluorescence micrograph (d) showing a collection of microcapsules.

In (c), the microcapsule diameters shown range from 2-10 μm, confirming this particle size range is consistent throughout the microcapsule sample batch. The

microencapsulation experiment using fluorophore doped cetyl alcohol as IP was carried out using a stirring speed of *ca.* 10,000 rpm. The particle sizes and particle size distribution of these microcapsules has been discussed and are larger compared to the toluene filled microcapsules made using the same stirring speed (Figure 2.6). Therefore, it can be concluded that upon increasing the IP viscosity, the microcapsule size increases also. The microcapsules are colourless to the eye, however when subjected to ultra violet (UV) radiation to excite the fluorophore doped internal phase, the resulting UV irradiated image is blue. The image was captured using a digital camera attached to the microscope and is shown in (d). The blue image is a manifestation of the filter used with no particular signification in itself. The internal phase is shown to be fully encapsulated within the melamine-formaldehyde polymer because no fluorophore is shown outside of the capsule. In (d), the blue fluorescence is shown to be more intense coming from the microcapsules which are grouped in the middle of the image than the periphery microcapsules. This can be explained by two reasons. Either the periphery microcapsules contain less fluorophore than the microcapsules shown at the centre of the image, which is unlikely since the fluorophore was fully dissolved into the internal phase and should therefore be uniformly distributed into each microcapsule, or the image shows the periphery microcapsules at a different depth of focus. Since optical microscopy is noted for having a limited depth of focus, this reason is more likely to explain the appearance of the image in (d). All four micrographs shown in Figure 2.10 were taken one year after microcapsule production. Therefore, these images show that microcapsules containing a solid internal phase at room temperature do not reduce in size or show any signs of deflation as was seen previously for toluene containing microcapsules.

The solid IP microcapsules at room temperature were gold coated and characterised using SEM (Figure 2.11). The SEM images confirm all the microcapsules containing cetyl alcohol have retained the spherical shape. Again, no apparent signs of "deflation" were observed as seen previously in SEM images of microcapsules containing toluene. The surface morphology is shown to be smooth in all SEM images. The particle size distribution appears to be between 2-10 μm. This correlates with the particle size distribution shown in the optical images (Figure 2.10). To conclude the microencapsulation procedure stated as method 1 in this thesis has been used to produce melamine-formaldehyde microcapsules containing organic liquid internal phases.

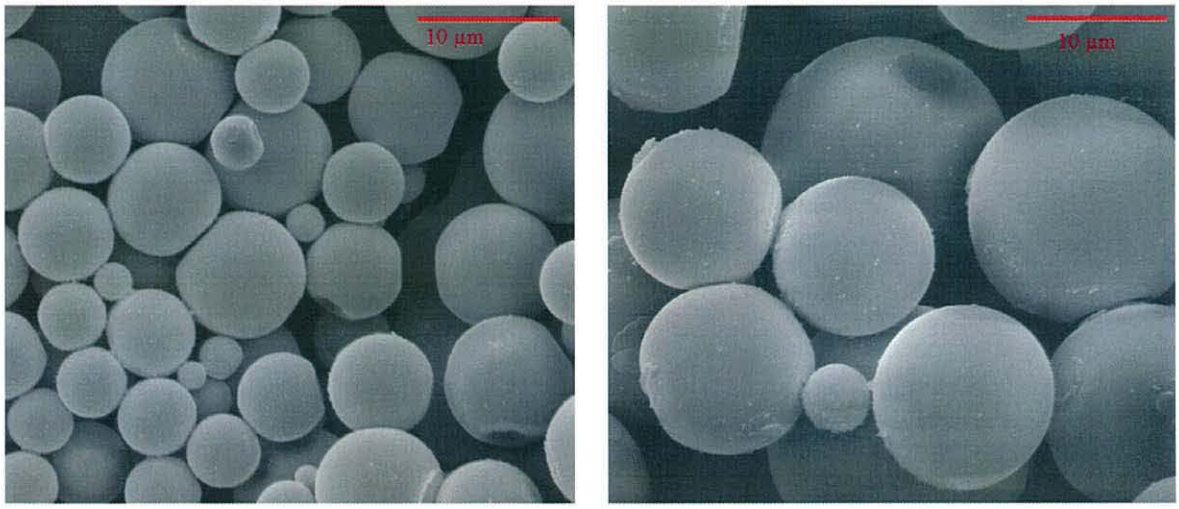

(a) (b)

Figure 2.11. SEM images showing microcapsules containing the fluorophore, 9,10-bisphenylethynylanthracene doped cetyl alcohol as IP.

This has been shown thus far by optical, fluorescence and SEM images. These micrographs show that when the IP possesses a low viscosity, the resulting microcapsules appear "deflated". However, such capsule anomaly is not seen when the IP possesses a high viscosity. Rather, the microcapsule shape is retained. Mixing speed tests carried out during the microencapsulation process confirmed the theory that faster emulsion mixing produces smaller sized microcapsules.

Although this microencapsulation procedure has been shown to encapsulate organic liquids, the biggest hindrance to using this procedure to microencapsulate homogeneous catalysts is the EMA emulsifier. The physicochemical properties of EMA are such that it causes severe agglomeration of microcapsules in the slurry after production, making it difficult to separate large quantities of microcapsules for both easier handling and further capsule analysis (*eg.* quantification of IP). Therefore, an alternative surfactant to EMA was sought for solution 1. This led to the development of a similar microencapsulation procedure, labelled "method 2" in this thesis.

2.3. Microencapsulation: method development

The literature was searched to find an alternative surfactant that still maintained a stable oil-in-water emulsion, yet enabling filtration of the microcapsules. A US patent (US

4,957,949) was found which addressed these problems. [14] The melamine-formaldehyde *in situ* microencapsulation procedure stated within this patent uses a commercially available surfactant, Demol NL (Kao, Japan) in solution 1 (the oil-supporting external aqueous phase). Demol NL is an aqueous solution of sodium 2-naphthalene sulfonate formaldehyde condensate (41% solids by weight), (Figure 2.12).

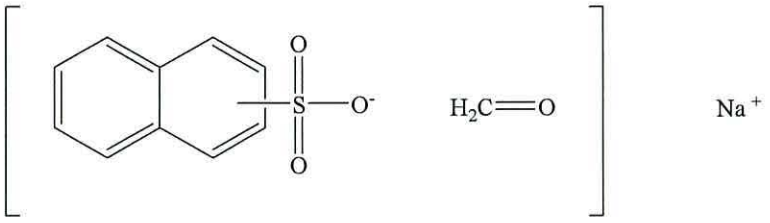

Figure 2.12. Chemical structure of the commercial surfactant Demol NL.

It is claimed in the patent that using Demol NL as surfactant in the external aqueous layer, allows the resultant microcapsule slurry to be easily filtered, yielding a free flowing powder of microcapsules. [14] Therefore, after obtaining Demol NL as a gift from Koa Inc. (Japan), microencapsulation experiments using toluene as IP were carried out to try to achieve a free flowing powder of microcapsules. Initially, microencapsulation method development focused upon the surfactant Demol NL directly replacing EMA in method 1. However, it was noted that EMA served two purposes in method 1, *i.e.* it had the function of creating and maintaining the optimum pH (4.2) for melamine-formaldehyde polymerization, and it acted as a surfactant. On this basis, an external acidic buffer consisting of 0.1 M potassium hydrogen phthalate and 0.1 M sodium hydroxide also was added with the Demol NL.

Initially the concentration of aqueous Demol NL solution used in the method was 1.5 % by weight in comparison with 3 % by weight for an aqueous EMA solution. The surfactant concentration was lowered to observe whether such a concentration level would stabilize the oil-in-water emulsion. It is known that emulsions consisting of microscopic droplets of 0.1- 50 μm and dispersed in a continuous phase are thermodynamically unstable, tending to coalesce so that there is a net reduction in the interfacial area (*i.e.* coalescence is a thermodynamic spontaneous process).[8] However, it is also known that the presence of a surfactant at an optimum concentration level will prevent such coalescence occurring. Microencapsulation trials were thus carried out

using this formulation and were initially unsuccessful. Instead the formation of large clumps of polymeric material soon appeared during the procedure after the pre-polymer was added to the oil-in-water emulsion.

(a) (b) (c)

Figure 2.13. Photographs showing resulting microcapsule slurry when solution 1 contains (a) too low surfactant concentration (1.5 %), (b) an excess surfactant concentration (10 %), and (c) an optimum surfactant concentration (3%).

The photograph shown in Figure 2.13 (a) is of a beaker containing such polymeric clumps obtained after a failed encapsulation due to the surfactant concentration being too low (1.5 %). In comparison, the photograph in Figure 2.13 (b) shows a failed encapsulation due to the surfactant concentration being too high (10%) and the photograph in Figure 2.13 (c) is of microcapsule slurry obtained after the optimum surfactant concentration was used (3%). From such observations, it was concluded that microcapsules were unable to be formed using Demol NL at such a low concentration of 1.5 % since this concentration was not able to support the oil-in-water emulsion.

Therefore, the methodology was developed by increasing the Demol NL concentration from 1.5 % to 3 % to increase the emulsion stability. The final method was modified from the aforementioned patent methodology and was labelled as method 2 throughout this thesis. It is summarized in the form of a flow diagram (Figure 2.14). To develop the method shown in Figure 2.14, the experimental conditions in the patent were closely followed. However, the polymer curing conditions were modified. Rather than curing the polymer by stirring at 363 K for 1 h with subsequent oven drying at 393 K for 2 h, similar curing conditions to method 1 were implemented by stirring with an overhead stirrer at 363 K for 3 h. Microcapsules were prepared using this modified

procedure. The resulting microcapsule slurry was filtered to yield a "polymer cake" which formed a free flowing powder after drying.

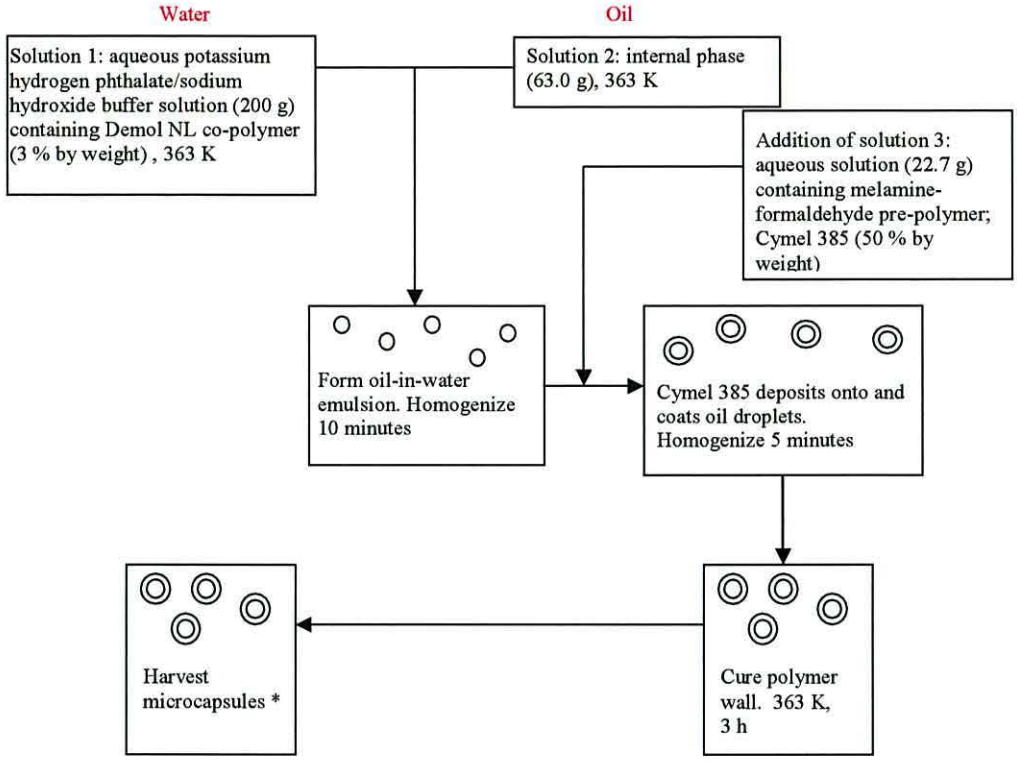

Figure 2.14. A flow diagram describing the microencapsulation process of method 2.

The filtered microcapsules containing toluene were characterized using SEM (Figure 2.15). Both SEM images show that the microcapsule size range is between 5-20 μm. This is a larger particle size diameter than for microcapsules formed using method 1. The reasons for this increased particle size diameter are two-fold. Firstly, a different surfactant was used. The change in surfactant may have bearing on the microcapsule size if a higher proportion of the Demol NL surfactant is incorporated into the microcapsule wall in comparison with the EMA surfactant. Secondly, a lower mixing speed (*ca.* 4,000 rpm) was used in this microencapsulation experiment since mixing speeds ($\geq$ 4000 rpm) caused excessive frothing of surfactant, which caused practical problems in handling the experiment. However, the toluene filled microcapsules formed using method 2 are still much larger (5-20 μm) than toluene filled microcapsules formed using method 1 (3-6 μm) when using the same mixing speed of 4,000 rpm. In the SEM images particulate matter adheres to the microcapsules. Such particulate matter is attributed to melamine-formaldehyde nanoparticles as described

elsewhere in the literature. [12] The SEM image in Figure 2.15 (a) shows a high number of microcapsules to be "deflated", as was seen in previous SEM images of microcapsules containing toluene. The microcapsules were imaged by SEM approximately two weeks after formation.

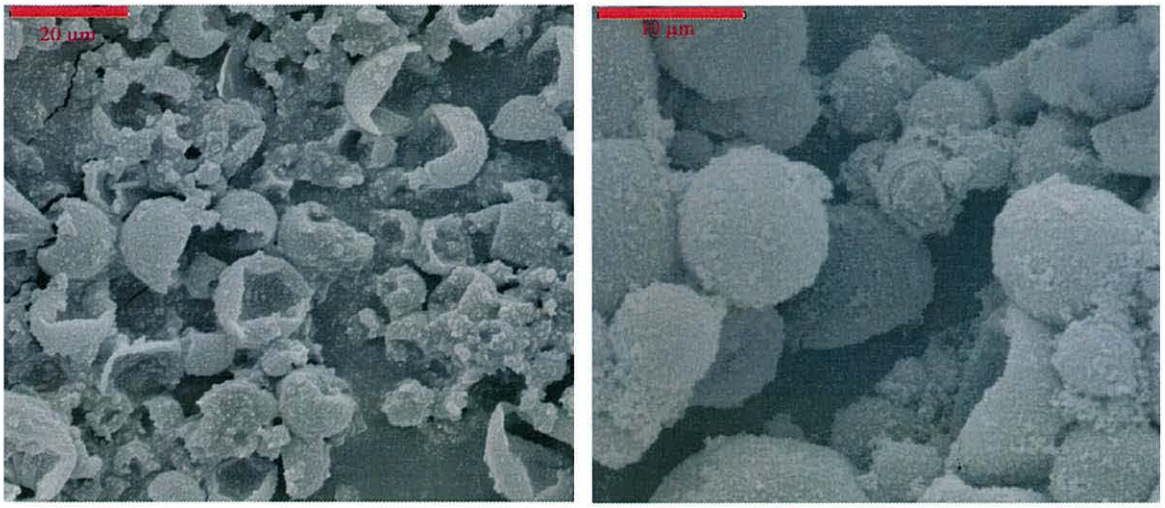

(a) (b)

Figure 2.15. SEM images of filtered toluene containing capsules made using microencapsulation method 2.

In a previously discussed experiment, microcapsules made using method 1 containing a fluorophore (9,10-bisphenylethynylanthracene) doped internal phase of cetyl alcohol were imaged using fluorescence microscopy, showing the internal phase to be fully encapsulated (see section 2.1). In a similar experiment to prove method 2 effectively encapsulates the internal phase, microcapsules were prepared using the same fluorophore, 9,10-bisphenylethynylanthracene. The IP used in method 2 encapsulations so far has been toluene. However, it was found that 9,10-bisphenylethynylanthracene was more soluble in chlorobenzene than toluene, therefore the IP used for the microencapsulation experiment was a chlorobenzene solution of 9,10-bisphenylethynylanthracene (1% as weight). Such a solution was chosen over cetyl alcohol since the aim of the experiment was to be able to visualise the internal phase of liquid filled microcapsules rather than solid filled (at room temperature) microcapsules. The resulting microcapsules were imaged using both optical microscopy and epi fluorescence (Figure 2.16). The microcapsules were imaged using optical microscopy immediately after production. The image in (a) shows slight deflation at the top and at

the sides of the microcapsules, yet the spherical shape is still maintained. The particle sizes shown range from *ca.* 3-10 μm, with the majority of microcapsules *ca.* 10 μm in diameter. These capsule sizes correlate with the SEM images of the toluene filled microcapsules made using method 2 which showed a capsule size distribution of *ca.* 5-20 μm. In (b), the image clearly shows the internal phase is fully encapsulated, and that the fluorophore is uniformly distributed within the IP. As seen before in Figure 2.10 (d), the green fluorescence is shown to be more intense coming from the microcapsules which are grouped in the middle of the image than the periphery microcapsules. Again, this is explained by the periphery microcapsules captured at a different depth of focus than the central microcapsules in the image.

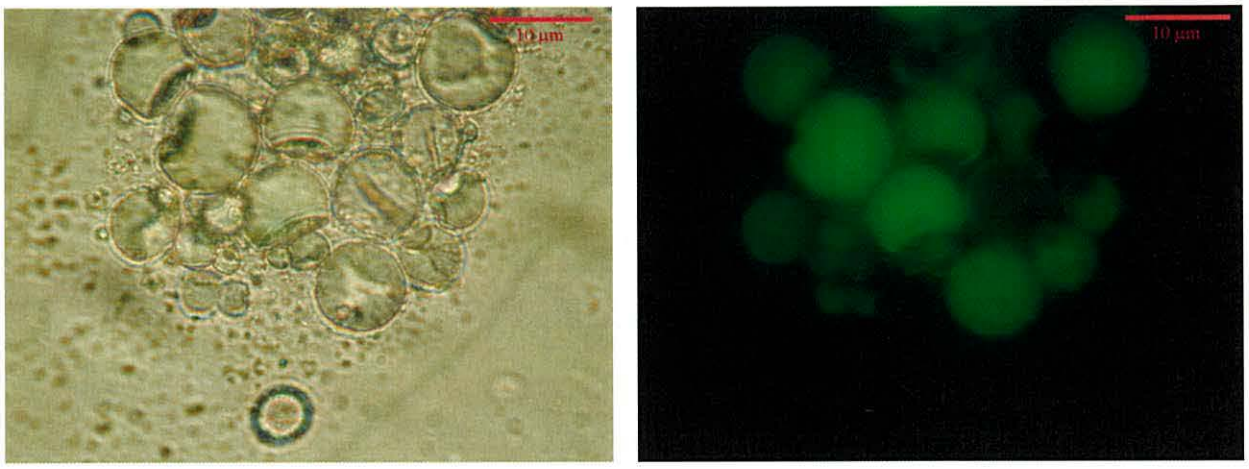

(a) (b)

Figure 2.16. Micrographs: optical (a) and epi fluorescent (b), showing microcapsules containing an internal phase of fluorophore, 9,10-bisphenylethynylanthracene doped chlorobenzene. All magnifications (x 1000).

The same batch of microcapsules was re-examined using fluorescence microscopy after approximately 1 month of storage (slurry form) in a sealed glass jar (Figure 2.17). The six images shown in Figure 2.17 are snapshots of different microcapsules from the same batch of aged slurry. The images show that although some microcapsules are spherical and intact with IP fully encapsulated as seen in Figure 2.17 (a), the majority of the microcapsules in the aged sample appear "deflated", as seen in the remaining five images shown in Figure 2.17. The size of the largest microcapsule in (a) is *ca.* 8 μm. In (b), the fluorescence image is stronger at the periphery of the microcapsules than the centre of the capsules, suggesting that the internal phase has migrated from the centre

towards the capsule walls. Also, the majority of capsules are *ca.* 5 μm in diameter which is a reduced size in comparison with the intact capsules shown in (a).

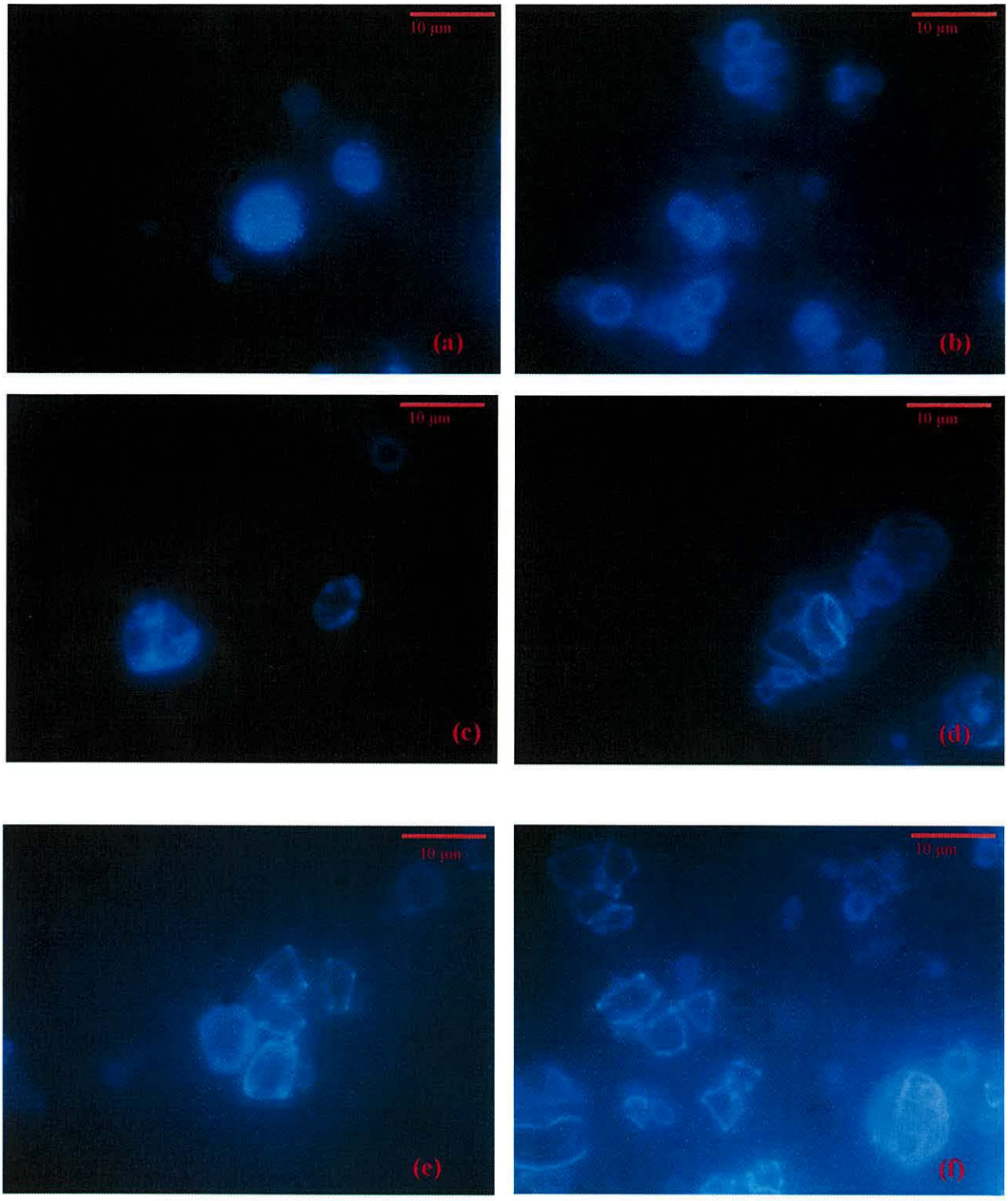

Figure 2.17. Fluorescent micrographs showing intact microcapsules (a), beginnings of IP leach (b) and (c), majority of capsules "deflated", yet retaining fluorophore within capsule wall after IP leaching (d), (e) and (f). Magnification (x 1000).

These observations are again made in the images labelled (d), (e), and (f). In (c), a large microcapsule is shown *ca.* 10 μm in diameter. Despite the retention of the large particle size, the shape of the capsule is non-spherical in comparison with the image shown in (a), thus suggesting the onset of "deflation". The images seen in (d), (e), and (f) show microcapsules that have lost the original spherical shape, and now appear irregular with the fluorophore located at the IP/polymer wall interface. Such images lead to the suggestion that IP is leaching from the microcapsules, and altering the capsule shape in the process.

As before (in section 2.1), to compare the difference in microcapsule morphology when using a more viscous internal phase, a batch of microcapsules was prepared using method 2 with an internal phase consisting of cetyl alcohol doped with the commercial blue dye, Pergascript blue (Ciba) (see section 5.3.6 for details). The resulting microcapsules were characterized using optical microscopy (Figure 2.18).

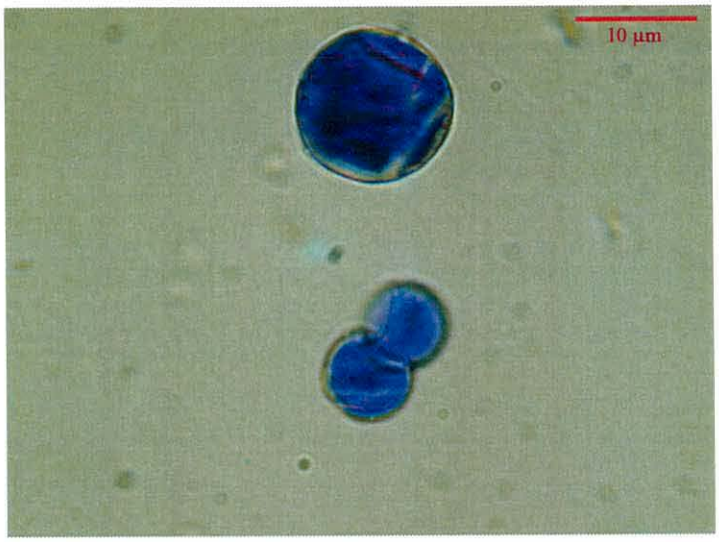

Figure 2.18. An optical micrograph showing intact microcapsules containing blue dye. Magnification (x 1000).

The image in Figure 2.18 shows that when a more viscous IP is used the microcapsule spherical shape is retained and microcapsule deflation is not apparent, as was seen earlier in method 1 encapsulations. The blue dye is seen to be fully encapsulated within the polymer wall. The particle size for the large microcapsule shown in Figure 2.18 is *ca.* 13 μm. The other two microcapsules shown are *ca.* 8 μm in diameter. These microcapsule sizes correlate with other microcapsule batches made using method 2.

Confocal laser scanning microscopy (CLSM)

Polymer wall imaging

Microcapsules made using method 2 were imaged using confocal scanning laser microscopy (CLSM) for the purposes of, visualizing polymer wall thickness, looking inside the microcapsule, and looking inside the polymer wall. Similar investigations using CLSM have been carried out on fluorophore tagged (rhodamine B, fluorescein isothiocyanate) gelatin-gum arabic microcapsules. [15] However, the fluorophore chosen in this work to image the melamine-formaldehyde polymer wall was 9-anthraldehyde (Aldrich). It was carefully selected because of the aldehyde functional group, reasoning that such a fluorophore could easily be incorporated into the melamine-formaldehyde pre-polymer because any free NH_2 end groups attached to the melamine moiety would be available for reacting with the aldehyde in the same way as formaldehyde reacts with melamine (see Chapter 1, Figure 1.9).

The pre-polymer was therefore fluorescently tagged by mixing 9-anthraldehyde and Cymel 385 together in a beaker at room temperature for 20 minutes. Observations of the resulting mixture after this time period showed the fluorophore to be only partially dissolved into the aqueous resin. Therefore, the suspension was subsequently heated to 363 K (the temperature used in method 2 microencapsulation experiments) in order to try to dissolve as much fluorophore as possible into the aqueous polymer mixture. After 10 minutes of stirring at this elevated temperature, the suspension was removed from the heat and centrifuged at 14,000 rpm for 5 minutes to separate the undissolved fluorophore particles from the fluorophore tagged pre-polymer supernatant. The yellow supernatant was decanted and was re-heated to 363 K to be used as solution 3 in accordance with the method 2 microencapsulation procedure.

Subsequently, a batch of microcapsules was made using the fluorescently tagged pre-polymer. The fluorophore (9-anthraldehyde) attaches to the melamine-formaldehyde pre-polymer by nucleophilic attack of the amine nitrogen onto the carboxyl group of the 9-anthraldehyde, to form an alcohol. An acidic proton bonded to the positively charged four co-ordinate nitrogen atom is removed by the basic environment, thus returning the nitrogen to a three co-ordinate neutral atom and resulting in the formation of a fluorescently tagged amine resin (Figure 2.19).

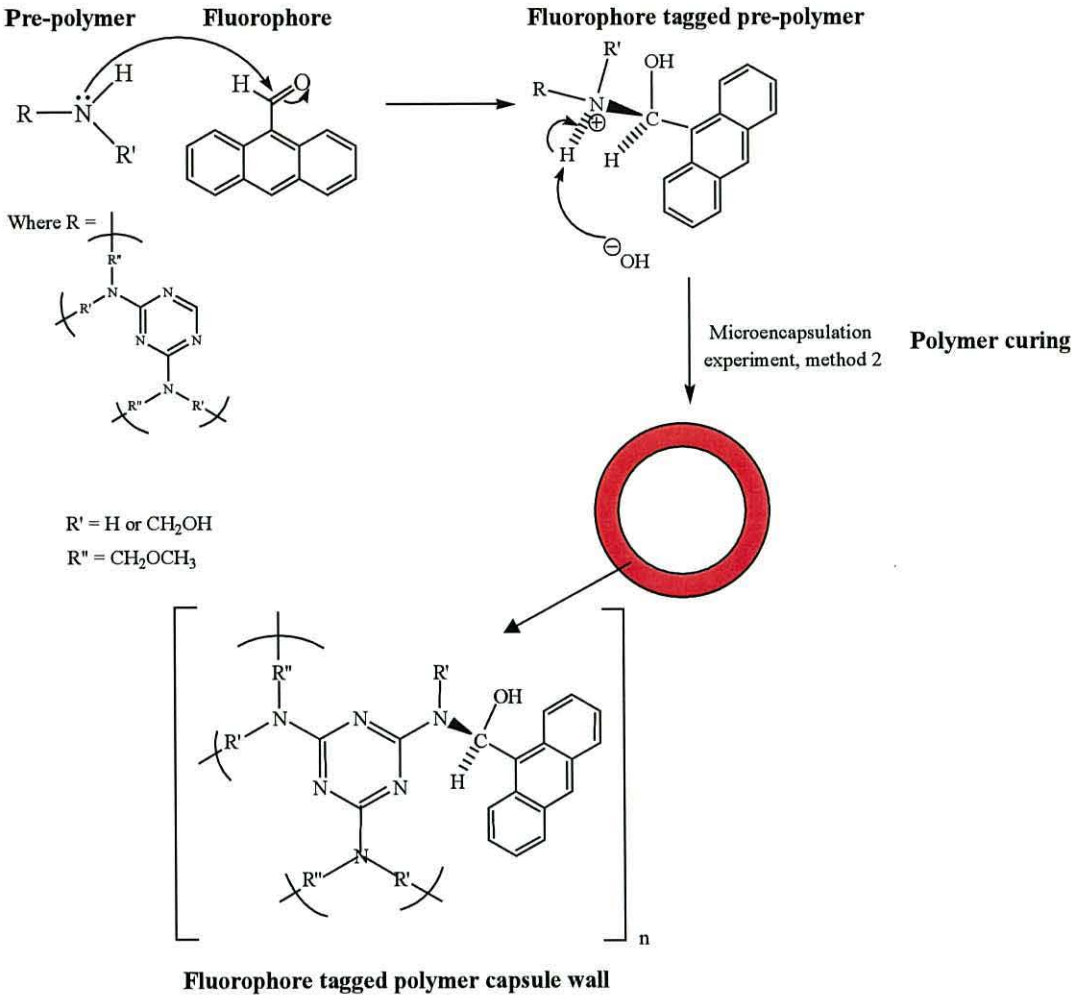

Figure 2.19. Schematic diagram showing how 9-anthraldehyde reacts with Cymel 385 to form the fluorophore tagged pre-polymer.

The microcapsules made contained a chlorobenzene solution of the organic dye; 5-[*p*-(dimethylamino)benzylidene]rhodanine. The optical properties of 9-anthraldehyde were required for configuring the confocal microscope as it was predicted that the fluorophore tagged polymer would possess similar optical properties. Therefore, the literature was checked and excitation and emission wavelengths of a solution of 9-anthraldehyde in methanol are λ_{max} = 390 nm and λ_{max} = 420 nm. [16,17] Subsequently, the confocal laser scanning microscope was configured using the laser line 488 nm (10 % intensity) as excitation source. Two beam splitters, HFT 488 nm and NFT 490 nm were employed in the configuration set up to direct the fluorescence emission towards the detector which was screened using a long pass filter 505 nm (LP 505 nm). A

schematic diagram of the confocal laser scanning microscope configuration for specific imaging of 9-anthraldehyde doped polymer wall microcapsules is shown (Figure 2.20).

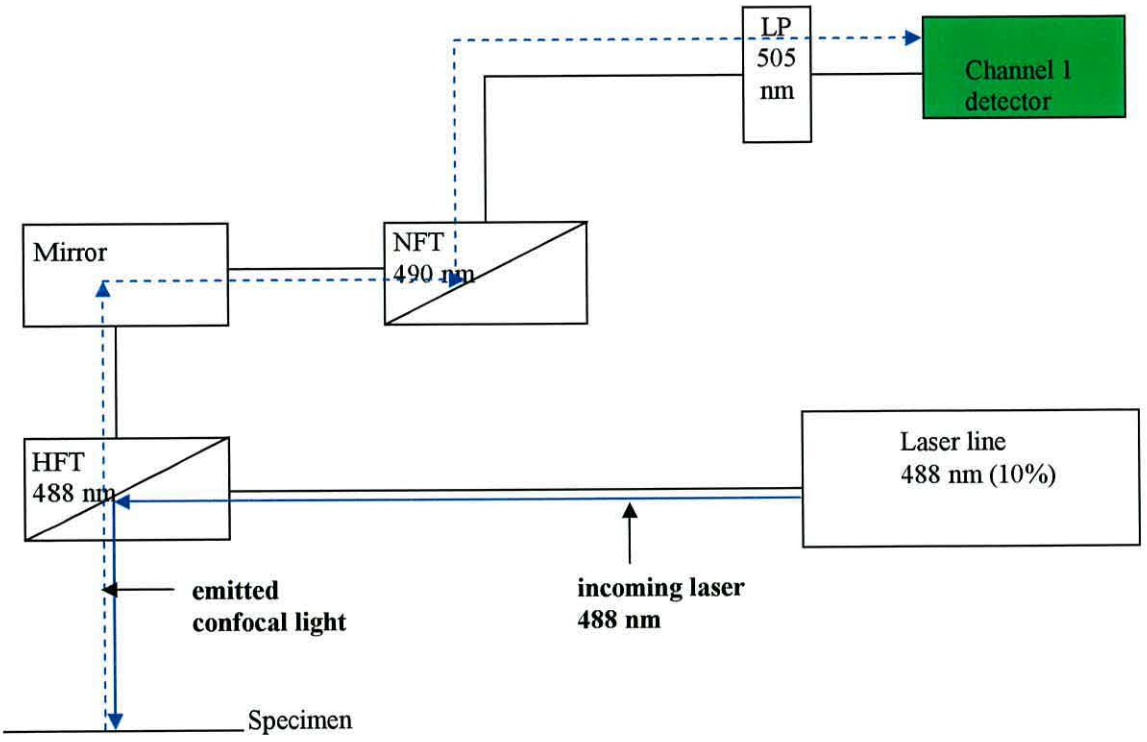

Figure 2.20. CLSM configuration used for imaging the 9-anthraldehyde tagged polymer wall.

The blue solid arrows in Figure 2.20 depict the laser path of the excitation wavelength at 488 nm. The first beam splitter (HFT 488) allows the excitation source to pass through targeting the specimen. The specimen is excited at this wavelength, producing a fluorescent emission. The fluorescence emission wavelengths (represented by the blue dashed arrows) above 488 nm pass through the beam splitter (which is a dichroic mirror), and are reflected by a normal mirror into another beam splitter (NFT 490). This beam splitter (also a dichroic mirror) only allows wavelengths above 490 nm to pass through to the detector. The detector is screened using a long pass filter (LP 505) which blocks off any wavelengths below 505 nm, allowing all others to penetrate through to the photomultiplier detector. The microcapsules were then prepared for imaging by firstly filtering the slurry to isolate the microcapsules. The retained microcapsules were dried for 1 h and the microscope slide was prepared by placing a drop of immersion oil onto the glass slide. A sub-sample of microcapsules (*ca.* 1 mg) was dispersed evenly into the immersion oil. Thereafter, a series of confocal

micrographs were taken of the fluorophore tagged polymer microcapsules. An example is shown in Figure 2.21.

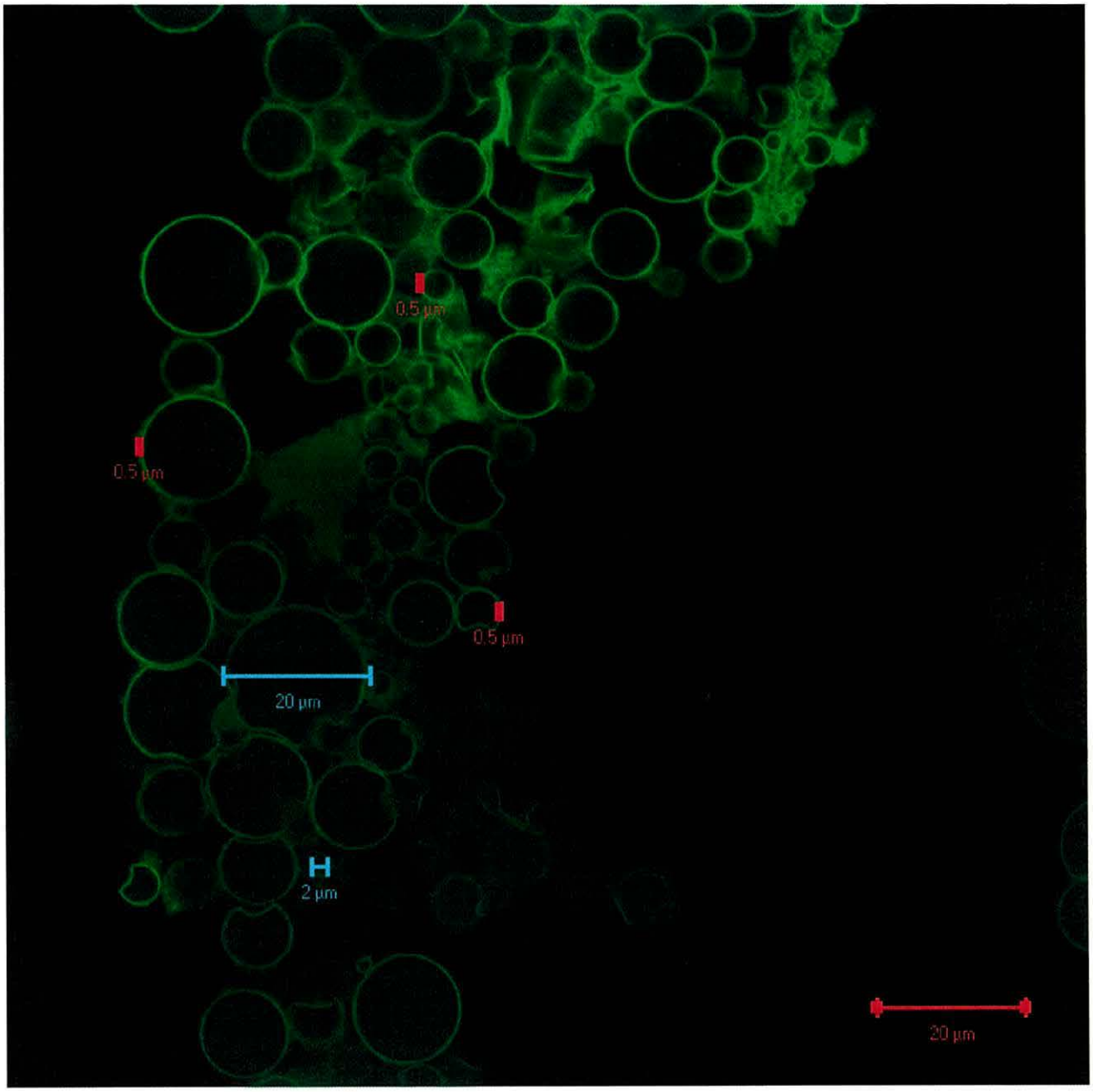

Figure 2.21. Confocal micrograph showing microcapsules with 9-anthraldehyde tagged polymer wall. Magnification (x 630).

The image in Figure 2.21 clearly shows that the fluorophore is uniformly distributed within the polymer wall. Also, a large particle size distribution amongst the microcapsules is seen, with capsule diameters ranging from *ca.* 2 µm to 20 µm. This particle size distribution correlates with previous method 2 particle size distributions which were all created using a stirring speed of 4,000 rpm. Despite the microcapsules

containing a liquid internal phase, the majority of capsules shown in Figure 2.21 have retained the spherical microcapsule shape. The polymer wall appears to be of uniform thickness (*ca.* 0.5 μm) for all microcapsules, regardless of microcapsule size. The inside of the microcapsules appear black in the confocal micrograph. This is because the dye molecule, (5-[p-(dimethylamino)benzylidene]rhodanine) is not excited using this particular confocal configuration. Since there is no reported fluorescence data of this molecule, [18] the inside of the microcapsules was expected to show as black in the confocal micrograph.

A separate batch of microcapsules was made using method 2 and a fluorescent probe was then applied to the internal phase and polymer wall to image them in tandem using confocal microscopy. The internal phase was imaged using the commercially available dye, Rhodamine B (Figure 2.22) which is a known fluorophore. The polymer wall was imaged using the same fluorophore as before, *i.e.* 9-anthraldehyde.

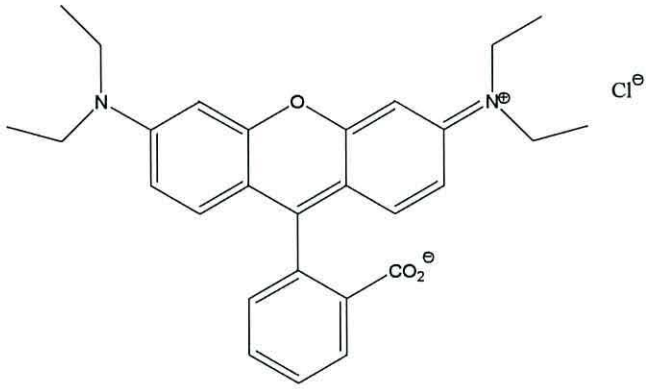

Figure 2.22. Chemical structure of Rhodamine B

Rhodamine B, is commonly used to attach non-covalently to non-fluorescent analytes, thereby enabling quantitative detection. [19] For the purpose of the microencapsulation experiment, it is a good choice for internal phase imaging because it is soluble in cetyl alcohol, one of the internal phases used in this thesis. Microcapsules were prepared using a cetyl alcohol solution of Rhodamine B (0.1 % by weight) as solution 2. 9-Anthraldehyde was tagged to the pre-polymer, Cymel 385 using the same preparative method described earlier. The microcapsules were prepared following method 2. The optical properties of Rhodamine B dissolved in methanol were measured using UV/Visible spectroscopy and fluorescence spectroscopy (Figure 2.23) to establish both

the excitation and emission maxima in order to configure the confocal microscope for imaging the microcapsules. The spectra in Figure 2.23 show an absorbance maxima at 555 nm, and emission maxima at 590 nm in accordance with the literature value. [20] The sharp signals occurring at 555 nm and 590 nm are "marker peaks" inherent to the software used with the fluorescence spectrometer. The markers indicate the excitation and emission values used to collect the emission and excitation scans, respectively.

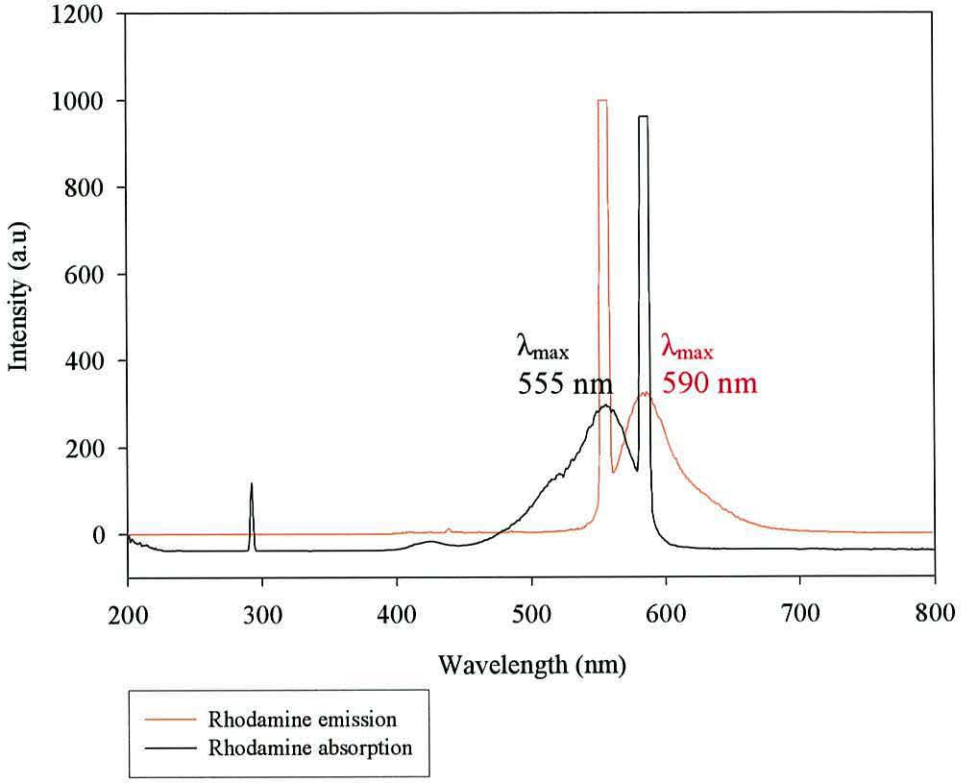

Figure 2.23. Rhodamine B absorption and emission spectra scanned between 200 and 800 nm.

Subsequently, the confocal microscope was configured using the laser line 543 nm (100 % intensity) as excitation source. Two beam splitters, HFT 488/543 and NFT 490 were used to direct fluorescence emission towards the two photomultiplier detectors. One detector was screened using a long pass filter (LP 505), the other detector was screened using a band pass filter (BP 565-615). A schematic diagram of this configuration is shown in Figure 2.24. The blue solid arrows in Figure 2.24 depict the laser path of the excitation wavelength at 543 nm. The first beam splitter (HFT 488/543) allows the excitation source to pass through and interact with the specimen. The specimen (9-

anthraldehyde polymer wall doped microcapsules containing an internal phase of Rhodamine B doped cetyl alcohol) is excited at this wavelength, producing two separate fluorescence spectra from the two different fluorophores. The fluorescence emission wavelengths (represented by the red and green dashed arrows) above 488/543 nm pass through the beam splitter (which is a dichroic mirror), and are reflected by a normal mirror into another beam splitter (NFT 490). This beam splitter (also a dichroic mirror) only allows wavelengths above 490 nm to pass through to the two detectors. One detector is screened using a long pass filter (LP 505) which blocks off any wavelengths below 505 nm, allowing all other wavelengths to penetrate through to the photomultiplier detector. This detector is given an arbitrary green label by the instrument software, LSM 510. The other detector is screened using a band pass filter (BP 565-615), which blocks all wavelengths above 615 nm and below 565 nm. This detector is given an arbitrary red label using the instrument software, LSM 510.

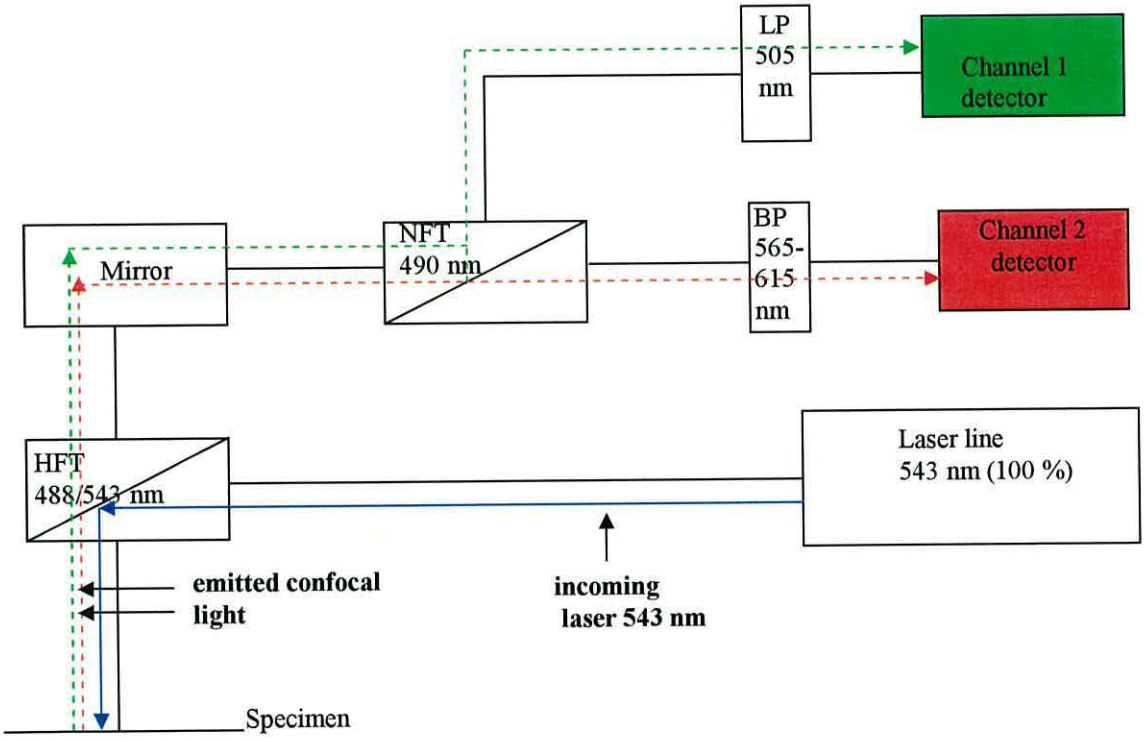

Figure 2.24. CLSM configuration used for imaging microcapsules containing Rhodamine B and anthraldehyde tagged polymer wall.

A series of confocal micrographs were then taken of the microcapsules. One example is shown in Figure 2.25.

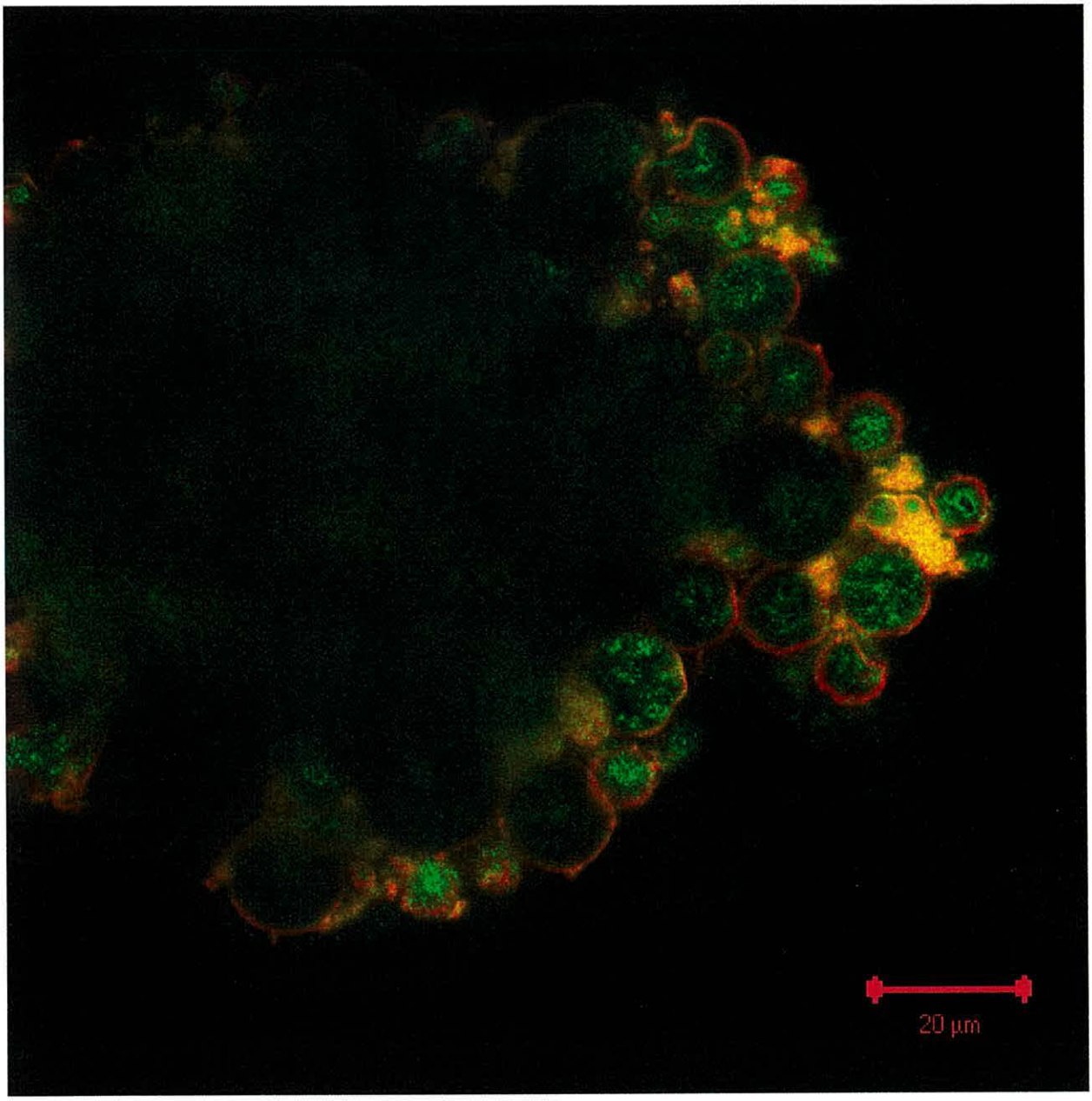

Figure 2.25. Confocal micrograph showing microcapsules containing Rhodamine B doped cetyl alcohol as IP, and 9-anthraldehyde doped polymer wall.

The microcapsules were made using a stirring speed of *ca.* 4,000 rpm following method 2 microencapsulation procedure. The resulting microcapsules particle size distribution is shown to be *ca.* 2-20 µm in diameter. This distribution correlates well with previous microcapsule batches made using method 2. The confocal micrograph was taken at room temperature. Since the microcapsules contain an internal phase of Rhodamine B

doped cetyl alcohol, at room temperature the microcapsules are solid. The solid internal phase explains the retention of spherical shape of these microcapsules with no apparent signs of deflation. Another example is shown in Figure 2.26.

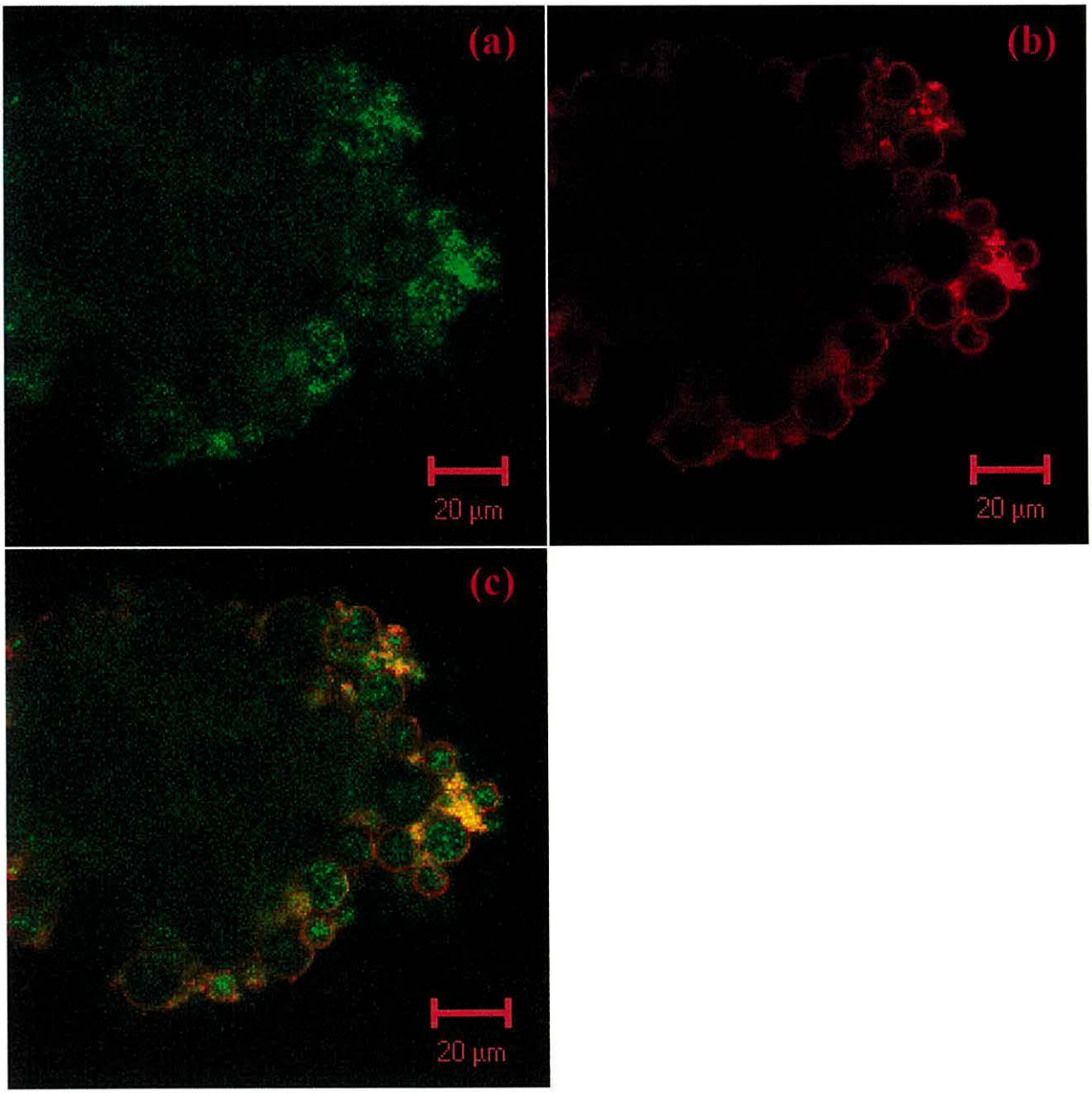

Figure 2.26. Confocal micrograph showing microcapsules containing (a) rhodamine B internal phase only, (b) 9-anthraldehyde derivative doped polymer wall, and (c) a composite of the images in (a) and (b).

Using the confocal configuration stated above, the green area in Figures 2.25 and 2.26 represents rhodamine B emission and the red area in these figures represents 9-anthraldehyde emission. Therefore, it can be concluded that rhodamine B is inside the

microcapsules and 9-anthraldehyde is present in the polymer wall. As discussed earlier, by using the preparative method described in this thesis for incorporating 9-anthraldehyde into the pre-polymer, it can be clearly seen from these micrographs and earlier micrographs that 9-anthraldehyde is uniformly distributed within the melamine-formaldehyde polymer at a macro scale. Again, as observed in earlier micrographs of microcapsules made using method 2, the polymer wall appears to be of uniform thickness (*ca.* 0.5 μm) for all microcapsules, regardless of microcapsule size.

The image in Figure 2.36 is a split image of the confocal image shown in Figure 2.35. In (a), the image of microcapsules is produced by the detector screened using the long pass filter 505 nm, therefore showing rhodamine B representation throughout the microcapsule batch. The image appears patchy which is due to the poor distribution of rhodamine throughout the cetyl alcohol. In (b), the image is produced by the detector screened using the band pass filter 565-615 nm, therefore showing 9-anthraldehyde representation throughout the microcapsule batch. The image shows the fluorophore is uniformly distributed within the polymer wall at a macro scale as described earlier. Finally, in (c) the image is a composite of the two images shown in (a) and (b), displaying signals from both detectors, thus showing both rhodamine B and 9-anthraldehyde representation at the same time.

2.4. Microencapsulation: further characterisation

Method 3 was a microencapsulation procedure developed at the sponsoring company (TMC) to make free-flowing microcapsules at a similar time to when method 2 was being developed at UWB. Therefore, two microencapsulation methods were effectively being developed in tandem for the purpose of eradicating the particle sticking problem associated with microencapsulation method 1. TMC subsequently proposed a "method 3" as an alternative procedure to be tested alongside method 2 for microencapsulation of target compounds. Microencapsulation experiments were thus carried out using this method and the resulting microcapsules were characterized using a variety of microscopy techniques such as optical microscopy, fluorescence microscopy, SEM, and confocal laser scanning microscopy (CLSM). Method 3 materials and procedure are detailed in section 5.1.3 of this thesis. Depending upon the experiment, solution 2 was either a chlorobenzene solution (130 g) of a known fluorophore (1 % by weight) or a

cetyl alcohol (130 g) solution of a known fluorophore (1 % by weight). Method 3 is summarized in the form of a flow diagram (Figure 2.27).

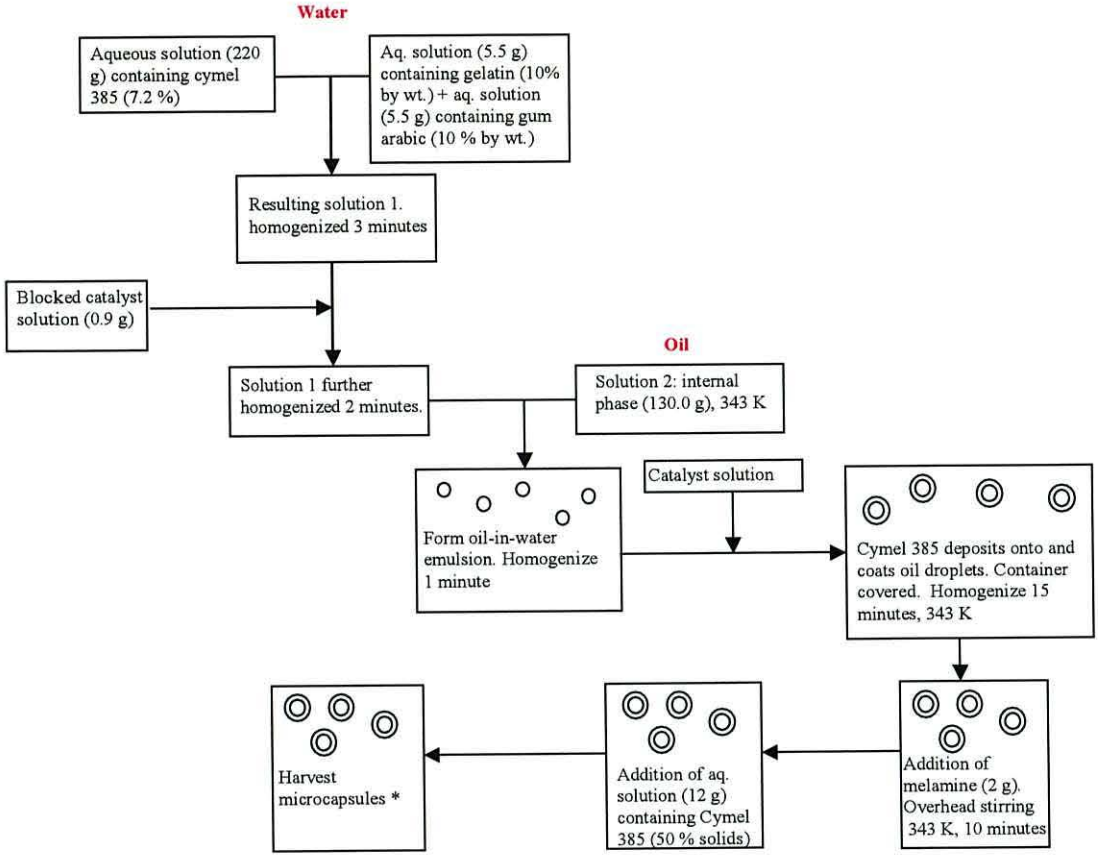

Figure 2.27. A flow diagram describing the microencapsulation process of method 3.

The key differences between method 3 and the methods already described in this thesis (methods 1 and 2) are; the addition of extra steps into the procedure, the sequence of steps in the procedure, and the different compounds used in the procedure. For example, both method 1 and 2 have 4 steps as seen previously in Figures 2.5 and 2.14, respectively. Whereas method 3 has 7 steps in the microencapsulation reaction. The sequence of mixing compounds is altered in method 3 in comparison with the other two methods. For example, the Cymel 385 pre-polymer is added to the surfactant at the beginning of method 3 and is later polymerised using the addition of a "catalyst" initiator. In comparison, the same pre-polymer is added towards the end of the microencapsulation experiment in method 1 and 2. Finally, method 3 uses the compounds gelatin and gum arabic as surfactant, whereas method 1 uses the co-polymer, EMA and method 2 uses Demol NL. Two additional solutions of "blocked

catalyst" and "catalyst" are used in method 3. The blocked catalyst solution is an aqueous solution (0.9 g) made up of *p*-toluene sulphonic acid (0.50 g), triethanolamine (0.16 g), isobutanol (0.16 g) and water (0.08 g), and is used to breakdown any large particles that may arise from the mixing of Cymel 385 pre-polymer and surfactant at high mixing speeds of *ca.* 10,000 rpm. The catalyst solution is an aqueous solution (1.1 g) made up of formic acid (0.45 g), phosphoric acid (0.25 g), *p*-toluene sulphonic acid (0.25 g) and water (0.15 g), and is used to initiate polymerisation of the Cymel 385 polymer.

Confocal Laser Scanning Microscopy

Internal phase imaging

The optical properties of 9,10-bisphenylethynylanthracene (Figure 2.28) are well known. [20] As a consequence, this fluorophore was encapsulated earlier using both method 1 and method 2 to image the internal phase of melamine-formaldehyde microcapsules using optical microscopy with epi-fluorescence.

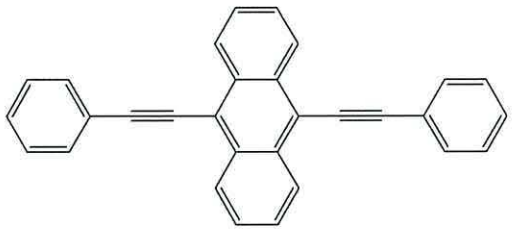

Figure 2.28. Chemical structure of 9,10-bisphenylethynylanthracene

The microcapsule images (Figure 2.10, and 2.16) showed 9,10-bisphenylethynylanthracene to possess good solubility in both cetyl alcohol and chlorobenzene, which were the microcapsule internal phases of method 1 and method 2, respectively. In a similar experiment, the same fluorophore was encapsulated for imaging the internal phase of microcapsules made using method 3. However, the characterisation method used to examine method 3 microcapsules was confocal laser scanning microscopy (CLSM). The advantages of using CLSM over optical microscopy with epi-fluorescence is, to be able to image the inside of the microcapsules, and to be able to build a three dimensional image of each microcapsule within the sample, thus enabling microcapsule surface and core to be examined in

greater detail. Two separate microencapsulation experiments were carried out using method 3. Firstly, microcapsules were prepared using an internal phase of cetyl alcohol solution containing 9,10-bisphenylethynylanthracene (1 % by weight). Secondly, microcapsules were prepared using an internal phase of chlorobenzene solution containing 9,10-bisphenylethynylanthracene (1 % by weight). By using different internal phases with distinctly different physical properties (*i.e.* physical states at room temperature), the resulting microcapsule morphology could be compared. A sample of 9,10-bisphenylethynylanthracene was donated from the research group laboratory at UWB. The absorbance maxima at 490 nm and emission maxima at 510 nm are known for 9,10-bisphenylethynylanthracene. [20] Therefore, the configuration of the confocal microscope was set up to be able to image microcapsules containing this compound. The microcapsules were prepared for imaging in the same way as before (see section 5.8.2 for details).

A series of confocal micrographs were taken of the microcapsules. One example of microcapsules containing 9,10-bisphenylethynylanthracene in cetyl alcohol is shown in Figure 2.29. The sample was relatively easy to image. The micrograph was taken using a magnification of (x 430) and was taken at room temperature, therefore the internal phase is solid (mp = 321 K). [21] The bright spots appearing on several of the microcapsules are caused by the internal phase solution (cetyl alcohol containing 9,10-bisphenylethynylanthracene) solidifying at room temperature. A large particle size distribution of microcapsules is shown, ranging from *ca.* 3 μm to 50 μm, although the majority of microcapsules shown are between the size range 40 -50 μm. Both particle sizes, and particle size distribution are much larger for method 3 microcapsules compared with method 1 (3-6 μm) and method 2 (5-20 μm) microcapsules. This could be explained by the surfactant used in method 3 experiments. That is, aqueous solutions of gelatin and gum arabic are mixed together at high speeds with Cymel 385 pre-polymer in method 3 (Figure 2.27). Since microcapsule walls can also be made from gelatin-gum arabic polymers, [22] it is feasible to suggest that a large concentration of gelatin and gum arabic from the method 3 experiment forms part of the polymer wall as the Cymel 385 cures and thus, accounting for the increased microcapsule particle sizes.

The smaller sized microcapsules (< 10 μm) appear spherical, although microcapsule detail cannot be seen clearly at this magnification. However, detail can be seen on the larger sized microcapsules (> 40 μm). The shapes of these larger sized

microcapsules are not fully spherical in comparison with the majority of the smaller sized microcapsules. Also, the microcapsule morphology appears to be layered. This is in contrast with optical microscopy images of method 1 microcapsules containing the same internal phase (Figure 2.10) which showed the capsule morphology to be smooth.

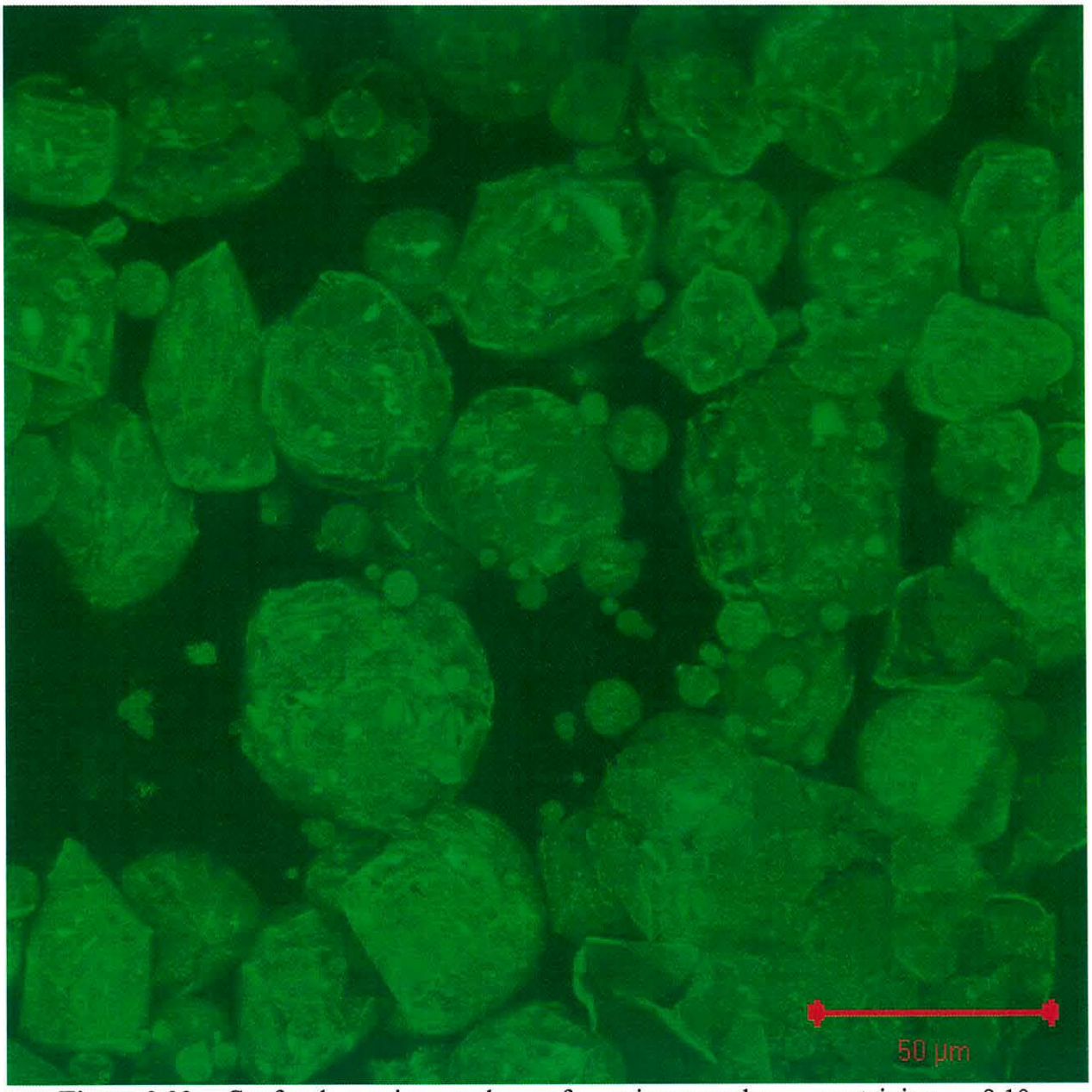

Figure 2.29. Confocal micrograph of microcapsules containing 9,10-bisphenylethynylanthracene doped cetyl alcohol as internal phase. Magnification (x 430).

Microcapsule shape and morphology is determined by the process of microencapsulation. Therefore, the larger microcapsule non spherical shape can be explained by events occurring within the procedure (such as change in surfactant and

also change in sequence of addition of microencapsulation reagents) that were unable to maintain a perfect sphere shape. The CLSM image in Figure 2.29 can be viewed as a "snapshot" of the microencapsulation process. Therefore, the observed microcapsule shapes are from the polymer coating the non perfect sphere in several layers. The CLSM micrograph in Figure 2.29 is generated from a series of stacked images that were taken from different focal planes through a selected microcapsule within the sample. Firstly, the microcapsule was sectioned into *ca.* 30 equal sections using the confocal software. The resulting images taken at each focal plane were subsequently used to form the composite confocal image shown in Figure 2.29.

In Figure 2.30, one example of a confocal micrograph of microcapsules containing 9,10-bisphenylethynylanthracene in chlorobenzene is shown. The microcapsules in Figure 2.30 were captured using a magnification of (x 630). The sample was easy to image. This image of the chlorobenzene containing microcapsules (doped with 9,10- bisphenylethynylanthracene) was generated from one focal plane only, which is in contrast with the previous image (Figure 2.29). The particle size distribution of the microcapsule diameters in Figure 2.30 appear to range from 4 μm to 8 μm. These capsules are *ca.* 10 times smaller than microcapsules containing cetyl alcohol produced using the same method 3.

Many microcapsules in Figure 2.30 have the appearance of a black circle surrounded with a fluorescent green circle. This is showing concentrated fluorophore at the polymer wall, indicating that the fluorophore has migrated from the centre of the microcapsule to the internal phase/polymer wall interface, thus supporting evidence of IP leaching seen earlier in various micrographs in this chapter. The leaching theory is again supported by the size of the microcapsules. The chlorobenzene containing microcapsules (maximum size, *ca.* 10 μm) appear approximately 20 % smaller than the cetyl alcohol containing microcapsules (maximum size, *ca.* 50 μm). Both microcapsules were generated following the same microencapsulation procedure (method 3). Some microcapsules in Figure 2.44 appear to have "collapsed". The polymer wall is seen to fold in towards the centre of the microcapsule. Again, the middle of the microcapsule is dark and the fluorophore appears to be concentrated at the polymer wall indicating leaching again.

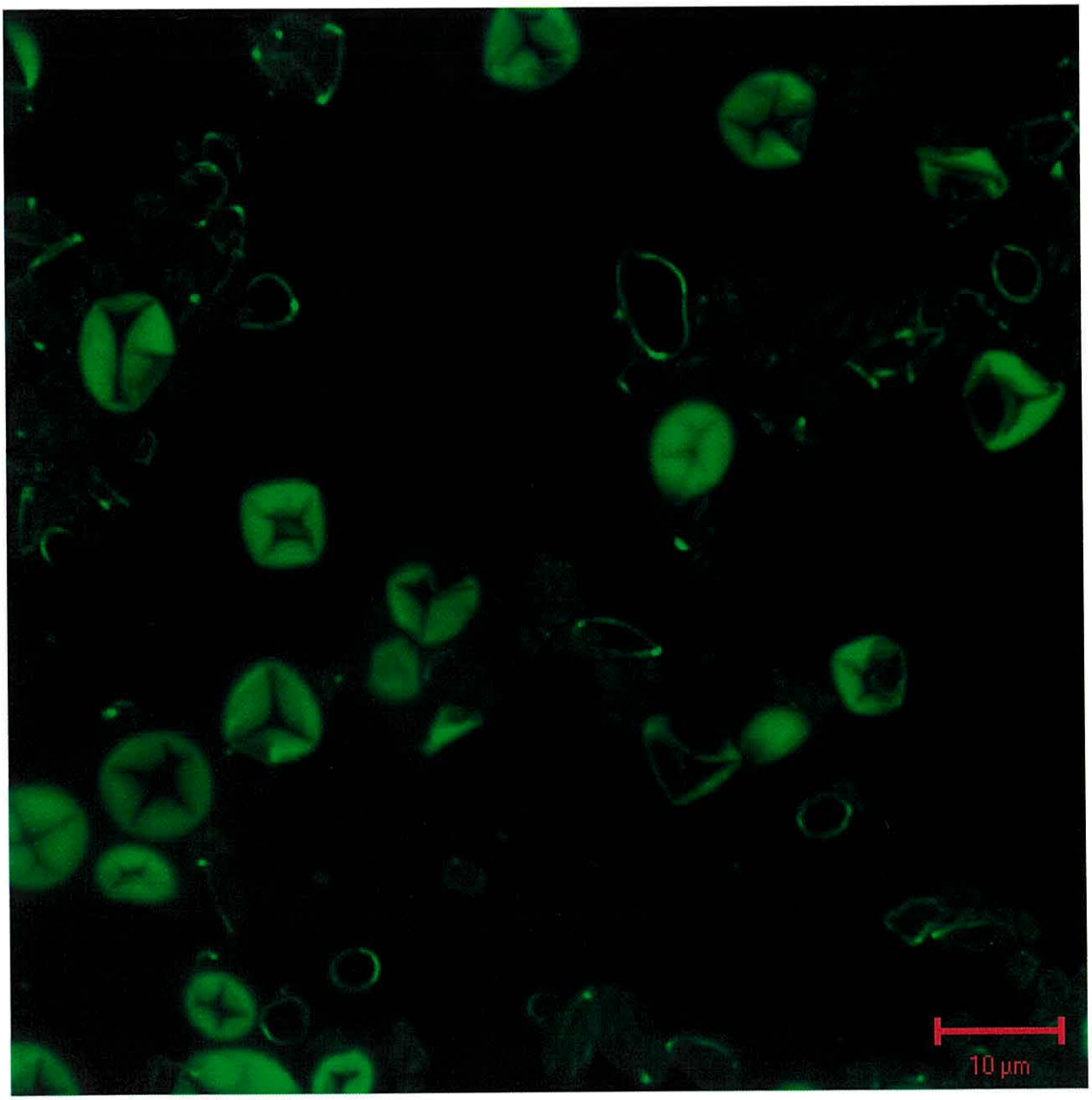

Figure 2.30. Confocal micrograph of method 3 microcapsules containing 9,10-bisphenylethynylanthracene doped chlorobenzene as internal phase. Magnification (x 630)

2.5. Formaldehyde Scavenging

All three microencapsulation procedures discussed within this chapter use melamine-formaldehyde as microcapsule polymer wall. A major problem associated with melamine-formaldehyde polymers is formaldehyde release post polymer production. [23] Formaldehyde has been designated a hazardous air pollutant (HAP) by the USEPA and

will contribute to the volatile organic compound (VOC) content of the coating. Formaldehyde in air has been detected using several methods. [24] A recent investigation was carried out to determine formaldehyde evolved during the curing of melamine-formaldehyde-based coatings using real time monitoring of formaldehyde by FT-IR. [25] A similar investigation has been carried out in this work using HPLC. It is known that dinitrophenylhydrazine (DNPH) reacts with various aldehydes to produce an aldehyde-DNPH derivative (Figure 2.31). [26]

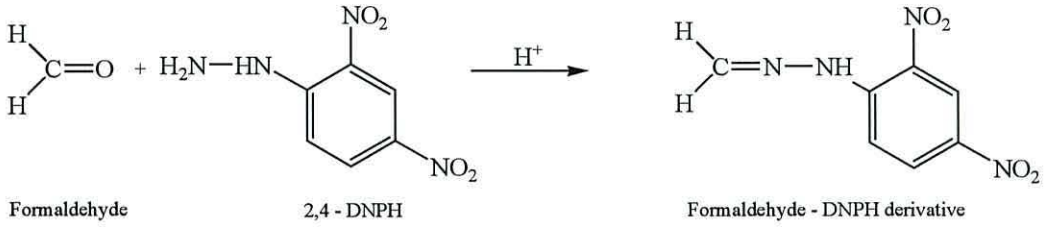

Figure 2.31. The reaction that occurs between formaldehyde and DNPH, forming the formaldehyde – DNPH derviative.

The formaldehyde-DNPH derivative is yellow and can be measured quantitatively using UV/Visible spectroscopy at its absorbance maxima, λ_{max} = 360 nm. [26] The derivative is formed by a 1:1 reaction of formaldehyde with DNPH, therefore quantification of this compound leads directly to accurate formaldehyde quantification. An analytical method to detect formaldehyde was set up using high performance liquid chromatography (HPLC), (see section 5.2.4 for details). To validate the method, a series of formaldehyde-DNPH derivative standards were made up and passed through the HPLC using a reverse phase column and a mobile phase of 70:30 (acetonitrile:water). The measured responses were plotted against concentration to produce a calibration curve (not shown). R^2 = 1.000 (3dp), BEC = 0.62 mg/L.

A series of tests were carried out to determine the accurate quantity of DNPH solution required for accurate quantitative formaldehyde detection. Slurry samples (1 g) were diluted using acetonitrile solution (100 ml). An aliquot of 10 ml was taken from this solution and acidified using 0.05 ml of concentrated HCl. Five further aliquots of 1 ml were taken from the acidified 10 ml slurry aliquot, and to them was added saturated DNPH solution. The volume of saturated DNPH solution added was 0.2 ml, 0.4 ml, 0.8 ml, 1.5 ml, and 3 ml for aliquot 1, 2, 3, 4, and 5, respectively. The samples were filtered using micropore filters and analyzed using the validated HPLC method. The

resulting HPLC traces showed that the optimum quantity of saturated DNPH solution required to detect formaldehyde in the 1 g slurry quantities analyzed was 0.4 ml.

Therefore, since formaldehyde was detected in all microencapsulation methods using HPLC in the quantities mentioned above, it was considered that a "scavenger" compound could be added to the microencapsulation process at the polymer curing stage to "mop up" excess formaldehyde. Therefore, a series of compounds were proposed as formaldehyde "scavengers" (Figure 2.32).

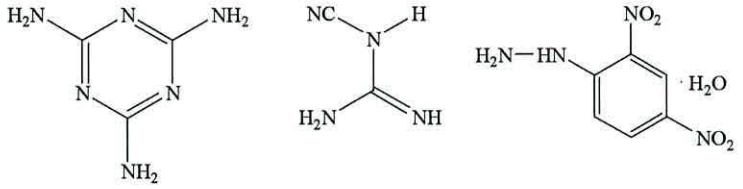

(a) (b) (c)

Figure 2.32. Proposed compounds to act as formaldehyde scavengers (a) melamine, (b) dicyandiamide, (c) hydrazine hydrate.

The compounds shown in Figure 2.32 were selected as possible "scavenger" contenders because all contain at least one amine functional group. It was postulated that the scavenger compounds would be incorporated into the melamine-formaldehyde polymer wall by attachment of the amine functional group to free sites on the polymer wall. The remaining amine group in the scavenger compound would then be able to react with any excess formaldehyde. In a parallel study, an alternative scavenger compound was also designed (Figure 2.33).

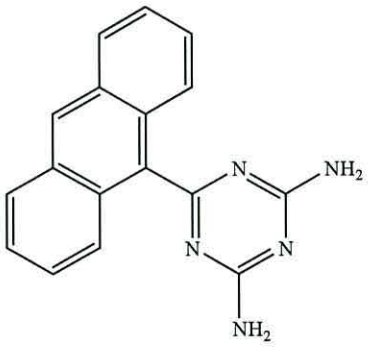

Figure 2.33. Chemical structure of the designed scavenger molecule.

This compound was chosen for two reasons. Firstly, it contains two amine functional groups; which means one group could attach to free sites on the polymer and the other

could react with excess formaldehyde. Secondly, it contains an anthracene moiety which is fluorescent. It was therefore considered that this scavenger compound could also be used for tagging into the polymer wall during the microencapsulation process, and that the resulting microcapsules could be imaged using fluorescent microscopy.

Literature searches to prepare the target molecule led to the discovery of similar compounds, such as 2,4-diamino-6-phenyl-1,3,5-triazine. [27] However, no anthracene derivative was found. Therefore, this is a new compound and the subsequent work is also new. Several attempts were made to prepare the anthracene derivative by adapting where appropriate the literature preparation of 2,4-diamino-6-phenyl-1,3,5-triazine. However, these attempts were unsuccessful, the ^{1}H NMR of the compound obtained after adaptation of the literature preparation for 2,4-diamino-6-phenyl-1,3,5-triazine showed mainly aldehyde starting material combined with a small proportion of nitrile intermediate. The ^{1}H NMR showed no indication of product formation. It is thought that the reaction is proceeding towards the imine intermediate which is a reversible reaction with the aldehyde under these conditions, and thus starting material is being obtained. Therefore, the target molecule was synthesized by a different route (Figure 2.34).

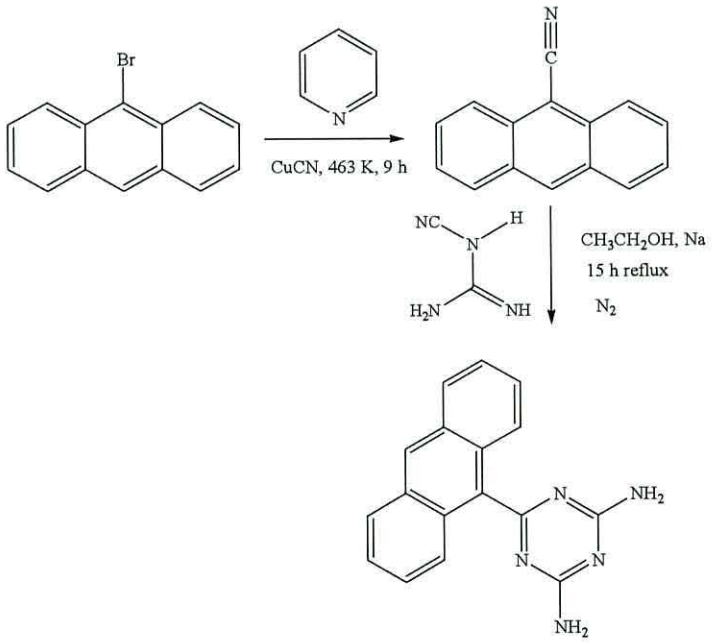

Figure 2.34. Reaction scheme of the preparation of 6-(9-anthracenyl) 2,4-diamino-1,3,5-triazine.

Firstly, cyanoanthracene was made from the starting material of 9-bromoanthracene following a literature procedure. [28] After purification, cyanoanthracene was reacted with sodium ethoxide and cyanoguanidine under a nitrogen atmosphere at reflux for 15 h to form a yellow solid. The solid was filtered and washed with ether to yield a yellow powder, which was recrystallized using hot methanol (1.55 g, 76 %). ^{1}H NMR, ^{13}C NMR and determination of accurate mass (see section 5.5.2 of this thesis for details) showed the yellow powder to be the required target molecule; 6-(9-anthracenyl) 2,4-diamino-1,3,5-triazine.

Microcapsules containing an internal phase of neat cetyl alcohol were prepared using method 3. Four stages of formaldehyde testing were carried out during method 3 (Figure 2.35). [29] The scavenger compounds were trialled individually by adding to the slurry after microcapsule production (see section 5.2.4 for details). Neat cetyl alcohol was chosen as internal phase to avoid leaching over the time scale of this experiment (1.5 h).

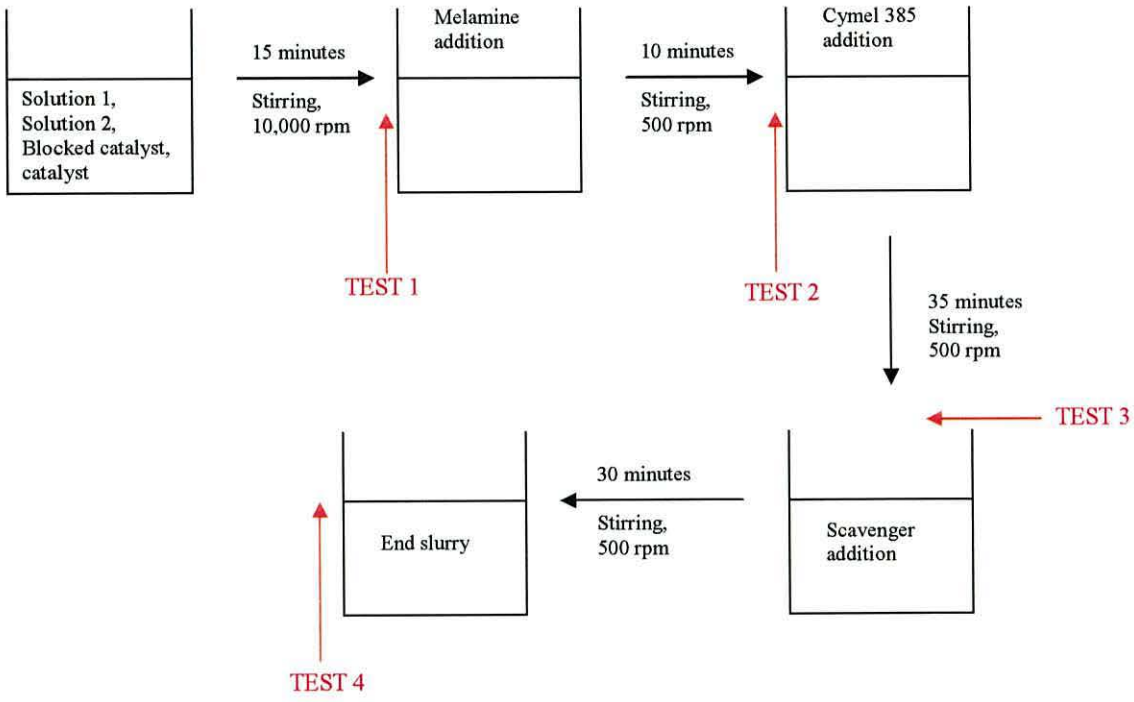

Figure 2.35. Schematic diagram showing the various testing points for formaldehyde testing.

The graph in Figure 2.36 shows a variation in formaldehyde concentrations at test point 1, ranging from 0.8-3.2 mg/L. This was unexpected since all three experiments at this stage of testing should contain similar formaldehyde levels. However, small changes in

quantities of solution 1 and 2 at the beginning of the experiment could explain such variation. After melamine addition (test point 2), the blue line shows a decrease in formaldehyde concentration whereas the other two profiles show an increase at similar increments. It was expected that a decrease in formaldehyde concentration occurred at test 2 since addition of melamine would react with excess formaldehyde.

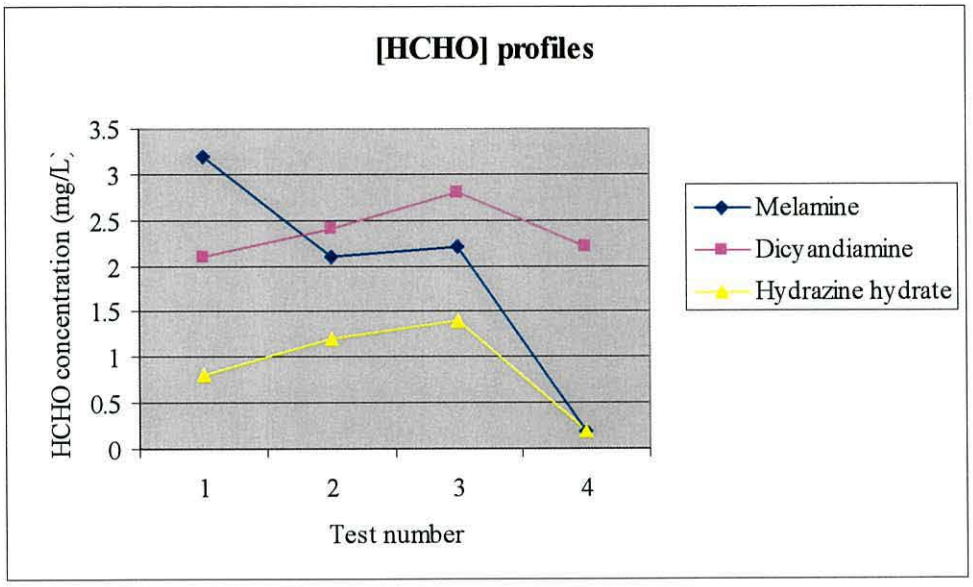

Figure 2.36. Formaldehyde concentration profiles obtained during microcapsule slurry testing before and after scavenger.

After Cymel 385 addition (test point 3), all three profiles show an increase in formaldehyde concentration as expected because Cymel 385 contains excess formaldehyde. The average concentration increase for all three samples tested is 0.2 mg/L. Finally, after addition of scavenger compound (test point 4), all profiles show a decrease in formaldehyde concentration. The compound shown to be the most effective formaldehyde scavenger was melamine, decreasing the formaldehyde concentration in the slurry sample by 2 mg/L. Hydrazine hydrate was the second most effective scavenger, decreasing the formaldehyde concentration in the slurry sample by 1.2 mg/L, and dicyandiamide was the least effective scavenger, decreasing the formaldehyde concentration in the slurry sample by 0.6 mg/L. Melamine was the most effective scavenger compound over hydrazine hydrate and dicyandiamine because it contains two amine functional groups in comparison with the other two scavenger compounds that contain only one amine functional group. This was confirmed by the result showing melamine decreased formaldehyde concentration twice as much as hydrazine hydrate

and almost four times the amount as dicyandiamine. Hydrazine hydrate was shown to be more reactive towards formaldehyde than dicyandiamine, despite both compounds containing one amine functional group. The hydrazine amine nitrogen is more nucleophilic towards the formaldehyde carbon due to its electron withdrawing nitro groups on the benzene ring within its structure. Also, upon reaction with formaldehyde the weaker nitrogen-nitrogen bond in hydrazine is broken more easily in comparison with the nitrogen-carbon bond in dicyandiamine (Figure 2.32).

The fourth scavenger compound, 6-(9-anthracenyl)-2,4-diamino-1,3,5- triazine (Figure 2.33) was used slightly differently in comparison with the three other scavenger compounds. The same four test points were used (Figure 2.35) to test formaldehyde concentration in slurry containing cetyl alcohol filled microcapsules made using method 3 as before. However, instead of the scavenger compound, 6-(9-anthracenyl)-2,4-diamino-1,3,5- triazine being added after test 3, it was added in place of melamine just after test 1. The reasons for the change in method were to incorporate the compound within the polymer wall for imaging, and to see if it behaved as a formaldehyde scavenger once incorporated within the polymer wall. Test results showed that this compound did not act as a formaldehyde scavenger in the quantity used. The resulting microcapsules were characterized using optical microscopy with epi-fluorescence (Figure 2.37).

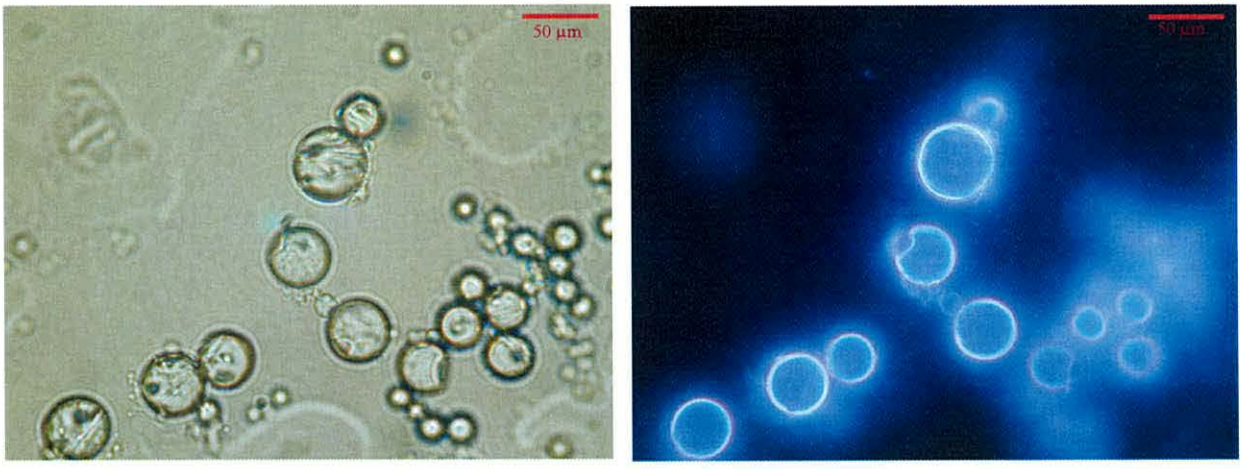

(a) (b)

Figure 2.37. Micrographs, optical (a) and fluorescent (b), showing a collection of microcapsules containing an internal phase of cetyl alcohol, and 6-(9-anthracenyl)-2,4-diamino-1,3,5- triazine tagged polymer wall. Magnification (x 1000).

The micrograph in Figure 2.37 (a) shows the microcapsules to be intact with a smooth polymer coating as seen in previous optical images of cetyl alcohol filled microcapsules in this chapter. In (b), the fluorescent scavenger molecule is seen localized at the polymer wall.

2.6. Conclusions

Three microencapsulation procedures have been discussed within this chapter. All three methods discussed are classed as *in situ* interfacial polymerisation, using the melamine-formaldehyde pre-polymer, Cymel 385 to form the microcapsule polymer wall. The basis of each method remains the same; an oil-in-water emulsion is prepared by high speed stirring of "oil" internal phase into an aqueous external phase. The external phase contains a surfactant that stabilizes the emulsion, thus retaining the oil droplet spherical shape which is subsequently coated by Cymel 385. The pre-polymer is then cured by heat to produce "oil" containing melamine-formaldehyde microcapsules.

In studying the three methods, it was observed that the microencapsulation variables; surfactant (structure and concentration), stirring speeds, and internal phase all play significant roles in the final microcapsule appearance and properties. For example, method 1 used the co-polymer EMA as surfactant and it was shown to be an effective emulsion stabilizer. This surfactant property is essential during the microencapsulation procedure, however it caused severe agglomeration after microcapsule production. In search of an alternative surfactant, method 2 was developed which employed the co-polymer sodium 2-naphthalene sulphonate formaldehyde condensate (trade name, Demol NL) as surfactant. In contrast to method 1, method 2 was shown to produce a free flowing powder of microcapsules. During method 2 experiments, it was shown by varying surfactant concentrations, that, in order to successfully maintain an oil-in-water emulsion, a surfactant concentration in excess of the critical micelle concentration was required. The surfactant used in method 3 was a gelatin-gum arabic co-polymer. This co-polymer is regularly used to form microcapsule walls, and therefore, a large proportion of this surfactant may be incorporated within the resultant microcapsule wall. Such a prediction could also account for the increased size of method 3 microcapsules. However, microcapsule size is strongly influenced by emulsion stirring speeds as was shown using method 1 experiments. By increasing homogeniser speed during emulsion formation, smaller microcapsules are produced. The internal phase

(IP) used to initially study method 1 microcapsules was neat toluene. Such microcapsules appeared to be "deflated". This was subsequently seen in method 2 and 3 microcapsules containing neat chlorobenzene. Therefore, experiments were carried out using methods 1, 2, and 3 to see the effect of a low melting solid IP (cetyl alcohol) upon microcapsule shape and surface morphology. Cetyl alcohol containing microcapsules were shown by optical microscopy to be spherical and smooth, with no signs of deflation. However, when examined in greater detail using confocal laser scanning microscopy, these microcapsules were shown to possess a slightly uneven microcapsule shape and the surface appeared to be layered. Such surface morphology was also observed on microcapsules containing toluene made using method 1. The reasoning behind this layered capsule surface effect stems from the oil-in-water emulsion stability. Lack of retention of perfect oil sphere causes the pre-polymer to deposit unevenly upon the oil droplet.

Microscopy was used as the main characterisation method to observe microcapsule structure and morphology of all microcapsules made using methods 1, 2 and 3. When using both confocal scanning laser microscopy (CLSM) and fluorescence microscopy to characterise microcapsules, the internal phase was doped with a fluorescent dye. It was shown from SEM, CLSM, optical and fluorescence microscopy that microcapsules containing a liquid internal phase appear to be "deflated". To further investigate "deflation", a series of microcapsule leaching experiments were carried out which will be presented in chapter 3 of this thesis. One piece of future work could be to monitor deflation and leaching of dye containing liquid filled capsules using time lapse confocal scanning laser microscopy. In another confocal experiment, the surfactant used in each microencapsulation method could be tagged using different fluorescent compounds to be able to observe the surfactant position within the microcapsules.

2.7. References

1 Han, H.K., Hong, S.C., *Molecular Crystals and Liquid Crystals*, 2000, **349**, 79

2 Hong, K., Park, S., *Materials Chemistry and Physics*, 1999, **58**, 128

3 Vasiliu, S., Popa, M., Rinaudo, M., *European Polymer Journal*, 2005, **41**, 923

4 Tao, X., Li, J.B., Mohwald, H., *Chemistry: A European Journal*, 2004, **10**, 3397

5 Krol, S., Cavalleri, O., Ramoino, P., Gliozzi, A., Diaspro, A., *Journal of Microscopy*, 2003, **212**, 239

[6] Prince, L. (Ed.)., *Microemulsions*, Academic Press, New York, 1977

[7] March, J., *Advanced Organic Chemistry (4th Ed)*, Wiley, USA, 1992

[8] Benita, S. (Ed.), *Microencapsulation: Methods and Industrial Applications*, Dekker, New York, 1996

[9] Dohányosová, P., Fenclová, D., Vrbka, P., Dohnal, V., *Journal of Chemical & Engineering Data*, 2001, **46**, 1533

[10] Mequanint, K., Sanderson, R., *Polymer*, 2003, **44**, 2631

[11] Cymel ® 385 resin brochure (Cytec, USA)

[12] Brown, E.N., Kessler, M.R., Sottos, N.R., White, S.R., *Journal of Microencapsulation*, 2003, **20**, 719

[13] Marrion, A.R. (Ed.), *The Chemistry and Physics of Coatings*, RSC, Cambridge, 1994

[14] Kamada, 1990, U.S.Patent, 4,957,949

[15] Lehr, C.M., Lamprecht, A., Schafer, U.F., *European Journal of Pharmaceutics* and Biopharmaceutics, 2000, **49**, 1

[16] Singh, A.K., Roy, M., *Canadian Journal of Chemistry*, 1990, **68**, 383

[17] Hirayama, S., *Journal of Chemistry Society Faraday Trans 1*, 1982, **78**, 2411

[18] Ikeda, H., Kawabe, Y., Sakai,T., Kawasaski, K., *Chemistry Letters*, 1989, 1803

[19] Graf C, Schartl W, Fischer K, Hugenberg N, Schmidt M, *Langmuir*, 1999, **15**, 6710

[20] Du, H., Fuh, R.A., Li, J., Corkan, A., Lindsey, J.S., *Photochemistry and Photobiology*, 1998, **68**, 141

[21] Budavari, S. (Ed)., *The Merck Index (12th Ed)*, Merck & Co, New Jersey, 1996

[22] Mayya, K.S., Bhattacharyya, A., Argillier, J.F., *Polymer International*, 2003, **52**, 644

[23] Mark, H.F.,(Ed.), *Encyclopedia of Polymer Science Technology (Vol 2),* Wiley, New York,1965

[24] Kawamura, K., Kerman, K., Fujihara, M., Nagatani, N., Hashiba, T., Tamiya, E., *Sensors and Actuators B – Chemical*, 2005, **105**, 495

[25] Phillips, J.H., Patterson, J.E., *Journal of Testing and Evaluation*, 2005, **33**, 73

[26] American Standards, American Society for Testing and Materials, Designation "D5197-92 standard", 1916 Race St, Philadelphia, PA 19103

[27] Shie, J.J., Fang, J.M., *Journal of Organic Chemistry*, 2003, **68**, 1158

[28] Bachmann, W.E., Kloetzel, M.C., *Journal of Organic Chemistry*, 1938, **3**, 55

[29] Personal disclosure: Dafydd Thomas, U.W.B

CHAPTER 3

RESULTS AND DISCUSSION

MICROCAPSULE LEACHING

3. Microcapsule Leaching

3.1. Area of Study

It was shown in Chapter 2 that melamine-formaldehyde microcapsules containing a volatile liquid internal phase appear to deflate over time and reduce in size after production, most probably releasing the internal phase in the process. However, melamine-formaldehyde is reported to be an impermeable thermosetting resin. [1] Thermosetting resins are polymers that are changed irreversibly under the influence of heat from a fusible and soluble material into one which is infusible and insoluble through the formation of a covalently crosslinked, thermally stable network. [2] The suggestion to rationalize the shrinkage of the capsules over time was that the melamine-formaldehyde polymeric capsule wall swells upon contact with volatile organic solvents, thus changing permeability and allowing solvent escape from the microcapsules. The work in this chapter seeks to investigate these observations.

It is well known that polymers swell in solvents. [2] Certain polymers can swell up to several times their original dry weight. For example, polyacrylamide swells to 400 times its original dry weight in water. [3] Such polymer types are classified in the literature as "super-absorbance polymers". [4] Swelling is the first stage of polymer solvation. Solvent molecules slowly diffuse into the polymer to produce a swollen gel, thereafter if the solvent–polymer interactions are a stronger force than the polymer-polymer intermolecular forces, the second stage of polymer dissolution takes place. [2] Melamine-formaldehyde resins possess high polymer-polymer intermolecular forces due to crosslinking and strong hydrogen bonding. It is known that crosslinked polymers do not dissolve, but do swell. [2] Therefore, it is feasible to suggest that such a polymer swelling process will occur within each individual microcapsule at the internal phase/melamine-formaldehyde polymer wall interface, and the resulting "swollen" polymer wall will then display semipermeable properties. In order to investigate such an occurrence, a series of separate leaching experiments were carried out and the data forms the basis of this chapter.

3.2. Microencapsulation of Phenanthroline

It is known from the literature that ferrous iron (Fe^{2+}) reacts with organic ligands; for example, upon reaction with *o*-phenanthroline, an orange-red complex of $[Fe(o\text{-phen})_3]^{2+}$ is formed (Figure 3.1.). Colour intensity is independent of acidity at pH 2-9 and the complex is stable for long periods. [5] The concentration of the complex in solution can be measured quantitatively using UV/Visible spectroscopy at an absorption maximum of 515 nm. [5]

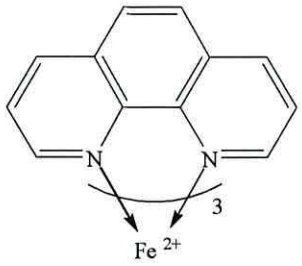

Figure 3.1. Structure of the phenanthroline-ferrous iron complex, formed upon reacting phenanthroline with aqueous iron(II). [5]

With the above information in mind, an experiment was designed using phenanthroline as a probe to test the "leakiness" of melamine-formaldehyde microcapsules that contained a volatile liquid internal phase. Phenanthroline, an organic ligand comprised of 2-(benzene-fused pyridinyl rings) was chosen to be a solute dissolved into the liquid internal phase reasoning that if this ligand leaked through the semi-permeable wall of the microcapsule its presence outside the capsule in a ferrous environment would be detected by the formation of the red iron-phenanthroline complex. To gain a valid result, it was important that any surface phenanthroline was removed from the outside of the capsules before dispersing in the aqueous iron(II)solution.

The first batch of microcapsules to be tested was microcapsules made using general method 1 microencapsulation procedure (see section 5.3.4 for experimental details). Upon addition of the Fe^{2+}(aq) standard to the diluted slurry solution, there was no immediate colour change from the white opaque solution to the expected orange-red colour, thus indicating no obvious phenanthroline on the capsule outer surface. The solution was then stirred at room temperature for *ca.* 1 h. Initial observations of the conical flask after this time period showed that the solution retained its original appearance; white and opaque. However, after a time period of 24 h (the solution was stopped stirring and left to stand at room temperature for approximately 24 h), observations of the conical flask showed the appearance of a pale orange/red colour. It

was concluded that this colour appearance had arisen from the formation of the phenanthroline - Fe^{2+} complex due to passage of phenanthroline across the capsule wall. Although a qualitative result was obtained from this experiment, quantification of phenanthroline was undetermined for this sample. This was because the microcapsules were unable to be separated by filtration from the solution and analyzing a suspension using UV/Visible spectroscopy would have interfered with the light scattering process leading to inaccurate results.

The experiment was therefore repeated with microcapsules that could be filtered (made using method 2) in order to gain quantitative results. The microcapsules containing phenanthroline were prepared using an adapted method 2 microencapsulation procedure (see section 5.3.4 for experimental details). The microcapsules were filtered from the slurry under vacuum. Initially, the filtrate was analysed for phenanthroline: small samples were taken from the filtrate and complexed with the iron standard as before. Upon addition of the iron standard to the filtrate sub-samples, a red colour appeared immediately, indicating the phenanthroline–Fe^{2+} (aq) complex had been formed. Following this result, a new experiment was set up to detect and quantify phenanthroline mass throughout the method 2 microencapsulation process.

A phenanthroline calibration curve was formed from measuring a series of phenanthroline standards with a known concentration of iron(II)solution using UV/Visible spectroscopy. The measured absorbance values were plotted against phenanthroline concentration (Figure 3.2). R^2 =1.000 (3 dp), BEC = 0.006 mg/L, equation of line: y = 0.2 x -0.003.

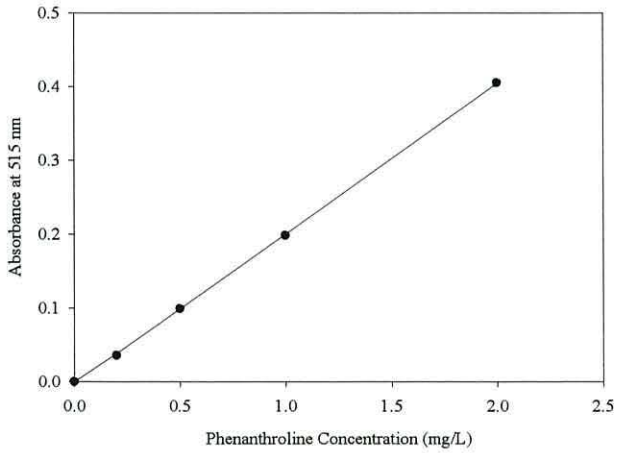

Figure 3.2. Calibration curve obtained for the phenanthroline-Fe^{2+} complex using different phenanthroline concentrations measured at fixed λ = 515 nm.

Monitoring the encapsulation of phenanthroline throughout method 2 was then attempted. At the beginning of the procedure 0.099 g of phenanthroline (dissolved in toluene) was dispersed in a surfactant containing aqueous solution. The emulsion was left to settle and the aqueous phase was analyzed for phenanthroline content using UV/Visible spectroscopy to examine whether phenanthroline was partitioning from the organic phase to the aqueous phase. A small amount (2 ml) of the aqueous phase was removed from a total volume of 200 ml using a pipette. Iron sulphate standard (0.5 ml) was added to this solution. A red solution was immediately formed giving an absorbance reading of 0.131 at 515 nm, which was converted using the phenanthroline calibration curve to give a concentration value of 0.67 mg/L. This concentration was then converted to give a phenanthroline mass, 134 µg in the aqueous layer (Figure 3.3).

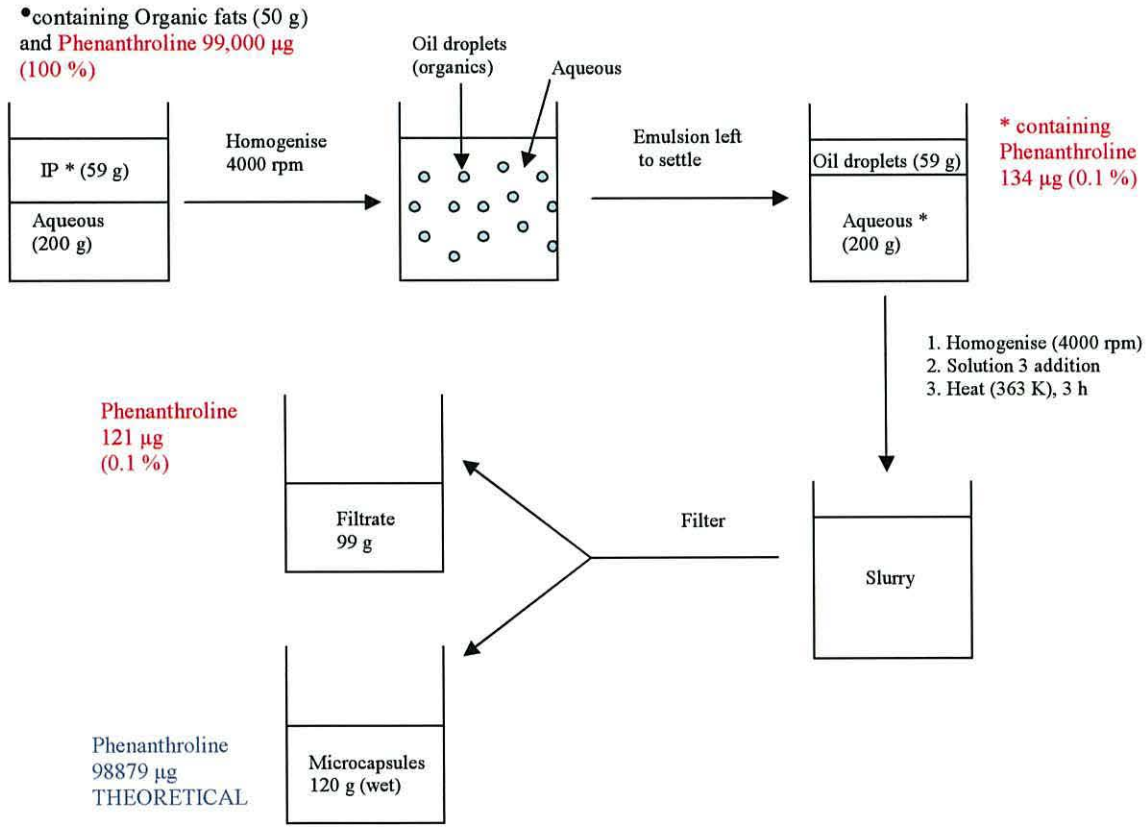

Figure 3.3. Schematic diagram showing phenanthroline monitoring during microencapsulation (adapted method 2).

The emulsion was set stirring again and solution 3 (an aqueous solution of melamine-formaldehyde pre-polymer) was added. The slurry was left stirring at 363 K for 3 h and the resulting microcapsules were subsequently filtered. Again, a small volume (2 ml)

was taken from the filtrate (total filtrate volume was 120 ml) and aqueous iron sulphate was added as before. A red colour was formed immediately giving an absorbance reading of 0.24 at 515 nm, which was converted to concentration using the calibration curve to give a value of 1.22 mg/L. The concentration was converted to give a phenanthroline mass, 121 μg in the aqueous filtrate layer. The mass of phenanthroline found in the filtrate is calculated to be 0.1 % of the total phenanthroline mass used at the beginning of the microencapsulation procedure. Therefore, it can be concluded from these calculations that a negligible amount of phenanthroline is found in the final microcapsule slurry and the remainder of the phenanthroline (*ca.* 98879 μg) must be inside the microcapsules, assuming 100 % inclusion of phenanthroline at the beginning of the experiment (Figure 3.3).

To quantify the phenanthroline inside the microcapsules the following tests were carried out; firstly, a sub-sample of microcapsules (12 g) was taken from a total mass of filtered microcapsules (120 g) and placed in 80 ml of deionised water to re-create a suspension. The microcapsules were filtered and the collected filtrate was diluted using an iron sulphate solution (80 ml). An immediate red colour was formed upon this dilution of the filtrate indicating the phenanthroline- Fe^{2+} complex had been formed. The red solution was measured in triplicate for phenanthroline content using UV/Visible spectroscopy as detailed earlier. The average absorbance reading was found to be 0.186, which was converted to give a solution concentration of 0.95 mg/L using the calibration curve. The concentration was converted to give a phenanthroline mass of 304 μg. Therefore, the data suggests that when a 120 g mass of microcapsules are dispersed into an aqueous environment, 3 % of the original mass of phenanthroline will be leached out into the aqueous phase.

In another experiment, a mass of microcapsules (12 g) were taken from the original mass of filtered microcapsules (120 g) and were "crushed" using a glass rod. The crushed microcapsules were dispersed and UV/Visible measurements were again carried out in triplicate and the average absorbance reading was found to be 0.189 which was converted to give a solution concentration of 0.94 mg/L using the calibration curve. At this stage, it should be noted that the concentration difference between the "crushed" microcapsules and "non-crushed" microcapsules is 0.010 mg/L. This small difference suggests either there is no phenanthroline inside the microcapsules or that the microcapsules do not break when using this method of crushing. The first suggestion of

phenanthroline absence inside the microcapsules could be explained by phenanthroline interacting with the acidic buffer in the aqueous solution 1 used to make the capsules, and therefore it is not present in the organic layer during the microencapsulation experiment. However, the data obtained thus far from UV/Visible spectroscopy measurements suggests that the concentration for phenanthroline from the "crushed" microcapsules is low due to an inefficient method of crushing and not because of interaction with the acidic buffer. This has been concluded because only 0.1 % of the original phenanthroline mass was detected in the filtrate after encapsulation. If phenanthroline was interacting with the acidic buffer in solution 1, then it is expected that a much higher mass of phenanthroline would be detected by UV/Visible spectroscopy measurements.

3.3. Microencapsulation of Ferrocene

Data obtained from section 3.2 indicated that the melamine-formaldehyde polymer wall was permeable to organic solutions of phenanthroline. As discussed previously, it was believed that such permeability occurs from the organic solvent interacting with the impermeable melamine-formaldehyde polymer, causing it to swell and become semi-permeable. Therefore, it was thought that this semi-permeable microcapsule polymer wall could act as a gradient barrier, *i.e.* a high concentration solution would pass through the polymer to a low concentration solution. To investigate this proposal, microcapsules containing an internal phase of a chlorobenzene solution of ferrocene were made following method 2 (see section 5.6.1 for experimental details). Another series of leaching tests were carried out which involved dispersing these ferrocene containing microcapsules into three different solvents; methanol, chloroform and hexane.

Ferrocene is an orange coloured compound, absorbing in the UV/Visible spectrum with an absorbance maximum occurring at 450 nm [6], thus allowing monitoring of microcapsule leaching by UV/Visible spectroscopy. It was expected that if the capsule walls act as semipermeable membranes, ferrocene would leach out of the capsules into the ferrocene free surrounding solvent by osmotic pressure. Three different solvents (hexane, chloroform and methanol) were chosen to compare the effect of each solvent upon ferrocene leaching. The orange coloured microcapsules obtained were not dried for the next step of the experiment to minimise any pre-measurement leaching (see section 5.4.2 for experimental details). To calibrate the UV/Visible

spectrometer, ferrocene standards were scanned between λ = 300 and 700 nm to confirm the literature absorbance maximum at 450 nm. Thereafter, ferrocene standards were measured at a fixed wavelength of 450 nm creating a calibration graph (Figure 3.4). R^2=1.000 (3 dp), BEC = 0.0028 mg/L, equation of line: y = 0.005 x -0.0014.

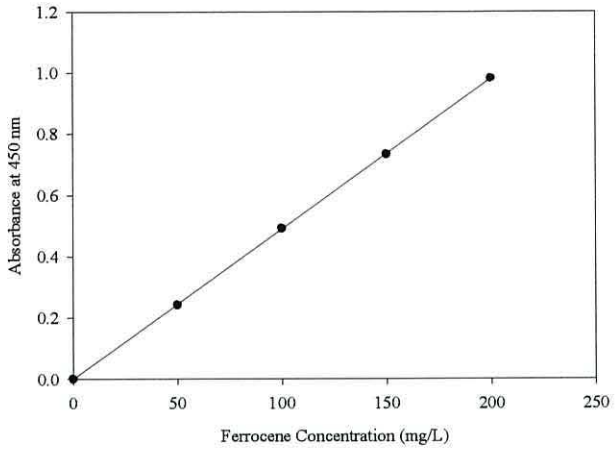

Figure 3.4. Calibration curve obtained for different ferrocene concentrations measured at fixed λ = 450 nm.

Test experiments consisted of shaking samples at a constant speed with aliquots of 4 ml being taken every hour for 3 h. After 3 h, an aliquot was taken at 24 h, then subsequently every 48 h up to 192 h. Control experiments simply consisted of microcapsule samples in the various solvent environments, standing still for the same allotted time period; as for the test experiments with removal of aliquots at the same time periods. In both test and control experiments, replacement solvent (4 ml) was added each time aliquots were removed. The dilution factor replacement solvent has been accounted for in the data presented in this section.

The graph in Figure 3.5 shows the ferrocene release profiles obtained when microcapsules containing ferrocene were placed into a neat hexane solution. The absorbance value for the first measurement (t = 0 h) for both control and test experiments should theoretically indicate the extent of "free core content" (*i.e.* non encapsulated ferrocene) which is measured under these specific experimental conditions to be 2 x 10^{-5} mg/L and 3 x 10^{-5} mg/L, respectively. After this, the release profile obtained for the test experiment closely follows the profile obtained for the control experiment. Both curves show rapid initial ferrocene release into the external hexane environment resulting from ferrocene being released intact from the capsules. The

gradients of the curves are measured to be 3.2 x 10^{-3} mg/L /48 h and 3.7 x 10^{-3} mg/L /48 h for the control and test experiments, respectively. After 48 h, a much slower release rate of ferrocene into the hexane solution is observed for both control and test experiments with gradients measured as 1.6 x 10^{-3} mg/L /148 h (equivalent to 5.2 x 10^{-4} mg/L /48 h) and 1.8 x 10^{-3} mg/L /148 h (equivalent to 5.8 x 10^{-4} mg/L /48 h), respectively.

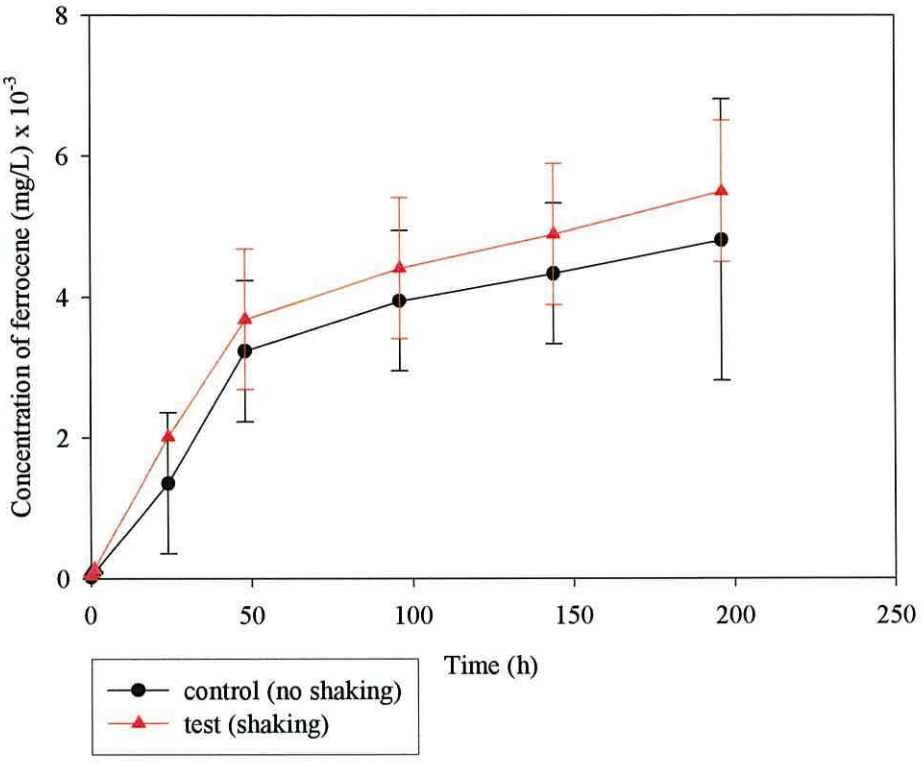

Figure 3.5. Graph to show concentration of ferrocene leaching into hexane solution from melamine-formaldehyde microcapsules over 192 h.

When the ferrocene containing microcapsules are placed into neat hexane, a concentration gradient between the internal phase of the microcapsules and hexane solvent is established. This concentration gradient is located within the polymer wall of the microcapsules. The control (no shaking) in this experiment shows that the release of ferrocene from the microcapsules into an external solvent of hexane is diffusion controlled. The test (shaking) causes the internal phase solution molecules of the microcapsules to strike the polymer wall at a greater force than in the control, thus kinetics causes a larger concentration of leached ferrocene in comparison to the control. The difference between the two curves shown in Figure 3.5 is the effect of shaking upon

the diffusion controlled leaching of ferrocene into hexane or alternatively it could be attributed to a sampling issue of the experiment. The concentration value for 100 % release ferrocene into solvent (theoretical) is 5880 mg/L. The error bars on both control and test hexane experiments show a variation within the data set. Compared to the chloroform and methanol data (see later), lower concentrations of ferrocene were leached in the hexane experiment. This can be explained by the wet microcapsules taking the form of two large polymeric clumps (Figure 3.6, (a)).

(a) (b) (c)

Figure 3.6. Photographs showing microcapsules containing ferrocene in an external solvent of (a) hexane, (b) chloroform, and (c) methanol.

It is observed in Figure 3.6 (a) that only the external layer capsules of the polymeric clumps seem to be wetted by the hexane molecules and that the hydrophobic hexane was unable to interact with capsules, still wet with water, to extract ferrocene from inside the microcapsules. Therefore, the higher ferrocene concentrations observed in the test experiment may also be arising from the break up of the large polymer clumps due to the continual shaking. In contrast, the photographs of ferrocene containing microcapsules in chloroform (Figure 3.6, (b)) and methanol (Figure 3.6, (c)) show that although these microcapsules were water wet, both chloroform and methanol easily dispersed the polymeric clumps that were originally seen in (a). The dispersed microcapsules in chloroform float on top of the denser chlorinated solvent as expected, and the microcapsules in methanol are seen to be fully dispersed forming a monodispersive array.

The graph in Figure 3.7 shows the ferrocene release profiles obtained when microcapsules containing ferrocene were placed into a neat chloroform solution. The control release profile obtained for the microcapsules in chloroform show a steady increase in ferrocene concentration in solution over 192 h. By comparison, the shaken capsules showed a marked increase in ferrocene concentration as the time increases

compared with the control (no shaking). Overall, more ferrocene was released in chloroform over hexane. For example, in the test experiment, the concentration of ferrocene released into chloroform after 48 h (28.9 x 10^{-3} mg/L) was *ca.* x 10 fold greater than the concentration of ferrocene released into hexane (3.7 x 10^{-3} mg/L). These larger ferrocene concentrations released into chloroform can be ascribed by several different factors.

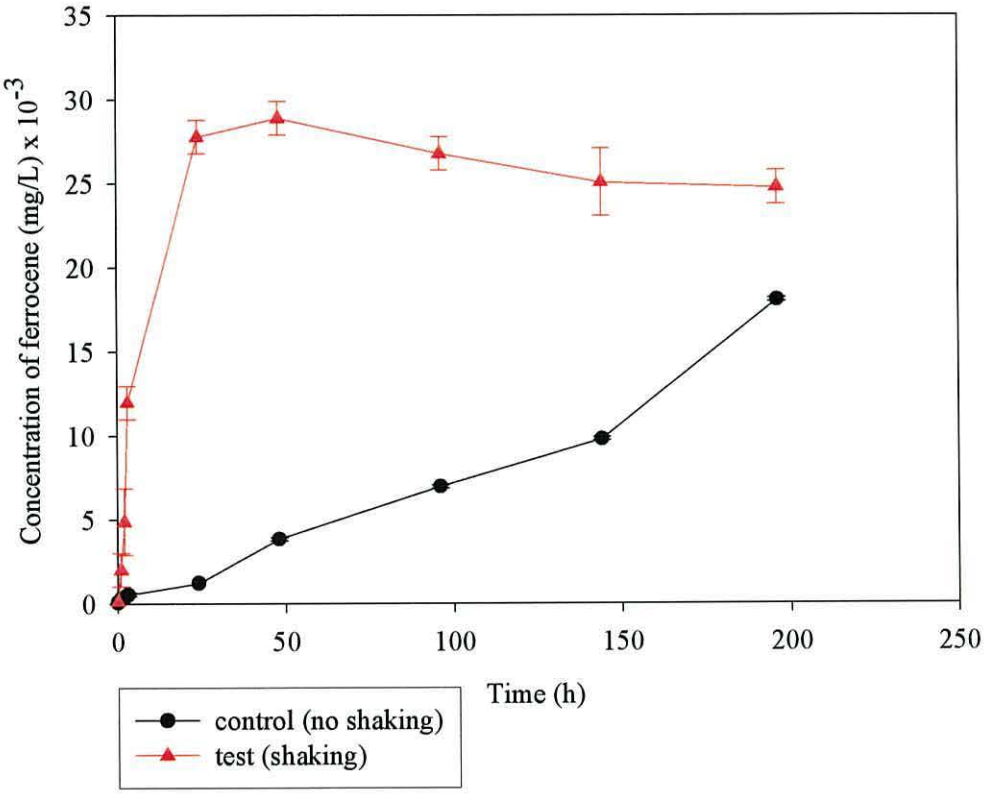

Figure 3.7. Graph to show concentration of ferrocene leaching into chloroform solution from melamine-formaldehyde microcapsules over 192 h.

Firstly, chloroform is a more polar solvent than hexane and as a result causes greater swelling of the polar melamine-formaldehyde polymer wall. [2] Secondly, the microcapsules in chloroform separate from the initial clump to form a dispersion (Figure 3.6 (b)). This exposes the entire surface of the microcapsules and allows a greater membrane surface area to be reached by the chloroform solvent, thereby releasing a greater concentration of ferrocene overall. Thirdly, ferrocene is more soluble in chloroform than hexane. Therefore, ferrocene being more soluble in

chloroform has a greater tendency to partition from the microcapsule internal phase into the surrounding chloroform solvent over hexane.

The graph in Figure 3.8 shows the ferrocene release profiles obtained when microcapsules containing ferrocene were placed into a neat methanol solution.

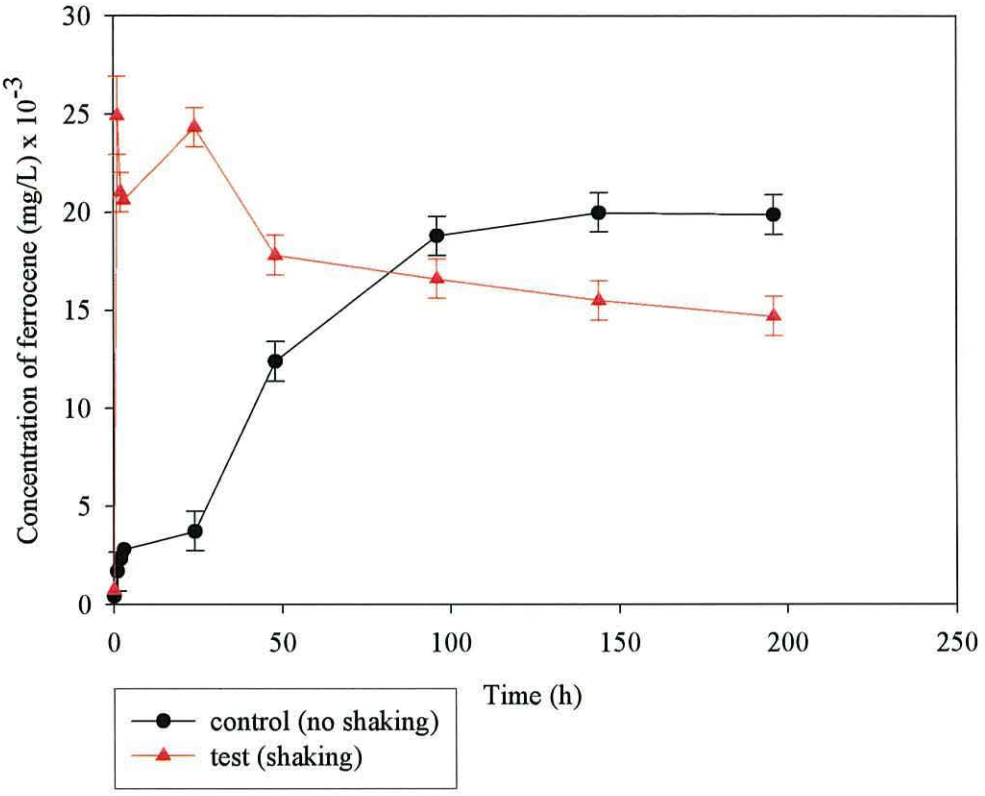

Figure 3.8. Graph to show concentration of ferrocene leaching into methanol solution from melamine-formaldehyde microcapsules over 192 h.

In methanol, the ferrocene leaching profile for the control (no shaking) increased rapidly for the first 48 h, and then slowly up to 196 h. By comparison, the test profile (depicted in red) increased to a maximum shortly after methanol addition (0-1 h). The ferrocene concentration then decreased which may indicate some uptake by the capsules. However, within experimental error this effect is believed to be small. Comparing the three solvents (Figure 3.9), the concentrations of ferrocene leached in methanol are similar to those for chloroform, both sets of ferrocene concentrations being much larger than for hexane. Such findings are partially ascribed to the methanol and chloroform dispersing capsules (still wet with water) more efficiently than hexane (Figure 3.6). The polar solvents, methanol and chloroform swell the polar melamine-

formaldehyde polymer more than hexane, therefore ferrocene is released into these solvents at a faster rate. Ferrocene is most soluble in chloroform in comparison to methanol and hexane. Therefore, the largest ferrocene concentrations leached are seen in this solvent (Figure 3.9).

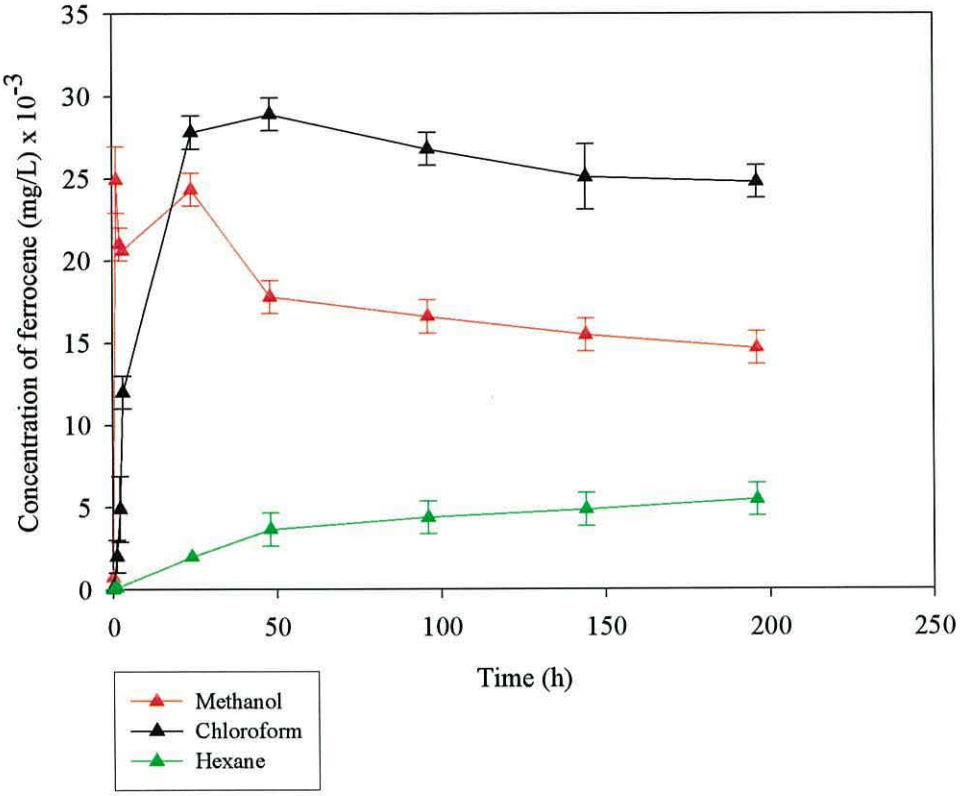

Figure 3.9. Graph to show concentration of ferrocene leaching into hexane, chloroform and methanol solutions from melamine-formaldehyde microcapsules over 192 h during tests (shaking).

3.4. Chlorobenzene Leaching

The leaching experiments discussed so far in this chapter were carried out on microcapsules formed using method 2 microencapsulation procedure. Such experiments have shown evidence for leaching of the microcapsule internal phase into an external liquid environment. One explanation put forward for these observations has been that leaching occurs by solvent swelling of the melamine-formaldehyde polymer capsule walls, making them semi-permeable. Thus, it is proposed that these

microcapsules can be viewed as "artificial cells", able to exchange solvent through the swollen polymer microcapsule wall following osmotic pressure gradients. "Artificial cells" were first postulated by Chang, [7] proposing that semi-permeable microcapsules containing proteins could be used for pharmaceutical applications. Since then, pharmaceutical research has made use of artificial cells for drug delivery. [8] Also, advances in artificial cells for therapeutic applications has been made by microencapsulating biotechnical materials such as hemoglobin, enzymes, cells and genetically engineered microorganisms. [9] Two experiments were thus designed to investigate the feasibility of solvent containing melamine-formaldehyde capsules as "artificial cells". Both experiments used microcapsules containing an internal phase of neat chlorobenzene. Experimental planning involved consideration of key variables such as selection of suitable external solvents and leachate monitoring procedure (see section 5.4.3) for experimental details.

3.4.1. Solvent Leaching Experiment 1

Preliminary data showed that chlorobenzene solutions leach from batches of microcapsules made following method 2 microencapsulation procedure. To investigate whether these leaching microcapsules could behave as "artificial cells", toluene (molecular size x = 4.3 Å, y = 5.9 Å, z = 1.8 Å) was selected as a suitable solvent to pass into the microcapsules to exchange with the similarly sized internal phase of chlorobenzene molecules (molecular size x = 4.4 Å, y = 5.7 Å, z = 0.99 Å). Results from the ferrocene leaching experiments in section 3.3 indicated that maximum ferrocene loss occurred in the presence of chloroform. Therefore, the decision was made to carry out experiment 1 in the presence of excess chloroform to maximize polymer swelling, thus aiding exchange of the two solvents (toluene and chlorobenzene) through the melamine-formaldehyde polymer wall.

As part of the experiment, two different "aged" batches of microcapsules were studied to compare the effects of aging upon solvent exchange. The literature was searched for melamine-formaldehyde aging data, however it appears that this subject has not been widely studied since the only relevant paper found reported heat capacity data of a cured (358 K for 20 h) melamine-formaldehyde resin. [10] "Old" and "fresh" microcapsules were used in both experiments. "Old" microcapsules were microcapsules that had been stored in a sealed glass container for two months and

"fresh" microcapsules were microcapsules which were made and left for one week standing in a similar sealed glass container. A control experiment consisting of neat chlorobenzene solvent (the "blank") was run alongside the two microcapsule batches for comparative purposes.

In this experiment, a small sample of microcapsules (1 g) was taken from the bulk batch of microcapsules for analysis to ensure sufficient target analytes were present for later analysis. A mass balance of the microcapsules was attempted in this experiment. However, since internal phase leaching appeared to occur almost immediately after the microcapsules were formed, this made the calculation more difficult to carry out. On this basis, a reasonable estimate (0.8 g) was made considering the weight of the internal phase present in one gram of microcapsules and considering the mass of individual components used in the microencapsulation experiment.

In planning this experiment; 1 ml of toluene in the presence of 19 ml of chloroform was used as external solvent volume for 1 g of microcapsules. The proposed chlorobenzene/toluene solvent exchange could occur either by mass, volume or molar exchange. If the estimate of internal phase in 1 g of microcapsules is correct at 0.8 g, then 0.8 g of toluene is required if solvent exchange is dependent upon mass. Such a mass of toluene is equivalent to *ca.* 0.9 ml in volume, therefore since the experiment uses 1 ml of toluene such experimental requirements are fulfilled.

Alternatively, solvent exchange could be dependent upon volume. A mass of 0.8 g of chlorobenzene internal phase is equivalent to *ca.* 0.7 ml. Again, the volume of toluene used in this experiment is in excess of this volume thus fulfilling such experimental requirements. Finally, solvent exchange could be molar dependent. In 1 g of microcapsules there is 7 mmol of chlorobenzene, therefore 7 mmol of toluene (*ca.* equivalent to 0.7 ml) would be required to pass into the microcapsules. To conclude, whether solvent exchange is dependent upon mass, volume or molar exchange, using 1 ml of toluene in the experiment ensured an excess of toluene was present if all chlorobenzene (0.8 g) leached out of the capsules.

To avoid evaporation of the volatile solvents during the experiment, the capsules and external solvent were sealed inside a round bottomed flask using a rubber Subaseal ™ and nesofilm.

Solvent exchange was monitored at regular time intervals; initially every 90 minutes for the first 3 h, then every 24 h until a time period of 120 h had elapsed. An aliquot (0.5 ml) was carefully withdrawn from the sealed flask using a syringe. The resulting suspension of solvent and microcapsules was filtered through a cotton wool plug and a sub-sample of the filtrate (0.1µl) injected into a gas chromatogram for analysis of the chlorobenzene, toluene and chloroform content. A method for GC analysis was developed, as part of this study, to ensure highly resolved data for these volatile compounds. The method used a splitless injector, a thick phase capillary column, and flame ionization detector (FID). An example of one GC chromatogram is shown in Figure 3.10.

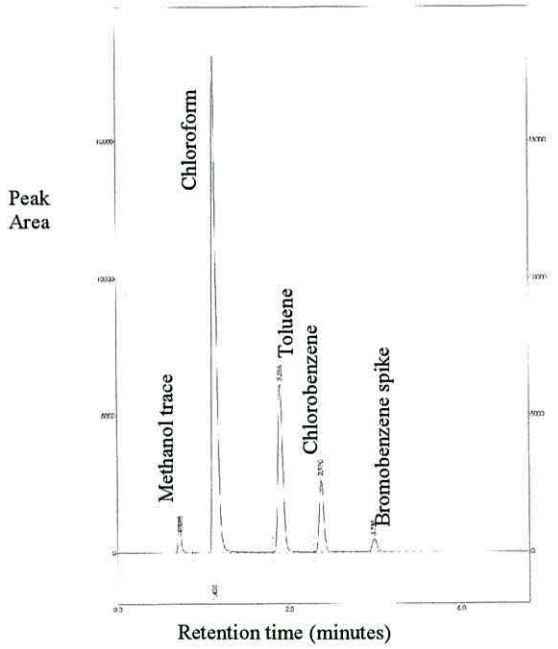

Figure 3.10. GC chromatogram showing resolution of the solvent peaks, chlorobenzene, chloroform, and toluene.

The chromatogram shown in Figure 3.10 is the resultant trace of an aliquot taken from the "fresh" microcapsule batch at 24 h. It shows peak area on the y axis and retention time in minutes on the x axis. Clearly, all solvent peaks are cleanly resolved in this chromatogram. The small first peak in the trace at 0.9 minutes is due to a methanol impurity in the chloroform solvent used. The second peak at 1.4 minutes is the largest of all peaks and is chloroform from the external solvent. The third peak at 2.3 minutes is toluene from the external solvent. The fourth peak at 2.9 minutes is chlorobenzene

leached from the microcapsules, and the final peak at 3.7 minutes is from a bromobenzene spike used to check the validity of these GC measurements.

The calibration curves in Figure 3.11 show data for a series of chlorobenzene standards and chloroform standards (a) and toluene standards (b). Standards were made from appropriate stock solutions in methanol and analyzed using GC-FID. All standards show an excellent linear response across a wide concentration range. Chlorobenzene: R^2 (3dp) = 1.000, BEC (mg/L) = 3820, equation of line; y = 49 x +1910. Toluene: R^2 (3dp) = 0.997, BEC (mg/L) = 5648, equation of line; y = 76 x + 2824. Chloroform: R^2 (3dp) = 0.999, BEC (mg/L) = 17,490, equation of line; y = 7 x + 8745.

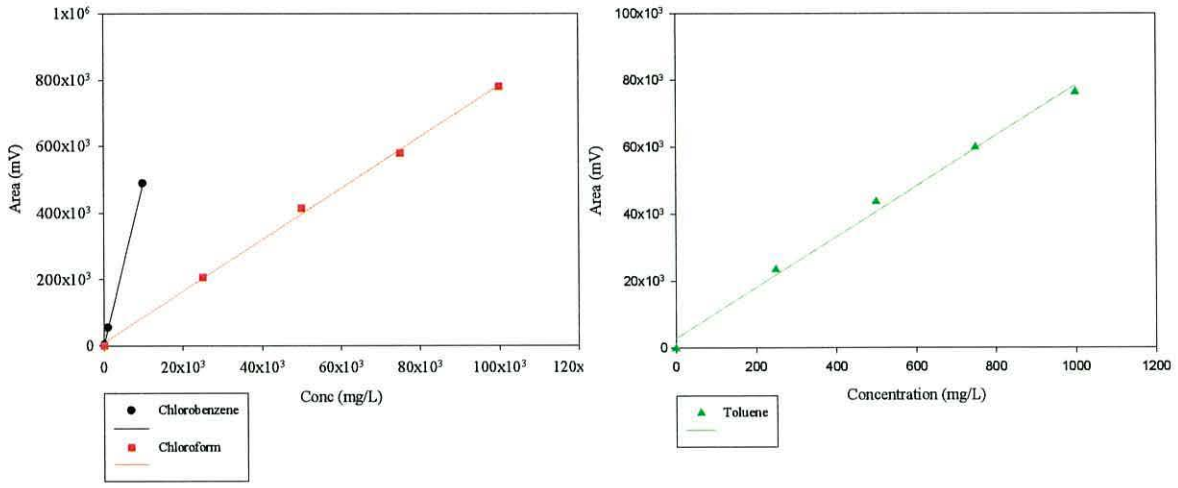

(a) (b)

Figure 3.11. Graphs to show peak area against solution concentration obtained by GC-FID for chlorobenzene and chloroform (a) and toluene (b).

Concentrations of chlorobenzene, toluene, and chloroform were calculated using the equations of the lines of best fit on the calibration graphs. The area under each solvent peak was converted to solvent mass (μg) taking into account the volume % aliquot. The chlorobenzene mass results were plotted against time (Figure 3.12).

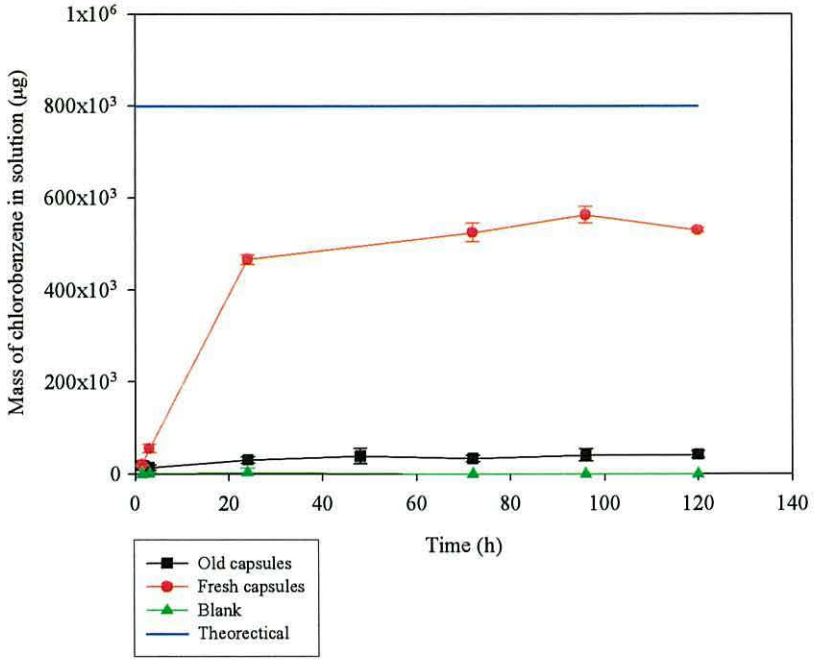

Figure 3.12. Graph showing chlorobenzene mass in solution over time (maximum mass of chlorobenzene encapsulated is estimated as 800,000 µg).

The graph in Figure 3.12 shows chlorobenzene mass against time taken as the average of three replicates with error bars shown. The black line corresponds to the measurements taken from the batch of "old" microcapsules, the red line corresponds to the measurements taken from the batch of "fresh" microcapsules and the green line corresponds to the measurements taken from the "blank". The data show that small amounts of chlorobenzene are leaching from the "old" microcapsules steadily over 120 h. In comparison, chlorobenzene leaches from the "fresh" capsules in much larger quantities over the same time frame. The "fresh" microcapsules appear to reach the "old" capsule rate after *ca.* 60 h. For example, after *ca.* 24 h the mass of chlorobenzene leached from the batch of "fresh" microcapsules is approximately 470,000 µg which is approximately fifteen times greater than the mass of chlorobenzene leached from the "old" microcapsules (*ca.* 30,000 µg). The leaching rate for the "fresh" microcapsules from the start of the experiment until 24 h is reached is calculated as 446869 µg/ 23 h (equivalent to 19,861 µg/ h). After this, the leaching continues but slows down to a rate of 96282 µg/ 72 h (equivalent to 1,337 µg/ h), reaching a plateau at *ca.* 560,000 µg until the end of the experiment at 120 h. The total mass of chlorobenzene released from the batch of fresh microcapsules after 120 h is therefore *ca.* 70 % of the internal phase

(based on our theoretical values). If chlorobenzene kept leaching from the batch of "fresh" microcapsules at the same rate measured at 120 h, then it would take approximately a further 180 h to leach all internal phase from microcapsules.

In comparison, the leaching rate for the "old" microcapsules from the start of the experiment until 24 h is reached is calculated as 11591 μg/ 23 h (equivalent to 515 μg/ h). Leaching continues after 24 h until the end of the experiment at a similar rate, 10332 μg/ 72 h (equivalent to 144 μg/ h). The low mass of the "old" microcapsules can be described by two different explanations. The first explanation suggests that the lower mass and lower leaching rate of chlorobenzene displayed by the "old" microcapsules is from continual leaching of the microcapsule internal phase over the two month post production aging period and therefore, the majority of the internal phase has already been "leached out". The data shows that the "old" capsules are releasing at 42,000 μg every 120 h. If the capsules have been releasing chlorobenzene at this rate during the past two months, then the mass of chlorobenzene leached from the microcapsules prior to the start of the experiment should be *ca.* (1440 h/ 120 h) x 42,000 μg = 504,000 μg. This predicted leached mass of chlorobenzene is 63 % of the total core content, therefore this could explain why the values are so low for the "old" capsules. Also, the "old" microcapsules may have been initially releasing chlorobenzene at a higher rate which then slowed down after a certain time period prior to the start of the experiment. This would account for loss of the majority of the total core content before the experiment.

The predicted leach rate is based upon findings from the data which involved the microcapsules dispersed in solution. However, the "old" microcapsules were stored in air over the two month period which may affect the leaching rate. A second explanation is that during the two month aging period, the microcapsule polymer wall has undergone further curing to create a more robust, less permeable polymer wall. Therefore, the internal phase is still encapsulated within the polymer wall but unable to escape as easily as in the case of the "fresh" microcapsules. The literature was searched for evidence to support this second theory, however there appears to be a dearth of papers concerning this topic. The slowing rate of leaching in the "fresh" capsules would be consistent with this second explanation.

The data for the mass of toluene for these capsules were also plotted against time to examine whether it was entering into the microcapsules and exchanging with the leaching chlorobenzene (Figure 3.13).

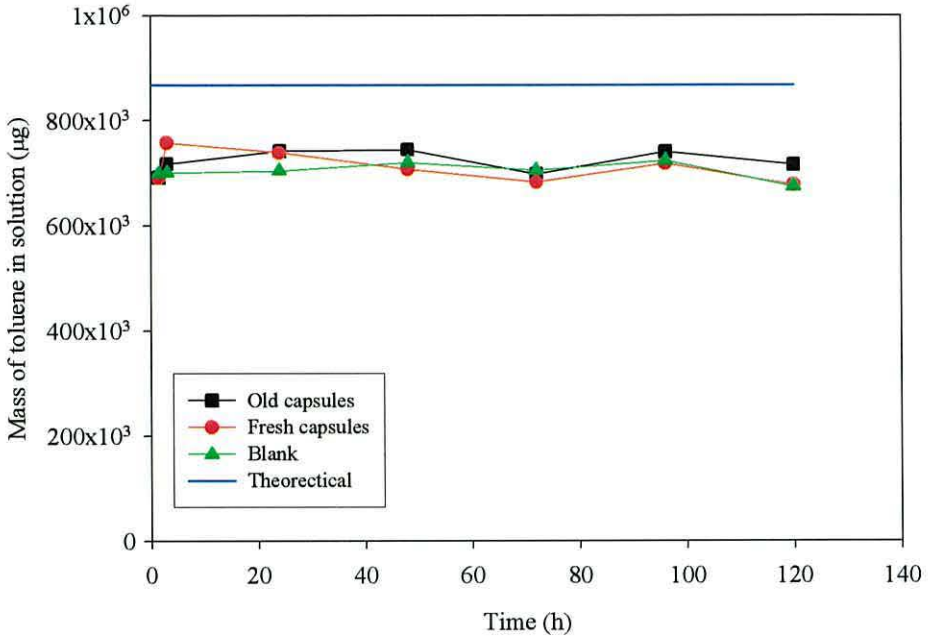

Figure 3.13. Graph showing the mass of toluene in solution over time.

All three experiments (old, fresh and blank) show a slight increase in toluene mass over time, but within experimental error the gradients of all lines can be reported as being approximately zero. From this data there is no evidence for toluene exchanging with the leaching chlorobenzene either in the "old" or "fresh" microcapsules. It was shown in Figure 3.11 that the mass of chlorobenzene displaced by one gram of the "fresh" microcapsules after 120 h in an environment of 20 ml of solvent (chloroform/toluene, 19:1) was *ca.* 560,000 µg. If such "fresh" microcapsules were behaving as "artificial cells" as proposed earlier in section 3.3, it is to be expected that *ca.* 560,000 µg of toluene would have entered the microcapsules if the solvent exchange was mass dependent (0.7 ml if volume dependent, and 6.1 mmol if molar dependent).

Explanation of the toluene data initially indicate towards the second theory proposed earlier to explain the chlorobenzene data, *i.e.* the microcapsule wall has undergone post production aging causing the wall to be more robust, thus retaining the internal phase, and hampering solvent exchange. However, all toluene data ("fresh",

"old" and blank) follow the same trends over 120 h. If post production ageing of the microcapsules had occurred, a difference in the toluene data trend-lines between the "old" and "fresh" batches of microcapsules would be expected. Therefore, it was concluded that the toluene data does not support the "post production ageing" theory and another explanation was required. Prior to this, the chloroform data was examined.

The data for the mass of chloroform for these capsules were plotted against time to examine whether this compound might be entering the microcapsules and exchanging with the leaching chlorobenzene (Figure 3.14).

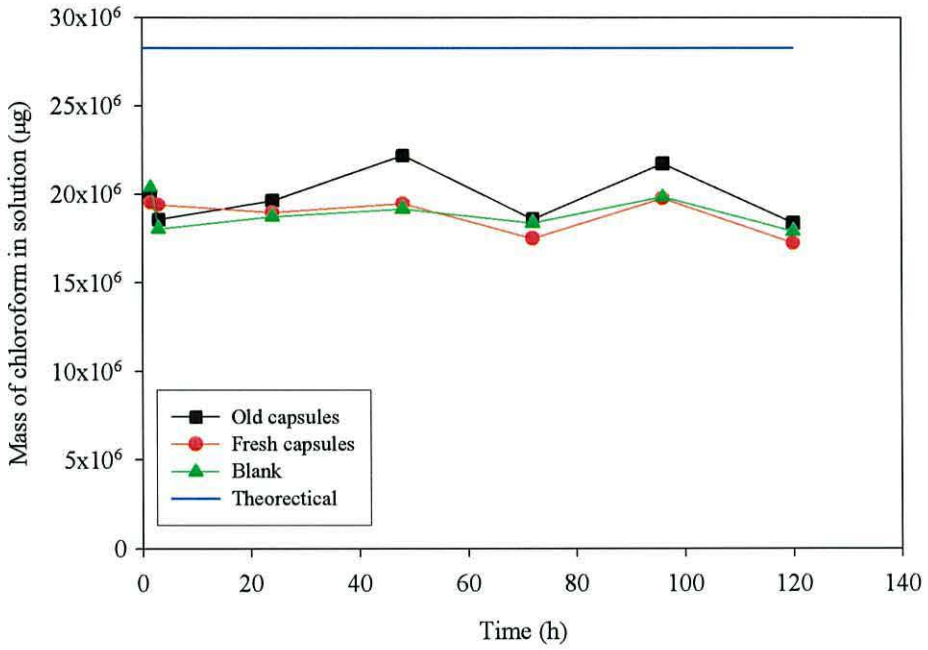

Figure 3.14. Graph showing mass of chloroform in solution over time.

All three experiments (old, fresh and blank) show a slight increase in chloroform mass over time, but within experimental error the gradients of all lines can be reported as being approximately zero. It was predicted that chloroform, a smaller molecule (molecular size as x = 1.8 Å, y = 2.4 Å, z = 1.8 Å) than toluene would exchange with the leaching chlorobenzene but from the data there is no evidence for chloroform exchanging with the leaching chlorobenzene either in the "old" or "fresh" microcapsules.

3.4.2. Solvent Leaching Experiment 2

This experiment was designed to compare with data gathered from the first leading experiment. The only change was to reverse the toluene/chloroform external solvent ratios from 1:19 to 19:1. The reasons for this change in ratio were twofold; firstly to see if a larger excess of toluene in the presence of chloroform would increase exchange with the internal core material of chlorobenzene and secondly, to study whether any changes to chloroform concentrations would be observable at lower overall chloroform levels. However, initial GC chromatograms for these samples (run using the same conditions as the first solvent leaching experiment) displayed poor peak separation due to the high toluene content in each sample (see Figure 3.15, (a)). The large toluene peak seen at 2.3 minutes overlapped and dwarfed the chlorobenzene peak at 2.9 minutes, making accurate integration of the smaller chlorobenzene content of the sample impossible. Therefore, the GC conditions were altered for this experiment by switching to a GC with a split/splitless injector which enabled resolution of the toluene and chlorobenzene peaks in the resulting chromatograms by venting off excess solvent vapour rather than it being passed down the column (Figure 3.15, (b)).

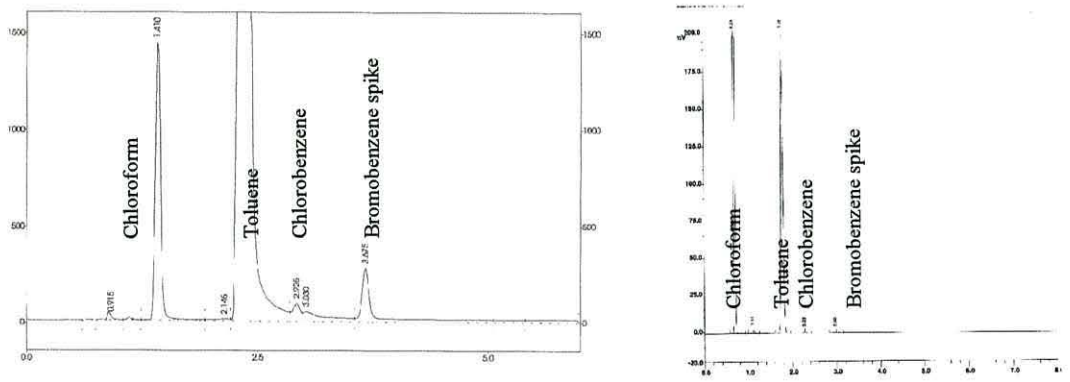

(a) (b)

Figure 3.15. GC chromatograms showing (a) poor solvent peak resolution, and (b) good solvent peak resolution.

The GC was then calibrated using a series of standards and calibration graphs were plotted for all the solvents under investigation (graphs not shown). Chlorobenzene: R^2

(3dp) = 0.996, BEC (mg/L) = 576, equation of line: y = 11 x + 288, toluene: R^2 (3dp) = 0.999, BEC (mg/L) = 57178, equation of line: y = 20 x - 28589, chloroform: R^2 (3dp) = 0.999, BEC (mg/L) = 200, equation of line: y = x + 100. The GC data obtained for chlorobenzene concentrations was converted to mass and then plotted against time (Figure 3.16).

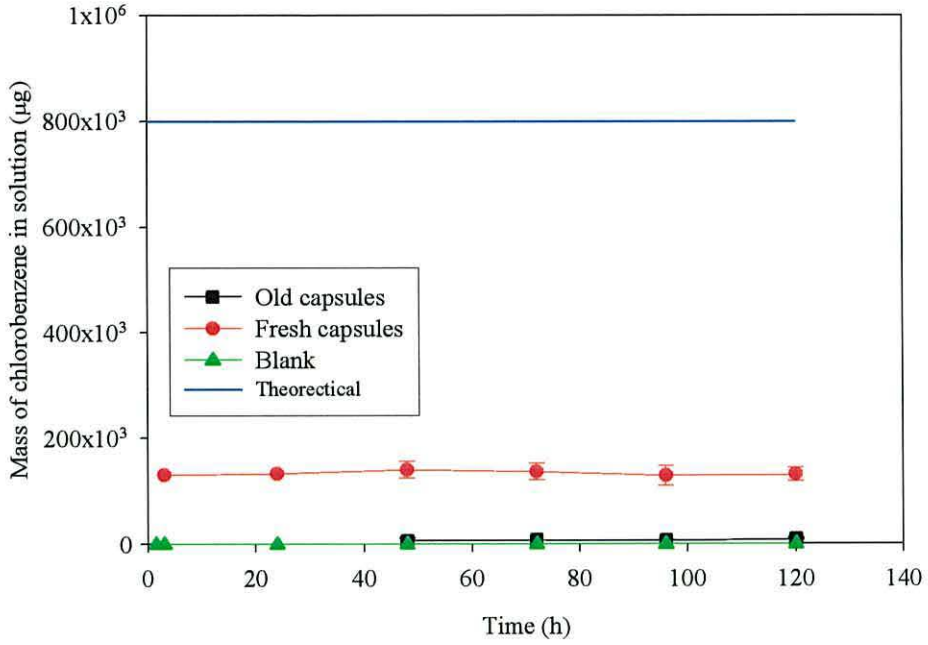

Figure 3.16. Graph showing mass of chlorobenzene in solution for "old" and "fresh" microcapsules over time.

The data show that very small amounts of chlorobenzene are leaching from the "old" microcapsules steadily over 120 h. Chlorobenzene appears to leach from the "fresh" capsules at the same rate as from the "old" capsules but in larger quantities. For example, after 120 h the "old" microcapsules have leached *ca.* 9,000 µg whereas the "fresh" microcapsules have leached *ca.* 13,000 µg. In comparison to the data from experiment 1, after 120 h the "old" capsules have leached almost 5 times less chlorobenzene and the "fresh" capsules have leached *ca.* 40 times less chlorobenzene. The control experiment (blank) shows no chlorobenzene in the aliquot samples tested as expected. The data for the mass of toluene in solution were plotted against time to examine whether this solvent was entering into the microcapsules in exchange for chlorobenzene (Figure 3.17). The data obtained for the old microcapsule batch shows the toluene to decrease in mass over time, whilst an increase in toluene mass over time is observed for both the fresh microcapsule batch and the control experiment. The error

bars show this increase to be within experimental error and can be reported as being approximately a line with a gradient of zero. Most importantly, observation of the "old" and "fresh" capsule data shows there is no variance from the blank. Therefore, it can be concluded that no toluene is leaching into the microcapsules.

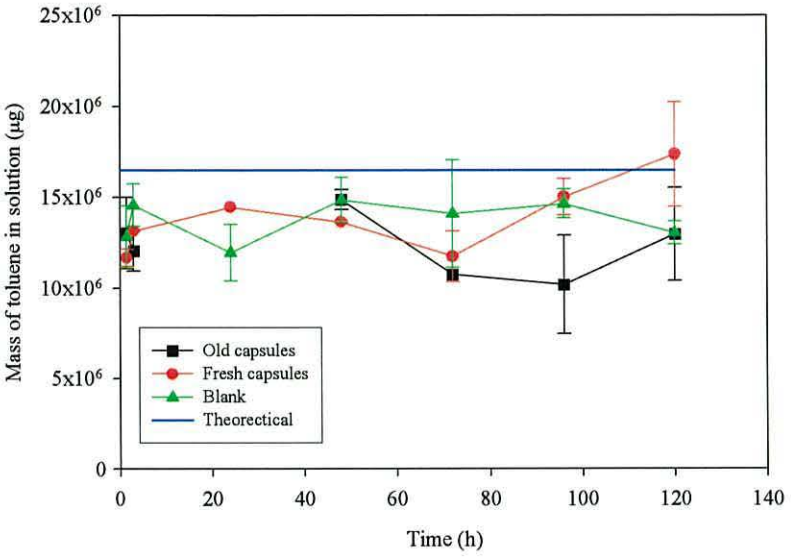

Figure 3.17. Graph showing mass of toluene in solution over time.

The data for chloroform were plotted against time to examine whether it was entering into the microcapsules and exchanging with the leaching chlorobenzene (Figure 3.18).

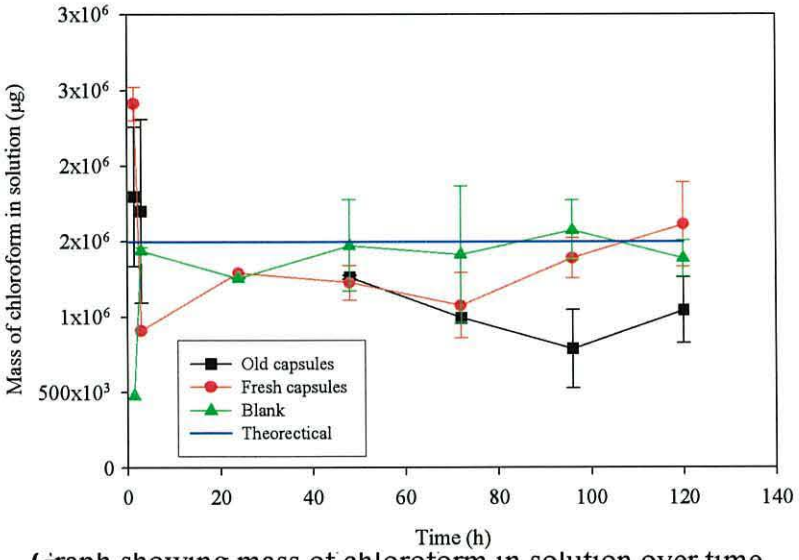

Figure 3.18. Graph showing mass of chloroform in solution over time.

The data for the "old" capsules appears to decrease whilst the lines that represent the "fresh" capsules and control experiments both increase as seen before in test 1 data.

Again, the data for the "old" and "fresh" microcapsules show no variance from the blank. Therefore, within experimental error it can be concluded that chloroform does not appear to leach into the batches of microcapsules. To investigate further the possible reasons why toluene and chloroform did not appear to enter into the "fresh" or "old" microcapsules either in experiment 1 or experiment 2, the capsule morphology was examined using optical microscopy (Figures 3.19 and 3.20).

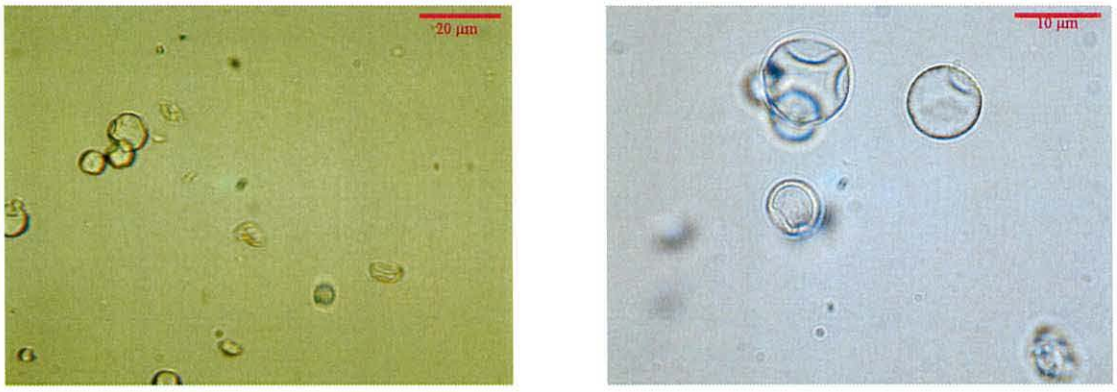

(a) (b)

Figure 3.19. Optical micrographs showing a sample of microcapsules containing chlorobenzene taken from the batch of "fresh" microcapsules: (a) (magnification = x 400), and (b) (magnification = x 1000).

The optical micrographs in Figure 3.19 show a sample of "fresh" chlorobenzene containing microcapsules at two different magnifications (x 400) and (x 1000). The majority of microcapsules shown in both (a) and (b) appear spherical and intact. A few of the microcapsules in (b) appear to have folded inwards. Such surface morphology was seen in various micrographs (optical, fluorescence, and SEM) in chapter 2 and explained by the onset of microcapsule deflation. The microcapsule particle size distribution shown in both (a) and (b) is shown to be 6-10 µm. These microcapsule sizes correlate with other batches of chlorobenzene containing microcapsules made using method 2 (see Chapter 2). The optical micrographs in Figure 3.20 show a sample of "old" chlorobenzene containing microcapsules at two different magnifications (x 400) and (x 1000). The optical micrograph in (a) shows "old" microcapsules are vastly shrunken in comparison with the "fresh" microcapsules at the same magnification (Figure 3.19 (a)). The particle size distribution is not distinguishable at this magnification, however it can be seen that all capsules are $\leq$ 1µm in diameter. In Figure 3.20 (b), the microcapsules are observed using a higher magnification. In both (a) and (b), it is difficult to observe "microcapsules", since the optical micrograph

shows an image which appears to look more like microscopic polymeric clumps rather than microcapsules. However, both optical micrographs clearly show the "old" batch of microcapsules to be dramatically reduced in size compared to the "fresh" batch of microcapsules.

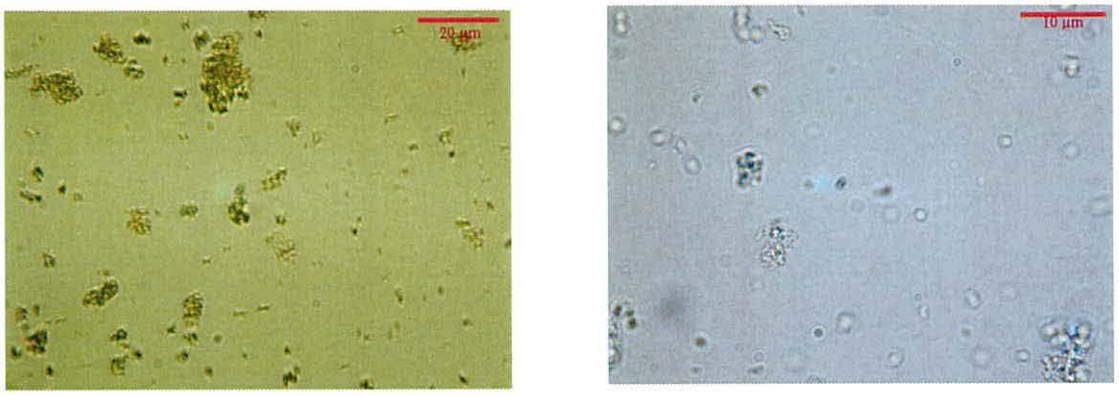

(a) (b)

Figure 3.20. Optical micrographs showing a sample of microcapsules containing chlorobenzene taken from the batch of "old" microcapsules: (a) (magnification = x 400), and (b) (magnification = x 1000).

3.5. Conclusions

Data gathered from the various leaching experiments presented in this chapter show that when melamine-formaldehyde microcapsules containing an internal phase (IP) of either neat chlorobenzene or a solute in chlorobenzene (or toluene) are removed from the aqueous "mother liquor", IP leaching occurs. The rate of IP leaching is highly dependent upon (i) the IP properties and (ii) the external environment in which the microcapsules reside. The IP properties such as size of molecule and solubility play an important role in rate of leaching. If the IP is more soluble in the external environment than the internal environment, a greater leach rate will ensue. Also if the polymer wall is slightly soluble in the IP, swelling of the polymer will occur thus increasing the IP leach rate.

The external environment is a key factor in controlling concentration gradients between the interior and exterior of the microcapsule. When a large concentration gradient exists between the interior and exterior of the microcapsule, larger quantities of IP will be driven out of the microcapsule by osmotic pressure. Again, if the polymer wall has a high capacity for swelling in the external environment, the IP leach rate will

be high. It was shown from the final leaching experiments in this chapter that the amount of IP leached from microcapsules depends upon the age of the capsule. "Fresh" microcapsules which were one week old leached significantly more IP (*ca.* 65 % more IP) than the "old" microcapsules which were two month old. Two explanations were initially put forward to describe why the batch of "old" microcapsules leached such lower masses of chlorobenzene in comparison with the "fresh" batch of microcapsules. However, after further leaching tests such low masses detected from the "old" microcapsules were attributed due to the IP having been pre-leached while in storage.

The original explanation of such internal phase leaching arose from the idea that the melamine-formaldehyde microcapsule polymer wall was acting as a semi-permeable membrane, allowing the solvent to pass through the wall. This was investigated further by the final leaching experiments that involved attempted exchange of toluene and chloroform solvents with chlorobenzene through the microcapsule wall driven by osmotic pressure. However, the data from these experiments showed no toluene or chloroform passed into the microcapsules, although chlorobenzene was shown to leach out. Such data can be interpreted by the following analogy (Figure 3.21)

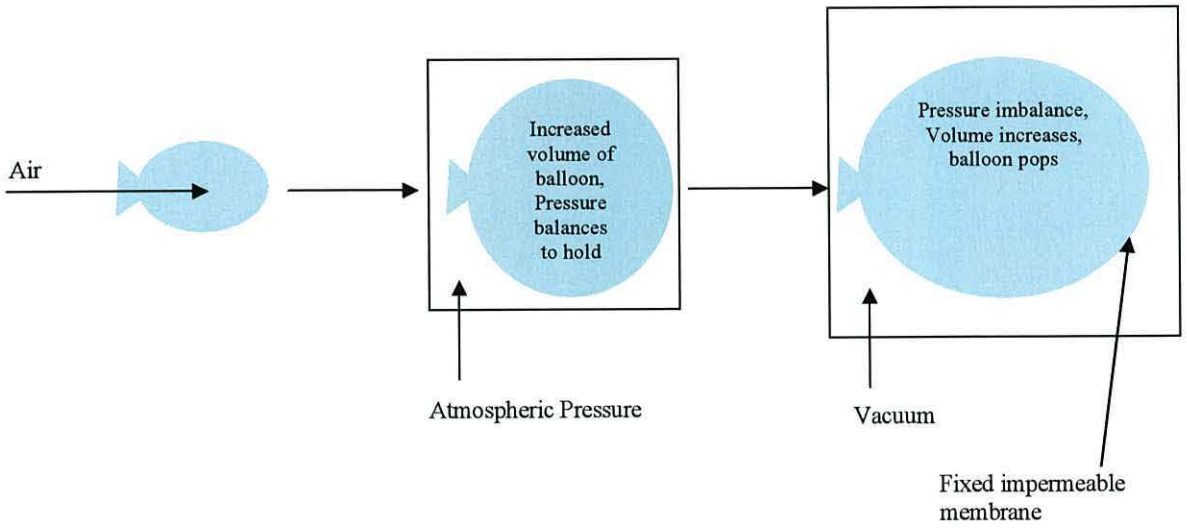

Figure 3.21. A schematic diagram showing the proceedings that follow an external pressure change upon an air filled balloon with a fixed impermeable membrane.

A balloon filled with air and stored under atmospheric pressure will contain a slightly higher internal pressure than the external atmospheric pressure. Therefore, the balloon

exhibits a slightly positive pressure in comparison to the external environment. If the balloon was to be transferred to a sealed vessel where upon evacuation of the vessel was followed, this would result in the balloon popping caused by the constraint of the fixed impermeable balloon membrane (Figure 3.21). If individual microcapsules are considered analogous to the balloon described above, this "balloon theory" could be used to describe the microcapsule leaching results obtained in this chapter. The microencapsulation procedure used throughout this thesis is based upon the process of *in situ* interfacial polymerization which produces solvent containing microcapsules suspended in aqueous slurry. Alternatively, the aqueous slurry could be thought of as the "mother liquor". When the microcapsules are suspended in this mother liquor, a pressure gradient specific for this environment will exist between the microcapsule polymer wall and the surrounding aqueous phase. If the microcapsules are taken from the mother liquor and placed into a different surrounding, for example air or a different solvent, then the pressure gradient will change to accommodate for such a change in surroundings. It is thought that the high concentration of chlorobenzene inside the microcapsules compared to the external environment creates a high pressure gradient across the melamine-formaldehyde polymer wall. Such a gradient causes the internal phase to expel from the microcapsules in such a manner that the capsules rapidly deflate with eventual release of all internal phase and leaving behind a collapsed polymeric shell. Therefore, attempting to pass solvent back into the microcapsules is in effect, attempting to try to "re-inflate" the microcapsules. The external solvent does not re-inflate the microcapsules but just causes polymer shell swelling (Figure 3.22).

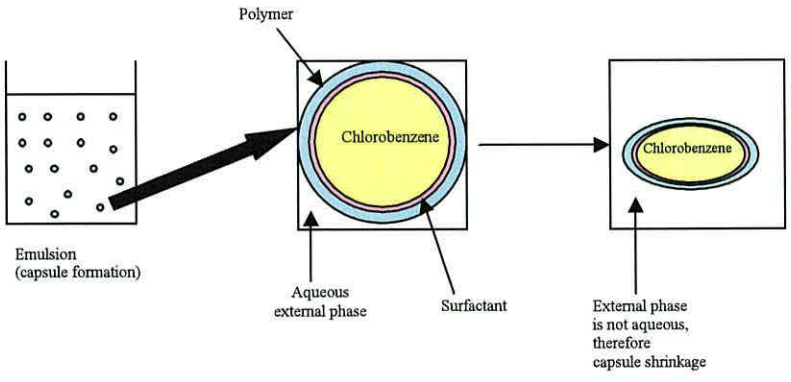

Figure 3.22. A schematic diagram showing the proceedings arising form removing microcapsules from the "mother liquor", *i.e.* microcapsule shrinkage.

3.6. References

1 Mark, H.F.,(Ed.), *Encyclopedia of Polymer Science Technology (Vol 2),* Wiley, New York,1965

2 Billmeyer, F.W., *Textbook of Polymer Science (3rd Ed),* Wiley, USA, 1994

3 Holliman, P.J., Clark J.A, Williamson, J.C, Jones, D.L., *Science of the Total Environment*, 2005, **336**, 13

4 Traub, B., Fritzhanns, T., Hafner, S., Spiess, H.W., *Colloid and Polymer Science*, 2000, **278**, 547

5 Sparks, D.L., (Ed.), *Methods of Soil Analysis, Part 3 Chemical Methods*, SSSA, USA, 1996

6 Kaplan, L., Kester, W.L., Katz, J.J., *Journal of the American Chemical Society*, 1952, **74**, 5531

7 Chang, T.M.S, *Science*, 1964, **146**, 524

8 Chang, T.M.S, Yu, W.P., Wong, J.P., *Journal of Microencapsulation*, 1998, **15**, 515

9 Chang, T.M.S., *European Journal of Pharmaceutics and Biopharmaceutics*, 1998, **45**, 3

10 Saiter, A., Devallencourt, C., Saiter, J.M, Grenet, J., *Materials Letters*, 2000, **45**, 180

CHAPTER 4

RESULTS AND DISCUSSION

CATALYSIS

4. Catalysis

Catalyst Synthesis

The organometallic complex; dichlorotris(triphenylphosphine)ruthenium (II) (Figure 4.1) was initially chosen for encapsulation because it is a versatile complex that is easily synthesized. [1] The complex is normally used as a catalyst in transfer hydrogenations [2], although it has been used to catalyse hydrogenation reactions. [3]

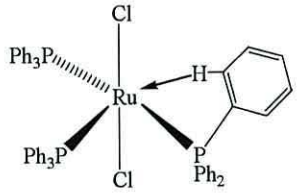

Figure 4.1. Chemical structure of tris(triphenylphosphine)dichlororuthenium (II) ($[RuCl_2(PPh_3)_3]$) in the solid state. [4]

The ruthenium complex was successfully synthesized by following a literature procedure. [1] Ruthenium trichloride trihydrate, in methanol was heated to reflux for 5 minutes under a nitrogen atmosphere. Thereafter, 6 equivalents of triphenylphosphine were added to the reaction vessel and the reaction mixture was left to reflux under nitrogen for 3 h. A black powder precipitate, which formed from the hot solution, was filtered and washed with ether giving a 94 % product yield. The black powder was characterised using elemental analysis (C, H, and N), ^{1}H NMR spectroscopy, ^{13}C NMR spectroscopy, ^{31}P NMR spectroscopy, and by melting point determination. The data was consistent with that reported in the literature [1] (see section 5.5.3 for details).

Catalyst Encapsulation

Microcapsules were prepared using an internal phase of chlorobenzene solution (63 g) containing dichlorotris(triphenylphosphine)ruthenium (II) (1 % by weight) following method 2 (see section 5.6.2 for details). Microcapsules were characterized using SEM and EDAX. Samples were prepared for SEM and EDAX by placing small amounts (*ca.* 0.1

mg) of filtered microcapsules on the prepared SEM aluminium stubs (see section 5.8.1 for preparation details).

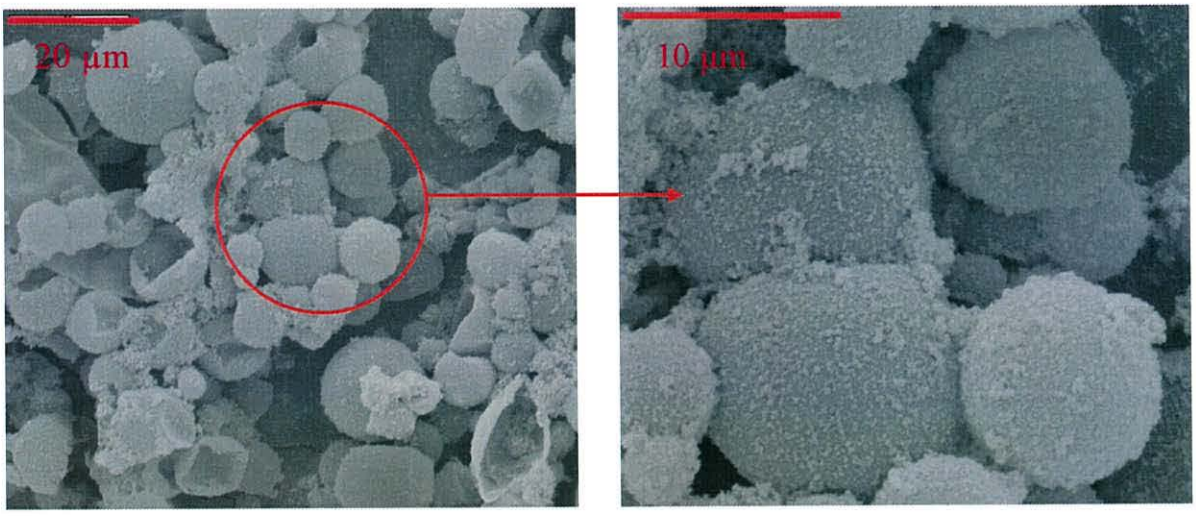

(a) (b)

Figure 4.2. SEM images (a) and (b), both of which show a sample of uncrushed ruthenium containing microcapsules.

A range of microcapsule sizes and morphologies are shown in the SEM image in Figure 4.2 (a). The microcapsule size distribution range appears to be *ca.* 2 – 20 μm. This size range correlates with previous method 2 microcapsule size ranges (see Chapters 2 and 3). Approx 50 % appear to possess some degree of deflation with approximately 50 % of the microcapsules fully intact (Figure 4.2 (a)). Several large clumps of polymeric material are shown to be resting alongside the microcapsules within this sample. The SEM image in (b) is a magnified image of the centralised microcapsules in (a). The large microcapsules shown are seen to be *ca.* 10 μm in diameter, and a few smaller microcapsules are also shown at the periphery of the micrograph. The microcapsules appear to be fully spherical and intact, showing no signs of deflation. The magnified image allows close examination of the microcapsule surface, showing it to be covered with nanoparticulate polymeric matter. Such nanoparticulate matter is consistently seen in other SEM images reported in this thesis when the microcapsule samples were made using method 2 (see chapters 2 and 3).

The EDAX trace shown in Figure 4.3 is the resultant trace from analyzing X-rays at the centre of the large microcapsule shown in Figure 4.2 (b). The trace shows qualitative detection of the element ruthenium within the sample of microcapsules as expected.

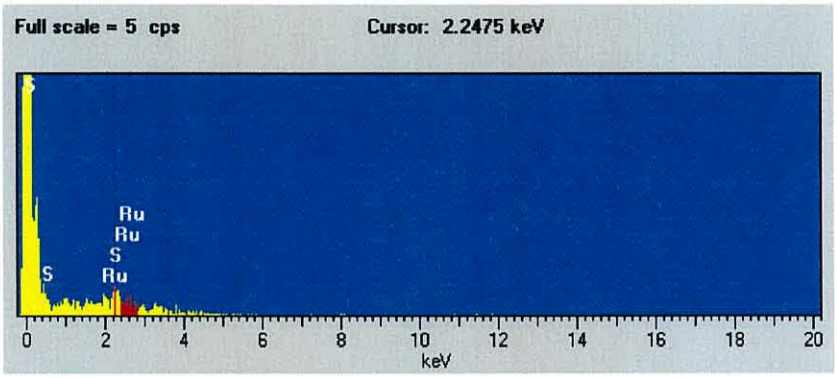

Figure 4.3. EDAX trace showing ruthenium signal obtained from uncrushed microcapsules shown in Figure 4.2 (b).

A fraction of the microcapsules were crushed using a mortar and pestle and the resultant capsules are shown in the SEM image in Figure 4.4.

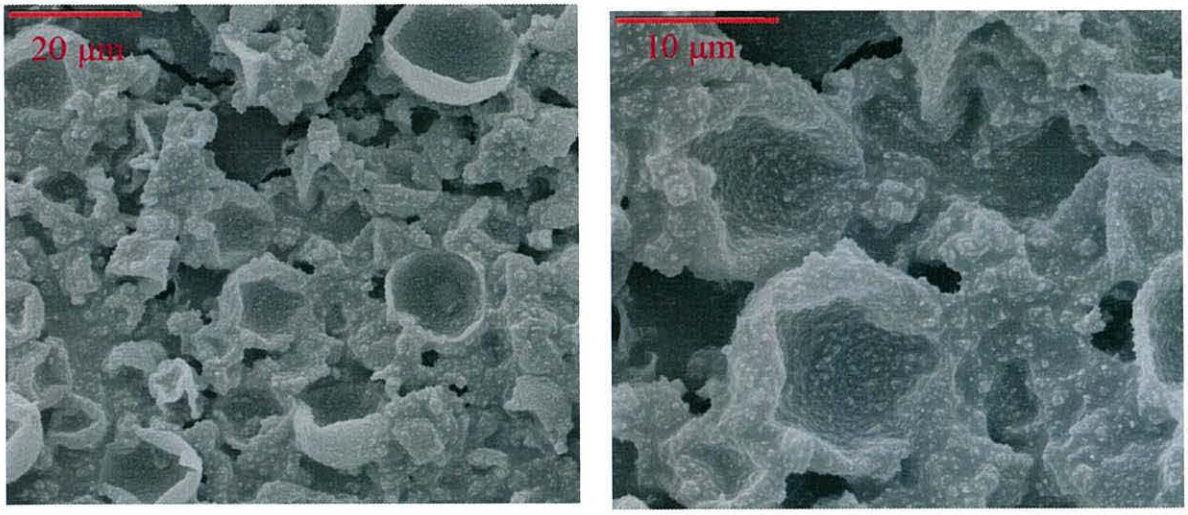

(a) (b)

Figure 4.4. SEM images (a) and (b) showing a large cross section of a sample of crushed microcapsules.

The majority of microcapsules shown in Figure 4.4 (a) appear to be crushed or "squashed". Again, a large microcapsule size distribution (*ca.* 2-20 μm) is shown in the SEM image in Figure 4.4 (a) which was seen earlier in Figure 4.2 (a), thus indicating that such a size distribution is representative of the microcapsule batch. The image in (b) is a magnified version of the crushed microcapsules shown in the centre of the image in (a). Both SEM images show that although the majority of microcapsules appear crushed using this method, the larger capsules still have retained part of the spherical shape, whereas the smaller microcapsules (≤ 5 μm) are shown to have completely lost shape. The microcapsule surface is shown to be uneven. It appears that crushing the microcapsule sample has forced the nanoparticulate matter that was previously resting on top of the microcapsules downwards, and thus embedding it into the polymeric capsule wall.

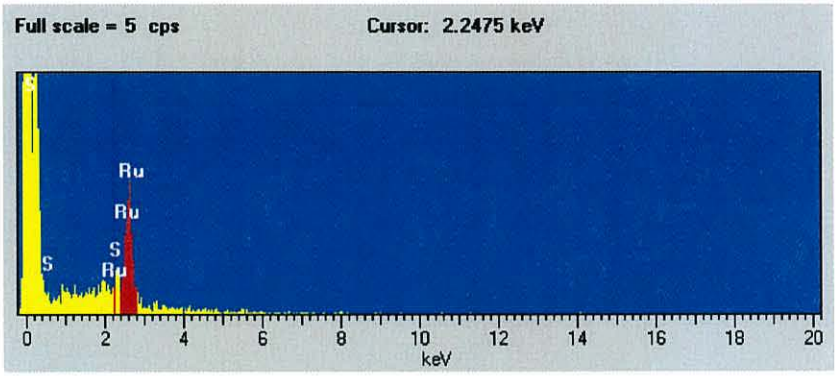

Figure 4.5. EDAX trace showing ruthenium signal obtained from crushed microcapsules seen above in Figure 4.4 (b).

An EDAX trace (Figure 4.5), resulting from directing X-rays at the centre of the large crushed microcapsule shown in Figure 4.4 (b) shows augmentation of the ruthenium content present which was expected since a greater surface area of the ruthenium complex within the microcapsule is exposed upon crushing.

Catalyst Modification

The ruthenium complex discussed above contains triphenylphosphine ligands and consequently was not too soluble in the chlorobenzene used for encapsulation. By changing all three triphenylphosphine ligands to tri-*n*-butylphosphine ligands which was

achieved by adapting the literature preparation used to make $RuCl_2(PPh_3)_3$, a more soluble complex was obtained. The crude product in solution was firstly washed with ether, dried using $MgSO_4$ and then the solvent was removed, yielding red oil (89%). The red oil was characterised using elemental analysis (C, H and N), ^1H NMR spectroscopy, ^{13}C NMR spectroscopy, ^{31}P NMR spectroscopy and mass spectrometry. Later, red crystals precipitated from the red oil and were characterised using X-ray crystallography (see Appendix). Elemental analysis confirmed the compound purity. As seen for the phenyl ligand, the three *n*-butyl groups attached to each phosphorus are all equivalent. Therefore, the 4 resonances that appear in the ^1H NMR spectrum are resulting from the different proton environments within the hydrocarbon chain. The triplet resonance that occurs at 1.39 ppm (C4) is the terminal methyl and the corresponding methylene reasonances occur at 1.81 ppm (C3), 2.00 ppm (C2), and 2.31 ppm (C1), where C1 is carbon attached to phosphorus. Direct insertion mass spectrometry was carried out on the compound and the parent molecular ion minus a chlorine atom ($[M\text{-}Cl^-]^+$ = 743) was observed in 53 % abundance. The butyl phosphine ligand was observed as a fragment in 100 % abundance.

The ruthenium complex, tris(tri-*n*-butylphosphine)dichlororuthenium (II) was trialled in an encapsulation experiment to test the integrity of the complex. The complex was encapsulated using method 1 (see section 5.6.2 for details). The internal phase was a toluene solution of the complex (0.5 % by weight).

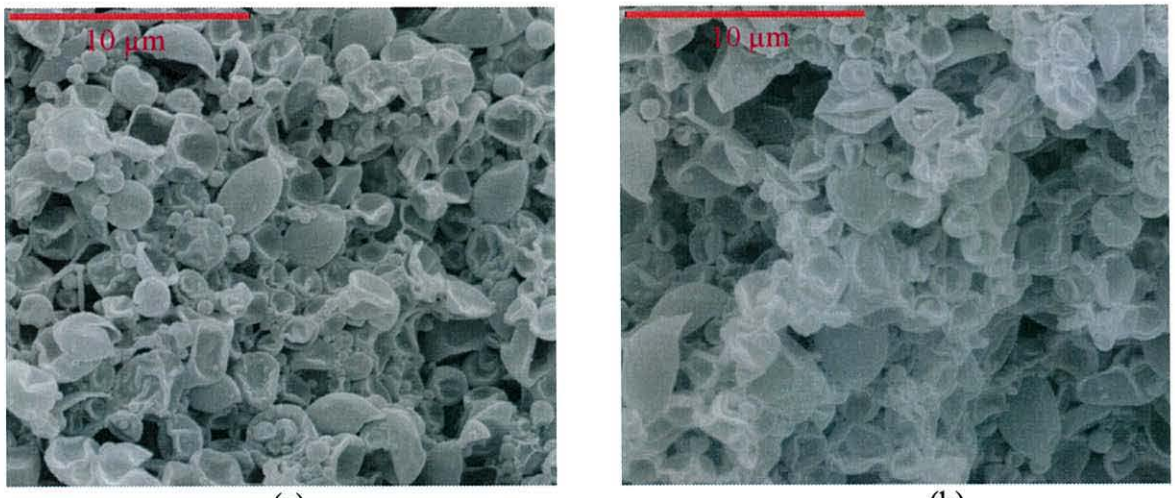

(a) (b)

Figure 4.6. SEM images of (a) uncrushed microcapsules and (b) crushed microcapsules.

The resulting microcapsules were characterized using SEM, EDAX, and particle size distribution (Figure 4.6). The majority of microcapsules shown in Figure 4.6 (a) appear intact. However, some of the larger microcapsules appear deflated due to internal phase leaching. A large capsule size distribution is seen, ranging from *ca.* 1-5 μm. This correlates with previous method 1 microcapsule size ranges (see chapter 2). This particle size range is seen again in the SEM image in (b), where the microcapsule sample was crushed using a mortar and pestle. The majority of microcapsules, in particular the larger capsules, are shown to be crushed or "squashed". The nanoparticulate matter seen in the earlier SEM image (Figure 4.4) is absent in both SEM images in Figure 4.6. This is due to a different microencapsulation method used, *i.e.* the change in surfactant.

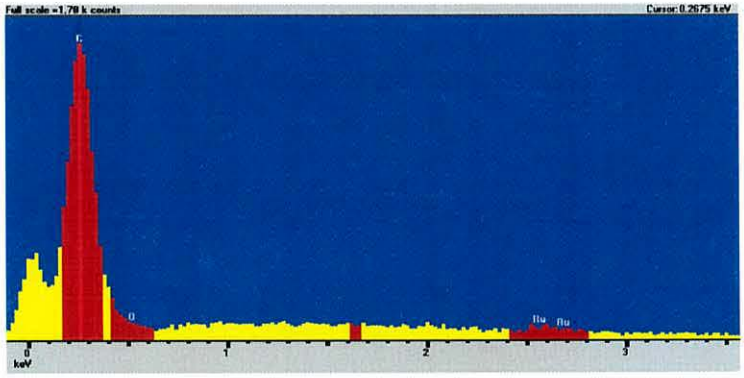

(a)

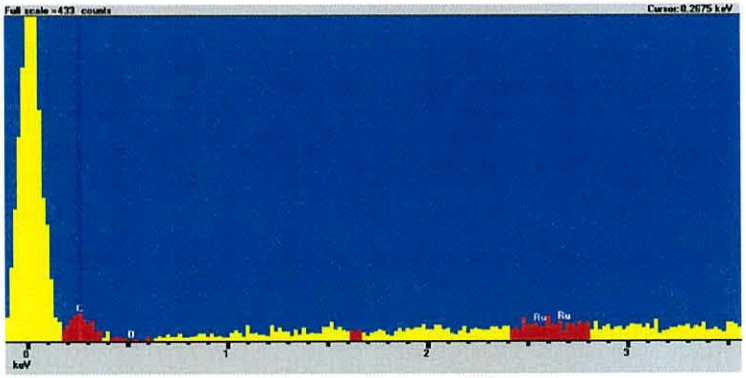

(b)

Figure 4.7. EDAX showing traces of ruthenium in (a) uncrushed microcapsules and (b) crushed microcapsules from microcapsules shown in Figure 4.6.

The EDAX shown in Figure 4.7 (a) is the resultant trace from directing X-rays at the centre of the large deflated microcapsule situated towards the centre of the SEM image shown in Figure 4.6 (a). The EDAX shows trace amounts of the element ruthenium within the sample of microcapsules. EDAX was carried out on the crushed microcapsule sample (Figure 4.7 (b)), by analyzing X-rays at the crushed microcapsule situated towards the centre of the SEM image shown in Figure 4.6 (b). Again, trace amounts of ruthenium were found in the crushed microcapsule sample.

The graph in Figure 4.8 shows particle size data whereby volume % is plotted against particle diameter. The graph shows that all microcapsule are below 25 μm in size, as was confirmed in the SEM images shown in Figure 4.6. The graph shows that approximately 50 % of the microcapsules in the slurry volume taken for analysis are *ca.* 2.5 μm in diameter.

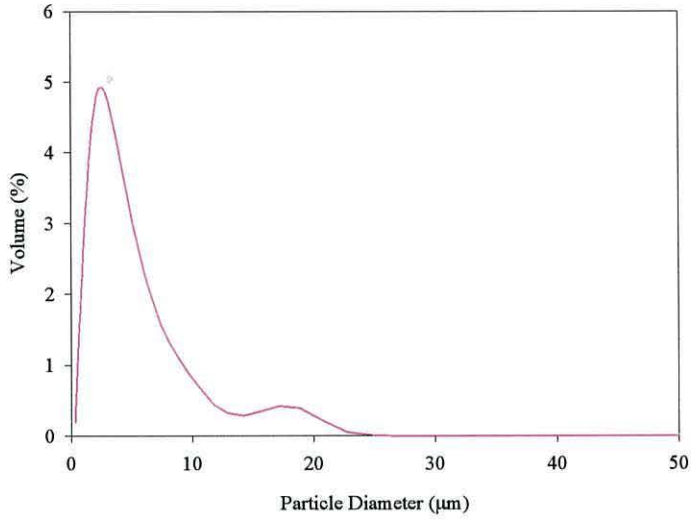

Figure 4.8. Graph showing particle size distribution of microcapsules containing a toluene solution of dissolved catalyst.

A small % of the microcapsules in the slurry (*ca.* 5 %) are *ca.* 17.5 μm in diameter. The ruthenium complex; $RuCl_2(P^nBu_3)_3$ is a new compound, however it is known that similar compounds have been made. [5] Therefore, when testing the catalytic activity of the

ruthenium containing microcapsules it was considered appropriate that the literature compound, $RuCl_2(PPh_3)_3$ with known catalytic data for comparison be tested before the unknown ruthenium complex, $RuCl_2(P^nBu_3)_3$.

Catalyst Testing

The EDAX traces obtained from analyzing X-rays at both batches of microcapsules clearly show ruthenium within the microcapsules. However, the EDAX traces do not discern whether the ruthenium complex is still intact after the microencapsulation process. To determine this, the microcapsules were tested for catalytic activity. As mentioned earlier: $[RuCl_2(PPh_3)_3]$ has been used to catalyze hydrogenation reactions. [3] It is known that transition metals such as ruthenium are unique in their ability to activate hydrogen under very mild conditions, thus accounting for their utility in catalytic hydrogenation. [6] One example is the hydrogenation reaction of 1-heptene under ambient conditions (Figure 4.9).[3]

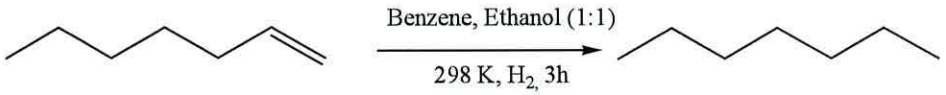

Figure 4.9. Hydrogenation of 1-heptene, *reagents and conditions*: $[RuCl_2(PPh_3)_3]$ (0.013 mol), 1-heptene (100 mol), benzene (25 ml), absolute ethanol (25 ml), H_2, 298 K, 3 h.

The hydrogenation reaction that converts 1-heptene to heptane can be easily monitored using gas chromatography. This reaction was considered an appropriate test reaction for the complex integrity. As a control reaction, the ruthenium complex was initially checked for catalytic activity in the hydrogenation reaction of 1-heptene before encapsulation and catalytic results were as found in the literature [3] (see section 5.7.1.1 for experimental details). The mechanism of hydrogenation of this complex has been studied and it is believed that the complex activates H_2 heterolytically. [7,8] A schematic diagram displaying the proposed catalytic mechanism is shown in Figure 4.10. It is reported in the literature that the likely intermediate in the heterolytic activation of H_2 is often a dihydrogen complex. [8] Following elimination of HCl, a ruthenium monohydride is produced which coordinates with the olefin substrate. Then following migration, addition of dihydrogen

and reductive elimination of product, the original monohydride is regenerated and recycled in the catalytic loop. Thus, the traditional oxidative addition step is avoided as this would necessitate Ru (II) being formally oxidised to Ru (IV) which is not a very stable oxidation state for ruthenium. [8]

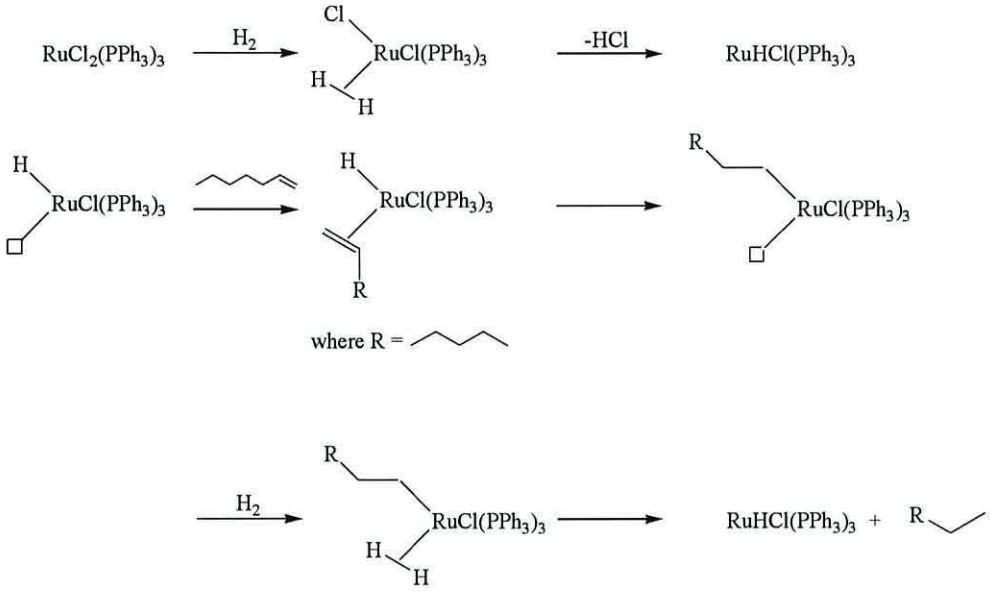

Figure 4.10. Reaction mechanism of the hydrogenation of 1-heptene using the ruthenium complex, $[RuCl_2(PPh_3)_3]$ as catalyst. [8]

The microcapsules containing dichlorotris(triphenylphosphine)ruthenium (1 g of microcapsules that contained an estimated 8 mg of ruthenium complex assuming complete encapsulation) were tested for catalytic activity under the same reaction conditions (1-heptene, 9.9 ml, 100 mmol; absolute ethanol, 25 ml; anhydrous benzene, 25 ml) and same GC monitoring conditions as stated earlier for the control reaction, *i.e.* "unencapsulated" complex (Figure 4.9). A small sample of the slurry containing the "catalyst microcapsules" was removed from the slurry masterbatch and the microcapsules were separated from the slurry by filtering under vacuum. Both crushed and non-crushed ruthenium containing microcapsules were tested for catalytic activity in the hydrogenation reaction of 1-heptene in separate reaction vessels (see section 5.7.1.2 for details). Firstly, a sample of uncrushed microcapsules was tested for activity. The reaction product, heptane was not detected by GC during the 4 h monitoring period when using uncrushed microcapsules. Therefore,

samples of crushed microcapsules (crushed using a variety of techniques; mortar and pestle, sonic bath, and re-homogenising) were subsequently tested for catalytic activity. However, the reaction product was not detected by GC at any time during the 4 h monitoring period for any of these reactions using crushed microcapsules.

Several reasons present themselves upon considering why no activity was observed. Firstly, the microcapsules may have been slightly wet during testing. However, this was rectified upon placing the microcapsules either inside a low temperature oven for *ca.* 2 h or leaving the capsules inside a dessicator overnight. Dried microcapsules were added to the reaction vessels. Again, no catalytic activity was observed from the dried microcapsules after 4 h of monitoring the reaction by GC. Secondly, the microcapsules may have not been crushed properly. Therefore, an experiment was carried out to show that the above techniques chosen for crushing the microcapsules were effective: four samples of ruthenium containing microcapsules (1 g) were placed in separate vials and absolute ethanol (15 ml) was added to each vial. The microcapsules in each vial were subjected to various crushing techniques (mortar and pestle, sonic bath for 7 minutes, and re-homogenising using a Silverson homogeniser for 10 minutes). The fourth vial was a control experiment and was therefore not treated to any of the crushing techniques. The supernatants were tested for chlorobenzene detection using GC-MS analysis. In each supernatant, chlorobenzene was detected and it was concluded that all crushing techniques employed were plausible for crushing microcapsules. Therefore, poorly crushed microcapsules were eliminated as a reason for lack of catalytic activity.

Thirdly, it was considered that the mass of microcapsules used in the hydrogenation reaction may not have contained a sufficient catalyst required to catalyze the volume of reagents used over the reaction time scale. In control hydrogenation reactions (conducted using unencapsulated complex $[RuCl_2(PPh_3)_3]$ 12 mg (0.13 mmol) of complex was used as catalyst when 9.9 ml of reagent was used. In comparison, the mass of microcapsules used as catalyst for the same volume of reagent was 1 g. The amount of ruthenium complex inside 1 g of microcapsules was unable to be quantified due the microcapsules leaching internal phase (as discussed in chapter 3 of this thesis). However, it is estimated that 1 g of microcapsules contains approximately 8 mg (8.4×10^{-3} mmol) of ruthenium complex. Providing this estimation is correct, the microcapsules used to catalyze the same reagent

volume as used for the unencapsulated catalyst contains 15 times less ruthenium complex. Scale up was considered but from a practical consideration, this was not possible because when the mass of microcapsules required for scale up was added to the required volume of solvent, a thick paste of microcapsules was formed. Low catalyst loading was not considered to be a main reason why the microcapsules were not catalytically active, since it was considered that even such small amounts of complex would have produced some product.

Fourthly, it was considered that the catalyst activity may be hindered by the presence of the melamine-formaldehyde polymer. Therefore, to eliminate polymer/solvent interactions as the reason for the failed hydrogenation of 1-heptene using the ruthenium microcapsules, separate washings of the non-crushed capsules and crushed capsules were carried out using an ethanol/benzene mixture (1:1) in order to remove the catalyst from the capsules. These washings were substituted for microcapsules in the test hydrogenation reactions. However, the washings did not catalyze the hydrogenation of 1-heptene, although this could be explained by the low complex loading in the washings but again, even a small loading would be expected to produce some product.

It was considered that surfactant/catalyst interaction could be a factor causing lack of microcapsule catalyst activity. Therefore, the ruthenium complex was encapsulated again using method 3 (different surfactant) instead of method 2 to eliminate surfactant/catalyst interactions as a cause of catalyst inactivity from the investigation. Two separate batches of microcapsules were made using method 3 (see section 5.6.2 for details). The internal phase for batch 1 microcapsules was a chlorobenzene solution of tris(triphenylphosphine)dichlororuthenium(II) (1 % by weight) as before in the encapsulation of the complex using method 2. The internal phase for batch 2 microcapsules was a cetyl alcohol solution of tris(triphenylphosphine)dichlororuthenium(II) (1 % by weight). Again, the ruthenium complex prior to encapsulation was checked for catalytic activity.

The activity testing was carried out under similar reaction conditions to that stated as before apart from that the experimental set up was altered slightly in order to carry out the hydrogenation tests in tandem. Therefore, a mass flow controller was incorporated into the experimental set up in order to control the volume of hydrogen in each reaction vessel.

The gas flow was monitored intermittently during the hydrogenation reactions using a flow meter. The modified experimental set up is shown in Figure 4.11. The grey box shown in the left of the photograph is part of the mass flow control unit which is fed hydrogen from a gas cylinder attached to the left of it (not shown in Figure 4.11). The reaction vessels are the two round bottomed flasks shown in the right hand side of the photograph which are attached to the mass flow control unit using thin plastic tubing. A condenser tube was connected to the reaction vessels for safety reasons. The three-necked round bottomed flasks were each charged with nitrogen before the reaction components were added. In a series of hydrogenation reactions, the "unencapsulated" ruthenium complex was tested alongside batches 1 and 2 of microcapsules containing ruthenium complex (1 g, "crushed" using a mortar and pestle and "non-crushed"). The hydrogen cylinder was opened to start the reaction, and this was recorded as time = 0 h. Aliquots were taken every 30 minutes during the 4 h reaction time period from each of the reaction vessels and the heptene and heptane responses were measured using GC.

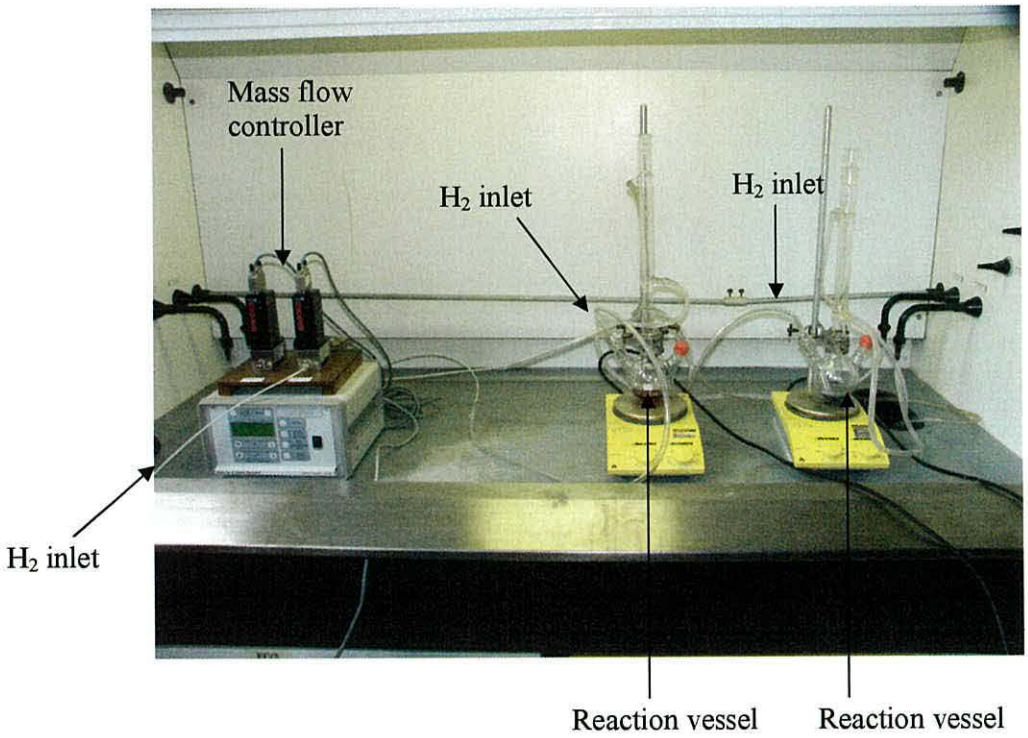

Figure 4.11. Photograph showing hydrogenation reaction set up.

The reaction using the unencapsulated catalyst showed complete heptene conversion to heptane after 3 h as before. However, microcapsule batches 1 and 2 containing the ruthenium complex (both non-crushed and crushed) showed no catalytic activity for the hydrogenation of 1-heptene under the reaction conditions stated above. At this point, choosing an alternative catalyst for encapsulation was an option. However, it was deemed good science to follow the problem through to try to find out the cause of such catalyst inactivity. Finally, it was postulated that lack of catalytic activity from the ruthenium containing microcapsules could be explained by the complex having changed chemical structure during the microencapsulation procedure.

Further microcapsule investigations

After the previously discussed tests to eliminate possible reasons why the microcapsules were not displaying signs of catalytic activity, it was decided to investigate the possibility that the catalyst is decomposing inside the microcapsules and is therefore different to the initial ruthenium complex used for encapsulation. These investigations were initiated on the basis of the following observations. During the hydrogenation tests, it was observed that the reaction solution containing the ruthenium complex was initially green in colour prior to hydrogen addition. However, after five minutes of a constant stream of hydrogen bubbling through the reaction, the solution changed from green to red and remained red whilst under the hydrogen atmosphere (Figure 4.12 (a)).

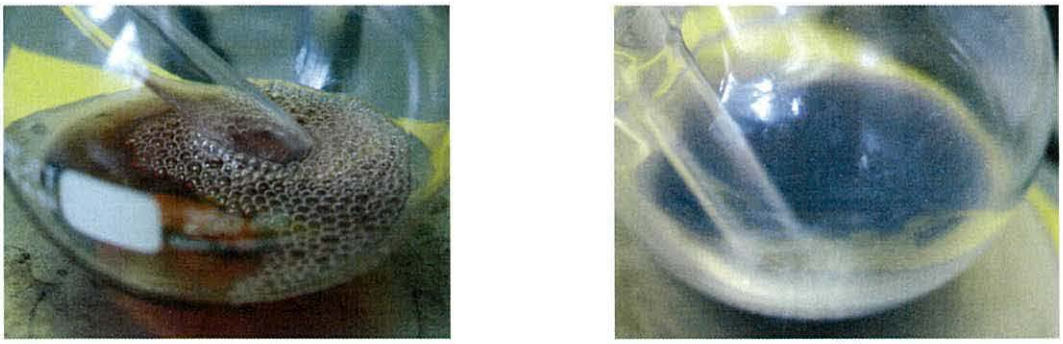

(a) (b)

Figure 4.12. Photograph showing (a) the reaction vessel containing the unencapsulated ruthenium complex under an atmosphere of hydrogen, and (b) the reaction vessel containing the ruthenium complex microcapsules under an atmosphere of hydrogen.

In contrast, the reaction solution containing the microcapsules appeared to be blue which was the same colour as the microcapsules. The reaction solution did not change colour during the 4 h hydrogenation period (Figure 4.12, (b)). Samples were taken from the catalyst solutions to be analyzed using UV/Visible spectrometry. These solutions were scanned between the wavelengths 350 nm – 800 nm in order to obtain the absorbance maximum for each coloured solution. The absorbance measurements are shown in Figure 4.13.

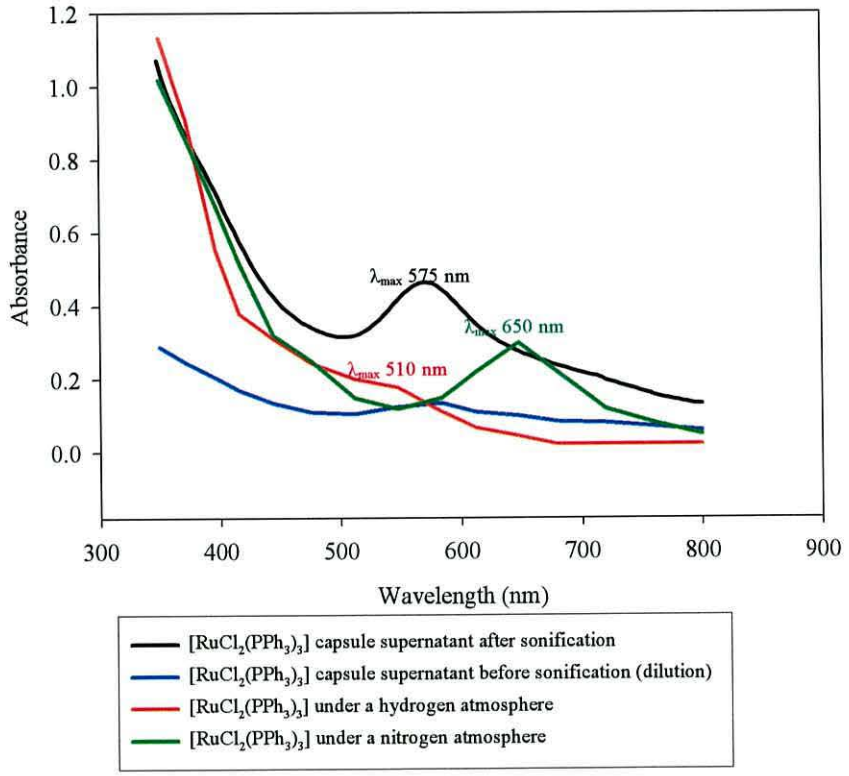

Figure 4.13. UV/Visible spectroscopy measurements obtained for the different coloured supernatants.

A series of absorbance maxima obtained using UV/Visible spectroscopy for the samples (labelled above as in figure) is shown in Figure 4.13. The green line is the resultant scan obtained from the unencapsulated ruthenium complex $[RuCl_2(PPh_3)_3]$ when dissolved in the solvent mix of benzene/ethanol (1:1) under an atmosphere of nitrogen. It can be seen

that upon solvation, the ruthenium complex has an absorbance maximum occurring at *ca.* 650 nm which causes the solution to appear its complementary colour, green. The green colour of the complex in solution is also observed under an atmosphere of air. The red trace is that of the unencapsulated ruthenium complex $[RuCl_2(PPh_3)_3]$ when dissolved in the solvent mix of benzene/ethanol (1:1) and hydrogen gas is bubbled through the solution. It can be seen under such conditions, the ruthenium complex has an absorbance maximum (λ_{max}) occurring at *ca.* 510 nm which causes the solution to appear its complementary colour, red. The blue trace is the resultant scan obtained from the supernatant of the non-crushed ruthenium containing microcapsules in the solvent mix benzene/ethanol (1:1) under an atmosphere of nitrogen, which has a λ_{max} at *ca.* 575 nm. Ruthenium containing microcapsules were crushed in solution by placing in a sonic bath for 10 minutes. The crushed microcapsules were subsequently added to the reaction mixture and hydrogen bubbled through for 2 h to see if catalysis would occur. Using GC monitoring there was no heptane product observed after 2 h, however a sample was taken from the reaction mixture and the supernatant was analyzed using UV/Visible spectroscopy under an atmosphere of air. This is shown as the black trace in Figure 4.12. From the spectra, it can be seen that the absorbance maximum again occurs at *ca.* 575 nm. Thus, it can be concluded from these results that the complex being released from the microcapsules is not the original ruthenium complex encapsulated, reasoning that if it was, the crushed microcapsules solution exposed to the hydrogen atmosphere would be expected to have a λ_{max} shifted towards that of the original ruthenium complex at 510 nm, yet the λ_{max} remains the same as the solution pre-crushing, at 575 nm.

It is known from the literature (see section 1.4 of this thesis) and from results in chapter 2 of this thesis, that formaldehyde is released from melamine-formaldehyde microcapsules during and post polymer curing. Therefore, it was considered a possibility that the original ruthenium complex could be binding or reacting with formaldehyde during the encapsulation process. A control reaction was carried out where the ruthenium complex, $[RuCl_2(PPh_3)_3]$ was dissolved into the solvent mixture of benzene/ethanol (1:1) to form a solution concentration (1 g/L). The solution was green at this stage as expected. Aqueous formaldehyde was added to the organic solution and it was left to stand for 30 minutes whereupon the solution (containing both organic and aqueous layers) changed

colour to the same blue colour that was observed previously in the supernatant which contained ruthenium microcapsules. The aqueous layer was separated from the organic layer and was analyzed using UV/Visible spectroscopy. The solution was scanned between the wavelengths 350 – 800 nm (Figure 4.14). The UV/Visible spectra in Figure 4.13 show the aqueous layer from the control reaction (black line) and the original microcapsule supernatant (red line). Both spectra shown follow a similar spectral pattern with λ_{max} occurring at 575 nm, thus indicating that both solutions contain the same chemical species. From hereon in this thesis, this chemical species with a λ_{max} at 575 nm is labelled as "unknown".

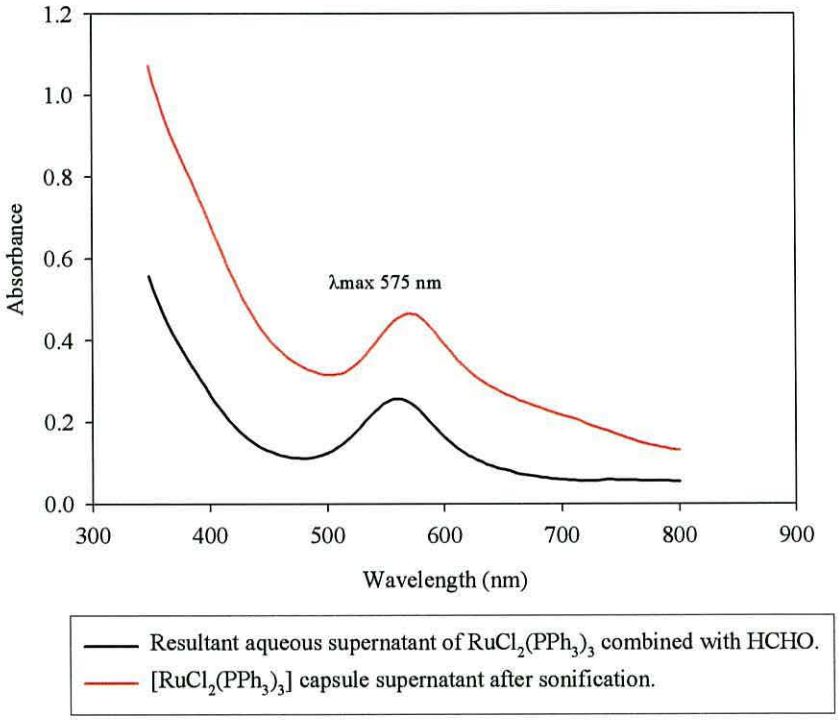

Figure 4.14. A graph showing UV/Visible spectrum of solution 1 (formaldehyde added to the ruthenium complex in solution) and solution 2 (supernatant of catalyst capsules).

To confirm these findings further structural analysis was carried out using infra-red spectroscopy on the supernatant containing the ruthenium microcapsules (Figure 4.15). The resulting spectra showed a medium absorbance observed at 1650 cm^{-1} which showed

the supernatant contained a carbonyl group. Other absorption peaks in the trace correspond mainly to absolute ethanol. The peak at 1650 cm^{-1} is thought to be from free formaldehyde washed from the capsules into the supernatant. At this stage, the possibility of formation of a formaldehyde complex with ruthenium cannot be ruled out but there is no evidence of such a compound from this infrared spectrum since any complex peaks are swamped by the excess solvent present in the supernatant solution. To confirm the assignment of the peak at 1650 cm^{-1} was from free formaldehyde, the spectrum of formalin was recorded over the same range and a similar medium absorbance at 1640 cm^{-1} was observed within the infra-red spectrum. Therefore it can be concluded that formalin is present in the microcapsule supernatant.

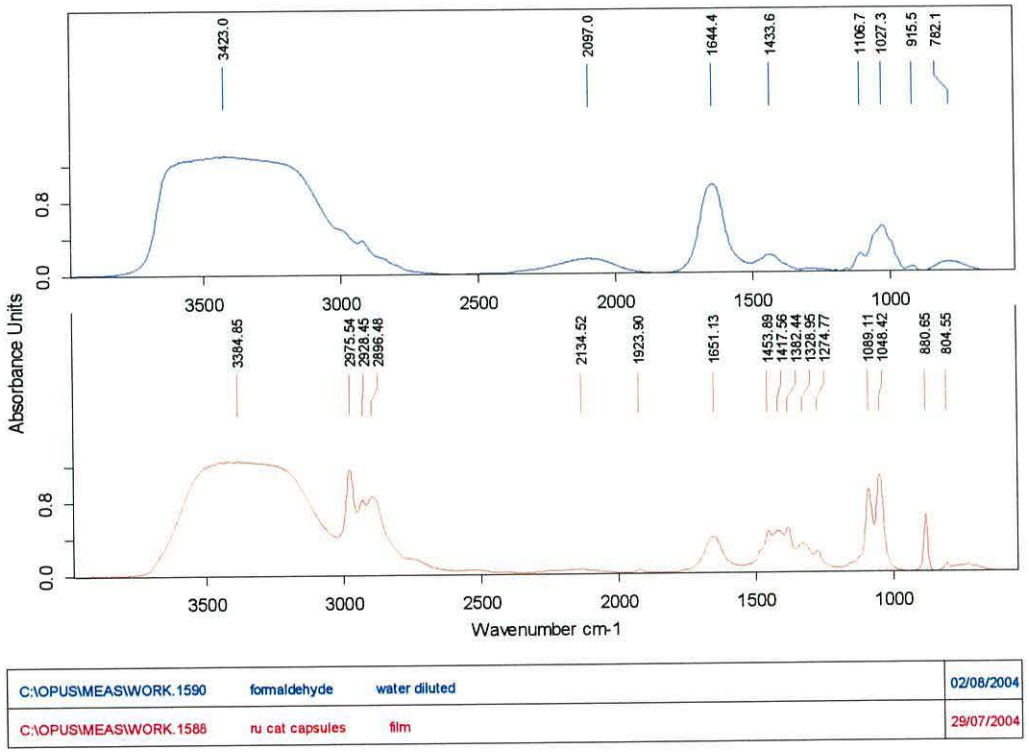

Figure 4.15. FTIR spectrum showing formaldehyde (blue) and the supernatant from the ruthenium containing microcapsules (red).

Further structural analysis was subsequently carried out on the "unknown". From the control reaction, the organic layer was separated from the aqueous layer and the organic

solvent was evaporated and dried using high vacuum. The powdered solid was re-dissolved in deuterated DMSO and submitted for analysis. ^{1}H NMR spectroscopy and ^{31}P NMR spectroscopy was carried out on the sample. A single resonance at 25.7 ppm was observed in the phosphorus NMR spectrum of the "unknown". In comparison, the original ruthenium complex has a single phosphorus resonance at 29.3 ppm, therefore the "unknown" complex is different from the original encapsulated. The proton NMR spectrum of the "unknown" also indicates the presence of a different complex from the original since there are many new resonances that were not in the original ruthenium complex spectrum. For example, the ^{1}H NMR for the original ruthenium complex has 3 resonances appearing at 7.5 ppm, 7.6 ppm, and 7.7 ppm which are due to the to phenyl protons on the ligand. Whereas the ^{1}H NMR spectrum for the probably solvated "unknown" has 12 resonances at 1.1 ppm, 2.5 ppm, 3.3 ppm, 3.5 ppm, 4.7 ppm, 4.9 ppm, 5.4 ppm, 5.8 ppm, 6.1 ppm, 6.4 ppm, 7.6 ppm, and 8.3 ppm (Figure 4.16). As before the resonances appearing in the aromatic region (7-8 ppm) are predicted to arise from phenyl protons in the ligand. However the remaining resonances are difficult to assign, because they clearly must arise from an interaction of the pre-catalyst with solvent and/or formaldehyde.

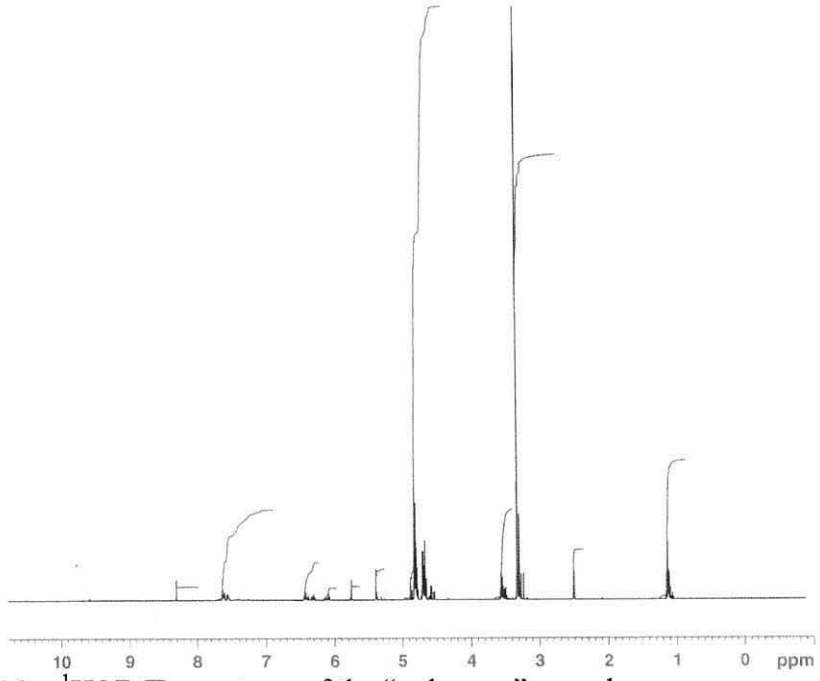

Figure 4.16. ^{1}H NMR spectrum of the "unknown" complex.

The same solution sample was submitted for TOF mass spectrometry. Not surprisingly, the mass spectrum of the "unknown" was difficult to interpret. However, the TOF mass spectrum obtained for the "unknown" (Figure 4.17, a) was consistent with that of the TOF mass spectral pattern obtained for the microcapsule supernatant (Figure 4.17, b).

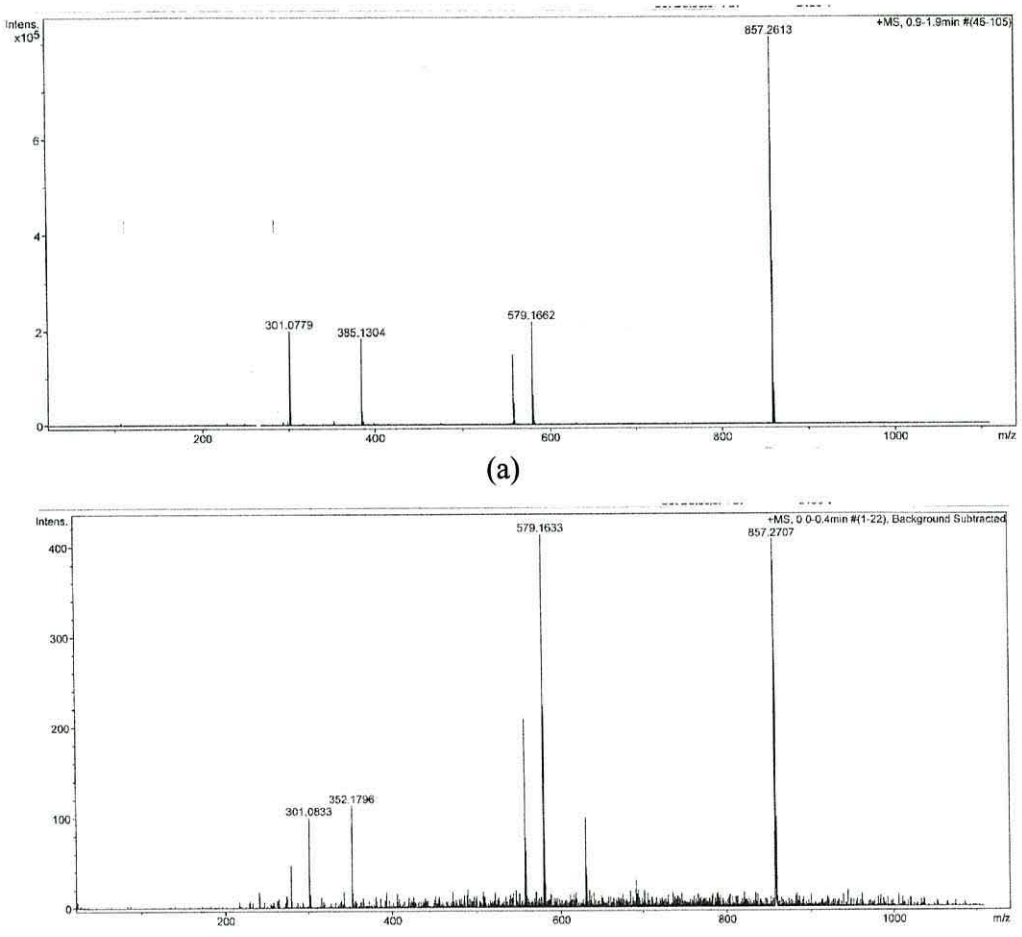

Figure 4.17. TOF mass spectrum of, (a) the "unknown" complex, and (b) microcapsule supernatant.

Both TOF mass spectra show a similar pattern of four main peaks at 301 m/z, 352 m/z, 579 m/z, and 857 m/z, which is consistent with the postulation that there are at least four separate compounds within the sample. The original ruthenium complex has a molecular weight of 958 which is not observed in either mass spectrum. The lack of this molecular

ion indicates the complex is different from the original. Since the characterisation carried out on both the "unknown" and microcapsule supernatant gave no definitive answer regarding the chemical structure of the "unknown", attempts were made to try to crystallise the complex. The "unknown" was dissolved in dichloromethane and this solution was layered with ether but the presence of a waxy material prevented crystallisation. The waxy material is similar to paraformaldehyde, which accounts, in part, for the NMR spectral data and the infrared data. Further work will be required to identify these complexes.

Conclusions

The ruthenium complex before encapsulation has been characterized using ^{1}H NMR spectroscopy, ^{13}C NMR spectroscopy, ^{31}P NMR spectroscopy, CHN analysis, melting point determination, and shown to be $[RuCl_2(PPh_3)_3]$. This complex was then dissolved in chlorobenzene and microencapsulated using the method 2 and 3 melamine-formaldehyde *in situ* interfacial polymerization process described elsewhere in this thesis. The resulting microcapsules were characterized using SEM to examine microcapsule integrity, surface structure and morphology, showing the majority of uncrushed microcapsules to be "deflated" and confirming that the mechanical crushing method of using a mortar and pestle effectively crushes such microcapsules. EDAX of the uncrushed and crushed microcapsule samples confirmed the presence of ruthenium inside the microcapsules.

The ruthenium containing microcapsules were tested for catalytic activity in the hydrogenation reaction, 1-heptene to heptane under ambient conditions. Prior to microcapsule testing, the complex itself was confirmed to be catalytically active for this reaction. All hydrogenation reactions carried out using the microcapsules showed no conversion of 1-heptene to heptane. Subsequently, further analysis was carried out to investigate the reason(s) for lack of catalytic activity from the microcapsules. A control reaction was carried out to determine whether the ruthenium complex had changed structure after microencapsulation. UV/Visible analysis of the product indicated such an occurrence, since the original ruthenium complex, $[RuCl_2(PPh_3)_3]$, in benzene/ethanol(1:1) has a λ_{max} at 510 nm in comparison with the "unknown", which has a λ_{max} at 575 nm. Both control reaction and microcapsule supernatant were treated as "new compounds" and were characterized using infrared spectroscopy, NMR spectroscopy and time of flight mass

spectroscopy. The characterisation indicated that the complex inside the microcapsules is different from the original ruthenium complex encapsulated. What this investigation has highlighted is that the method and materials of encapsulation is clearly important when dealing with reactive intermediates and that the use of formaldehyde-based encapsulation methods are probably not suitable for the generation of catalysts where the active catalyst is prone to attack by a carbonyl group. This will have important consequences for the future development of microencapsulation procedures for catalyst protection and release.

References

1 Wilkinson, G., Hallman, P.S., Stephenson, T.A., *Inorganic Syntheses*, 1970 237

2 James, R., *Homogeneous Hydrogenation*, Wiley, New York, 1973

3 Wilkes, L.M., Nelson, J.H., McCusker, L.B., Seff, K., Mathey, F., *Inorganic Chemistry*, 1983, **22**, 2476

4 Cotton, F.A., Wilkinson, G., *Advanced Inorganic Chemistry*, Wiley, New York, 1988

5 O Haly, A., Razzah, A., Nixon, J.F., *Inorganic Chimia Acta*, 1985, **103**, 83

6 Hegedus, L.S., *Transition Metals in the Synthesis of Complex Organic Molecules*, University Science Books, California, 1999

7 Evans, D., Osborn, J.A., Jardine, F.H., Wilkinson, G., *Nature*, **208**, 1203, 1965

8 Crabtree, R.H., *The Organometallic Chemistry of the Transition Metals*, Wiley, USA, 1998

Future Work

The work in this thesis concerning the encapsulation of homogeneous catalysts could be continued in a variety of ways. The work presented in chapter 4 showed that problems occur when encapsulating a ruthenium catalyst using a formaldehyde based microcapsule polymer wall. Therefore, one way to tackle this problem would be to select a range of non-formaldehyde based polymers as an alternative to melamine-formaldehyde microcapsules and see if the ruthenium complex previously used in this work behaved the same way. Alternatively, homogeneous catalysts with a different metal centre to ruthenium could be trialled in microencapsulation experiments, for example, palladium. If specific microencapsulation equipment was available, it would be interesting to trial catalyst encapsulation using a range of different microencapsulation methods that are discussed in chapter 1 to see firsthand what effects the varying methods have upon the type of capsule produced.

CHAPTER 5

EXPERIMENTAL

5. Experimental

In this chapter, sections 5.1 - 5.4 and 5.6 focus upon the material science aspect of microencapsulation. Therefore, full details of microcapsule characterisation for these sections are reported and discussed in the appropriate results and discussion chapters of this thesis (chapters 2, 3, and 4) in accordance with standard material science method reporting. Sections 5.5 and 5.7 are synthesis and catalysis, respectively. Therefore, characterisation data is reported in full in these sections in compliance with standard synthetic method reporting. The final section; 5.8 reports instrumentation details used for all characterisation.

5.1. Microencapsulation

The photograph in Figure 5.1 shows the experimental set up used for a typical microencapsulation experiment. In the right hand side of the photograph is a Silverson homogenizer, model L4R. This piece of equipment is used to homogenize both internal and external phase by creating high shear (typically it operates at 2,000 rpm to 10,000 rpm ± 500 rpm) to create an oil-in-water emulsion. In the left hand side of the photograph is a water bath with an overhead mechanical stirrer attached. These pieces of equipment are used for the final stage of microencapsulation, *i.e.* curing the microcapsule polymer wall.

Figure 5.1. Microencapsulation equipment used for the work in this thesis.

5.1.1. General microencapsulation; method 1

Materials: the surfactant used for these encapsulations was an ethylene-maleic anhydride co-polymer (EMA) obtained as a fine white powder from commercial suppliers (Zeeland Chemicals Inc, USA). The pre-polymer used to form the polymer wall was Cymel 385 obtained from commercial suppliers (Cytec, USA). Cymel 385 (79 % melamine-formaldehyde pre-polymer) was used "as received" from commercial suppliers in all method 1 microencapsulation experiments unless otherwise stated. The internal phase (IP) used for each microencapsulation experiment is stated in each experimental section as appropriate. All other reagents used were from Aldrich (reagent grade) and used as received unless otherwise stated.

Method: an aqueous solution (84.6 g) of EMA (3 % by weight), neat internal phase (77.0 g), and an aqueous solution (38.4 g) of Cymel 385 (50 % by weight) were solutions 1, 2 and 3, respectively. The three solutions (in separate glass beakers) were covered using aluminium foil and transferred to a water bath (maintained at 348 K ± 2 K) for 15 minutes. Solution 1 was removed from the water bath and homogenized at full speed measured as *ca.* 10,000 rpm using a Tenma digital photo tachometer, model: 72-6633 (Fischer). This speed was used in all method 1 encapsulations (unless otherwise stated) for 3 minutes using a Silverson homogenizer, model: L4R. Solution 2 was removed from the water bath and was poured slowly for 30 seconds at a constant rate into solution 1 whilst homogenizer was operating at full speed. The resulting oil-in-water emulsion was homogenized at the same rate for 5 minutes. Capsule size and morphology were initially observed using optical microscopy during this stage by taking a small drop of emulsion, diluting with water and placing onto a microscope slide. Solution 3 was removed from the water bath and poured slowly at a constant rate into the oil-in-water dispersion. The resulting emulsion was homogenized for a further 5 minutes. The opaque slurry was covered using aluminium foil and transferred to the water bath (maintained at 348 K ± 2 K) and stirred using an overhead mechanical stirrer at full speed (*ca.* 500 rpm) for 3 h. The slurry was then transferred to screw cap glass bottles for storage and later analysis (details in the results and discussion chapters). Immediate analysis of the structure and morphology of the microcapsules was carried out using a Nikon optical microscope. Microcapsules were viewed at (x 1000) magnification using an optical microscope, model: Eclipse E600 (Nikon, Japan) with an oil immersion lens (numerical aperture 1.30), and eyepiece (x 10/22). Images were

recorded using a digital camera, model: Coolpix 950 (Nikon, Japan) attached to the optical microscope.

5.1.2. General microencapsulation; method 2

Materials: the surfactant used for these encapsulations was sodium 2-naphthalene sulfonate formaldehyde condensate (trade name, Demol NL) obtained as an aqueous solution of surfactant (41 % by weight) from commercial suppliers (Kao Corporation, Chemical Business Division, Tokyo, Japan). The pre-polymer used to form the polymer wall was Cymel 385 obtained from commercial suppliers (Cytec, USA). Cymel 385 (79 % melamine-formaldehyde pre-polymer) was used "as received" from commercial suppliers in all method 2 microencapsulations unless otherwise stated. The internal phase (IP) used for each microencapsulation experiment is stated in each experimental section as appropriate. All other reagents used were from Aldrich (reagent grade) and used as received unless otherwise stated.

Method: an aqueous solution (200 g) of a mixture of potassium hydrogen phthalate (2-$(HO_2C)C_6H_4CO_2K$) (0.1 M) and sodium hydroxide (0.1 M) of the ratio 16.7: 1, respectively, formed an acidic buffer solution (pH 4.2 ± 0.1). [1] An aqueous solution (14.6 g) of Demol NL (41 %) was added to the buffer to form solution 1. Neat internal phase (63.0 g) and an aqueous solution (22.7 g) of Cymel 385 (50 % by weight) were solutions 2 and 3, respectively. The solutions (in separate glass beakers) were covered using aluminium foil and transferred to a water bath (maintained at 363 K ± 2 K) for 15 minutes. Solution 1 was removed from the water bath and homogenized at a speed measured as *ca.* 4,000 rpm using a Tenma digital photo tachometer, model: 72-6633 (Fischer) unless otherwise stated for 3 minutes using a Silverson homogenizer, model: L4R. Solution 2 was removed from the water bath and was poured slowly for 30 seconds at a constant rate into solution 1 whilst homogenizer was operating at a speed of *ca.* 4,000 rpm. The resulting oil-in-water emulsion was homogenized at the same rate for 10 minutes. Capsule size and morphology was initially observed using optical microscopy during this stage by taking a small drop of slurry, diluting with water and placing onto a microscope slide. Solution 3 was removed from the water bath and was poured slowly at a constant rate into the oil-in-water emulsion. The resulting emulsion was homogenized for a further 5 minutes. The opaque slurry was covered using aluminium foil and transferred to a water bath (maintained at 363 K ± 2 K) and

stirred using an overhead mechanical stirrer at full speed (*ca.* 500 rpm) for 3 h. The slurry was then transferred to screw cap glass bottles for storage and later analysis (details in the results and discussion chapters). Immediate analysis of the morphology of the microcapsules took place using a Nikon optical microscope. Microcapsules were viewed at (x 1000) magnification using an optical microscope, model: Eclipse E600 (Nikon, Japan) with an oil immersion lens (numerical aperture 1.30), and eyepiece (x 10/22). Images were recorded using a digital camera, model: Coolpix 950 (Nikon, Japan) attached to the optical microscope.

5.1.3. General microencapsulation; method 3

Materials: the surfactant used for these encapsulations was a mixture of gelatin and gum arabic, both obtained separately as white powders from commercial suppliers (Aldrich, UK). The pre-polymer used to form the polymer wall was Cymel 385 obtained from commercial suppliers (Cytec, USA). Cymel 385 (79 % melamine-formaldehyde pre-polymer) was used "as received" from commercial suppliers in all method 3 microencapsulations unless otherwise stated. The internal phase (IP) used for each microencapsulation experiment is stated in each experimental section as appropriate. All other reagents were from Aldrich (reagent grade) and used as received unless otherwise stated.

Method: an aqueous solution (5.5 g) of gelatin (10 % by weight) and aqueous solution (5.5 g) of gum arabic (10 % by weight) was added to an aqueous solution (220 g) of Cymel 385 (7.2 %) to form solution 1. Neat internal phase (130 g) formed solution 2. The solutions (in separate glass beakers) were covered using aluminium foil and transferred to a water bath (maintained at 363 K ± 2 K) for 15 minutes. Solution 1 was removed from the water bath and homogenized at a speed measured as *ca.* 2,000 rpm using a Tenma digital photo tachometer model: 72-6633 (Fischer) unless otherwise stated for 3 minutes using a Silverson homogenizer, model: L4R. A "blocked catalyst" solution (0.9 g) made up of *p*-toluene sulphonic acid (0.50 g), triethanolamine (0.16 g), isobutanol (0.16 g) and water (0.08 g) was added to the homogenizing solution 1. The resulting solution was subsequently homogenized at the same rate as before for a further 2 minutes. Solution 2 was removed from the water bath and slowly poured at a constant rate into the homogenizing solution. The resulting oil-in-water emulsion was homogenized for 1 minute at the same rate as before. Capsule size and morphology was

initially observed using optical microscopy during this stage by taking a small drop of slurry, diluting with water and placing onto a microscope slide. A "catalyst" solution (1.1 g) made up of formic acid (0.45 g), phosphoric acid (0.25 g), *p*-toluene sulphonic acid (0.25 g) and water (0.15 g) was added to the homogenizing emulsion. The emulsion was covered using aluminium foil and further homogenized at an increased speed of *ca.* 10,000 rpm for 15 minutes. The emulsion was removed from the homogenizer and placed into a water bath (maintained at 343 K ± 2 K) fitted with a mechanical overhead stirrer. The beaker containing the emulsion was set stirring at a reduced speed of *ca.* 500 rpm. At this stage, melamine (2 g) was added to the slurry. The mixture was covered using aluminium foil and stirred at the same rate as before for a further 10 minutes using the overhead stirrer. An aqueous solution (12 g) of Cymel 385 (50 % by weight) was added dropwise to the stirring slurry. The mixture was again covered using aluminium foil and left to stir for a remaining 35 minutes at the same rate as before using an overhead stirrer. The resulting slurry was transferred to screw cap glass bottles for storage and later analysis (details in the results and discussion chapters). Immediate analysis of the morphology of the microcapsules took place using an optical microscope. Microcapsules were viewed at (x 1000) magnification using an optical microscope, model: Eclipse E600 (Nikon, Japan) with an oil immersion lens (numerical aperture 1.30), and eyepiece (x 10/22). Images were recorded using a digital camera, model: Coolpix 950 (Nikon, Japan) attached to the optical microscope.

5.2. Microencapsulation Variables

5.2.1. Preparation of microcapsules: effect of homogenizer speed upon particle size

Microencapsulation was carried out as stated above under section 5.1.1. Solution 2 (IP) used for this experiment was neat toluene (77.0 g). The variable in this experiment was homogenizer speed therefore five separate encapsulations of neat toluene (77.0 g) were carried out using the following homogenizer speeds *ca.*: 2000 rpm, 4000 rpm, 6000 rpm, 8000 rpm and 10,000 rpm. These homogenizer speeds were verified using a photo digital tachometer (details as stated in section 5.1.1). The resulting microcapsules from each of the five encapsulation experiments were characterised by (i) particle size analysis, using a Coulter LS particle size analyzer, (model, LS 100 Q), (ii) optical microscopy (using a Nikon optical microscope, (model, Eclipse E600), and (iii)

scanning electron microscopy (using a Hitachi scanning electron microscope, (model, S-520). Sample preparation and instrument details are given in section 5.8 for each of these methods.

5.2.2. Preparation of microcapsules: increasing viscosity of IP

Microencapsulation was carried out as stated above under section 5.1.1. Solution 2 for this experiment was cetyl alcohol (77.0 g) containing an in-house prepared sample of 9,10-bisphenylethynylanthracene (1 % by weight) determined as pure. The resulting microcapsules were characterized by (i) optical microscopy (using a Nikon optical microscope, (model, Eclipse E600) attached with an epi fluorescence attachment, Y-Fl Epi –fl, and (ii) scanning electron microscopy (using a Hitachi scanning electron microscope, (model, S-520). Sample preparation and instrument details are given in section 5.8 for each of these methods.

5.2.3. Preparation of microcapsules: surfactant modification

Initially, a microencapsulation experiment was carried out as stated above under section 5.1.1 using an aqueous solution (84.6 g) of PVA (10 % by weight) as solution 1. Solution 2 used for this experiment was neat toluene (77.0 g). Characterisation was not carried out after this experiment since the surfactant concentration was found to be too high, producing a sticky mess, and therefore microcapsules were not formed (see Figure 2.13 (b)). Thereafter, a microencapsulation experiment (primarily concerned with modifying the surfactant) was carried out which led to the modification of method 1 (5.1.1) into method 2 (5.1.2). In the first experiment, the following mixture was used as solution 1: an aqueous solution (84.6 g) of a mixture of potassium hydrogen phthalate (2-(HO_2C)$C_6H_4CO_2K$) (0.1 M) and sodium hydroxide (0.1 M) of the ratio 16.7: 1 respectively, to form an acidic buffer solution (pH 4.2 ± 0.1) [1], and an aqueous solution (3.1 g) of Demol NL (41 %). Solution 2 was a neat toluene solution (77.0 g). Solution 3 was an aqueous solution (38.4 g) of Cymel 385 (50 % by weight). Microencapsulation was carried out as stated above in section 5.1.1. Characterisation was not carried out after this experiment since the surfactant concentration was found to be too low, and microcapsules were not formed (see Figure 2.13 (a)). The experiment was repeated except that the experimental conditions stated in the patent were followed more closely. [2] However, the polymer curing conditions in the patent procedure were modified to be the same curing conditions as that stated in method 1 (5.1.1). Solution 1

was an aqueous solution (200 g) of a mixture of potassium hydrogen phthalate (2-$(HO_2C)C_6H_4CO_2K$) (0.1 M) and sodium hydroxide (0.1 M) of the ratio 16.7: 1, respectively, and an aqueous solution (14.6 g) of Demol NL (41 %). Solution 2 was neat toluene (63 g), and solution 3 was an aqueous solution (22.7 g) of Cymel 385 (50 % by weight). Microcapsules were formed by following a procedure now stated in this thesis as method 2 (5.1.2). The resulting microcapsules were characterized using SEM (details in section 5.8).

5.2.4. Preparation of microcapsules: formaldehyde testing

A high performance liquid chromatography (HPLC) method was developed to test for formaldehyde concentration in microcapsule slurries. Firstly, dinitrophenylhydrazine (DNPH) was purified by the following procedure. A supersaturated solution of DNPH was made by boiling excess DNPH in 200 ml of acetonitrile for *ca.* 1 h. The solution was allowed to cool to 313 K and this temperature was maintained until *ca.* 95 % solvent had evaporated. The remaining crystals were washed with acetonitrile and the whole procedure was again repeated. The crystals were collected and dissolved into 250 ml of acetonitrile to make a saturated stock solution.

Secondly, a DNPH–formaldehyde derivative was prepared by the following procedure. Dilute HCl (50 ml) was added to the recrystallized DNPH (2 g, 10 mmol) to create a saturated solution. Formalin (1 ml, 12 mmol) was added to this acidified saturated DNPH solution. The DNPH-formaldehyde precipitate was filtered, washed with dilute HCl and water, and dried in air. A standard stock solution (100 mg/L) of the DNPH-formaldehyde was made by dissolving 0.025 g into 250 ml of acetonitrile. From this solution a series of standards were made and analysed using HPLC to create a calibration curve. The optimised method was carried out using a Hewlett Packard HPLC (series 1050). The UV detector was set to 360 nm. The column used was Thames Restek (SpherSIL) 5μm ODS-2 250 x 4.6 mm and the eluent used was an acetonitrile/water mix (70:30). Each sample run time was 14 minutes.

Thereafter, microencapsulation experiments, 1, 2, and 3 were carried out as stated above under sections 5.1.1, 5.1.2, and 5.1.3, respectively. Solution 2 for all three experiments was neat cetyl alcohol. The resulting microcapsules were tested qualitatively for formaldehyde content using the optimised HPLC method by taking 1 g of microcapsule slurry which was diluted using 100 ml of acetonitrile. An aliquot of 10

ml was removed from the diluted slurry suspension. Concentrated HCl (0.05 ml) was added to the diluted slurry suspension followed by addition of saturated DNPH solution (2 ml). Samples were filtered using a micropore filter and analysed using the verified HPLC method. Thereafter, to determine the correct quantity of saturated DNPH solution to be added to each slurry sample (method 1, 2, and 3) for quantitative formaldehyde detection, a series of tests were carried out whereby slurry samples (1 g) were diluted using acetonitrile solution (100 ml). An aliquot of 10 ml was taken from this solution and acidified using 0.05 ml of concentrated HCl. Five further aliquots of 1 ml were taken from the acidified 10 ml slurry aliquot, and to them was added saturated DNPH solution. The volume of saturated DNPH solution added was 0.2 ml, 0.4 ml, 0.8 ml, 1.5 ml, and 3 ml for aliquot 1, 2, 3, 4, and 5, respectively. The samples were filtered using micropore filters and analyzed using the validated HPLC method.

Thereafter, method 3 was chosen to be tested quantitatively for formaldehyde concentration at various stages during the microencapsulation experiment. The experimental procedure was as follows. Microcapsules were made by following method 3 (outlined under section 5.1.3), except the experiment was scaled down by a factor of 10. Solution 2 was neat cetyl alcohol (13 g). During method 3, four aliquots of microcapsule slurry (1 g) were removed at the following times for formaldehyde testing. Aliquot 1 (test 1) was removed after 15 minutes (the start of the microencapsulation experiment = 0 h). Aliquot 2 (test 2) was removed after 25 minutes, aliquot 3 (test 3) was removed after 60 minutes. Immediately after the removal of aliquot 3, scavenger compound (melamine, 4 g) was added to the microencapsulation experiment. Aliquot 4 (test 4) was removed at 90 minutes. Each slurry aliquot was prepared for HPLC analysis by firstly diluting into acetonitrile (100 ml). A further aliquot (10 ml) was taken from this solution and acidified using concentrated HCl (0.05 ml). A saturated solution of DNPH (0.4 ml) was then added and the resulting solution was filtered using micropore filters and analyzed using the validated HPLC method. This formaldehyde test was repeated twice with the exception that the scavenger compound used was dicyandiamine (4 g), and hydrazine hydrate (4.8 g), respectively.

5.3. Microencapsulation of organic target species

5.3.1. Microencapsulation of 9,10-Bisphenylethynylanthracene

Microencapsulation was carried out as stated above under section 5.1.1. Solution 2 for this experiment was cetyl alcohol solution (77.0 g) containing an in-house prepared sample of 9,10-bisphenylethynylanthracene (1 % by weight) determined as pure. Microcapsules were characterized by (i) optical microscopy (using a Nikon optical microscope, (model, Eclipse E600), with an epi fluorescence attachment, Y-Fl Epi –fl (details in section 5.8). The experiment was repeated except that microencapsulation was carried out as stated above under section 5.1.2. Solution 2 for this experiment was chlorobenzene solution (63.0 g) containing 9,10-bisphenylethynylanthracene (0.1 % by weight) determined as pure. Microcapsules were characterized by (i) optical microscopy (using a Nikon optical microscope, (model, Eclipse E600), with an epi fluorescence attachment, Y-Fl Epi –fl (details in section 5.8). The experiment was again repeated except that microencapsulation was carried out as stated above under section 5.1.3. Solution 2 for this experiment was a cetyl alcohol solution (130 g) of 9,10-bisphenylethynylanthracene (0.1 % by weight). Microcapsules were characterized using confocal laser scanning microscopy (using a Zeiss confocal laser scanning microscope, (model LSM 510). The experiment was again repeated except that solution 2 was a chlorobenzene solution (130 g) of 9,10- bisphenylethynylanthracene (0.1 % by weight). Microencapsulation was carried out as stated above under section 5.1.3. Microcapsules were characterized using confocal laser scanning microscopy (using a Zeiss confocal laser scanning microscope, (model LSM 510). Sample preparation and instrument details are given in section 5.8.

5.3.2. Fluorescent doping of Cymel 385 using 9-Anthraldehyde

Microencapsulation was carried out as stated above under section 5.1.2. Solution 2 for this experiment was a chlorobenzene solution (63 g) of 5-[*p*-(dimethylamino)benzylidene]rhodanine in chlorobenzene (1 % by weight). Solution 2 was prepared by weighing the dye, 5-[*p*-(dimethylamino)benzylidene]rhodanine into a beaker containing chlorobenzene, covering and heating to 363 K for 10 minutes. The dye appeared to be only partially soluble in the solvent therefore the suspension was filtered under vacuum, with the majority of the compound retained on the filter paper. The filtrate containing dye was covered with aluminium foil and re-heated until it

reached 363 K. Solution 3 for this experiment was formed by mixing an aqueous solution (22.7 g) of Cymel 385 (50 % by weight) and 9-anthraldehyde (100 mg) together at room temperature for 20 minutes. The mixture was then covered and heated to 363 K to try to fully dissolve 9-anthraldehyde into the aqueous solution. After 10 minutes of stirring, the resulting suspension was removed from the heat and centrifuged at 14,000 rpm for 5 minutes. The yellow supernatant was decanted and placed into a separate beaker which was re-heated by placing into a water bath at 363 ± 2 K. Microcapsules were characterized using confocal laser scanning microscopy (using a Zeiss confocal laser scanning microscope, (model LSM 510). Sample preparation and instrument details are given in section 5.8.

5.3.3. Microencapsulation of Rhodamine B

Microencapsulation was carried out as stated above under section 5.1.2. Solution 2 for this experiment was a cetyl alcohol solution (63 g) of Rhodamine B (0.1 % by weight). Solution 3 for this experiment was formed by mixing an aqueous solution (22.7 g) of Cymel 385 (50 % by weight) and 9-anthraldehyde (100 mg) together at room temperature for 20 minutes. The mixture was then heated to 363 K to dissolve 9-anthraldehyde into the aqueous solution. After 10 minutes of stirring, the resulting suspension was removed from the heat and centrifuged at 14,000 rpm for 5 minutes. The yellow supernatant was decanted and placed into a separate beaker which was re-heated by placing into a water bath at 363 ± 2 K. Microcapsules were characterized by confocal laser scanning microscopy (using a Zeiss confocal laser scanning microscope, (model LSM 510). Sample preparation and instrument details are given in section 5.8.

5.3.4. Microencapsulation of Phenanthroline

Microencapsulation was carried out as stated above under section 5.1.1. Solution 2 was a toluene solution (77.0 g) of phenanthroline (1 % by weight). The experiment was repeated except that microencapsulation was carried out as stated above under section 5.1.2. Solution 2 was comprised of a toluene solution (9.0 g) of phenanthroline (1 % by weight), laurel alcohol (30 g), and myristyl alcohol (20 g). Both batches of microcapsules were used in leaching experiments. See section 5.4 for further details.

5.3.5. Fluorescent doping of Cymel 385 using 6-(9-anthracenyl)-2,4-diamino-1,3,5-Triazine

Microencapsulation was carried out as stated above under section 5.1.3, except the experiment was scaled down by a factor of 10. Solution 2 was a neat solution of cetyl alcohol (13 g). The compound; 6-(9-anthracenyl)-2,4-diamino-1,3,5-triazine (0.2 g) was directly substituted for melamine (0.2 g) in this experiment following the above procedure. Microcapsules were characterized by (i) optical microscopy (using a Nikon optical microscope, (model, Eclipse E600), with epi fluorescence attachment, Y-Fl Epi –fl, and (ii) formaldehyde testing (see 5.2.4 for details). Sample preparation and instrument details are given in section 5.8 for each of these methods.

5.3.6. Microencapsulation of TMC Blue IP.

Microencapsulation was carried out as stated above in section 5.1.2. Solution 2 was a solution of TMC blue IP (63 g) which consisted of Pergascript blue (5.0 g, Ciba), Bis phenol A (5.7 g, Whyte), Span 60 (2.5 g, Black), Cetyl alcohol (12.6 g, Salim) and Stearyl alcohol (37.2 g, Salim). Microcapsules were characterized by (i) optical microscopy (using a Nikon optical microscope, (model, Eclipse E600)). See section 5.8 for details.

5.4. Microcapsule Leaching

All chemicals listed in this section were purchased from Aldrich (reagent grade) and used as received unless otherwise stated.

5.4.1. Phenanthroline microcapsules

Two microencapsulation experiments were carried out as stated above under section 5.3.4. Batch 1 microcapsules (method 1) were tested qualitatively for leakiness. A small amount of slurry (1 g) was taken from the batch, which was then diluted using deionised water (100 ml) into a 100 ml volumetric flask. Thereafter, a small volume (20 ml) of the diluted slurry was accurately pipetted into a conical flask and the pH was tested and found to be slightly acidic at pH 6.2 ± 0.1. Therefore, the pH was lowered to 3.0 ± 0.1 by adding a few drops of dilute H_2SO_4 (2M). An aqueous iron(II)sulphate ($FeSO_4.7H_2O$) stock solution (100 mg/L) was prepared by dissolving $FeSO_4.7H_2O$ (0.1 g, 0.36 mmol) in deionised water into a volumetric flask (1 L). A small volume (20 ml) was accurately pipetted from the iron stock solution into the conical flask containing the

diluted slurry, thus further diluting the slurry by 50 %. Observations of the conical flask after 24 h showed the appearance of a pale orange/red colour. A phenanthroline calibration curve was formed: an aqueous phenanthroline stock solution (100 mg/L, 5.55 x 10^{-4} M) was prepared by dissolving phenanthrolinemonohydrate (0.11 g, 0.6 mmol) in deionised water into a volumetric flask (1 L). From this stock solution, five phenanthroline standards (0 – 10 mg/L) were prepared. Subsequently, each standard was complexed with an aqueous Fe^{2+} standard (10 mg/L) and diluted by a factor of 5. Absorbance measurements of each standard were made using an ATi Unicam, model UV 4 UV/Visible spectroscopy measuring at a fixed wavelength of 515 nm. This wavelength was chosen by scanning a phenanthroline- Fe^{2+} standard (1 mg/L) through the wavelengths 300 – 700 nm and the maximum absorbance value was detected at 515 nm. A series of phenanthroline- Fe^{2+} standards (0.1 - 2 mg/L) were then measured. The second microencapsulation experiment (method 2) was monitored for phenanthroline release at various stages of the procedure using an ATi Unicam, model UV 4 UV/Visible spectroscopy as before (see section 3.1 in chapter 3 for details). Sample preparation and instrument details are given in section 5.8.

5.4.2. Ferrocene microcapsules

Microencapsulation was carried out as stated above under section 5.1.2. Solution 2 was a chlorobenzene solution (63 g) of ferrocene (5 % by weight). The following leaching experiments were carried out in triplicate, *i.e.* three replicates were taken from one batch of capsules. The general procedure for each experiment consisted of weighing 7g of wet capsules into 150 ml glass jars. An accurately measured volume of solvent (50 ml) was added to the capsules and the lids of the jars were screwed tightly in order to create a sealed system. Three solvents of differing polarity; hexane, chloroform and methanol were chosen to investigate any release of ferrocene internal phase into these solvents. Ferrocene release was monitored using an ATi Unicam, model: UV 4 UV/Visible spectrometer measuring at 450 nm. This wavelength was chosen by scanning a ferrocene standard (10 μg/L) through the wavelengths 300 – 700 nm and the maximum absorbance value was detected at 450 nm. A series of ferrocene standards (50 - 250 μg/L) were then measured at the fixed wavelength of 450 nm creating a calibration curve for reference. The test experiments consisted of shaking the full jars for an overall time period of 192 h, with aliquots of 4ml being taken every h for the first

3 h, then at 24 h, and then after every 48 h. Each time an aliquot was replaced with 4 ml of fresh solvent. The control experiments were the same experimental set up with the exception that the jars remained stationary as opposed to being shaken. The first aliquot of 4 ml for analysis was taken from the jar immediately after the 50 ml of solvent was added to the capsules. The depleted volume was replenished using 4ml of fresh solvent, thereby diluting the concentration of the original liquid. Subsequent aliquots of 4ml were taken every hour for the first 3 h, then at 24 h, and then after every 48 h until a total time period of 192 h had elapsed. Each aliquot was sequentially replaced with 4 ml of fresh solvent. All aliquots were measured at 450 nm against a reference cuvette containing the appropriate solvent. Sample preparation and instrument details are given in section 5.8.

5.4.3. Chlorobenzene microcapsules

Microencapsulation was carried out as stated above under section 5.1.2. Solution 2 was neat chlorobenzene (63 g). The following leaching experiments were carried out in triplicate, *i.e.* three replicates were taken from one batch of capsules. A sample of microcapsules (1 g) was placed inside a 100 ml round bottomed flask which contained a solvent mix (20 ml) of chloroform/toluene (19:1). The flask was sealed using an airtight Subaseal™ stopper. A reference flask contained only the solvent mix. Solvent (0.5 ml) was withdrawn from the flask using a syringe after 90 minutes of contact with the capsules. The capsules were filtered through a cotton wool plug and a sample of the filtrate (0.1 µl) was manually injected into a Chrompack GC, model: CP 9001. The optimised method used was splitless using a Restek MTX -1 (30 m) wide bore column (7µl), internal diameter, 0.53 µm. The oven was ramped from 373 K to 433 K over a time period of 3 minutes and the sample was run for a further 2 minutes at this final temperature. An FID detector was used at 573 K. Data was integrated using Maestro Chromatography software. The instrument was calibrated using chlorobenzene dissolved in methanol standards; 5,000 mg/L, 10,000 mg/L and 25,000 mg/L. After initial sampling, aliquots (0.5 ml) were removed for analysis after an additional 90 minutes had passed. Further aliquots (0.5 ml) were removed for analysis every 24 h over a total time period of 120 h. In a second experiment, an identical procedure was followed with the single exception that the chloroform/toluene solvent mixture ratio was 1:19 in this instance as opposed to 19:1 in the first experiment. Microcapsules

were also characterized by optical microscopy (using a Nikon optical microscope, (model, Eclipse E600)). Sample preparation and instrument details are given in section 5.8.

5.5. Synthesis

Solvents were dried by standard methods unless otherwise stated. Chemicals were obtained from Aldrich, UK (reagent grade) and were used as received unless otherwise stated. Details of all instrumentation used for characterization can be found in section 5.8.

5.5.1. Preparation of 9-Cyanoanthracene

The reaction was carried out under a nitrogen atmosphere using standard Schlenk line techniques. Copper (I) cyanide (4.5 g, 50.0 mmol) was added to dry pyridine (40 ml). 9-bromoanthracene (10 g, 38.9 mmol) was then added to the resulting green "paste". The reaction mixture was heated to 463 K using a silicone oil bath and left to reflux for 9 h. TLC observations at this point showed the reaction mixture to be mostly starting material. Therefore, excess pyridine (*ca.* 30 ml) was distilled from the reaction mixture and the reaction at reduced volume was refluxed at 463 K for a further 9 h. TLC observations at this point showed the reaction to be complete therefore the reaction was quenched with aqueous ammonium hydroxide (10 ml, 2 M). The product was extracted with diethylether (3 x 50 ml). The ethereal layer was subsequently washed with water (50 ml), dilute HCl (50 ml, 2M) and again water (50 ml) to extract the pyridine. The ethereal layer was dried using $MgSO_4$ and the solvent removed using a rotary evaporator to yield a yellow powder (5.73g, 57 %), δ_H(500 MHz; d_6-DMSO) 7.71 (2H, d.d.d, $^3J_{HH}$ = 7.0 Hz, $^4J_{HH}$ = 1.5 Hz), 7.86 (2H, d.d.d, $^3J_{HH}$ = 7.0 Hz, $^4J_{HH}$ = 1.5 Hz), 8.28 (4H, d.d.d, (overlapping)), 9.10 (1H, s), δ_C(125 MHz; $CDCl_3$) 105.51, 117.28, 125.35, 126.39, 128.98, 130.69, 132.77, 133.37. m.p. 446-448 K, in accordance with the literature 447-448 K. [3]

5.5.2. Preparation of 6-(9-anthracenyl)-2,4-Diamino-1,3,5-Triazine

The reaction was carried out under a nitrogen atmosphere using standard Schlenk line techniques. Sodium ethoxide was formed by adding sodium (0.35 g) to ethanol (35 ml). 9-Cyanoanthracene (2.03 g, 10 mmol) and dicyanamide (1.68 g, 20 mmol) were added to this solution. The reaction mixture was heated at reflux for 15 h. The solid formed

from solution was filtered and washed with ether to yield a yellow powder, which was recrystallised using hot methanol (1.55 g, 76 %). δ_H(500 MHz; d_6-DMSO), 7.76 (2H, ddd, $^3J_{HH}$ = 6.9 Hz, $^4J_{HH}$ = 1.7 Hz), 7.91 (2H, ddd, $^3J_{HH}$ = 6.9 Hz, $^4J_{HH}$ = 1.7 Hz), 8.35 (4H, ddd (overlapping)), 9.13 (1H, s); δ_C(125 MHz; d_6-DMSO), 103.8, 116.9, 124.3, 126.7, 129.5, 129.9, 130.2, 132.6, 133.7. TOF: m/z (%) 288 (M^+, 100). m/z 288.1234 calc 288.1244, Δ = 3.2 ppm.

5.5.3. Preparation of Tris(triphenylphosphine)dichlororuthenium (II) [$RuCl_2(PPh_3)_3$]

The reaction was carried out under a nitrogen atmosphere using standard Schlenk line techniques. Ruthenium trichloride trihydrate (1.0 g, 3.8 mmol, 99.9 % purity) was dissolved in methanol (250 ml) and refluxed under nitrogen for 5 minutes. After cooling, triphenylphosphine (6.0 g, 22.9 mmol) was added in the ratio of 6 moles of phosphine per one mole of ruthenium trichloride trihydrate. The solution was again refluxed under nitrogen for 3 h. The complex precipitated from the hot solution as black crystals. Upon cooling the crystals were filtered under nitrogen, washed three times with dry ether and dried under vacuum. Yield: 3.45 g, (94%). δ_H(500 MHz; $CDCl_3$) 7.48 (2H, d), 7.56 (1H, b s), 7.69 (2H, m). δ_C(125 MHz; $CDCl_3$) 128.52, 132.0, 132.11, 134.8. δ_P(202 MHz; $CDCl_3$) 29.32. Found: C, 66.7; H, 4.7; N, 0; [$RuCl_2(PPh_3)_3$] requires C, 67.6; H, 4.7; N, 0. m.p. 402-404 K in accordance with the literature value, 405-407 K. [4]

5.5.4. Preparation of Tris(tri ^{n}butylphosphine)dichlororuthenium (II) [$RuCl_2(PBu_3)_3$]

The reaction was carried out under a nitrogen atmosphere using standard Schlenk line techniques. Ruthenium trichloride trihydrate (1.0 g, 3.8 mmol) was dissolved in methanol (250 ml) and refluxed under nitrogen for 5 minutes. After cooling, *n*-butyl phosphine (6.0 g, 22.9 mmol) was added in the ratio of 6 moles of phosphine per one mole of ruthenium trichloride trihydrate. The solution was again refluxed under nitrogen for 3 h. The complex formed red-brown oil which was washed three times with dry ether and dried using $MgSO_4$. The solvent was removed using a rotary evaporator and the oil was further dried using a high vacuum line. Yield: 0.9 g (89 %), δ_H(250 MHz; $CDCl_3$) 1.39 (3H, t), 1.81 (2H, q), 2.00 (2H, broad singlet), 2.31 (2H,

broad singlet). δ_C(125 MHz; $CDCl_3$) 14.08, 22.68, 25.75, 29.60. δ_P(202 MHz; $CDCl_3$) 29.49 DI: m/z ($[M\text{-}Cl^-]^+$, 53%), 743 (53), 203 (100). Found: C, 55.7; H, 10.7; N, 0; $[RuCl_2(PBu_3)_3]$ requires C, 55.5; H, 10.4; N, 0 %. Red crystals precipitated from the oil and were characterised using X-ray crystallography (see Appendix).

5.6. Microencapsulation of organometallic target species

All chemicals listed in this section were purchased from Aldrich, UK and used as received unless otherwise stated.

5.6.1. Microencapsulation of Ferrocene

Microencapsulation was carried out as stated above under section 5.1.2. Solution 2 was a chlorobenzene solution (63 g) of ferrocene (5 % by weight). Microcapsules were characterized by leaching experiments carried out by using UV/Visible spectroscopy using an ATi Unicam UV/Visible spectrometer, (model, UV 4). See section 5.4 for details.

5.6.2. Microencapsulation of Tris(triphenylphosphine)dichlororuthenium (II) $[RuCl_2(PPh_3)_3]$

Microencapsulation was carried out as stated above under 5.1.2. Solution 2 was a chlorobenzene solution (63 g) of tris(triphenylphosphine)dichlororuthenium(II) (1 % by weight). Microcapsules were characterized by SEM and EDAX (see section 5.8 for details). The experiment was repeated twice, except that in both cases microencapsulation was carried out as stated above under 5.1.3 (both experiments were scaled down by a factor of 10). Solution 2 for the first repeat was a cetyl alcohol solution (13 g) of tris(triphenylphosphine)dichlororuthenium(II) (1 % by weight) and the IP for the second repeat was a chlorobenzene solution (13 g) of tris(triphenylphosphine)dichlororuthenium(II) (1 % by weight). Both batches of microcapsules were tested for catalytic activity (see 5.7.1.1 for details).

5.6.3. Microencapsulation of Tris(tri ^{n}butylphosphine)dichlororuthenium (II) $[RuCl_2(PBu_3)_3]$

Microencapsulation was carried out as stated above under section 5.1.1. Solution 2 used for this experiment was a toluene solution (77.0 g) of Tris(tri ^{n} butylphosphine)dichlororuthenium (II) $[RuCl_2(PBu_3)_3]$ (0.5 % by weight).

Microcapsules were characterized by (i) particle size analysis, and (ii) SEM and EDAX. See section 5.8 for details.

5.7. Catalysis

5.7.1.1. Hydrogenation of 1-Heptene using $[RuCl_2(PPh_3)_3]$

In early testing experiments, absolute ethanol (25ml) and anhydrous benzene (25ml) were added to a 3-necked flask pre-flushed with nitrogen. 1-Heptene (9.9 ml, 100 mmol) was added to the stirring solution. The ruthenium catalyst; $[RuCl_2(PPh_3)_3]$ (0.12 g, 0.13 mmol) was added to the flask using a powder funnel. Hydrogen gas was bubbled through the stirring solution for 4 h at ambient temperature and pressure. Aliquots of solution (0.5 ml) were withdrawn from the reaction vessel every 15 minutes for the first hour, then at 30 minutes intervals thereafter to monitor the reaction by GC. A sub-sample of this filtrate (0.1 µl) was manually injected into a Chrompack GC, model: CP 9001. The optimised method used was splitless using a Restek MTX -1 (30 m) wide bore column (7µl), internal diameter, 0.53 µm. Each sample was run isothermally at 303 K for a time period of 12 minutes. An FID detector was used at 573 K. Data was integrated using Maestro Chromatography. The instrument was calibrated using standards; 50,000 mg/L, 75,000 mg/L and 100,000 mg/L of heptane in methanol. In later testing experiments, a mass flow controller (see Figure 4.10 in chapter 4 of this thesis) was incorporated into the testing apparatus in order to monitor hydrogen flow into the round bottomed flasks. The sampling method remained the same, however, the instrument was changed from a Chrompack GC to a Varian GC, model: CP 3800. The optimized method (column and instrumental conditions) used remained the same as before. Data was integrated using Varian Star software.

5.7.1.2. Hydrogenation of 1-Heptene using microencapsulated $[RuCl_2(PPh_3)_3]$

Absolute ethanol (25ml) and anhydrous benzene (25ml) were added to a 3-necked flask pre-flushed with nitrogen. 1-Heptene (9.9 ml, 100 mmol) was added to the stirring solution. In separate experiments, both batches of uncrushed catalyst microcapsules (1.0 g) theoretically containing 0.008 g of catalyst microencapsulated in chlorobenzene were added to the flask using a powder funnel. Hydrogen gas was bubbled through the stirring solution for 4 h at ambient temperature and pressure. Aliquots of solution (0.5 ml) were withdrawn from the reaction vessel every 15 minutes for the first hour, then at

30 minutes intervals thereafter to monitor the reaction. The reaction was monitored using gas chromatrography (GC) using the same GC column and conditions as stated in section 5.7.1.1. The procedure was repeated several times with the exception that the catalyst microcapsules were crushed before addition to the reaction mixture. Sample preparation for crushing the microcapsules involved either (i) grinding microcapsules using a mortar and pestle or (ii) sonification using a sonic bath for 7 minutes.

5.8. Characterisation Techniques

5.8.1. Scanning Electron Microscope (SEM) and Energy Dispersive Analysis X-ray (EDAX)

Preparation of the aluminium stubs for SEM analysis was carried out as follows. A small square of double sided carbon sticky tape was firstly attached to the aluminium stub. Then, one drop of emulsion slurry was placed into a 1000 ml volumetric flask and diluted accordingly using distilled water. This diluted dispersion of microcapsules was then passed through a 0.45 μm micropore filter paper, which retained the majority of microcapsules. The filter paper was gently pressed onto the exposed side of the carbon sticky tape, transferring the majority of microcapsules to the pre-prepared stub. The stub was placed into a dessicator and left to dry overnight. In an alternative preparation, microcapsule slurry (1 ml) was placed into a 2 ml eppendorf centrifuge tube and diluted with distilled water (1 ml). This diluted dispersion was centrifuged at 14,000 rpm for 5 minutes. The supernatant was removed to leave microcapsules. A sub-sample of these microcapsules was taken from the eppendorf centrifuge tube and placed gently onto the sticky carbon pre-prepared aluminium stub. The stub was placed into a dessicator and left to dry overnight. In later SEM analyses, sample preparation was either (i) firstly filtering the slurry to give a powdered sample of microcapsules, then placing a sub-sample of these microcapsules onto the sticky carbon pre-prepared aluminium stub, or (ii) highly diluting the slurry using distilled water (as before), then placing a drop of this diluted dispersion directly onto the sticky carbon pre-prepared aluminium stub, leaving the water to evaporate overnight by placing the stub in a dessicator. All sample coated stubs were sputtered with a gold coating (using the sputter coater, Polaron (model, E5000) at 1.2 KV for 7 minutes) and then, placed into the microscope for analysis. Scanning electron microscopy (SEM) was carried out using a Hitachi–S-520 instrument (Hitachi, Japan) typically operating at 10^{-5} mm/Hg, 10-14 KV, and emission current of

100 μA. The condenser lens was set to an aperture of 6. Early SEM photos were recorded using a film camera, whereas later SEM photos were taken using a digital camera incorporated into the EDAX system. Samples prepared for EDAX were prepared in the same way as for SEM analysis. EDAX was carried out using an Oxford ISIS-III EDS system (Oxford, UK). The condenser lens was changed from 6 to 4 when using EDAX in order to widen the electron beam.

5.8.2. Confocal Laser Scanning Microscopy (CLSM)

Preparation of the microscope slides for confocal laser scanning microscopy was carried out as follows. A small drop of slurry was mixed with immersion oil and placed onto a glass microscope slide. The slide was covered using a glass cover slip and placed under the microscope. One drop of immersion oil was placed on top of the glass cover slip when the microscope oil lenses were being used. In an alternative preparation, a dispersion of dry microcapsules in immersion oil was prepared, and a cover slip placed on top of the sample. Again, one drop of immersion oil was placed on top of the cover slip when the microscope oil lenses were used. A Zeiss (model, LSM 510) Laser Scanning Confocal Imaging System (Zeiss, Germany), equipped with a Coherent multiphoton laser (model, Mira 900) (Coherent, USA) and a Zeiss axioplan 2 optical microscope (Carl Zeiss, Germany), was used to investigate the structure and morphology of the microcapsules. All confocal fluorescence pictures were taken with an x 40 objective (oil immersion, numeric aperture 1.30) or an x 63 objective (oil immersion, numeric aperture 1.40). The configuration (laser line, filters, etc.) for each micrograph taken is detailed in the relevant results and discussion sections of this thesis. The software used for CLSM imaging was LSM 5 image examiner.

5.8.3. Optical/Fluorescence Microscopy

Preparation of the microscope slides for both optical and fluorescence microscopy was carried out as stated in 5.8.2. A Nikon (model, Eclipse E600) optical microscope (Nikon, Japan) fitted with a Nikon epi fluorescence attachment, Y-Fl Epi –fl (Nikon, Japan) was used to characterise microcapsules in both optical (transmission) and fluorescence (reflectance) modes, where appropriate. All optical/fluorescence microscope pictures were taken with an x 100 objective (oil immersion, numeric

aperture 1.30). The pictures were recorded using a Nikon (model, Coolpix 950) digital camera (Nikon, Japan) attached to the microscope.

5.8.4. Gas Chromatography (GC)

Samples were prepared for gas chromatography as stated in the relevant experimental sections of this thesis. All GC samples were run using a Chrompack, CP 9001 unless otherwise stated. The gas chromatography conditions used (unless otherwise stated) was splitless using a Restek MTX -1 (30 m) wide bore column (7µl), internal diameter, 0.53 µm. The oven was ramped from 373 K to 433 K over a time period of 3 minutes and samples were run for a further 2 minutes at this final temperature. An FID detector was used at 573 K. Data was integrated using Maestro Chromatography software.

5.8.5. UV/Visible Spectroscopy

Samples were prepared for UV/Visible spectroscopy as stated in the relevant experimental sections of this thesis. The spectrometer used for all UV/Visible measurements was an ATi Unicam, (model, UV 4) (Unicam, UK). Depending upon the experiment, the instrument was either run in scan or fixed wavelength mode. Standards and a blank were always measured before each sample batch. A deuterium lamp was used for scanning between the wavelengths 200 nm and 325 nm which was then switched to a tungsten lamp for scanning between the wavelengths 325 nm and 800 nm. Each UV/Visible Spectroscopy measurement was carried out using a 2.0 nm band width. The software used to analyze the samples was Vision, V3.40.

5.8.6. Fluorescence Spectroscopy

Samples were prepared for fluorescence spectroscopy by dissolving solid samples in an appropriate solvent and using neat solvent as a blank measurement. All samples were measured at known concentrations, details of which are stated within the relevant experimental section. Fluorescence measurements were made using a Varian instrument (Cary Eclipse) which is fitted with a photomultiplier (PMT) detector. Measurements were taken using 2.5 nm slit width. Excitation wavelengths used for measuring fluorescence is stated in the relevant experimental sections of this thesis.

5.8.7. Particle size analyzer

Samples were prepared for particle size analysis by taking 1 ml of slurry and diluting using distilled water (1 ml). From the diluted sample, a sub-sample (*ca.* 1 ml) was pipetted into the particle size analyzer. The instrument used for all particle size measurements was a Coulter LS Particle Size Analyzer (model, LS 100Q) which is capable of analyzing particles in the size range, 0.4 – 9.5 μm. Data was analyzed using Beckman Coulter particle characterization v 2.0 software, using optical model; Garnet.

5.8.8. Infrared Spectroscopy

Infrared samples were prepared by placing a small drop of the sample (either neat or using chloroform as mulling agent) between two NaCl discs. The instrument used for all infrared measurements was a Bruker (model, Tensor 27) (Bruker, Germany). Each sample was scanned from 400 cm^{-1} to 4000 cm^{-1} using 40 scans unless otherwise stated. A background reading was measured each time before a sample was scanned. Data was analyzed using Opus (2) software.

5.8.9. Elemental Analysis (CHN)

Sample preparation for CHN analysis is described in the relevant experimental sections of this thesis. CHN analysis was obtained using a Carlo Erba EA 1108 – Elemental Analyser.

5.8.10. Nuclear Magnetic Resonance (NMR)

^{1}H nmr, ^{13}C nmr, and ^{31}P nmr spectra were recorded on a Bruker AVANCE 500 MHz instrument using deuterated chloroform as the solvent unless otherwise stated, (assignment notation used; s = singlet, d = doublet, d.d = doublet doublet, d.d.d = doublet doublet doublet, t = triplet, q = quartet, m = multiplet.)

5.8.11. Mass Spectrometry

Sample preparation for mass spectrometry is described in the relevant experimental sections of this thesis. Mass spectra were obtained by direct infusion (DI) using a time of flight (TOF) Bruker Esquire 3000 plus (Bruker, Germany) unless otherwise stated.

5.8.12. High Pressure Liquid Chromatography (HPLC)

Samples were prepared for high pressure liquid chromatography as stated in the relevant experimental section of this thesis. Analysis was carried out using a Hewlett Packard HPLC (series 1050). The UV detector was set to 360 nm. The column used was Thames Restek (SpherSIL) 5µm ODS-2 250 x 4.6 mm and the eluent used was an acetonitrile/water mix (70:30).

References

1 Weast, R.C., (Ed.), *CRC Handbook of Chemistry and Physics (52nd Ed)*, The Chemical Rubber Company, USA, 1972

2 Kamada, 1990, U.S. Patent, 4,957,949

3 Bachmann, W.E., Kloetzel, M.C., *Journal of Organic Chemistry*, 1938, **3**, 55

4 Wilkinson, G., *Inorganic Syntheses*, 1970, **12**, 237

APPENDIX

University of Southampton · School of Chemistry
EPSRC National Crystallography Service

Table 1. Crystal data and structure refinement.

Identification code	**2005src0352**	
Empirical formula	$C_{96}H_{216}Cl_7P_8Ru_3$	
Formula weight	2169.81	
Temperature	120(2) K	
Wavelength	0.71073 Å	
Crystal system	Monoclinic	
Space group	*C*2/*c*	
Unit cell dimensions	a = 35.086(7) Å	α = 90°
	b = 14.184(3) Å	β = 119.17(3)°
	c = 26.639(5) Å	γ = 90°
Volume	11575(4) Å^3	
Z	4	
Density (calculated)	1.245 Mg / m^3	
Absorption coefficient	0.698 mm^{-1}	
F(000)	4652	
Crystal	Plate; Pale Orange	
Crystal size	0.54 × 0.26 × 0.05 mm^3	
θ range for data collection	3.00 – 27.48°	
Index ranges	$-45 \le h \le 44$, $-17 \le k \le 18$, $-34 \le l \le 34$	
Reflections collected	50708	
Independent reflections	13201 [R_{int} = 0.0646]	
Completeness to θ = 27.48°	99.3 %	
Absorption correction	Semi–empirical from equivalents	
Max. and min. transmission	0.9660 and 0.7045	
Refinement method	Full-matrix least-squares on F^2	
Data / restraints / parameters	13201 / 300 / 568	
Goodness-of-fit on F^2	1.034	
Final *R* indices [$F^2 > 2\sigma(F^2)$]	*R1* = 0.0494, *wR2* = 0.1187	
R indices (all data)	*R1* = 0.0877, *wR2* = 0.1385	
Largest diff. peak and hole	1.462 and –1.261 e Å^{-3}	

Diffractometer: *Nonius KappaCCD* area detector (ϕ scans and ω scans to fill *asymmetric unit* sphere). **Cell determination:** DirAx (Duisenberg, A.J.M.(1992). J. Appl. Cryst. 25, 92-96.) **Data collection:** Collect (Collect: Data collection software, R. Hooft, Nonius B.V., 1998). **Data reduction and cell refinement**: *Denzo* (Z. Otwinowski & W. Minor, *Methods in Enzymology* (1997) Vol. **276**: *Macromolecular Crystallography*, part A, pp. 307–326; C. W. Carter, Jr. & R. M. Sweet, Eds., Academic Press). **Absorption correction**: *SADABS Version 2.10.* (G. M. Sheldrick (2003)) Bruker AXS Inc., Madison, Wisconsin, USA. **Structure solution**: *SHELXS97* (G. M. Sheldrick, Acta Cryst. (1990) A**46** 467–473). **Structure refinement**: *SHELXL97* (G. M. Sheldrick (1997), University of Göttingen, Germany). **Graphics:** *ORTEP3 for Windows* (L. J. Farrugia, J. Appl. Crystallogr. 1997, 30, 565).

Special details:

All hydrogen atoms were fixed.
There was some disorder in the butyl chains which was modelled.

Table 2. Atomic coordinates [× 10^4], equivalent isotropic displacement parameters [$Å^2$ × 10^3] and site occupancy factors. U_{eq} is defined as one third of the trace of the orthogonalized U^{ij} tensor.

Atom	*x*	*y*	*z*	U_{eq}	*S.o.f.*
C1	991(1)	3649(3)	4133(2)	22(1)	1
C2	1082(1)	2786(3)	4512(2)	25(1)	1
C3	1077(2)	3025(3)	5065(2)	40(1)	1
C4	1240(2)	2259(4)	5507(2)	61(2)	1
C5	1631(1)	3215(2)	3779(1)	20(1)	1
C6	1979(1)	3634(3)	4348(2)	25(1)	1
C7	2431(1)	3560(3)	4406(2)	31(1)	1
C8	2790(1)	3901(3)	4984(2)	34(1)	1
C9	1101(1)	4843(2)	3361(2)	23(1)	1
C10	814(1)	5539(2)	3462(2)	26(1)	1
C11	871(1)	6542(3)	3310(2)	31(1)	1
C12	575(2)	7245(3)	3376(2)	35(1)	1
C13	1124(1)	831(3)	3663(2)	22(1)	1
C14	801(1)	340(3)	3806(2)	25(1)	1
C15	1029(1)	−48(3)	4414(2)	29(1)	1
C16	727(1)	−510(3)	4591(2)	40(1)	1
C17	602(1)	367(2)	2482(2)	22(1)	1
C18	836(1)	−580(3)	2575(2)	28(1)	1
C19	535(1)	−1345(3)	2176(2)	30(1)	1
C20	420(2)	−1219(3)	1557(2)	49(1)	1
C21	1430(1)	1309(3)	2871(2)	24(1)	1
C22	1841(1)	803(3)	3323(2)	34(1)	1
C23	2243(2)	1047(5)	3253(2)	67(2)	1
C24	2666(2)	709(5)	3766(3)	77(2)	1
C25	708(1)	2285(3)	1560(2)	24(1)	1
C26	351(1)	2338(3)	931(2)	24(1)	1
C27	301(1)	1413(3)	621(2)	30(1)	1
C28	−48(2)	1450(3)	−11(2)	41(1)	1
C29	402(1)	4176(3)	1562(2)	24(1)	1
C30	479(1)	5184(3)	1782(2)	30(1)	1
C31	224(2)	5897(3)	1308(2)	38(1)	1
C32	373(2)	5967(4)	858(2)	63(2)	1
C33	1303(1)	3701(3)	2281(2)	24(1)	1
C34	1395(1)	4007(3)	1793(2)	36(1)	1
C35	1832(4)	4490(14)	2029(6)	68(4)	0.55(2)
C36	2169(3)	4533(14)	2483(4)	64(5)	0.55(2)
C135	1880(3)	3990(15)	1988(5)	42(4)	0.45(2)
C136	2203(4)	3736(18)	2422(6)	70(6)	0.45(2)
P1	1056(1)	3566(1)	3485(1)	18(1)	1
P2	929(1)	1345(1)	2941(1)	18(1)	1
P3	752(1)	3244(1)	2063(1)	19(1)	1
Cl1	0	4030(1)	2500	19(1)	1
Cl2	115(1)	2136(1)	3161(1)	18(1)	1
Ru1	541(1)	2744(1)	2712(1)	16(1)	1
C41	2082(1)	−1165(3)	5746(2)	29(1)	1
C42	1874(1)	−1032(3)	6130(2)	35(1)	1
C43	1756(2)	−16(3)	6162(2)	40(1)	1
C44	1521(2)	118(4)	6507(2)	51(1)	1
C45	1777(1)	−3084(3)	5555(2)	33(1)	1
C46	1345(1)	−2850(3)	5016(2)	33(1)	1
C47	952(1)	−3172(3)	5060(2)	36(1)	1
C48	937(2)	−4231(3)	5137(2)	47(1)	1
C49	2632(1)	−2694(3)	6421(2)	40(1)	1
C50	3012(2)	−2012(4)	6753(2)	58(2)	1
C51	3435(5)	−2206(19)	7306(6)	66(7)	0.328(11)
C52	3621(4)	−1952(10)	7801(5)	40(4)	0.328(11)
C151	3293(4)	−2449(9)	7352(4)	77(5)	0.672(11)
C152	3220(4)	−2395(8)	7742(4)	101(5)	0.672(11)
P41	2248(1)	−2356(1)	5678(1)	28(1)	1
Cl41	2085(1)	−3888(1)	4621(1)	35(1)	1

Cl42	1896(1)	−1579(1)	4339(1)	33(1)	1
Ru41	2500	−2500	5000	24(1)	1

Table 3. Bond lengths [Å] and angles [°].

C1–C2	1.519(5)	C18–H18B	0.9900
C1–P1	1.852(4)	C19–C20	1.507(6)
C1–H1A	0.9900	C19–H19A	0.9900
C1–H1B	0.9900	C19–H19B	0.9900
C2–C3	1.521(5)	C20–H20A	0.9800
C2–H2A	0.9900	C20–H20B	0.9800
C2–H2B	0.9900	C20–H20C	0.9800
C3–C4	1.495(6)	C21–C22	1.534(5)
C3–H3A	0.9900	C21–P2	1.858(4)
C3–H3B	0.9900	C21–H21A	0.9900
C4–H4A	0.9800	C21–H21B	0.9900
C4–H4B	0.9800	C22–C23	1.550(6)
C4–H4C	0.9800	C22–H22A	0.9900
C5–C6	1.528(5)	C22–H22B	0.9900
C5–P1	1.841(3)	C23–C24	1.523(7)
C5–H5A	0.9900	C23–H23A	0.9900
C5–H5B	0.9900	C23–H23B	0.9900
C6–C7	1.517(5)	C24–H24A	0.9800
C6–H6A	0.9900	C24–H24B	0.9800
C6–H6B	0.9900	C24–H24C	0.9800
C7–C8	1.516(5)	C25–C26	1.529(5)
C7–H7A	0.9900	C25–P3	1.864(4)
C7–H7B	0.9900	C25–H25A	0.9900
C8–H8A	0.9800	C25–H25B	0.9900
C8–H8B	0.9800	C26–C27	1.515(5)
C8–H8C	0.9800	C26–H26A	0.9900
C9–C10	1.525(5)	C26–H26B	0.9900
C9–P1	1.862(4)	C27–C28	1.525(5)
C9–H9A	0.9900	C27–H27A	0.9900
C9–H9B	0.9900	C27–H27B	0.9900
C10–C11	1.519(5)	C28–H28A	0.9800
C10–H10A	0.9900	C28–H28B	0.9800
C10–H10B	0.9900	C28–H28C	0.9800
C11–C12	1.512(5)	C29–C30	1.519(5)
C11–H11A	0.9900	C29–P3	1.854(4)
C11–H11B	0.9900	C29–H29A	0.9900
C12–H12A	0.9800	C29–H29B	0.9900
C12–H12B	0.9800	C30–C31	1.523(5)
C12–H12C	0.9800	C30–H30A	0.9900
C13–C14	1.528(5)	C30–H30B	0.9900
C13–P2	1.849(4)	C31–C32	1.526(6)
C13–H13A	0.9900	C31–H31A	0.9900
C13–H13B	0.9900	C31–H31B	0.9900
C14–C15	1.516(5)	C32–H32A	0.9800
C14–H14A	0.9900	C32–H32B	0.9800
C14–H14B	0.9900	C32–H32C	0.9800
C15–C16	1.504(5)	C33–C34	1.546(5)
C15–H15A	0.9900	C33–P3	1.844(4)
C15–H15B	0.9900	C33–H33A	0.9900
C16–H16A	0.9800	C33–H33B	0.9900
C16–H16B	0.9800	C34–C35	1.511(10)
C16–H16C	0.9800	C34–C135	1.519(10)
C17–C18	1.530(5)	C34–H34A	0.9900
C17–P2	1.834(3)	C34–H34B	0.9900
C17–H17A	0.9900	C35–C36	1.211(11)
C17–H17B	0.9900	C35–H35A	0.9900
C18–C19	1.527(5)	C35–H35B	0.9900
C18–H18A	0.9900	C36–H36A	0.9800

C36–H36B	0.9800	C46–H46A	0.9900
C36–H36C	0.9800	C46–H46B	0.9900
C135–C136	1.215(12)	C47–C48	1.520(6)
C135–H35C	0.9900	C47–H47A	0.9900
C135–H35D	0.9900	C47–H47B	0.9900
C136–H36D	0.9800	C48–H48A	0.9800
C136–H36E	0.9800	C48–H48B	0.9800
C136–H36F	0.9800	C48–H48C	0.9800
P1–Ru1	2.2889(12)	C49–C50	1.533(7)
P2–Ru1	2.3134(10)	C49–P41	1.835(4)
P3–Ru1	2.2976(10)	C49–H49A	0.9900
Cl1–Ru1^{i}	2.4915(10)	C49–H49B	0.9900
Cl1–Ru1	2.4915(10)	C50–C51	1.521(12)
Cl2–Ru1	2.4797(10)	C50–C151	1.538(10)
Cl2–Ru1^{i}	2.4967(13)	C50–H50A	0.9900
Ru1–Cl2^{i}	2.4967(13)	C50–H50B	0.9900
C41–C42	1.531(5)	C51–C52	1.208(14)
C41–P41	1.823(4)	C51–H51A	0.9900
C41–H41A	0.9900	C51–H51B	0.9900
C41–H41B	0.9900	C52–H52A	0.9800
C42–C43	1.513(6)	C52–H52B	0.9800
C42–H42A	0.9900	C52–H52C	0.9800
C42–H42B	0.9900	C151–C152	1.188(11)
C43–C44	1.517(6)	C151–H51C	0.9900
C43–H43A	0.9900	C151–H51D	0.9900
C43–H43B	0.9900	C152–H52D	0.9800
C44–H44A	0.9800	C152–H52E	0.9800
C44–H44B	0.9800	C152–H52F	0.9800
C44–H44C	0.9800	P41–Ru41	2.3758(12)
C45–C46	1.531(5)	Cl41–Ru41	2.3626(10)
C45–P41	1.837(4)	Cl42–Ru41	2.3787(12)
C45–H45A	0.9900	Ru41–Cl41^{ii}	2.3626(11)
C45–H45B	0.9900	Ru41–P41^{ii}	2.3758(12)
C46–C47	1.510(5)	Ru41–Cl42^{ii}	2.3787(12)

C2–C1–P1	119.1(3)	C6–C5–H5A	107.4
C2–C1–H1A	107.6	P1–C5–H5A	107.4
P1–C1–H1A	107.6	C6–C5–H5B	107.4
C2–C1–H1B	107.6	P1–C5–H5B	107.4
P1–C1–H1B	107.6	H5A–C5–H5B	106.9
H1A–C1–H1B	107.0	C7–C6–C5	111.4(3)
C1–C2–C3	111.5(3)	C7–C6–H6A	109.3
C1–C2–H2A	109.3	C5–C6–H6A	109.3
C3–C2–H2A	109.3	C7–C6–H6B	109.3
C1–C2–H2B	109.3	C5–C6–H6B	109.3
C3–C2–H2B	109.3	H6A–C6–H6B	108.0
H2A–C2–H2B	108.0	C8–C7–C6	113.1(3)
C4–C3–C2	114.8(4)	C8–C7–H7A	109.0
C4–C3–H3A	108.6	C6–C7–H7A	109.0
C2–C3–H3A	108.6	C8–C7–H7B	109.0
C4–C3–H3B	108.6	C6–C7–H7B	109.0
C2–C3–H3B	108.6	H7A–C7–H7B	107.8
H3A–C3–H3B	107.5	C7–C8–H8A	109.5
C3–C4–H4A	109.5	C7–C8–H8B	109.5
C3–C4–H4B	109.5	H8A–C8–H8B	109.5
H4A–C4–H4B	109.5	C7–C8–H8C	109.5
C3–C4–H4C	109.5	H8A–C8–H8C	109.5
H4A–C4–H4C	109.5	H8B–C8–H8C	109.5
H4B–C4–H4C	109.5	C10–C9–P1	118.6(3)
C6–C5–P1	119.8(3)	C10–C9–H9A	107.7

P1–C9–H9A	107.7	C20–C19–H19B	108.8
C10–C9–H9B	107.7	C18–C19–H19B	108.8
P1–C9–H9B	107.7	H19A–C19–H19B	107.7
H9A–C9–H9B	107.1	C19–C20–H20A	109.5
C11–C10–C9	112.0(3)	C19–C20–H20B	109.5
C11–C10–H10A	109.2	H20A–C20–H20B	109.5
C9–C10–H10A	109.2	C19–C20–H20C	109.5
C11–C10–H10B	109.2	H20A–C20–H20C	109.5
C9–C10–H10B	109.2	H20B–C20–H20C	109.5
H10A–C10–H10B	107.9	C22–C21–P2	120.5(3)
C12–C11–C10	113.5(3)	C22–C21–H21A	107.2
C12–C11–H11A	108.9	P2–C21–H21A	107.2
C10–C11–H11A	108.9	C22–C21–H21B	107.2
C12–C11–H11B	108.9	P2–C21–H21B	107.2
C10–C11–H11B	108.9	H21A–C21–H21B	106.8
H11A–C11–H11B	107.7	C21–C22–C23	111.3(4)
C11–C12–H12A	109.5	C21–C22–H22A	109.4
C11–C12–H12B	109.5	C23–C22–H22A	109.4
H12A–C12–H12B	109.5	C21–C22–H22B	109.4
C11–C12–H12C	109.5	C23–C22–H22B	109.4
H12A–C12–H12C	109.5	H22A–C22–H22B	108.0
H12B–C12–H12C	109.5	C24–C23–C22	111.6(4)
C14–C13–P2	119.8(2)	C24–C23–H23A	109.3
C14–C13–H13A	107.4	C22–C23–H23A	109.3
P2–C13–H13A	107.4	C24–C23–H23B	109.3
C14–C13–H13B	107.4	C22–C23–H23B	109.3
P2–C13–H13B	107.4	H23A–C23–H23B	108.0
H13A–C13–H13B	106.9	C23–C24–H24A	109.5
C15–C14–C13	111.3(3)	C23–C24–H24B	109.5
C15–C14–H14A	109.4	H24A–C24–H24B	109.5
C13–C14–H14A	109.4	C23–C24–H24C	109.5
C15–C14–H14B	109.4	H24A–C24–H24C	109.5
C13–C14–H14B	109.4	H24B–C24–H24C	109.5
H14A–C14–H14B	108.0	C26–C25–P3	119.2(3)
C16–C15–C14	114.1(3)	C26–C25–H25A	107.5
C16–C15–H15A	108.7	P3–C25–H25A	107.5
C14–C15–H15A	108.7	C26–C25–H25B	107.5
C16–C15–H15B	108.7	P3–C25–H25B	107.5
C14–C15–H15B	108.7	H25A–C25–H25B	107.0
H15A–C15–H15B	107.6	C27–C26–C25	111.6(3)
C15–C16–H16A	109.5	C27–C26–H26A	109.3
C15–C16–H16B	109.5	C25–C26–H26A	109.3
H16A–C16–H16B	109.5	C27–C26–H26B	109.3
C15–C16–H16C	109.5	C25–C26–H26B	109.3
H16A–C16–H16C	109.5	H26A–C26–H26B	108.0
H16B–C16–H16C	109.5	C26–C27–C28	112.8(3)
C18–C17–P2	116.4(2)	C26–C27–H27A	109.0
C18–C17–H17A	108.2	C28–C27–H27A	109.0
P2–C17–H17A	108.2	C26–C27–H27B	109.0
C18–C17–H17B	108.2	C28–C27–H27B	109.0
P2–C17–H17B	108.2	H27A–C27–H27B	107.8
H17A–C17–H17B	107.4	C27–C28–H28A	109.5
C19–C18–C17	112.1(3)	C27–C28–H28B	109.5
C19–C18–H18A	109.2	H28A–C28–H28B	109.5
C17–C18–H18A	109.2	C27–C28–H28C	109.5
C19–C18–H18B	109.2	H28A–C28–H28C	109.5
C17–C18–H18B	109.2	H28B–C28–H28C	109.5
H18A–C18–H18B	107.9	C30–C29–P3	117.6(3)
C20–C19–C18	113.7(3)	C30–C29–H29A	107.9
C20–C19–H19A	108.8	P3–C29–H29A	107.9
C18–C19–H19A	108.8	C30–C29–H29B	107.9

P3–C29–H29B	107.9	C17–P2–C21	103.12(17)
H29A–C29–H29B	107.2	C13–P2–C21	101.86(16)
C29–C30–C31	112.5(3)	C17–P2–Ru1	112.17(12)
C29–C30–H30A	109.1	C13–P2–Ru1	118.93(12)
C31–C30–H30A	109.1	C21–P2–Ru1	117.45(12)
C29–C30–H30B	109.1	C33–P3–C29	101.55(17)
C31–C30–H30B	109.1	C33–P3–C25	100.90(17)
H30A–C30–H30B	107.8	C29–P3–C25	102.04(17)
C30–C31–C32	114.0(4)	C33–P3–Ru1	122.92(12)
C30–C31–H31A	108.7	C29–P3–Ru1	114.80(12)
C32–C31–H31A	108.7	C25–P3–Ru1	111.86(13)
C30–C31–H31B	108.7	$Ru1^{i}$–Cl1–Ru1	85.86(4)
C32–C31–H31B	108.7	Ru1–Cl2–$Ru1^{i}$	86.00(3)
H31A–C31–H31B	107.6	P1–Ru1–P3	96.75(4)
C31–C32–H32A	109.5	P1–Ru1–P2	95.45(4)
C31–C32–H32B	109.5	P3–Ru1–P2	95.72(4)
H32A–C32–H32B	109.5	P1–Ru1–Cl2	98.05(4)
C31–C32–H32C	109.5	P3–Ru1–Cl2	163.80(3)
H32A–C32–H32C	109.5	P2–Ru1–Cl2	89.40(3)
H32B–C32–H32C	109.5	P1–Ru1–Cl1	90.65(4)
C34–C33–P3	116.8(3)	P3–Ru1–Cl1	95.31(3)
C34–C33–H33A	108.1	P2–Ru1–Cl1	166.67(3)
P3–C33–H33A	108.1	Cl2–Ru1–Cl1	77.99(3)
C34–C33–H33B	108.1	P1–Ru1–$Cl2^{i}$	168.32(3)
P3–C33–H33B	108.1	P3–Ru1–$Cl2^{i}$	83.99(4)
H33A–C33–H33B	107.3	P2–Ru1–$Cl2^{i}$	96.08(4)
C35–C34–C135	28.6(6)	Cl2–Ru1–$Cl2^{i}$	80.18(4)
C35–C34–C33	111.4(6)	Cl1–Ru1–$Cl2^{i}$	77.68(3)
C135–C34–C33	111.6(6)	C42–C41–P41	117.4(3)
C35–C34–H34A	109.3	C42–C41–H41A	108.0
C135–C34–H34A	83.2	P41–C41–H41A	108.0
C33–C34–H34A	109.3	C42–C41–H41B	108.0
C35–C34–H34B	109.3	P41–C41–H41B	108.0
C135–C34–H34B	130.6	H41A–C41–H41B	107.2
C33–C34–H34B	109.3	C43–C42–C41	112.7(4)
H34A–C34–H34B	108.0	C43–C42–H42A	109.0
C36–C35–C34	137.3(12)	C41–C42–H42A	109.0
C36–C35–H35A	102.8	C43–C42–H42B	109.0
C34–C35–H35A	102.8	C41–C42–H42B	109.0
C36–C35–H35B	102.8	H42A–C42–H42B	107.8
C34–C35–H35B	102.8	C42–C43–C44	113.4(4)
H35A–C35–H35B	105.0	C42–C43–H43A	108.9
C136–C135–C34	134.4(12)	C44–C43–H43A	108.9
C136–C135–H35C	103.6	C42–C43–H43B	108.9
C34–C135–H35C	103.6	C44–C43–H43B	108.9
C136–C135–H35D	103.6	H43A–C43–H43B	107.7
C34–C135–H35D	103.6	C43–C44–H44A	109.5
H35C–C135–H35D	105.3	C43–C44–H44B	109.5
C135–C136–H36D	109.5	H44A–C44–H44B	109.5
C135–C136–H36E	109.5	C43–C44–H44C	109.5
H36D–C136–H36E	109.5	H44A–C44–H44C	109.5
C135–C136–H36F	109.5	H44B–C44–H44C	109.5
H36D–C136–H36F	109.5	C46–C45–P41	116.0(3)
H36E–C136–H36F	109.5	C46–C45–H45A	108.3
C5–P1–C1	103.25(16)	P41–C45–H45A	108.3
C5–P1–C9	99.78(16)	C46–C45–H45B	108.3
C1–P1–C9	99.35(17)	P41–C45–H45B	108.3
C5–P1–Ru1	117.77(12)	H45A–C45–H45B	107.4
C1–P1–Ru1	117.94(12)	C47–C46–C45	112.7(3)
C9–P1–Ru1	115.65(12)	C47–C46–H46A	109.1
C17–P2–C13	100.92(17)	C45–C46–H46A	109.1

C47–C46–H46B	109.1	C50–C51–H51B	102.3
C45–C46–H46B	109.1	H51A–C51–H51B	104.9
H46A–C46–H46B	107.8	C152–C151–C50	125.3(9)
C46–C47–C48	113.8(4)	C152–C151–H51C	106.0
C46–C47–H47A	108.8	C50–C151–H51C	106.0
C48–C47–H47A	108.8	C152–C151–H51D	106.0
C46–C47–H47B	108.8	C50–C151–H51D	106.0
C48–C47–H47B	108.8	H51C–C151–H51D	106.3
H47A–C47–H47B	107.7	C151–C152–H52D	109.5
C47–C48–H48A	109.5	C151–C152–H52E	109.5
C47–C48–H48B	109.5	H52D–C152–H52E	109.5
H48A–C48–H48B	109.5	C151–C152–H52F	109.5
C47–C48–H48C	109.5	H52D–C152–H52F	109.5
H48A–C48–H48C	109.5	H52E–C152–H52F	109.5
H48B–C48–H48C	109.5	C41–P41–C49	103.7(2)
C50–C49–P41	115.6(3)	C41–P41–C45	103.62(18)
C50–C49–H49A	108.4	C49–P41–C45	99.7(2)
P41–C49–H49A	108.4	C41–P41–Ru41	114.26(13)
C50–C49–H49B	108.4	C49–P41–Ru41	116.62(15)
P41–C49–H49B	108.4	C45–P41–Ru41	116.83(14)
H49A–C49–H49B	107.4	Cl41–Ru41–Cl41^{ii}	180.00(5)
C51–C50–C49	127.4(11)	Cl41–Ru41–P41	90.95(4)
C51–C50–C151	25.1(9)	Cl41^{ii}–Ru41–P41	89.05(4)
C49–C50–C151	106.3(7)	Cl41–Ru41–P41^{ii}	89.05(4)
C51–C50–H50A	105.4	Cl41^{ii}–Ru41–P41^{ii}	90.95(4)
C49–C50–H50A	105.4	P41–Ru41–P41^{ii}	180.0
C151–C50–H50A	128.9	Cl41–Ru41–Cl42	90.01(4)
C51–C50–H50B	105.4	Cl41^{ii}–Ru41–Cl42	89.99(4)
C49–C50–H50B	105.4	P41–Ru41–Cl42	89.27(4)
C151–C50–H50B	102.7	P41^{ii}–Ru41–Cl42	90.73(4)
H50A–C50–H50B	106.0	Cl41–Ru41–Cl42^{ii}	89.99(4)
C52–C51–C50	139(2)	Cl41^{ii}–Ru41–Cl42^{ii}	90.01(4)
C52–C51–H51A	102.3	P41–Ru41–Cl42^{ii}	90.73(4)
C50–C51–H51A	102.3	P41^{ii}–Ru41–Cl42^{ii}	89.27(4)
C52–C51–H51B	102.3	Cl42–Ru41–Cl42^{ii}	180.00(5)

Symmetry transformations used to generate equivalent atoms:
(i) –x,y,–z+1/2 (ii) –x+1/2,–y–1/2,–z+1

Table 4. Anisotropic displacement parameters [Å^2× 10^3]. The anisotropic displacement factor exponent takes the form: $-2\pi^2[h^2a^{*2}U^{11} + \cdots + 2\,h\,k\,a^*\,b^*\,U^{12}]$.

Atom	U^{11}	U^{22}	U^{33}	U^{23}	U^{13}	U^{12}
C1	19(2)	25(2)	23(2)	−3(2)	11(2)	2(2)
C2	19(2)	27(2)	25(2)	1(2)	7(2)	−1(2)
C3	51(3)	41(3)	31(2)	2(2)	23(2)	7(2)
C4	73(4)	65(4)	46(3)	11(3)	31(3)	16(3)
C5	13(2)	22(2)	22(2)	−2(1)	7(2)	−2(1)
C6	16(2)	27(2)	25(2)	−3(2)	5(2)	−1(2)
C7	21(2)	33(2)	31(2)	0(2)	8(2)	−3(2)
C8	17(2)	36(2)	39(2)	0(2)	7(2)	−3(2)
C9	19(2)	20(2)	26(2)	−2(2)	9(2)	−3(2)
C10	24(2)	22(2)	29(2)	−1(2)	11(2)	−3(2)
C11	35(2)	21(2)	42(2)	2(2)	23(2)	−1(2)
C12	43(3)	26(2)	40(2)	6(2)	22(2)	6(2)
C13	16(2)	24(2)	26(2)	−2(2)	10(2)	−1(2)
C14	19(2)	25(2)	28(2)	4(2)	9(2)	2(2)
C15	25(2)	29(2)	31(2)	11(2)	13(2)	6(2)
C16	35(2)	44(3)	41(3)	17(2)	19(2)	7(2)
C17	16(2)	19(2)	26(2)	−2(2)	5(2)	−1(1)
C18	26(2)	24(2)	29(2)	−1(2)	9(2)	2(2)
C19	32(2)	20(2)	32(2)	−1(2)	12(2)	0(2)
C20	69(4)	32(3)	32(2)	−6(2)	13(2)	−8(2)
C21	21(2)	24(2)	28(2)	−2(2)	13(2)	1(2)
C22	17(2)	47(3)	35(2)	5(2)	10(2)	7(2)
C23	28(3)	120(5)	49(3)	12(3)	16(2)	26(3)
C24	35(3)	103(5)	84(4)	2(4)	21(3)	15(3)
C25	20(2)	25(2)	26(2)	−3(2)	10(2)	0(2)
C26	25(2)	25(2)	23(2)	0(2)	15(2)	1(2)
C27	33(2)	29(2)	27(2)	−2(2)	14(2)	0(2)
C28	46(3)	41(3)	30(2)	−10(2)	15(2)	4(2)
C29	23(2)	27(2)	25(2)	5(2)	13(2)	3(2)
C30	32(2)	22(2)	39(2)	4(2)	21(2)	3(2)
C31	41(3)	27(2)	53(3)	11(2)	30(2)	8(2)
C32	76(4)	53(3)	77(4)	35(3)	52(3)	22(3)
C33	20(2)	30(2)	28(2)	−2(2)	16(2)	−5(2)
C34	27(2)	51(3)	35(2)	4(2)	20(2)	−4(2)
C35	64(8)	80(10)	77(8)	−10(8)	49(7)	−33(7)
C36	36(6)	111(13)	49(6)	−20(7)	24(5)	−38(7)
C135	34(6)	72(11)	37(6)	−6(7)	32(5)	−17(6)
C136	26(6)	118(17)	73(10)	1(9)	30(7)	−19(8)
P1	12(1)	19(1)	19(1)	−1(1)	5(1)	−1(1)
P2	14(1)	18(1)	21(1)	0(1)	7(1)	0(1)
P3	15(1)	21(1)	21(1)	1(1)	8(1)	−1(1)
Cl1	13(1)	18(1)	24(1)	0	7(1)	0
Cl2	14(1)	21(1)	20(1)	2(1)	8(1)	1(1)
Ru1	10(1)	17(1)	17(1)	0(1)	5(1)	0(1)
C41	22(2)	31(2)	33(2)	−4(2)	14(2)	−1(2)
C42	28(2)	40(3)	36(2)	−1(2)	15(2)	4(2)
C43	37(3)	46(3)	40(3)	−6(2)	22(2)	2(2)
C44	51(3)	49(3)	62(3)	−15(3)	35(3)	2(2)
C45	32(2)	32(2)	36(2)	2(2)	18(2)	2(2)
C46	29(2)	33(2)	39(2)	3(2)	19(2)	0(2)
C47	30(2)	42(3)	40(2)	−4(2)	19(2)	−6(2)
C48	53(3)	42(3)	52(3)	−11(2)	31(3)	−15(2)
C49	33(2)	52(3)	33(2)	5(2)	13(2)	13(2)
C50	31(3)	90(4)	36(3)	−19(3)	3(2)	13(3)
C51	15(9)	115(15)	47(11)	21(10)	−2(8)	−3(9)
C52	25(7)	39(8)	31(8)	−17(6)	−5(6)	−7(6)
C151	28(6)	115(10)	56(7)	−44(6)	−6(4)	32(6)
C152	117(11)	105(9)	43(6)	21(6)	10(6)	−14(7)

P41	22(1)	30(1)	28(1)	1(1)	10(1)	2(1)
Cl41	28(1)	29(1)	47(1)	−11(1)	17(1)	−6(1)
Cl42	26(1)	34(1)	34(1)	2(1)	12(1)	8(1)
Ru41	18(1)	24(1)	28(1)	−2(1)	9(1)	0(1)

Table 5. Hydrogen coordinates [$\times 10^4$] and isotropic displacement parameters [$Å^2 \times 10^3$].

Atom	*x*	*y*	*z*	U_{eq}	*S.o.f.*
H1A	1184	4162	4376	26	1
H1B	687	3849	4005	26	1
H2A	1370	2522	4606	30	1
H2B	858	2298	4299	30	1
H3A	1259	3594	5236	48	1
H3B	775	3184	4970	48	1
H4A	1073	1681	5338	91	1
H4B	1205	2451	5835	91	1
H4C	1549	2141	5637	91	1
H5A	1645	2521	3825	23	1
H5B	1717	3362	3485	23	1
H6A	1911	4305	4369	30	1
H6B	1976	3298	4671	30	1
H7A	2487	2894	4353	37	1
H7B	2438	3936	4098	37	1
H8A	2728	4549	5049	51	1
H8B	3070	3882	4987	51	1
H8C	2804	3492	5289	51	1
H9A	1408	5033	3610	27	1
H9B	1037	4918	2958	27	1
H10A	504	5352	3227	31	1
H10B	888	5515	3871	31	1
H11A	1178	6736	3559	37	1
H11B	812	6555	2907	37	1
H12A	270	7103	3098	53	1
H12B	646	7883	3308	53	1
H12C	615	7204	3767	53	1
H13A	1355	370	3728	27	1
H13B	1264	1344	3947	27	1
H14A	573	794	3765	30	1
H14B	656	−183	3531	30	1
H15A	1250	−514	4447	35	1
H15B	1185	474	4684	35	1
H16A	505	−56	4556	60	1
H16B	895	−721	4991	60	1
H16C	585	−1053	4342	60	1
H17A	348	274	2542	27	1
H17B	488	555	2076	27	1
H18A	1088	−502	2506	34	1
H18B	951	−780	2979	34	1
H19A	678	−1966	2312	35	1
H19B	262	−1350	2201	35	1
H20A	254	−633	1408	74	1
H20B	243	−1753	1330	74	1
H20C	688	−1187	1529	74	1
H21A	1349	1017	2494	28	1
H21B	1513	1969	2852	28	1
H22A	1792	113	3285	41	1
H22B	1899	990	3712	41	1
H23A	2211	748	2898	80	1
H23B	2257	1738	3213	80	1
H24A	2696	993	4119	116	1
H24B	2914	896	3715	116	1
H24C	2660	21	3794	116	1
H25A	992	2246	1565	29	1
H25B	669	1684	1718	29	1
H26A	70	2502	912	28	1
H26B	423	2843	734	28	1
H27A	226	911	816	36	1
H27B	585	1245	647	36	1

H28A	−329	1618	−40	61	1
H28B	−72	832	−188	61	1
H28C	32	1925	−210	61	1
H29A	439	4155	1217	29	1
H29B	94	4014	1437	29	1
H30A	795	5329	1960	35	1
H30B	393	5245	2083	35	1
H31A	252	6526	1484	45	1
H31B	−89	5722	1113	45	1
H32A	684	6129	1047	94	1
H32B	204	6457	577	94	1
H32C	327	5360	661	94	1
H33A	1356	4250	2537	29	1
H33B	1517	3208	2511	29	1
H34A	1390	3445	1569	43	1
H34B	1162	4442	1530	43	1
H35A	1934	4290	1757	81	0.55(2)
H35B	1751	5161	1937	81	0.55(2)
H36A	2120	4284	2790	96	0.55(2)
H36B	2264	5191	2566	96	0.55(2)
H36C	2394	4158	2459	96	0.55(2)
H35C	1897	3635	1679	50	0.45(2)
H35D	1946	4652	1940	50	0.45(2)
H36D	2127	3624	2726	105	0.45(2)
H36E	2427	4227	2546	105	0.45(2)
H36F	2314	3152	2345	105	0.45(2)
H41A	2342	−754	5894	34	1
H41B	1872	−937	5356	34	1
H42A	1607	−1424	5980	42	1
H42B	2080	−1257	6523	42	1
H43A	1568	221	5767	48	1
H43B	2026	367	6337	48	1
H44A	1247	−239	6328	76	1
H44B	1457	789	6515	76	1
H44C	1707	−108	6901	76	1
H45A	1849	−3751	5531	39	1
H45B	1733	−3024	5893	39	1
H46A	1327	−2160	4952	40	1
H46B	1340	−3155	4679	40	1
H47A	684	−2979	4707	43	1
H47B	952	−2849	5390	43	1
H48A	944	−4559	4818	70	1
H48B	667	−4394	5142	70	1
H48C	1189	−4423	5501	70	1
H49A	2467	−2759	6634	48	1
H49B	2754	−3321	6416	48	1
H50A	3102	−1797	6473	69	1
H50B	2882	−1455	6837	69	1
H51A	3426	−2899	7343	79	0.328(11)
H51B	3658	−2098	7187	79	0.328(11)
H52A	3730	−1308	7824	60	0.328(11)
H52B	3866	−2375	8028	60	0.328(11)
H52C	3417	−1965	7954	60	0.328(11)
H51C	3311	−3131	7287	93	0.672(11)
H51D	3591	−2193	7496	93	0.672(11)
H52D	3490	−2495	8104	151	0.672(11)
H52E	3006	−2877	7699	151	0.672(11)
H52F	3103	−1768	7744	151	0.672(11)